

**AN INVESTIGATION ON THE SURFACE WATER
EFFECT IN LANDSLIDE SUSCEPTIBILITY MAPPING:
AN EXAMPLE FROM YENİCE (KARABÜK) BASIN**

**HEYELAN DUYARLILIĞI HARİTALAMARINDA
YÜZEY SUYUNUN ETKİSİNİN ARAŞTIRILMASI:
YENİCE (KARABÜK) HAVZASI ÖRNEĞİ**

M. CAN CANOĞLU

PROF. DR. HÜSNÜ AKSOY

Supervisor

Submitted to Institute of Sciences of Hacettepe University

as a Partial Fulfilment to the Requirements

for the Award of the Degree of Doctor of Philosophy

in Geological Engineering

2015

ETHICS

In this thesis study, prepared in accordance with the spelling rules of Institute of Graduate Studies in Science of Hacettepe University,

I declare that

- all the information and documents have been obtained in the base of the academic rules
- all audio-visual and written information and results have been presented according to the rules of scientific ethics
- in case of using others Works, related studies have been cited in accordance with the scientific standards
- all cited studies have been fully referenced
- I did not do any distortion in the data set
- and any part of this thesis has not been presented as another thesis study at this or any other university.

17/06/2015

MUSTAFA CAN CANOĞLU

ABSTRACT

AN INVESTIGATION ON THE SURFACE WATER EFFECT IN LANDSLIDE SUSCEPTIBILITY MAPPING: AN EXAMPLE FROM YENİCE (KARABÜK) BASIN

M. Can CANOĞLU

Doctor of Philosophy, Department of Geological Engineering

Supervisor: Prof. Dr. Hüsnü AKSOY

June 2015, 140 Pages

Considering the dramatic results as life losses and economic damages, landslides are the second most important type of natural hazards in Turkey following the earthquakes. The Western Black Sea region is well known with its frequent landslide events. In this study, Yenice Watershed, which embodies Derebaşı and Cebeciler landslides, was investigated within the context of water effect on landslide susceptibility. The relation between the landslide occurrence and variations in the saturation degree was attempted to be investigated in a watershed scale. In this way, landslide susceptibility variations could be analysed in space and time evolving out of triggering factors as water effect in terms of saturation degree of soil. This study presents an integrated approach which utilize the Soil Moisture Distribution and Routing (SMDR) model and Frequency Ratio Analysis with conventional parameters of landslide susceptibility. Saturation Degree Index (SDI) is proposed as a new index reflecting the temporal effect of hydrodynamic variations on landslide susceptibility. The water effect is usually represented with the Topographic Wetness Index (TWI) in conventional landslide susceptibility studies. The new proposed Spatio-Temporal Landslide Susceptibility approach is used in Yenice Watershed to explicate the

triggering effect of soil saturation for the occurrence date of Derebaşı Landslide. The comparison results of landslide susceptibility maps obtained from this new approach utilizing the proposed SDI and conventional TWI are quite noticeable. SDI reveals the effect of water as a triggering factor for landslide susceptibility. Accordingly, a new substantial method is proposed using the attainable monthly mean meteorological data to generate monthly landslide susceptibility maps. The verification of the proposed method was carried out by applying the procedure on the Cebeciler Landslide existing in the same watershed as Derebaşı Landslide.

Keywords: Landslide Susceptibility, Saturation Degree, Frequency Ratio Analysis, Soil Moisture Distribution and Routing, Karabük-Yenice.

ÖZ

HEYELAN DUYARLILIĞI HARİTALAMARINDA YÜZEY SUYUNUN ETKİSİNİN ARAŞTIRILMASI: YENİCE (KARABÜK) HAVZASI ÖRNEĞİ

M. Can CANOĞLU

Doktora, Jeoloji Mühendisliği Bölümü

Tez Danışmanı: Prof. Dr. Hüsnü AKSOY

Haziran 2015, 140 Sayfa

Heyelanlar, ekonomik zararlar ve can kayıpları göz önüne alındığında, Türkiye’de depremlerden sonra ikinci derecede önemli doğal afet olarak kabul edilmektedir. Batı Karadeniz Bölgesi sıkça rastlanan heyelan olaylarıyla bilinir. Bu çalışmada, Derebaşı ve Cebeciler heyelanlarını bünyesinde barındıran Yenice Havzası, suyun heyelan duyarlılığı üzerindeki etkisi kapsamında araştırılmıştır. Heyelan oluşumu ve doygunluk derecesi değişimleri arasındaki ilişki bir havza ölçeğinde analiz edilmiştir. Bu sayede, zaman ve mekandaki tetikleyici faktörlerden kaynaklanan heyelan duyarlılığı değişimleri, doygunluk derecesi açısından analiz edilmiştir. Bu tez çalışmasında, Soil Moisture Distribution and Routing (SMDR) modelini ve Frekans oranı analizini heyelan duyarlılığının alışılagelmiş parametreleri ile kullanan birleştirilmiş bir yaklaşım sunulmaktadır. Doygunluk Derecesi İndeksi (SDI), hidrodinamik değişimlerin heyelan duyarlılığında zamansal etkilerini yansıtan yeni bir indeks olarak önerilmiştir. Genelde, su etkisi geleneksel heyelan duyarlılığı çalışmalarında Topoğrafik Nemlilik İndeksi (TWI) ile temsil edilir. Yeni önerilen zamansal-mekânsal heyelan duyarlılık yaklaşımı, Derebaşı Heyelanının oluşum tarihindeki toprak doygunluğunun

tetikleyici etkisinin yorumlanması için Yenice Havzasında kullanılmıştır. Önerilen yeni yaklaşım SDI ve geleneksel TWI kullanılarak elde edilen Heyelan duyarlılığı haritalarının karşılaştırılması dikkat çekicidir. SDI su etkisini heyelan duyarlılığında tetikleyici faktör olarak ortaya çıkartmıştır. Buna bağlı olarak, elde edilebilir aylık ortalama meteorolojik veriyi kullanarak, aylık heyelan duyarlılığı haritalarını oluşturan yeni bir yöntem önerilmiştir. Önerilen yöntemin doğruluğu, Derebaşı Heyelanı ile aynı havzada bulunan Cebeciler Heyelanına yöntemin uygulanması ile gerçekleştirilmiştir.

Anahtar Kelimeler: Heyelan Duyarlılığı, Doygunluk Derecesi, Frekans Oranı Analizi, SMDR, Karabük-Yenice.

GENİŞLETİLMİŞ ÖZET

HEYELAN DUYARLILIĞI HARİTALAMARINDA YÜZEY SUYUNUN ETKİSİNİN ARAŞTIRILMASI: YENİCE (KARABÜK) HAVZASI ÖRNEĞİ

M. Can CANOĞLU

Doktora, Jeoloji Mühendisliği Bölümü

Tez Danışmanı: Prof. Dr. Hüsnü AKSOY

Haziran 2015, 140 Sayfa

Heyelan afeti, Türkiye’de ekonomik zararlar ve can kayıpları açısından önemli bir doğal afettir. Heyelan felaketinin olumsuz etkileriyle, nüfus artışı ve kontrolsüz şehirleşme nedeniyle her geçen gün daha fazla karşılaşılmaktadır. Türkiye’de Batı Karadeniz Bölgesi’nde heyelan olaylarına sıkça rastlanmaktadır. İncelenen Derebaşı heyelanında sismik ve meteorolojik kayıtlara göre, ana tetikleyici faktörün su etkisi olduğu, depremler ve insan faktörünün ikincil düzeyde tetikleyici faktör olduğu ifade edilebilmektedir.

Heyelan duyarlılık çalışmalarında, su etkisinin yansıtılabilmesi için genellikle Topoğrafik Nemlilik İndeksi (TWI) kullanılmaktadır. Bu indeks, toprağın nem içeriğinin mekansal dağılımını temsil eden bir gösterge olarak aşağıdaki eşitlikteki gibi tanımlanmıştır.

$$TWI = \ln (A/\tan \beta)$$

Bu eşitlikte “A” özgül havza alanı, “ β ” ise lokal eğimi ifade etmektedir. Ancak bu indeks, homojen ve izotrop ortam, tek tip zemin koşulu ve durağan

meteorolojik kořullarda geerli olup havza ierisindeki yaėıř ile yzeysel akıř arasındaki iliřkiyi ortaya koyamamaktadır. rneėin; aynı topoėrafyaya sahip biri öl ikliminde diėeri amazon ikliminde olan iki havzanın da yukarıdaki eřitliėe gre topoėrafik nemlilik indeksleri aynı hesaplanacaktır. Ancak, gerekte iki havzanın nemlilik kořulları tamamen farklı olacaktır. Bu nedenle, Topoėrafik Nemlilik İndeksi (TWI)'nin heyelan duyarlılıėındaki dinamik sreleri yansıtamadıėı ve tetikleyici mekanizmaların heyelan duyarlılıėına yansıtılmasında etkili olmayacaėı dřnlmektedir.

Bu alıřmada, Derebařı ve Cebeciler heyelanlarını bnyesinde barındıran Yenice Havzası, yzey sularının heyelan duyarlılıėı zerindeki etkisi kapsamında arařtırılmıřtır. alıřma iin seilen Derebařı heyelanı, oluřum tarihi bilindiėi iin tercih edilmiřtir. Genellikle, Batı Karadeniz Blgesi'ndeki heyelanların ařırı yaėıřlardan sonra gerekleřtiėi ifade edilir. Ancak, meteorolojik kayıtlara gre Derebařı heyelanının gerekleřtiėi 5 Haziran 2000 tarihindeki yaėıř miktarı sadece 7.3 mm'dir. Ayrıca, bu tarihte heyelanı tetikleyecek dzeyde herhangi bir sismik kayıt da bulunmamaktadır. Bu nedenle, Derebařı heyelanı iin yaėıř ile yzeysel akıř arasındaki iliřkinin ortaya koyulabilmesi iin doygunluk fazlası yzeysel akıř ilkesini temel alan SMDR (Soil Moisture Distribution and Routing) modeli kullanılmıřtır. Heyelan duyarlılıėı kavramına su etkisinin birleřtirilebilmesi iin mevcut meteorolojik veriler kullanılarak SMDR modelinden elde edilen doygunluk derecesi haritaları Doygunluk Derecesi İndeksi'ne (SDI) dnřtrlmřtr. Bu dnřtrme iřlemi iin frekans oranı analizini heyelan duyarlılıėının alıřılagelmiř parametreleri ile kullanan birleřtirilmiř bir yaklařım ortaya koyulmuřtur. SDI, hidrodinamik deėiřimlerin heyelan duyarlılıėında zamansal etkilerini yansıtan yeni bir indeks olarak nerilmiřtir.

Heyelan duyarlılıėında yeni bir indeks olarak nerilen Doygunluk Derecesi İndeksi (SDI) ile Topoėrafik Nemlilik İndeksi (TWI) kullanılarak elde edilen Heyelan Duyarlılık haritaları karřılařtırıldıėında SDI kullanılarak oluřturulan Heyelan Duyarlılık haritasının Derebařı heyelanının oluřum mekanizmasını daha iyi temsil ettiėi ve daha gereki sonu verdiėi grlmřtr. Ancak, heyelanların birbirinden baėımsız zamansal ve mekansal srelerin sonucu

olarak oluşmasından dolayı SDI'nin matematiksel olarak ifade edilebilmesi mümkün olamamıştır. Bunun nedeni, zamansal faktörlerin mekansal olarak sabit ancak zamansal olarak değişkenlik göstermesi, mekansal faktörlerin ise zamansal olarak sabit ancak mekansal olarak değişkenlik göstermesi olarak açıklanabilir.

Yeni bir indeks olarak önerilen SDI'nin doğrulamasının yapılabilmesi için Yenice Havzası içinde gerçekleşmiş olan Cebeciler heyelanı, Derebaşı heyelanı ile aynı yöntem kullanılarak analiz edilmiştir. Ancak Cebeciler heyelanının oluşum tarihi net olarak bilinmemekle beraber, Afet İşleri Genel Müdürlüğü'nün Cebeciler Heyelanı ile ilgili Jeolojik Araştırma Raporu 1998 tarihli'dir. Bu nedenle, aylık ortalama meteorolojik veriler derlenerek SMDR modeli çalıştırılmış, elde edilen aylık doygunluk derecesi verileri frekans oranı yöntemiyle heyelan duyarlılığına SDI olarak entegre edilmiştir. Bu yöntemle elde edilen SDI değerleri ve önerilen yöntemin sonuçlarına göre, 1998 yılının Mayıs ayının Cebeciler heyelanının tetiklenmesi açısından bakıldığında en duyarlı ay olduğu görülmektedir.

Elde edilen sonuçlara dayanılarak, suyun zamansal etkilerini heyelan duyarlılığına yansıtılabilmek için Yenice Meteoroloji İstasyonu'nun kayıt altına aldığı tüm verileri kapsayan 1989-2009 yılları arasındaki meteorolojik verilerin 12 aylık ortalaması kullanılmış ve SMDR modeli tekrar çalıştırılmıştır. Elde edilen doygunluk derecesi haritaları aynı yöntemle "SDI"ye çevrilerek 12 aylık duyarlılık haritaları elde edilmiştir.

Heyelan duyarlılığında "SDI"nin kullanımı ile daha determinist bir yaklaşım ortaya konulmuş ve bu yöntem ile yüzey suyunun zamansal etkisi tetikleyici bir faktör olarak daha doğru bir şekilde heyelan duyarlılığı kavramına yansıtılmıştır.

ACKNOWLEDGEMENTS

I would like to thank Prof. Dr. Hüsnu Aksoy for his constant supervision, encouragement, valuable suggestions and constructive comments throughout my doctoral education, which greatly helped to shape up my academic perspective in the right course.

I want to express my gratitude to thesis supervising committee members, Prof. Dr. Murat Ercanođlu and Assis. Prof. Dr. Bedri Kurtuluş for their constructive suggestions and constant technical support for the improvement of this thesis.

I would like to express my thanks to Prof. Dr. Mehmet Ekmekçi and his team members and Prof. Dr. Ali İhsan Karayiđit for their support during determination of hydraulic conductivity and organic matter content tests performed in Hacettepe University Geological Engineering Department Laboratories.

I am also indebted to SUYAPI Engineering and Consulting Inc. management for their patience and tolerance during my studies in context of my professional and academic progress.

At last but not the least, I would like to express grateful appreciation to my family for their patience and encouragement during my studies. And finally, I would not have gone so far without support from my wife “Nagihan Canođlu” who met halfway during my ambiguous periods.

TABLE OF CONTENTS

	<u>Page</u>
ABSTRACT	i
ÖZ	iii
GENİŞLETİLMİŞ ÖZET	v
ACKNOWLEDGEMENTS.....	viii
TABLE OF CONTENTS	ix
SYMBOLS and ABBREVIATIONS	xi
1. INTRODUCTION.....	1
1.1 RESEARCH OBJECTIVES	3
2. GENERAL CHARACTERISTICS OF THE STUDY AREA.....	5
2.1 REGIONAL GEOLOGICAL PROPERTIES OF THE STUDY AREA	7
2.2 SEISMICITY of STUDY AREA	10
3. PREVIOUS STUDIES	12
3.1 LANDSLIDE STUDIES and DEFINITIONS	12
3.1.1 Causes and Triggering Factors of Landslides.....	15
3.1.2 Triggering and Causal Factors of The Derebaşı Landslide.....	16
3.1.3 Landslide Susceptibility Studies and Basic Concepts	17
3.2 GEOLOGICAL STUDIES IN YENICE and NEAR ENVIRON	24
3.3 SMDR STUDIES	27
4. ANALYSIS AND DEVELOPMENT OF METHODOLOGY	30
4.1 DESK STUDIES	30
4.2 FIELD STUDIES	31
4.3 LABORATORY STUDIES	33
4.3.1 Specific Gravity Test	34
4.3.2 Moisture Content Test.....	35
4.3.3 Organic Matter Content Test.....	35
4.3.4 Determination of Grain Size Distribution	36
4.3.5 Determination of Atterberg Limits.....	36
4.3.6 Soil Classification.....	37
4.3.7 Determination of Hydraulic Conductivity	39
4.4 STRUCTURE of SMDR MODEL and ITS PARAMETRISATION	41

4.4.1 Structure of the SMDR Model	41
4.4.1.1 Working Principle of SMDR Model.....	43
4.4.1.2 Main Components of SMDR Model.....	45
4.4.1.2.1 Meteorological Components.....	45
4.4.1.2.2 Drainage Component	47
4.4.1.2.3 Evapotranspiration Component	49
4.4.1.2.4 Lateral Flow Component	51
4.4.1.2.5 Percolation Component.....	54
4.4.2 Input Data of SMDR Model and Data Production.....	54
4.4.2.1 Raster Maps	54
4.4.2.1.1 Digital Elevation Model Map.....	55
4.4.2.1.2 Watershed Boundary Map.....	55
4.4.2.1.3 Aspect Map	58
4.4.2.1.4 Vegetation Map	59
4.4.2.1.5 Soil Type Map	60
4.4.2.2 Lookup Tables	62
4.4.2.2.1 Meteorological Data Table	63
4.4.2.2.2 Vegetation Characteristics Table.....	63
4.4.2.2.3 Soil Characteristics Table.....	65
4.5 FREQUENCY RATIO ANALYSIS IN TERMS OF LANDSLIDE SUSCEPTIBILITY	71
5. RESULTS and CONCLUSIONS.....	100
REFERENCES	116
APPENDİX 1. Seismic parameters of the earthquakes that occurred in the period of 01.06.2000-10.06.2000 for a radius of 300km from Yenice Watershed.	129
APPENDİX 2. Saturation degree maps of last ten days before the occurrence date of Derebaşı Landslide	132
CURRICULUM VITAE	139

SYMBOLS and ABBREVIATIONS

Symbols

A	Specific Catchment
β	Local Slope
C^0	Degree Celcius
G_s	Specific Gravity
w	Moisture Content
K	Coefficient of Hydraulic Conductivity (m/s)
r_t^2	Manometer Radius (cm ²)
r_o^2	Radius of Soil Sample (cm ²)
L	Length of Soil Sample (cm)
h_1	Hydraulic Head Loss at t_1 (cm)
h_2	Hydraulic Head Loss at t_2 (cm)
t	Time Difference between the Records of h_1 ve h_2 (s)
W	Grid Size (square) (m)
θ	Cell Average Water Content (m ³ .m ⁻³)
Δt	Time Step (d)
RF	Rainfall Volume (m ³)
SM	Snowmelt Volume (m ³)
Q_i	Volume Of Water Received Through Lateral Flow From Surrounding Upslope Cells
Q_o	Volume of water lost through lateral flow to surrounding downslope cells
ET	Volume of Water Lost By Evapotranspiration
P	Volume of Water Lost By Percolation
SE	Saturation Excess Runoff
T_i	Local Temperature of Cell "i" (°C)
T_{ref}	Daily Average Temperature Measured at Reference Point (°C)
H_i	Elevation of Cell "i" (m)
H_{ref}	Reference Elevation (m)

$T_i(t)$	Local Temperature of Cell "i" at Time "t" (°C)
$T_{s/r}$	Snowfall – Rainfall Limit (°C)
$RF_i(t)$	Rainfall of Cell "i" at Time "t" (mm)
$TP(t)$	Total Precipitation at Time "t" (mm)
$SF_i(t)$	Snowfall of Cell "i" at Time "t" (mm)
$T_i(t)$	Local Temperature of Cell "i" at Time "t" (°C)
T_{SM}	Temperature of Snowmelt (°C)
$SM_{pot;i}(t)$	Potential Snowmelt of Cell "i" at Time "t" (mm)
m_i	Snowmelt Factor of Cell "i" (mm. °C ⁻¹ day ⁻¹)
k_i	Snowmelt Constant of Cell "i" (mm.day ⁻¹)
Δt	Time Difference (day)
θ	Volumetric Water Content of Soil (m ³ .m ⁻³)
t	Time (day)
q	Flow Velocity (m.day ⁻¹)
z	Depth (m)
$K(\theta)$	Hydraulic Conductivity as a Function of Soil Water Content (m.day ⁻¹)
H	Hydraulic Head (m)
K_{sat}	Saturated Hydraulic Conductivity (m.day ⁻¹)
θ_{sat}	Volumetric Water Content at Saturation (m ³ .m ⁻³)
θ_r	Residual Water Content (m ³ .m ⁻³)
α	Constant Equal to 13
$u(z)$	Root Extraction Rate at Position z (m.day ⁻¹)
E_{Ti}	Evapotranspiration Rate (m.day ⁻¹)
Ω	Dimensionless Coefficient
Z_A	Thickness of Evapotranspiration Zone (m)
E_{Tp-ref}	Reference Potential Evapotranspiration Rate (m.day ⁻¹)
θ	Water Content (m ³ .m ⁻³)
θ_{wp}	Wilting Point (m ³ .m ⁻³)
θ_{etl}	Evapotranspiration Limit (m ³ .m ⁻³)
R_a	Solar Radiation (MJ.m ⁻² day ⁻¹)
δ_T	Difference Between Mean Monthly Maximum and Mean Monthly Minimum Temperatures (°C)

T_{av}	Daily Average Temperature (°C)
ρ_w	Density of Water (kg.m ⁻³)
λ_H	Latent Heat of Vaporization Of Water (MJ.kg ⁻¹)
γ_{sc}	Solar Constant (118.20 MJ.m ⁻² gün ⁻¹)
ω_s	Sunset Hour Angle (rad)
d_r	Relative Distance Between the Earth and Sun on a Given Day
ϕ	Latitude (rad)
δ	Angle Between Sunrays and the Normal to the Surface (rad)
J	Julian Day Number
n_Y	Number of Days of Year Y
k	Neighbour Cell
int	Integer Part of the Expression in Parenthesis
α	Cell Slope Aspect (°)
Φ_k	The Proportion of Water Income to Cell “k”
Φ_{k+1}	The Proportion of Water Income to Cell “k+1”
P_{ij}	Water Proportion Transferred From Cell “i” to Cell “j”
Z_i	Depth of the Cell i
Z_j	Depth of the Cell j
L_j	Distance From Centre of the Cell “i” to Centre of the Cell “j”
n	Number of Neighbour Cell Situated Downslope of Cell “i”
w	Width of the cell (m)
$(dh/dL)_i$	The Local Slope of Cell “i”
$K(\theta)_i$	Coefficient of Hydraulic Conductivity of Cell “i”
ET	Evapotranspiration
Fr_i	Frequency Ratio of Class “i”
$N_{pix(Si)}$	The Number of Pixels Containing Landslide in Class “i”
$N_{pix(Ni)}$	Total Number of Pixels Having Class “i” in Whole Area of the Watershed
$\sum N_{pix(Si)}$	Total Number of Pixels Containing Landslide
$\sum N_{pix(Ni)}$	Total Number of Pixels In The Whole Area Of The Watershed

Abbreviations

AHP	Analytic Hierarchy Process
ANN	Artificial Neural Network
ANSWERS	Areal Nonpoint Source Watershed Environmental Response Simulation
ASTER	Advanced Spaceborne Thermal Emission and Reflection Radiometer
ASTM	American Society for Testing and Materials
AVSWAT	Soil and Water Assessment Tool
DEM	Digital Elevation Model
DSLAM	Distributed Shallow Landslide Analysis Mode
FULLSA	Fuzzy Logic Applications on Landslide Susceptibility Assessments
GPS	Global Positioning System
HAA	Hydrologically Active Areas
IDW	Inverse Distance Weighting
LISA	The Level I Stability Analysis
LS	Landslide Susceptibility
MCDM	Multi-Criteria Decision Making
NPS	Non Point Source
OMC	Organic Matter Content
PCA	Principal Component Analysis
PET	Potential Evapotranspiration
SD	Saturation Degree
SDI	Saturation Degree Index
SHALSTAB	Shallow Landsliding Stability
SMDR	Soil Moisture Distribution and Routing
SSURGO	Soil Survey Geographic Database
Temp	Temperature
TN	Sample Preserved In Plastic Bag
TWI	Topographic Wetness Index
USCS	Unified Soil Classification System
USDA	United States Department of Agriculture

USLE	Universal Soil Loss Equation
ULS	Unclassified Landslide Susceptibility
VSFL	Variable Source Loading Function

1. INTRODUCTION

Natural disasters are catastrophic events caused by nature or the natural processes of the earth. The severity of a disaster is measured in lives lost, economic loss, and the ability of the population to rebuild. More and more people are affected by disasters because of the increasing population and uncontrolled urbanization process. In many countries the economic losses and casualties due to the landslides are greater than commonly recognized, and generate a yearly loss of property larger than any other natural disaster, including earthquakes, floods and windstorms [1]. Following the earthquakes, landslides are the second significant natural hazards in Turkey, in terms of economic losses and casualties [2]. The work performed by “General Directorate of Natural Disasters” shows that the residential units subjected to natural disasters happened between the years 1951-2008 are affected mostly from landslide [3]. For this period 13494 landslides occurred in Turkey and from economic point of view the cost of these landslides is approximately 5 billion TL to the national economy [3].

In mapping the landslides many approaches were developed and tested [2, 4, 5, 6, 7, 8, 9, 10, 11, 12]. Landslide susceptibility mapping, in terms of spatio-temporal assessment at national, regional and local scales, is being considered in this study as an important decision making tool for detailed mitigation plan for landslide hazard. Landslides in western part of Black Sea Region (Turkey) have been studied by many researchers, because the region is most widely known as a landslide prone region in the country [13, 14, 15, 16, 17, 18, 19, 20]. The major triggering factor for landsliding in this region is the effect of water, the information obtained by the seismic records, and field studies show that earthquakes and human activities are secondary factors for landslide triggering.

TWI (Topographic Wetness Index) is commonly used index to involve the water effect in Landslide Susceptibility. TWI is defined as an indicator of the spatial distribution of soil water content by Moore et al. [21]:

$$TWI = \ln (A/\tan \beta) \quad (\text{eq. 1.1})$$

Where “A” is specific catchment and “ β ” is local slope. However, this index is valid under steady state meteorological conditions and not representative for rainfall-runoff processes. For example; considering two watersheds having the same topography, one located in a desert climate and the other in Amazon climate, TWI of the first watershed will be the same as the TWI of the second, but in reality, the wetness conditions will be completely different. Under this circumstance, TWI can not reflect dynamic processes on Landslide Susceptibility. Furthermore, occurrence of landslide after excessive rainfall is a general expression mentioned by many researchers [22, 23, 24, 25]. However, there might be cases of landslides that are not directly related to excessive rainfall. For example, during the occurrence date of Derebaşı Landslide which is located in the study area (Yenice Watershed), the only rainfall is 7.3 mm, additionally; no seismic activity was recorded at or just before the occurrence date. Thus, it is thought that the triggering factor of the Derebaşı Landslide could be the water effect rather than excessive rainfall and/or earthquake. For the reflection of the rainfall runoff process on landslide susceptibility concept in “Derebaşı Landslide”, the most suitable model is decided as a fully spatially distributed model based on the saturation excess runoff generation phenomenon.

Therefore, to enlighten the water effect of landslide susceptibility including the triggering process, a model envisaged the spatial and temporal variation of the soil moisture emerged to be combined with the landslide susceptibility concept. For this purpose the SMDR (Soil Moisture Distribution and Routing) model developed by Soil and Water Laboratory [26] was utilized.

SMDR is a fully spatially distributed model, based on the saturation excess runoff phenomena, where the soil hydrodynamic processes are captured at each pixel of the selected watershed. In this way SD (Saturation Degree) map could be obtained as an output of SMDR model is utilized for the occurrence date of a selected landslide, basing on the meteorological data.

With the aim of integrating the water effect and the Landslide Susceptibility concept, the saturation degree map was converted to SDI (Saturation Degree Index)

map of which the details will be given in the following sections by frequency ratio analysis method.

1.1 RESEARCH OBJECTIVES

The main aim of the present research is to reveal the effect of the water on landslide susceptibility in terms of saturation degree. The following specific objectives are set to achieve these aims:

- Select a landslide of known date triggered by water effect (not heavy rainfall no seismic relation).
- Conduct fieldwork for determination of landslide susceptibility input data and gathering temporal and spatial data and information.
- Determine the saturation degree by modelling the rainfall-runoff process.
- Use of frequency ratio analysis to assess the spatio-temporal landslide susceptibility map.
- Suggest a new index as a layer of landslide susceptibility representing the wetness on the scale of watershed for a selected landslide.
- Validation of the suggested index for another landslide in the watershed

To determine the quantitative and qualitative effect of water for landslide susceptibility, a landslide of a known date (Derebaşı Landslide) is selected. Based on the above aims and objectives, the main outputs of the research are envisaged as follows:

- Generation of landslide susceptibility map of the study area for the occurrence date of Derebaşı Landslide.
- Comparison of landslide susceptibility maps obtained by TWI and new suggested index SDI
- Suggestion of new method for landslide susceptibility phenomena integrating the SMDR and frequency ratio analysis. Generating the spatio-temporal landslide susceptibility maps.
- Validation of the new method in terms of spatio-temporal landslide susceptibility with another landslide of known year.

In brief, the general perspective of this study includes;

(a) Generating the saturation degree map of the Yenice Watershed for the occurrence date of Derebaşı Landslide with processing SMDR model.

(b) Converting the saturation degree map to SDI map using frequency analysis.

(c) Comparing the landslide susceptibility maps rendered by TWI and by SDI.

(d) Generating landslide susceptibility maps for 12 months as a new method using SDI with monthly mean meteorological data.

(e) Validation of the new method with another landslide in the Yenice Watershed.

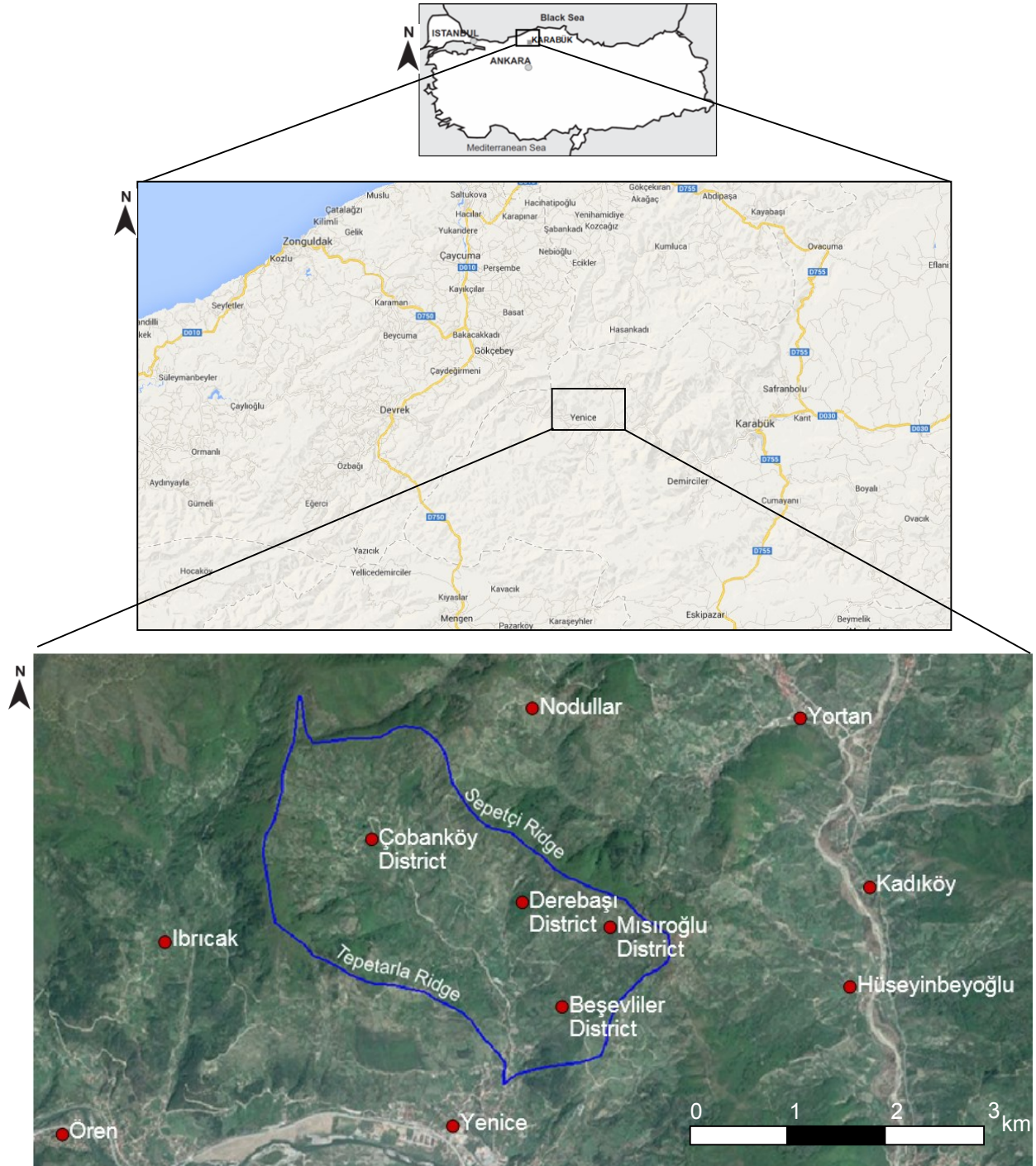
2. GENERAL CHARACTERISTICS OF THE STUDY AREA

The study area is located in the Western Black Sea Region of Turkey, and approximately 2km north of Yenice County and 26 km west of Karabük city (see Fig. 2.1). The approximate distance to Zonguldak and Bartın is 45 km, to Bolu 145km, and to Ankara 240 km. The study area is known as Yenice Watershed (see Figs. 2.1 and 2.2), covers an area of 15.34 km² and located in 1/25000 scaled Zonguldak F28-c1 and F28-b4 topographic maps prepared by National Mapping Agency of Turkey [27]. According to vegetation characteristics map acquired from the Directorate of Yenice Regional Forestry, at the occurrence date of Derebaşı Landslide 20.3% of the area Yenice Watershed was covered by forest and the rest of the area was defined as improper forest area [28]. The climate is typical Black Sea climate with high and distributed rainfall the year round. Summers are warm and humid, winters are cool and damp. The Black Sea is the region which receives the greatest amount of precipitation and is the only region of Turkey that receives high precipitation throughout the year. Based on the meteorological data (between the years 1989-2009) obtained from General Directorate of Meteorological Service of Turkey snowfall is quite common between the months of December and March, snowing for a week or two, and it can be heavy once it snows. Mean annual snowy day number is 25, maximum precipitation is seen at spring season. Mean annual temperature is 13⁰C. Mean temperature at summer season is 30⁰C, mean temperature at winter season is 1⁰C. Maximum temperature is recorded as 44⁰C in August, minimum temperature is recorded as -11⁰C in January. Mean annual precipitation is 1100 mm approximately [29]. The vegetation activity of forest area is much more efficient than improper forest area. The structure of the terrain in the study area has the typical characteristics of Western Black Sea Region. Flat and lowland areas are found rarely and agricultural activities are limited due to the topographic conditions.

According to census study realized by Turkish Statistical Institute in 2009 the population of the Karabük city is 218.564 and the population of the Yenice County is 21.671 [30]. The mining activities in terms of iron mine have a place in Karabük in the form of iron and steel works.

Elevations in the area range between 165 and 837m; and the highest point in the study area is located on the Sepetçi Ridge. Tepetarla Ridge is another

important topographic feature (see Fig. 2.1). In Yenice Watershed slope angles range between 0° and 41° with an average of 19° . Farmlands exist in gentle slopes while extensive and thick forests cover the highest and steepest elevations. Çobanköy, Derebaşı, Mısıroğlu, Beşevliler are the main districts of the study area.



— Watershed Delineation

Fig. 2.1: Location map of the study area (modified from google maps [31])



Fig. 2.2: General view of Yenice (towards NW)

2.1 REGIONAL GEOLOGICAL PROPERTIES OF THE STUDY AREA

The geological properties of the study area are shown in Figure 2.3. The oldest geological unit in the study area and its near environ is Precambrian aged Dirgine Metagranitoids which consist of granite, granitoite, tonalite and monzonite. The Precambrian aged Marbles and Granites superimpose on the Dirgine Metagranitoids by faulting [32]. Jurassic aged limestones represented as İnaltı formation overlie the Precambrian units. The lower cretaceous aged geological units can be observed on the Jurassic limestones by an angular disconformity. The upper cretaceous is represented by Ulus formation in the study area. Ulus formation which has flysch character can be observed as sandy shale, siltstone, sandy limestone, calcareous claystone and sandstone intercalation. All these geological units are superimposed unconformably by Quaternary aged alluviums (Qa) and slope debris (Q). Alluvial deposits formed around the riverbed, consist of materials in the size of gravel, sand, silt and clay. Fine material ratio decreases and blocks occur where riverbed steepens. The slope debris consists of loosely stuck or unstuck blocky and gravelly materials. Slope debris is a product of bedrock which has been weathered, eroded and deposited on slopes in the study area.

The study area which is located in the Western Black Sea Region, is exposed to compression regime during Dogger, after closure of Paleothetis in Triassic. Due to the shoaling during Malm the carbonates got around to deposit. Owing to facies

and thickness variations, the Cretaceous sequences of northern Turkey have been divided into a number of formations with local names that cause a great deal of confusion. Lower Cretaceous sediments are generally rare around the Black Sea Basin. They crop out extensively in the Central Pontides, in particular in the Ulus and the Zonguldak Basins [33]. Ulus basin which gives the name of the Ulus formation, formed in the beginning of the Lower Cretaceous. It was from stratigraphic studies of these two basins that the Ulus Group represents the syn-rift deposits of the western Black Sea. The NE–SW trending Ulus Basin is the largest Lower Cretaceous basin of the Pontides. In contrast to the Zonguldak Basin, the Ulus Basin is described as a single unit: the Ulus formation. It starts at the bottom with coarse clastic rocks and grades rapidly into turbiditic sandstones and shales. In the eastern part of the Ulus Basin the flysch deposits are poor in fossils, indicating an Early Cretaceous age [34]. This group is a 200–1300 m thick sequence of grey to black marls, shales, claystone, siltstone and sandstone intercalations. Its clastic nature contrasts with the underlying grey to white limestone [35].

The geological units of the Ulus formation are not reliably dated. Locally, foraminifera of Early Cretaceous age was found by [35]. This stratigraphic perspective considers an Aptian–Cenomanian age for the overlying clastic Ulus formation. The Ulus formation is overlain, with a slight angular unconformity, by red to pinkish, thinly bedded pelagic limestones, with volcanoclastic intercalations in its upper part. The age of the clastic sequence in the Ulus basin, is older than along the Black Sea coast. However, the geodynamic significance of the age of onset of detritic sedimentation in this basin is not as clear as along the Black Sea coast. Effectively, in this basin, large normal faults could not be observed as along the Black Sea coast [33].

Moreover, there are conspicuous compressional structures with intensity of deformation increasing toward the south and the east that is toward the accreted highpressure–low-temperature complexes of the Early Cretaceous subduction zone [36]. According to the studies realized in the Ulus Basin, the Ulus formation representing a typical flysch sequence which is highly susceptible to weathering [37, 38].

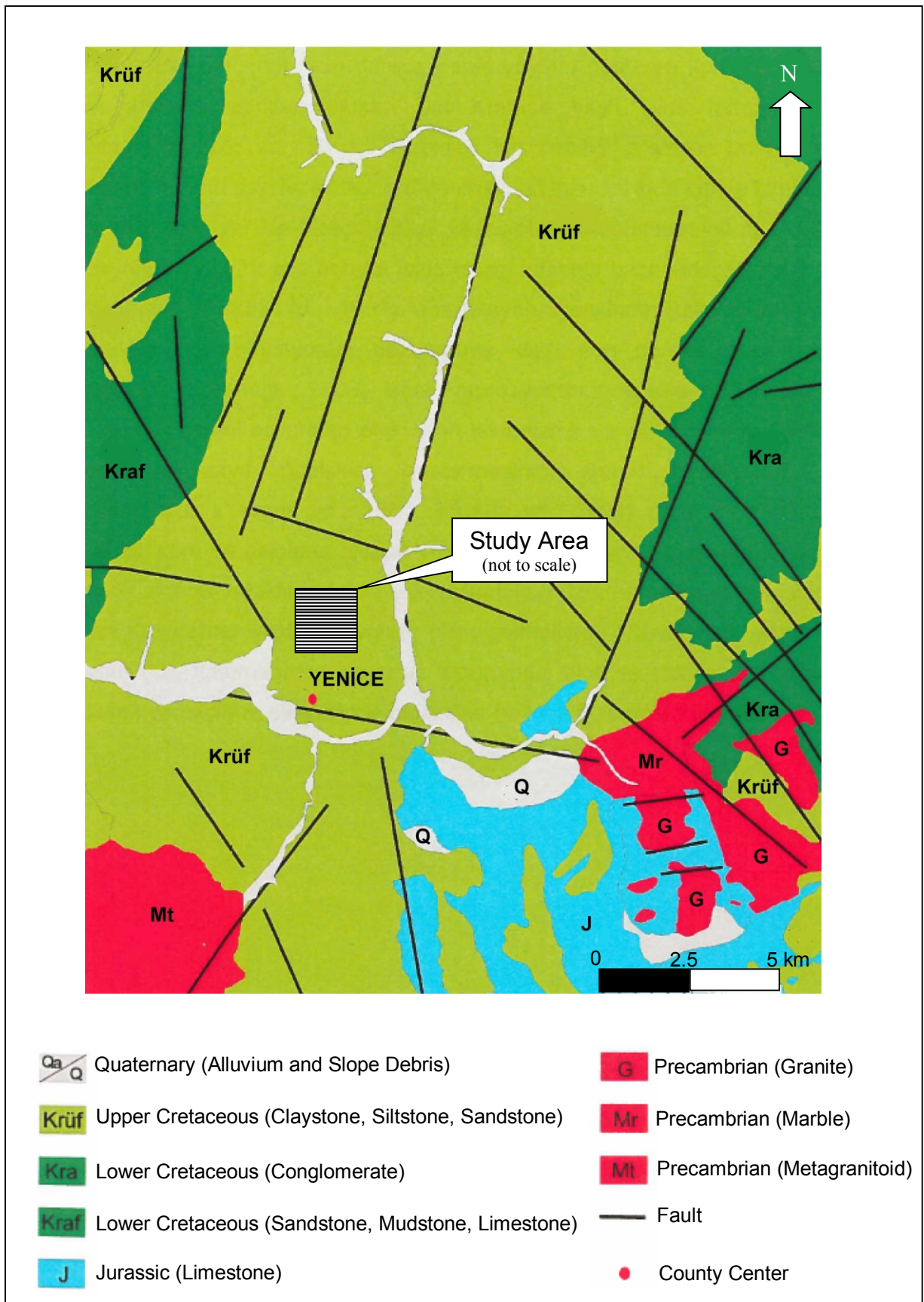


Figure 2.3: Geological map of the study area and its near environ, from Yergök et al. [39]

2.2 SEISMICITY of STUDY AREA

Anatolia is under influence of two major tectonic factors, namely North Anatolian Fault Zone and East Anatolian Fault Zone. The study area is adjacent to the North Anatolian Fault Zone (45km north of North Anatolian Fault). Study area and near environ is located in the first degree earthquake zone, according to “Earthquake Zonation Map of Turkey” published by Ministry of Public Works and Settlement in 1996 (Fig. 2.4).

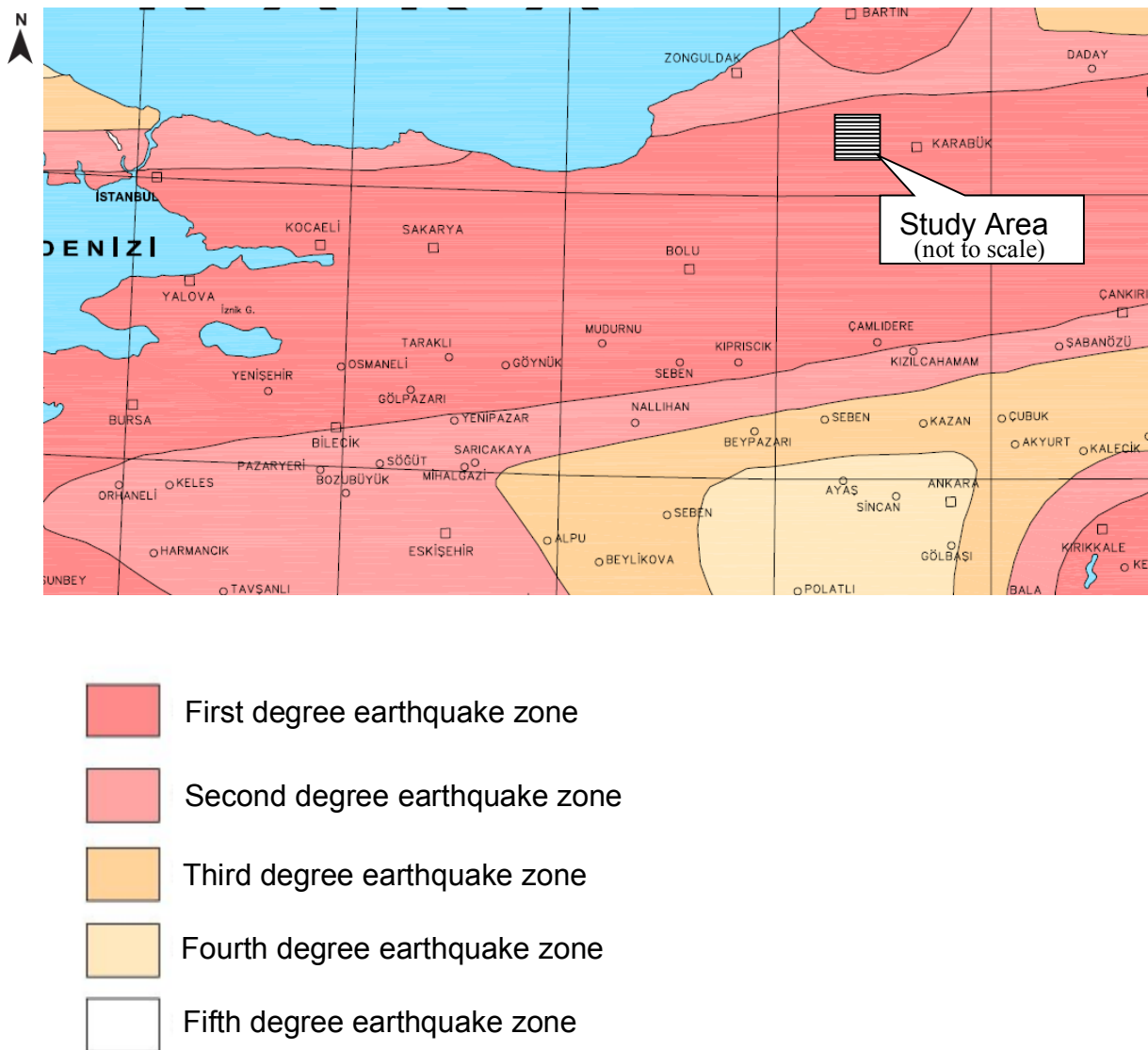


Fig. 2.4: Earthquake zonation map of Turkey [40]

According to the active fault and earthquake location map of Turkey published by Republic of Turkey Prime Ministry, Disaster and Emergency Management Presidency [41], no historical earthquake is recorded in the study area. However, due to the distance to North Anatolian Fault Zone the near environ of the study area is exposed to earthquakes (Fig. 2.5).

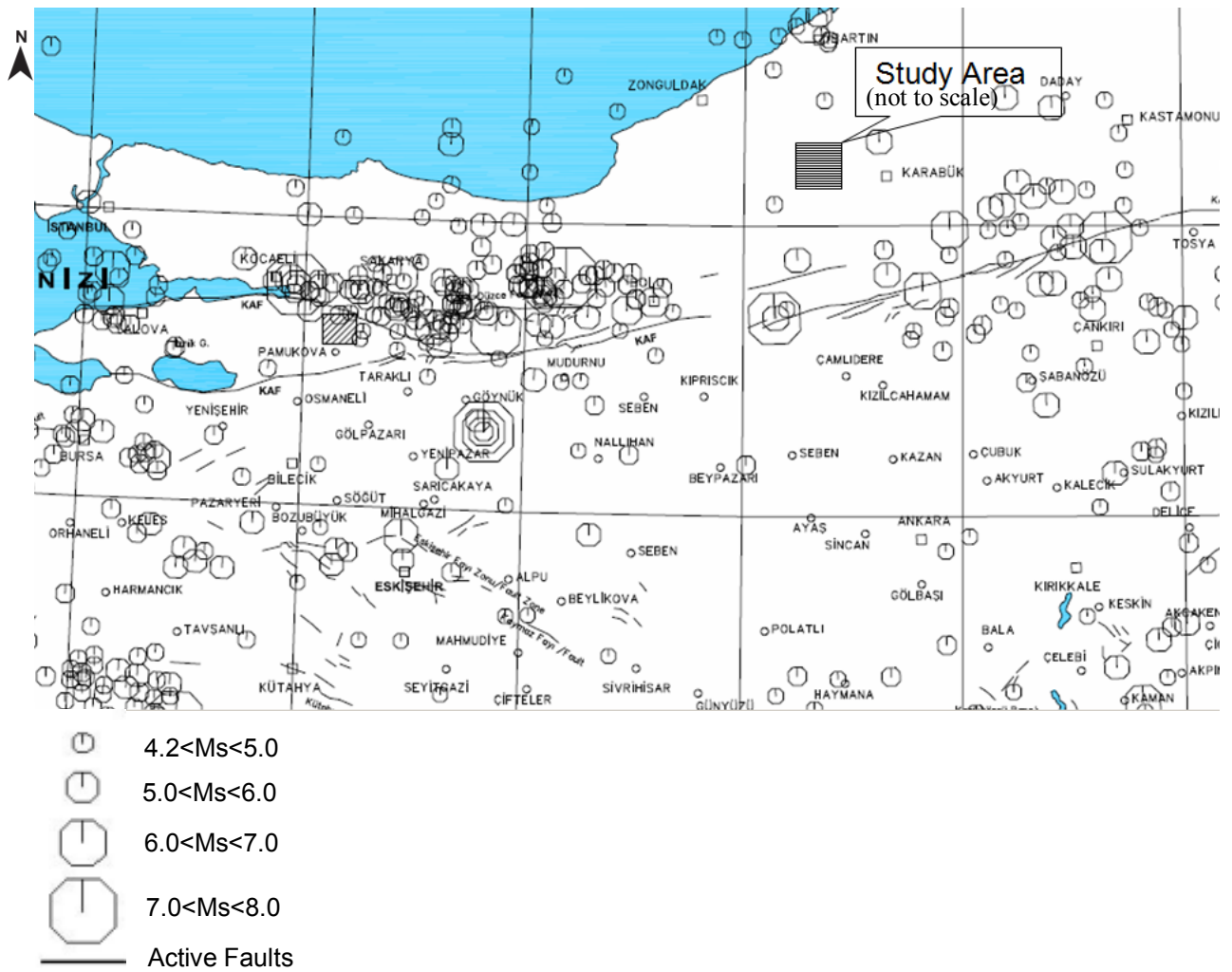


Fig. 2.5: Active fault and earthquake epicentre location map of Turkey [41]

3. PREVIOUS STUDIES

3.1 LANDSLIDE STUDIES and DEFINITIONS

Landsliding is a natural process that includes a wide range of ground movements under certain geological conditions. Landslides do not necessarily involve sliding as most people think [42]. The “landslide” concept may be defined as a wide variety of processes involving downward and outward movement of a part of slope- forming materials including soil, rock, artificial fill, or a combination of these along a plane of failure, caused due to shear failure along this plane [43]. The materials may move by falling, toppling, sliding, spreading, flowing or combination of them [43, 44].

The actual literature analysis shows that researchers do not agree on a univocal landslide classification. Classification of landslides were studied by many researchers such as Ladd [45], Sharpe [46], Campbell [47], Varnes [43, 48], Crozier [49], Wieczorek [50], Cruden and Varnes [44] and Hungr et al. [51]. However, the most widely used classification system today, is the one proposed by Varnes [43, 48]. Different parameters utilized by Varnes [43, 48] for the classification of landslides are as follows:

- Type of material: Rock, debris and earth are the terms which usually utilized for the classification of landslide process
- Type of movement: Clarification of landslide mechanism is generally used to identify the movement type as fall, topple, slide, spread, and flow.

In addition to the parameters utilized by Varnes [43, 48], following parameters can be considered for the classification of landslides.

- Rate of movement: Based on the site observations and case history type of landslide and hazard evaluation can be determined. The rate of movement is usually classified as; slow (mm/y), moderate (m/hr), rapid (m/sec)

- Water condition: water condition is an important parameter for landslide classification. This effect can be observed as intense rainfall, snowmelt, and change in groundwater level and saturation degree of soil.

- Triggering mechanisms: Triggering can be defined as the effect which initiate an action. Triggering mechanism for landsliding are identified as rainfall, earthquake, and human activities. But, a landslide can be triggered by any temporal factor.

On the other hand, state of activity represents the activity of a landslide particularly related by the evaluation of future events. According to Hungr et al. [51], a landslide can be classified based on the state of activity as active, inactive, dormant, and stabilized, etc.

Varnes classification [43] is the most widely accepted classification of landslides, as modified by Cruden and Varnes [44] (Table 3.1 and Figure 3.1) [52]. Type of material and type of movement are the basis of this classification.

Table 3.1 Classification of different types of landslides in different parent materials [43, 48].

Type of movement	Types of material		
	Bed rock	Engineering Soil	
		Predominantly coarse	Predominantly fine
Falls	Rock fall	Debris fall	Earth fall
Topples	Rock topples	Debris topples	Earth topples
Slides:			
Rotational	Rock slump	Debris slump	Earth slump
Translational	Rock slide	Debris slide	Earth slide
Lateral Spreads	Rock spread	Debris spread	Earth spread
Flows	Rock flow	Debris flow	Earth flow
Complex	Combination of two or more types of mass movement		

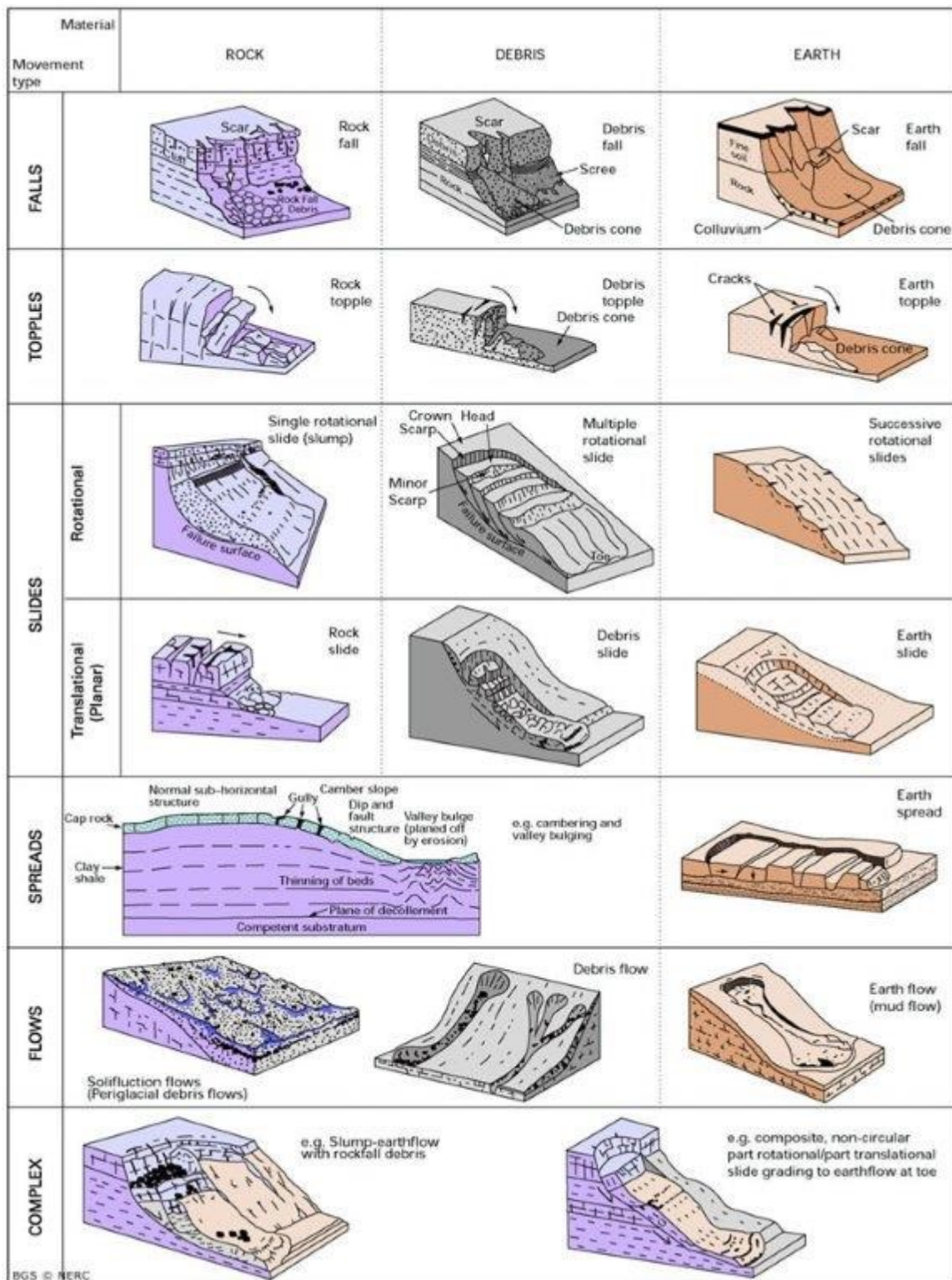


Figure 3.1: Types of landslides, modified after Varnes [43] and Cruden and Varnes [44]. [52].

3.1.1 Causes and Triggering Factors of Landslides

Landsliding starts when the stability of the subjected slope changes from a stable to an unstable condition under many causal factors [53]. Causes of landslide are the factors which transform the slope susceptible to failure. Landslide causal factors can be subdivided temporal causal factors and spatial causal factors. But, the triggering factor is the single event which initiate the landslide. In other words, causal factor prepare the conditions to make a slope susceptible to failure, and the triggering factor initiates the movement. However, there is a fine border between triggering factor and temporal causal factor. All triggering factors can be considered as a temporal causal factor but any spatial causal factor can never be a triggering factor. In addition, landslide can have many causes but can only have one triggering factor. Because of this, determining the exact triggering factor is not always easy due to the complexities of landsliding processes.

Different researchers such as Varnes [43, 54], Hoek and Bray [55], Cruden and Varnes [44] and Sidle and Ochiai [56] had pointed out the general potential causes of landslide. The major factors that contributed directly or indirectly to the occurrence of landslides can be listed as follows [53]:

(1) Natural Causes:

a) Geological causes:

- Weak or sensitive materials (spatial causal factor)
- Weathered materials (spatial causal factor)
- Sheared, jointed or fissured materials (spatial causal factor)
- Adversely oriented discontinuity (bedding, schistosity, fault, unconformity, contact and so forth) (spatial causal factor)
- Variation of permeability (spatial causal factor)
- Stiffness of materials (spatial causal factor)

b) Morphological causes:

- Tectonic uplift (temporal causal factor)
- Glacial rebound (temporal causal factor)
- Fluvial, wave or glacial erosion of slope toe or lateral margins (temporal causal factor)
- Subterranean erosion (temporal causal factor)

- Deposition loading slope or its crest (temporal causal factor)
- Vegetation removal by fire or drought (temporal causal factor)

(2) Physical causes

- Intense rainfall (temporal causal factor)
- Rapid snowmelt (temporal causal factor)
- Prolonged exceptional precipitation (temporal causal factor)
- Rapid drawdown of floods (temporal causal factor)
- Earthquake (temporal causal factor)
- Thawing (temporal causal factor)
- Freeze-and-thaw weathering (temporal causal factor)
- Shrink-and-swell weathering (temporal causal factor)
- Flooding (temporal causal factor)
- Saturation excess runoff (temporal causal factor)

(3) Anthropogenic causes (human activities)

- Excavation of slope or its toe (temporal causal factor)
- External loading (temporal causal factor)
- Drawdown and filling of reservoirs (temporal causal factor)
- Deforestation (temporal causal factor)
- Irrigation (temporal causal factor)
- Mining activities (temporal causal factor)
- Artificial vibration or dynamic loads (temporal causal factor)
- Water leakage from utilities (temporal causal factor)
- Diversion of river current (temporal causal factor)
- Use of unstable earth fills, for construction (temporal causal factor).

The landslide causing factors for the Derebaşı Landslide in Yenice Watershed can be summarized as follows:

3.1.2 Triggering and Causal Factors of The Derebaşı Landslide

The most profound natural cause affecting the Derebaşı landslide is geology. The Yenice Watershed, which embodies the Derebaşı landslide, is covered by Upper Cretaceous Ulus formation. The Ulus formation represents a typical flysch

sequence which is highly susceptible to weathering [57, 38]. Although the term flysch refers to “rock material”, the landslides in the study area occur within the weathering zone of flysch layers. In other words, landslides in the region occur in the zone of soil type material [2]. Occurrence of landslides frequently in Ulus formation for the studies in Western Black Sea Region is underlined by Ercanoğlu [15]. The change of grain size distribution along the landslide is a primary observation during detailed site observations. From crest to toe of the Derebaşı landslide, the proportion of fine material increases. The change of material size along the Derebaşı Landslide area can be explained from the sedimentation processes of the different layers of flysch material and its weathering products. Accordingly, the change in hydraulic conductivity and the variation of water flux along the slope affect the landsliding. Considering the change in hydraulic conductivity, Derebaşı Landslide starts from the crown as earthflow due to the saturation excess runoff processes. The topographic parameters such as slope, aspect and elevation are important factors for the Derebaşı landslide. All these parameters are preparative for saturation degree variations which initiate the landsliding.

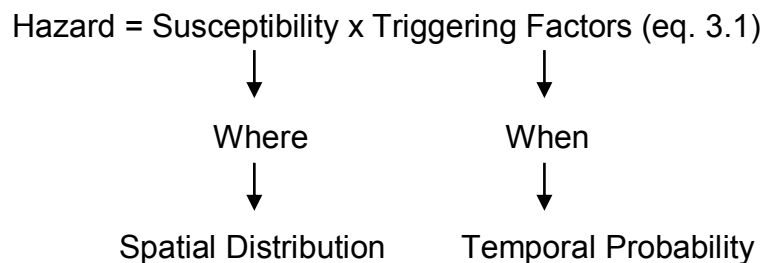
The earthquake records gathered from the Boğaziçi University Kandilli Observatory and Earthquake Research Institute shows that during the occurrence date of the Derebaşı landslide no significant seismic activity was recorded in radii of 50km, 100km and 300km (Appendix 1). So, the Derebaşı landslide should not have been triggered by earthquake. Furthermore, no mining activities which can trigger the landslide exist in and near environ of the Yenice Watershed. The only triggering factor can be the “water effect” which can initiate the landsliding. Therefore, in the present study the effect of water will be qualitatively and quantitatively studied to enlighten the effect of the saturation degree in the context of landslide susceptibility.

3.1.3 Landslide Susceptibility Studies and Basic Concepts

Conventional landslide susceptibility can be defined as likelihood of a landslide occurring in an area on the basis of local terrain conditions. In other words, landslide susceptibility is a relative spatial likelihood for the occurrence of landslides of a particular type and volume as indicated by Van Westen [4]. Landslide susceptibility usually involves preparing a landslide inventory together with an

assessment of the areas with a potential to experience landsliding in the future, but with no assessment of the frequency of the occurrence of landslides [58].

Landslide hazard is defined as the probability of occurrence of a particular landslide type (initiation and run out, volume, speed) within a specified period of time and in a given area. Landslide hazard defined by Guzzetti et al. [6] as the probability of occurrence in a specified period and within a given area of a potentially damaging landslide of a given magnitude. Landslide risk is expected losses (monetary, or in number of buildings and/or people) due to specific landslide type initiation and run out, volume, speed) within a specified period of time and in a given area [4]. Van Westen et.al. [4] explained the relation between landslide susceptibility, landslide hazard and landslide risk as follow;



However, in some studies triggering factors are involved to susceptibility concept in terms of spatio-temporal distribution [59, 60, 61, 62]. The present study integrates the effect of water as saturation degree into the landslide susceptibility concept within the context of spatio-temporal perspective.

All the available methods used for landslide susceptibility and hazard zonation are based upon some widely accepted principles or assumptions [6, 54, 63, 64, 65, 66], as indicated below;

- According to Varnes [54], the past and present are keys to the future. The past and the present landslides indicate the preparative conditions for the landsliding in the future such as geological, geomorphological, hydrogeological and climatic conditions. In this way, the landslide types, frequency of occurrence, landslide susceptibility zonation can be estimated for the future.

- The main conditions that cause landslides are identifiable [54]. The causal factors can be mapped and classified through field surveys and remote sensing image interpretations [43, 67].
- Degrees of hazard can be estimated when the causes and factors that trigger landslides are identified, it is often possible to measure degrees of hazard [54].
- Landslide occurrence, in space or time, can be derived from heuristic investigations, computed through the analysis of environmental information or inferred from physical models. Therefore, a region can be zoned into different susceptible and hazard classes ranked according to different probabilities [6].

Different methods have been applied by different researchers for the landslide assessment and hazard. Overviews of the different landslide susceptibility mapping are given by Varnes [54], Carrara et al. [11], Hutchinson [64], Aleotti and Chowdhury [5], Guzzetti et al. [6], Gorsevski et al. [60]. Literature reviews made out that landslide susceptibility approaches can be analysed into 2 groups as qualitative or quantitative, and direct or indirect.

Qualitative methods are subjective and based entirely on the judgment of the expert carrying out the susceptibility or hazard assessment [5]. Quantitative methods are objective ways of producing numerical estimates, i.e. probabilities of the occurrence of landslide phenomena in any susceptibility and hazard zone [6].

In direct mapping methods, existing landslides and/or specifically known potential landslide areas are identified. The aerial photographs [68] and satellite images [67] can be utilized for direct mapping method.

In indirect mapping methods, landslide causal factors, are used to predict the potential landslide areas. Indirect methods utilize large amount of parameters and statistical or deterministic analysis of all these possible contributing factors in relation to the occurrence of landsliding phenomena, determining in this way the relation between the terrain conditions and the occurrence of landslides [4].

According to Guzzetti et al. [6], the required steps for indirect mapping methods can be summarized as follows;

- 1) Recognition and mapping of landslides over a target region or a subset obtained by preparing a landslide inventory map.
- 2) Identification and mapping of the physical factors, which are directly or indirectly correlated with slope instability.
- 3) Estimate of the relative contribution of the instability factors in generating slope failures.
- 4) Classification of the land surface into domains of different levels of susceptibility
- 5) Assessment of the model performance.

The well-known approaches utilized in the literature can be grouped into six categories [5, 6, 64]:

(1) Direct geomorphological mapping

Direct geomorphological mapping of landslide susceptibility is a relative determination of the spatial variability of existing or potential landslide areas based on the engineering judgement. This method is based on the ability of the expert to evaluate the reliable information. Disadvantages of this approach is summarized by Leroi [69] as follow;

- Comparison of the landslide susceptibility zonation maps prepared by different experts can vary due to the subjectivity of the decision rules.
- Updating the landslide susceptibility map is not always easy when a new data becomes available.
- Extensive field surveys should be realized.

(2) Analysis of landslide inventories

The simplest technique of landslide mapping is the landslide inventory [6]. Collection of aerial photographs, satellite imagery and site observations realized to map the existing or potential landslides by use of GPS. Landslide inventory maps provide the characterization of each landslide, degree of activity and its size. Due to lack of historical database in most places of the world, these maps provide no insight into temporal changes in landslide distribution and provide information of landslides for a short period of time [70].

(3) Heuristic methods

In heuristic methods, weighting of each causal factor used in landslide susceptibility mapping, is specified by the expert. This subjective perspective of the method depends on the expert's knowledge about the site properties and landsliding dynamics in terms of geomorphological process upon the study area [6]. The method for landslide susceptibility mapping involves a number of steps listed as following [70]:

- a) Selection and mapping of the causative factors
- b) Preparation of thematic data layer with relevant categories of the factors
- c) Assignment of weights and ratings to factors and their categories, respectively
- d) Integration of thematic data layers
- e) Preparation of landslide susceptibility map showing different zones.

This method became popular due to its convenience [71]. The weights may vary from expert to expert and also from region to region. Some techniques were developed to make the analysis more objective for weight assignment procedure of each landslide causal factor.

Analytical Hierarchy Process (AHP) developed by [72] is a Multi-Criteria Decision Making tool which converts subjective assessments of relative importance to a set of overall scores or weights. Ayalew et al. [73] used AHP method to obtain the relative weights of landslide controlling factors, and used GIS to prepare landslide hazard assessment map. Hasekioğulları [74] used the AHP method for assessing landslide susceptibility in Western Black Sea Region.

(4) Statistical methods

Statistical methods have been adapted to landslide susceptibility concept for minimizing the uncertainties in weight assignment procedure. These are indirect and quantitative methods in which the functional relationships between instability factors, and the past and present distribution of slope failures are described [6]. Two types of statistical methods, namely bivariate and multivariate methods are utilized for the landslide susceptibility studies. In bivariate analyses, the core of the analysis is to get the densities of landslide occurrence within each parameter map's classes and to get the data driven weights based on the class distribution and the landslide density [75]. Different researchers have proposed different bivariate methods, such as: general instability index [76], frequency index [77], surface percentage index

[78], information value method [79] statistical index method [80], weighting factor [81], frequency ratio [82], and landslide susceptibility analysis [83].

Multivariate statistical methods consider the relation between a dependent variable and several independent variables that might affect the probability of the searched situation [75]. Frequently used techniques in multivariate methods are: multiple linear regression ([84, 85, 86], discriminant analysis ([87, 88, 89], and logistic regression ([90, 91, 92]. Principal component analysis (PCA) is also used to reduce the number of variables and to limit their interdependence when many factors are available [93]. According to Wang et al. [94], the limitations of multivariate statistical technique are listed as follows:

- 1) Discriminant and regression analyses require data derived from a normally distributed population that is frequently violated.
- 2) A mixture of continuous (i.e. slope, aspect, elevation, distance from drainage, distance from lineaments, etc.) and categorical (i.e. geology, land use, soil type, etc.) factors may lead to incorrect results.
- 3) Some of the factors may have a weak physical relationship with landslide occurrences. Combination of such factors with other factors may generate data, which is very difficult to interpret, unreliable and sometimes meaningless.

(5) Fuzzy logic and artificial neural networks

To achieve limitations of the qualitative and quantitative methods, fuzzy logic, neural networks, or their combination have been adapted to the landslide susceptibility concept. To determine the relationship between the causal factor and the landslide occurrence fuzzy set theory [95, 17] is utilized.

According to Garrett [96], an artificial neural network (ANN) is a computational mechanism able to acquire, represent and compute a mapping from multivariate space of information to another given set of data representing that mapping.

An intelligent hybrid system known as “Fuzzy neural network” is formed with the combination of fuzzy logic and ANN. The main stages of this combined hybrid system are listed as follow by [97]:

- 1- Determination of weights of thematic layers through ANN connection-weight approach
- 2- Determination of ratings for categories of thematic layers

- 3- Integration of ratings and weights using GIS to obtain a landslide susceptibility map.

(6) Physically based modelling

Physical models are based on physical laws of conservation of mass, energy or momentum. This approach is more deterministic and the parameter employed are generally determined in the field or in the laboratory. These models (mono-, bi- and tri-dimensional) are commonly used in soil engineering for slope-specific stability studies [5]. The parameters utilized for the calculation of slope stability are normal stress, angle of internal friction, cohesion, pore water pressure, external weights, etc. A factor of safety defined as the ratio of resisting forces to driving forces is most commonly calculated to quantify the degree of stability of a simple soil mass [55].

Some popular deterministic models for slope stability are:

- A GIS based conceptual model named as Distributed Shallow Landslide Analysis Model (DSLAM) has been developed for the analysis of shallow rapid landslides at catchment scale by Wu and Siddle [98]. This model includes; infinite slope stability analysis, continuous temporal changes in root cohesion and vegetation surcharges, and stochastic influence of actual rainfall patterns on pore water pressures [99].
- The infinite slope model which is based on the limit equilibrium approach is frequently used to analyse the stability of shallow landslides [62]. This model considers the slope inclination is constant for an unlimited and uniform slope extension. This model has been used by Ray et al [62] to enlighten the impact of soil moisture on slope stability.
- Hammond et al. [100] introduce the Level I Stability Analysis (LISA) for U.S. Forest Service]. This model utilizes the Monte Carlo simulation technique for the estimation for the probability of slope failure.
- SHALSTAB was developed to predict the probable locations of shallow landslide, based on the infinite slope concept, considering the slope angle, drainage area, and degree of concentration of water from upslope stability [101]. SHALSTAB is

employed by Gorsevski et al. [60] for a spatially and temporally distributed landslide susceptibility study.

3.2 GEOLOGICAL STUDIES IN YENICE and NEAR ENVIRON

Yenice and its near environ is interested by many researchers in terms of geological studies [2, 14, 17, 18, 32, 67, 102, 103, 104, 105, 106, 107, 108].

Güner [102] determines the geomorphological map and the geomorphological features of Filyos Valley in Northern Anatolia furnished some critical data to better understand Quaternary development of Northern Anatolia. The investigations of numerous river terraces performed by Güner [102] leads to the conclusion that the study area suffered severe epeirogenic movements during Quaternary.

Koçyiğit [103] determines the stratigraphic nature of the Karabük – Safranbolu Tertiary basin. With regards to the findings of Koçyiğit [103], Karabük – Safranbolu basin is NE-SW oriented and funnel shaped. In its southwest section, both northern and southern margins of the basin are tectonic in character, and therefore, much narrower. The northwestern margin of basin displays diverse characteristics such as thrust fault, overturned fold and angular unconformity. In the Karabük region, sediments of this basin are shallow marine deposits of Lower Lutetian age and fluvial deposits. The present shape of basin has been formed at the end of Upper Lutetian; it has characteristics of an intermontane basin. Since the Upper Pliocene time, it might have been uplifted at least twice [103].

Okay [104] analysed the geology of Pontides in three tectonic units (İstanbul Zone, Istranca Massif and Intra Pontide Suture) juxtaposed in Mid. to Late Mesozoic times. According to findings of Okay [104] about the western part of Intra Pontide Suture, the reactivation time correspond to Late Cretaceous. Pelagic limestones, serpentinite and blueschist of probable Late Cretaceous age also occur as fault slivers in southern part.

Ercanoğlu and Gökçeoğlu [14] worked on the assessment of landslide susceptibility study in and near Yenice by performing fuzzy approach. Ercanoğlu and Gökçeoğlu [14] utilized the fuzzy logic approach to satisfy the lack of uncertainties of the available methods for regional landslide susceptibility assessments. As a result of this study, the performance of the fuzzy approach

appear to be satisfactory comparing with the conventional landslide susceptibility methods [14].

Biryol [105] studied Eskipazar tectonic basin located approximately 25 km east of Yenice. According to Biryol [105] Eskipazar Basin is 3-5 km wide, 10 km long and NW-SE trending depression bounding by a complex array of oblique-slip normal faults and strike-slip faults as a part of North Anatolian Fault System and the basin fill is composed of two different units deposited under the control of different tectonic regimes, namely the paleotectonic and the neotectonic regimes. The Eskipazar formation constituted from poorly consolidated fluviolacustrine deposits are susceptible to landsliding and triggered nearby the active faults within the basin [105].

Ercanoğlu et al. [18] realized the landslide susceptibility zoning with performing the multivariate statistical techniques in north of Yenice which embodies Yenice Watershed. The study area of this work [18] is covered completely by the Ulus formation that has a flysch character. Ercanoğlu et al. [18] determined the importance weights of the conditioning factors contributing to landsliding by multivariate statistical techniques and index maps for each factors. As a result landslide susceptibility map is obtained by overlying all factors taking into consideration with their weights.

Ercanoğlu and Gökçeoğlu [17] employed fuzzy set theory to determine the relationship between landslide occurrence and responsible causative factors for the north of Yenice including Yenice Watershed. Ercanoğlu and Gökçeoğlu [17] developed a computer program (FULLSA) which utilizes the fuzzy relations and procedures, and produces the landslide susceptibility map automatically to analyse the landslide inventory and parameter maps together. The approach employed by Ercanoğlu and Gökçeoğlu [17] mainly prevents the subjectivity sourced from the parameter selection and provides a support to improve the landslide susceptibility mapping studies.

Tüysüz et al. [32] analysed the lithostratigraphic units of the Western Black Sea Region. According to Tüysüz et al. [32] Upper Cretaceous aged Ulus formation is defined as flysch and observed frequently in the Western Black Sea and this unit is formed by claystone, sandstone, siltstone and marl intercalations.

Ercanoğlu [2] determined landslide susceptibility by artificial neural networks approximately 30 km southwest of Yenice Watershed. Slope angle, slope aspect,

topographical elevation, topographical shape, wetness index, and vegetation index were utilized as input parameters and statistical index values were used to express the parameter effects on landslide occurrence. Then, landslide susceptibility analyses were performed using artificial neural networks approach [2].

Kuterdem [106] studied for the identification of some surface features within the North Anatolian Fault Zone for the area between Eskipazar and North Anatolian Fault Zone. In the morphotectonic study of Kuterdem [106], various landforms related to right lateral strike slip faults such as offset streams, pressure ridges, etc. were observed in the study area and recognized from Landsat ETM+ satellite data and relief maps.

Akın [107] studied in investigation of deterioration of Eskipazar (Karabük) travertines which is a highly preferred rock type in building stone market due to its physical properties such as colour and texture besides its easy process.

Alkeveli [67] investigated the usage of the ASTER (Advanced Spaceborne Thermal Emission and Reflection Radiometer) satellite data on landslide inventory mapping for Yenice and Gökçebey. Based on the analyses, it was revealed that the best approach related to landslide inventory mapping was found as stereoscopic image analysis. However, according to findings of Alkeveli [67] ASTER satellite image can be used in regional and medium scale landslide inventory studies as a result of testing DEM (Digital Elevation Model) obtained from the ASTER image.

Yılmaz et al. [20] realized a landslide susceptibility study using bivariate statistical analysis for Devrek (Zonguldak-Turkey) quite close to Yenice. In this study three different approaches in seed cell concept such as (1) crowns and flanks, (2) only crowns, (3) only flanks of the landslides were considered for the evaluation and comparison of the resulting landslide susceptibility maps obtained from use of bivariate statistical index.

Within the context of Tefen Hydroelectric Power Plant Project which is located 7.5 km southwest of Yenice Watershed, Tefen Dam axis, reservoir area and natural structure materials resources has been investigated by Suyapı [108]. In this study [108], stratigraphy, tectonic setting, seismicity have been mentioned and the results of in-situ and laboratory tests interpreted in terms of engineering geology.

3.3 SMDR STUDIES

Soil Moisture Distribution and Routing (SMDR) model is utilized by many researchers for watershed modelling as a variable source area concept. [109, 110, 111, 112, 113, 114, 115, 116].

Veith et al. [109] examined the hydrologic response of an agricultural watershed (FD 36) in the Appalachian Valley and Ridge physiographic region by three computer simulation models. Areal Nonpoint Source Watershed Environmental Response Simulation (ANSWERS2000), Soil and Water Assessment Tool (AVSWAT2000), and Soil Moisture Distribution and Routing (SMDR) – were used to simulate the surface hydrologic processes by Veith et al. [109]. As a result of this study [109], annual surface runoff was mapped with three different hydrologic model and compared.

According to Marchant et al. [110], successful implementation of the best management practices for reducing non-point source (NPS) pollution requires knowledge of the locations of saturated areas that produce runoff. In this study [110], SMDR model was used to simulate runoff production on a 164 ha farm watershed in Delaware County, New York, in the headwaters of New York City water supply. The validation of SMDR model is verified by comparing the detailed records of runoff at the watershed outlet and the SMDR simulation results. As a conclusion, the results of the SMDR model simulated by Marchant et al. [110] found satisfactory considering the minimal calibration.

Easton et al. [111] simulated hydrologic processes in an urban upstate New York watershed by considering the impact of impervious surfaces, hydraulic control structures (detention basins) and land use on the water balance by modification of the SMDR model. SMDR model is adapted for an urban watershed to predict areas of the landscape prone to elevated soil moisture levels and saturation excess runoff. Then validation of the variable source model is tested by comparing the modelled and measured runoff amounts [111].

Alwis et al. [112] studied on the description of a methodology to determine the spatial variability of saturated areas using a temporal sequence of remotely sensed images. The derived maps which show the runoff producing locations by saturation excess processes on hydrologically active areas were validated by comparison with two distributed hydrologic simulation models developed for

watersheds such as Town Brook specifically, SMDR model and VSFL model [112]. The results of the validation have shown the remotely sensed data to adequately represent the spatial distribution of saturated areas for most land covers in the watershed. According to Alwis et al. [112], this technique of delineating saturated areas shows promise for many applications requiring knowledge of HAAs, such as hydrologic modelling, land use planning, zoning, or implementing management practices to reduce pollution.

Campos et al. [113] studied on a joint implementation of spatially distributed runoff and soil erosion analysis in watersheds allowing subsequent modelling of nutrients transport processes originating from distributed sources. For this purpose, Campos et al. [113] presented a distributed application for modelling the hydrological cycle of a watershed (using the SMDR model), computing the soil erosion products (with the USLE implementation) and obtaining a nutrient creation and transportation model (combining both outputs). This application is already running with real data from the Itoiz location to better understand the ecological cycles in which this nutrients take part.

Rao et al. [114] studied on the reducing loss of sediments and nutrients in agricultural areas in terms of nonpoint source pollution determining with saturation excess processes from variable source area concept in Catskill Mountain Watershed New York. In this context, saturation probability map is prepared by SMDR model [114].

Frey et al. [115] studied on herbicide losses which diffuse to surface waters often originate from a limited part of a catchment called as critical source area. The predictability of critical source areas tested by Frey et al. [115] with a modified version of SMDR in a small agricultural catchment in Switzerland, in which herbicide losses to surface waters had been experimentally investigated. SMDR which is slightly modified the code to incorporate drainage flow and the effects of sink areas in a simple way is utilized as a fully distributed hydrological model with the objective to identify the location and the spatio-temporal dynamics of areas contributing to fast-flow processes. In conclusion, causing factors for spatial heterogeneity of runoff formation is analysed within the context of diffuse herbicide losses.

Frey et al. [116] used a distributed hydrological model to simulate the distribution of fast runoff formation as a proxy for critical source areas for herbicide pollution in a small agricultural catchment in Switzerland. SMDR model is utilized for

critical source areas prediction and the prediction degree is tested based on prior knowledge without local measurements improved upon relying on observed discharge by Frey et al. [116].

4. ANALYSIS AND DEVELOPMENT OF METHODOLOGY

Within the context of this doctoral research the water effect on landslide susceptibility in terms of spatio-temporal variations of the water content will be studied, and a new parameter on this issue will be attempted to be integrated as a new parameter that has been integrated to the landslide susceptibility concept.

For this purpose, to understand the relationship between the water effect and the landslide susceptibility, a new methodology will be introduced using the SMDR technique and conventional landslide susceptibility analyses.

For this purpose, the following specific steps are set:

- 1) Desk Studies
- 2) Field Studies
- 3) Laboratory Studies
- 4) Parameterisation of SMDR Model,
- 5) Frequency Ratio Analysis in Terms of Landslide Susceptibility

4.1 DESK STUDIES

The desk study stage included the collection and processing of available data. During this stage, relevant documents and maps were identified, collected and studied to obtain preliminary information on landslides. The visual interpretations such as computer-based digital image processing methods were used for the preliminary field reconnaissance. This stage comprised the following main sub-activities:

- Collection and compilation of data (topographic maps, vegetation map, meteorological data etc.) and literature review;
- Selection of a landslide of known date
- Finding of a suitable model for the simulation of soil moisture distribution
- Analysis of meteorological data;
- Pre-consultation with key personnel to clarify the triggering mechanism of Derebaşı Landslide.

In this context;

- 1) Landslide reports prepared by “Republic of Turkey Prime Ministry Disaster and Emergency Management Presidency [41]” were obtained. In these reports only the Derebaşı landslide’s occurrence date was mentioned.
- 2) Daily meteorological data prepared by the “General Directorate of Meteorological Service of Turkey [29]” for Yenice Station between the years 1989-2009 were obtained. These data were utilized for “Soil Moisture Distribution and Routing” model for the next stages of this study. Monthly mean meteorological data between the years 1989-2009 including monthly precipitation, mean temperature and monthly potential evapotranspiration (PET) are given in Table 4.1.

Table 4.1: Mean Meteorological Data (1989-2009) [29]

	Precipitation (mm)	Mean Temperature (C°)	PET (mm)
January	44.2	4.8	0
February	41.8	5.6	0
March	40.4	8.7	0
April	49.2	12.7	96
May	42.9	16.6	144
June	56.9	20.6	144
July	27.6	23.5	207
August	37.2	23.5	135
September	35.0	19.1	84
October	49.5	14.9	42
November	57.8	8.8	0
December	50.8	5.4	0

- 3) The vegetation characteristics map and vegetation characteristics parameters were collected from the “Directorate of Yenice Regional Forestry [28]”. These data were also utilized for SMDR model for the next stages of this study.

4.2 FIELD STUDIES

Within the context of field studies, soil sampling, in situ soil strength surveying with pocket penetrometer based on the standard described in ASTM WK27337 [117] and soil type mapping based on field observations were performed. As a first stage, preliminary field observation was realized in Yenice Watershed. The variation of soil type in Yenice Watershed was mapped based on the field observation, and the soil

sampling strategy was specified. Then soil sampling operation was performed considering the conservation of soil moisture between the dates 03.08.2013-08.08.2013. During the field studies, it was observed that, for the top elevations of the landslide area, sand size material is abundant, while lower elevations the finer material increases. Subject to availability, the soil samples were taken from the depths varying between 50cm and 100cm below the vegetable soil thickness, then the strength of the soil profile is determined by pocket penetrometer in accordance with the standards described in ASTM WK27337 [117] (Fig. 4.1).



Figure 4.1: Determination of soil strength with pocket penetrometer and soil sampling in plastic bag

The results of pocket penetrometer test are given in Table 4.2.

Table 4.2: Pocket penetrometer test results

Sample No	Pocket Penetrometer Test Results (kg/cm ²)
TN-1	1.50
TN-2	1.50
TN-3	1.75
TN-4	1.25
TN-5	2.25
TN-6	2.00
TN-7	1.50
TN-8	2.50
TN-9	1.00
TN-10	1.00

Based on the information obtained from “Republic of Turkey Prime Ministry Disaster and Emergency Management Presidency” [118] the occurrence date of Derebaşı landslide was the first week of June 2000. This information is cross-checked from the local people discourses and village headman recording protocol and the date was recorded as 5 June 2000. The report in concern, indicated that the type of the landslide is morphologically determined as rotational (Fig. 4.2)

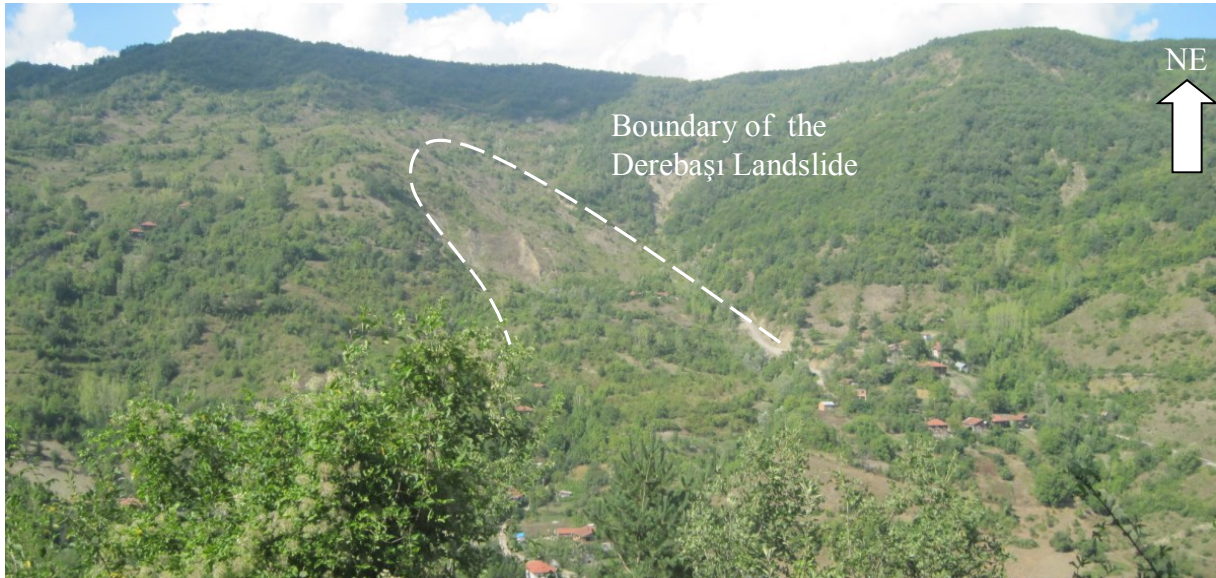


Figure 4.2: General view of Derebaşı landslide (Towards NE)

4.3 LABORATORY STUDIES

For the determination of soil hydraulic properties, ten soil samples were collected from the study area (see Fig. 4.3) and put in plastic bags (named as TN) to preserve the in-situ moisture content. Specific gravity (G_s), moisture content (w), organic matter content (OMC), grain size distribution, Atterberg limits and coefficient of hydraulic conductivity values of the samples were collected in the soil mechanics and hydrogeology laboratories of Geological Engineering Department of Hacettepe University. The soil class of each soil sample was specified by Unified Soil Classification System with grain size distribution and Atterberg limits. Additionally, soil samples were classified using with the classification system proposed by Rawls et al. [119] and Rawls and Brakensiek [120]. In this way, the index textural properties (residual water content, porosity, wilting point, field capacity etc.) of each soil class were determined.

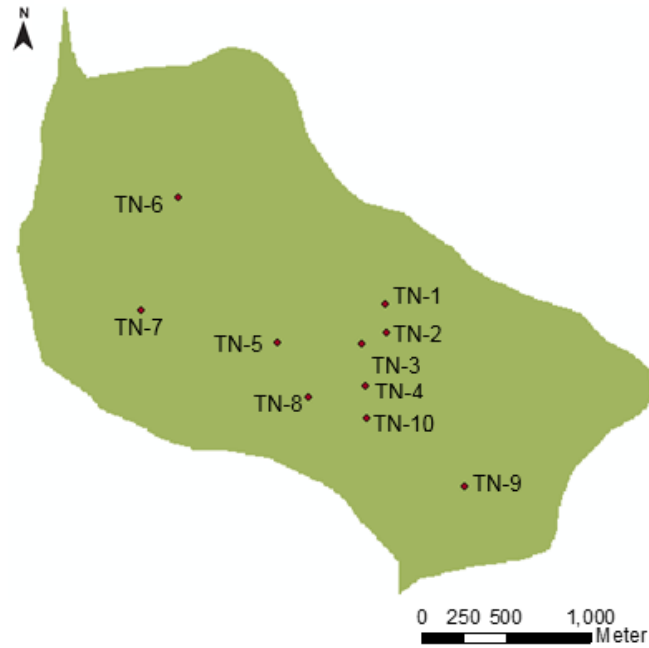


Figure 4.3: Sample location map

In order to be more representative more soil samples could be collected, but due to the apeak topography of the study area only 10 soil sample could be taken.

4.3.1 Specific Gravity Test

Specific gravity was obtained by pycnometer test based on the standard proposed by ASTM [121] for the material grain size smaller than 4.75mm. Three tests were performed per each soil sample, then the average was calculated as ASTM [121] indicates. The specific gravity test results are given in Table 4.3.

Table 4.3: Specific gravity test results

Sample No	Gs
TN-1	2.47
TN-2	2.38
TN-3	2.45
TN-4	2.38
TN-5	2.48
TN-6	2.37
TN-7	2.35
TN-8	2.50
TN-9	2.55
TN-10	2.45

4.3.2 Moisture Content Test

The moisture content tests were performed based on the standard proposed by ASTM [122]. For the moisture content test also, three tests were realized per each soil sample then the average was calculated as ASTM [122] indicates. Test results of the moisture content tests by mass are given in Table 4.4

Table 4.4: Moisture content by mass test results

Sample No	w (%)
TN-1	4.80
TN-2	16.85
TN-3	10.31
TN-4	14.67
TN-5	7.92
TN-6	13.87
TN-7	17.04
TN-8	17.33
TN-9	9.81
TN-10	13.04

4.3.3 Organic Matter Content Test

Organic matter content (by mass) tests were performed based on the standard proposed by ASTM [123] in the coal laboratory of Hacettepe University Geological Engineering Department. For the organic matter content (OMC) determination, three tests were realized per each soil sample. The average of the test results was calculated as ASTM [123] indicates. The organic matter content test results are given in Table 4.5.

Table 4.5: Test results of organic matter content by mass

Sample No	OMC (‰)
TN-1	5.3
TN-2	4.1
TN-3	6.6
TN-4	4.7
TN-5	5.5
TN-6	4.3
TN-7	5.7
TN-8	5.0
TN-9	6.7
TN-10	6.6

4.3.4 Determination of Grain Size Distribution

The grain size distribution of the soil samples were carried out by hydrometer analysis for fine grained material, and sieve analysis for coarse grained material, proposed by ASTM [124]. The grain size distribution curves for the analysed soils are shown in Figure 4.4. In this figure, it can be observed that fine grained material is dominant in general. But, the samples TN-3 and TN-6 contain more sand than other samples.

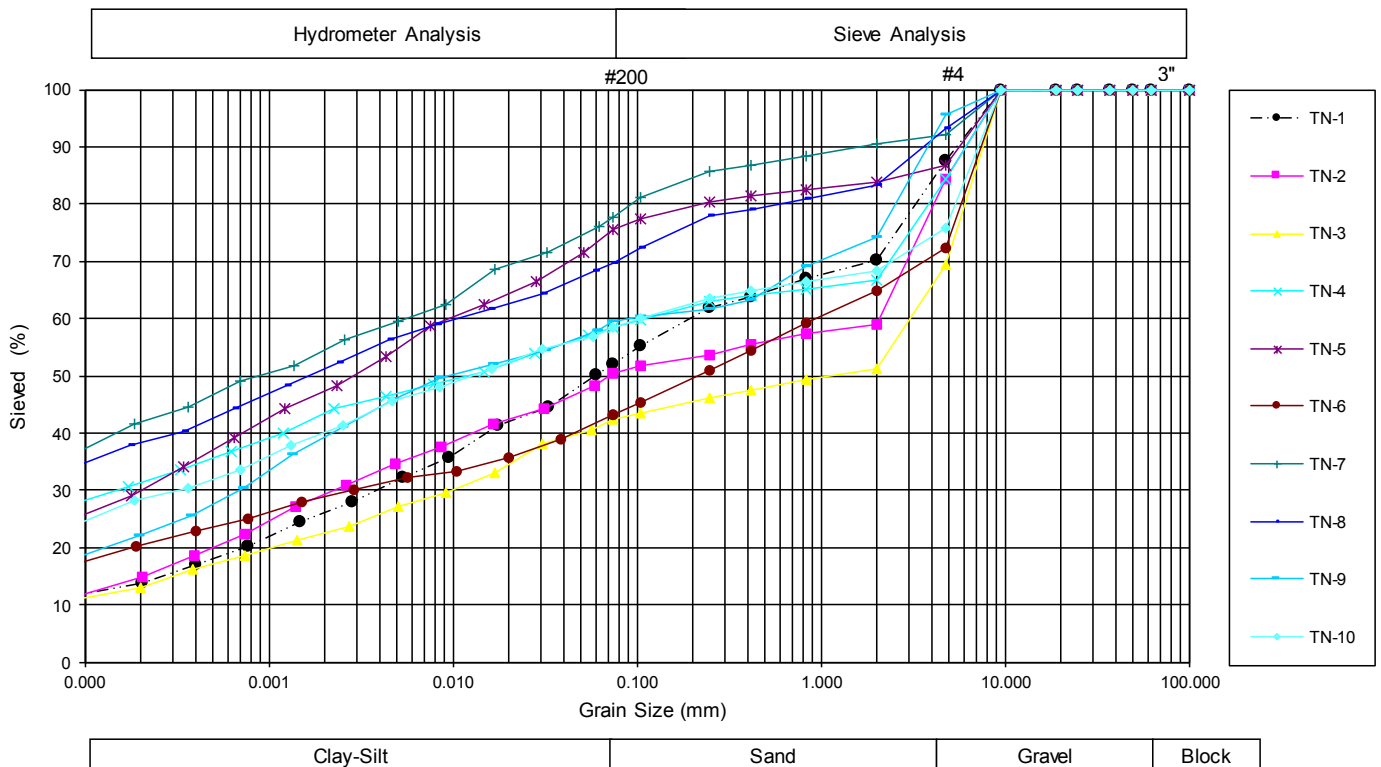


Figure 4.4: The grain size distributions of the soil samples

4.3.5 Determination of Atterberg Limits

Determination of the liquid limit, plastic limit and plasticity index values was realized based on the standard proposed by ASTM [125] and the shrinkage limit was determined as proposed by ASTM [125]. The results of the tests in concern are given in Table 4.6.

Table 4.6: Atterberg limits of the soil samples

	Liquid Limit	Plastic Limit	Plasticity Index	Shrinkage Limit
TN-1	37.86	23.73	14.13	15.32
TN-2	43.82	25.59	18.22	19.74
TN-3	47.23	27.47	19.77	22.19
TN-4	47.36	26.37	20.99	22.65
TN-5	39.47	26.82	12.66	15.62
TN-6	41.37	27.50	13.87	25.06
TN-7	44.36	27.99	16.37	13.51
TN-8	48.37	26.67	21.70	35.76
TN-9	37.32	22.87	14.45	12.33
TN-10	42.47	28.85	13.61	21.80

4.3.6 Soil Classification

After determining the grain size distribution and the Atterberg Limits, the soil class of each sample was specified according to the Unified Soil Classification System. Gravel, sand, silt and clay percentages and the soil class of each soil sample taken from the study area are shown on Table 4.7.

Table 4.7: Soil classes (USCS) and percentages of gravel, sand, silt, clay

	TN-1	TN-2	TN-3	TN-4	TN-5	TN-6	TN-7	TN-8	TN-9	TN-10
Soil Class (USCS)	CL	CL	GC	CL	ML	SC	ML	CL	CL	ML
Gravel (%)	12.49	15.55	30.59	15.69	13.19	27.80	7.78	6.86	4.36	24.25
Sand (%)	35.58	34.11	27.06	25.87	11.16	28.89	14.53	23.42	36.05	17.30
Silt (%)	27.40	23.31	21.19	18.46	31.33	15.27	25.84	21.51	23.35	20.54
Clay (%)	24.53	27.03	21.16	39.98	44.32	28.04	51.85	48.21	36.24	37.90
Clay + Silt (%)	51.93	50.34	42.35	60.36	75.65	43.31	77.69	69.72	59.59	58.45

To compose the soil characteristics table which is the most important input data for the hydrodynamic components of SMDR model, each soil sample was classified according to USDA (United States Department of Agriculture) soil texture classification system [126]. This method is suggested by the Soil and Water Laboratory [26] also. Textural classification of the soil samples by USDA soil texture classification system is represented on a ternary diagram (Fig 4.5).

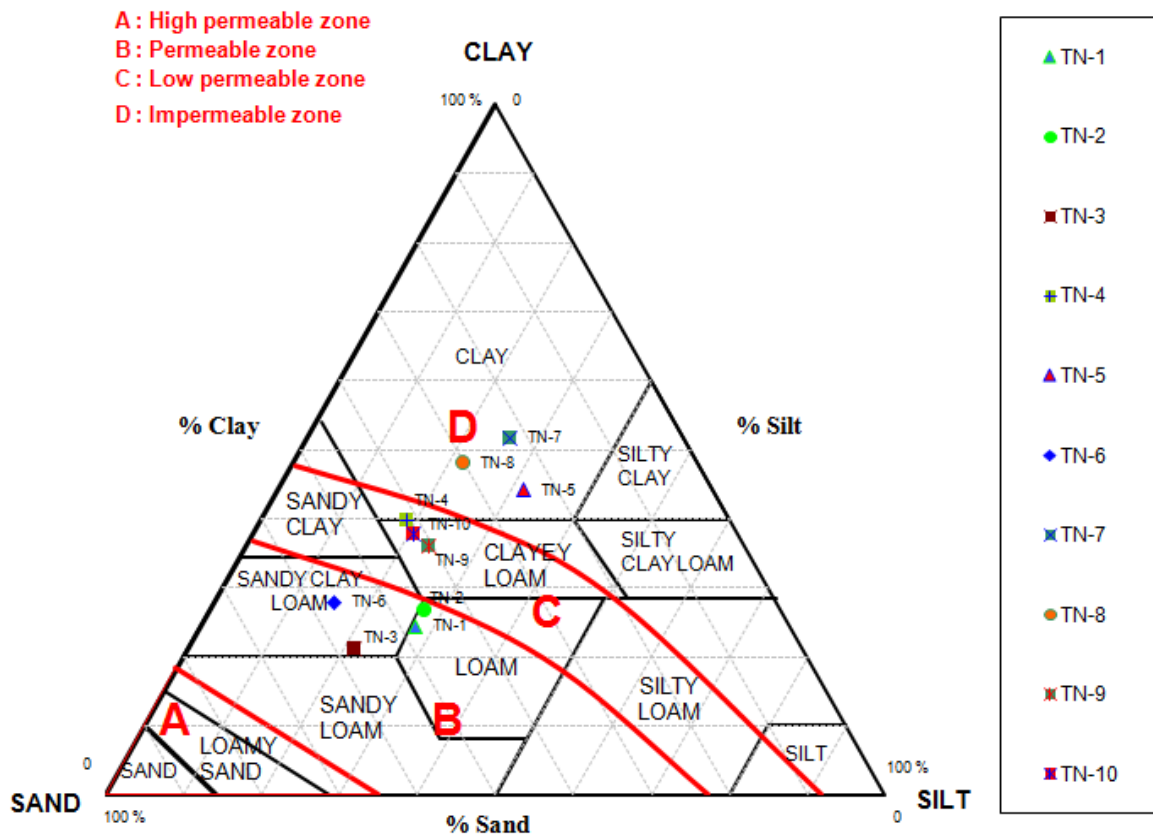


Figure 4.5: Textural classification of the soil samples in the study area according to USDA soil texture classification system [126].

According to USDA soil texture classification system, the soil samples taken from the study area are represented by 4 different soil classes. TN-7, TN-8 and TN-5 are represented as "clay", TN-4, TN-9 and TN-10 are represented as "clayey loam", TN-6 and TN-3 are represented as "sandy clayey loam", TN-1 and TN-2 are represented as "loam" textural class.

The parameters required for the soil characteristics table of SMDR model are, porosity, residual water content, wilting point, available water capacity, field capacity, water content at saturation, maximum available water content, potential evapotranspiration limit, macroporal drainage limit, coefficient of vertical hydraulic conductivity and coefficient of horizontal hydraulic conductivity. The explanations of these terms will be given in detail in Chapter 4.4.2. The soil characteristics table is determined by "the hydrologic soil properties index table based on the soil texture" proposed by Rawls et al. [119]. The parameters of this table is utilized as soil characteristics table for SMDR model and shown on Table 4.8.

Table 4.8: Hydrologic soil properties index table based on soil texture [119]

Textural Class	Porosity (cm ³ /cm ³)	Residual Water Content (%)	Wilting Point (%)	Field Capacity (%)	Water Content at Saturation (%)	Max. Available Water Content (%)	Ksat Vertical (mm/d)
Clayey Loam	46.4	7.5	19.7	31.8	39	31.5	48
Clay	47.5	9	27.2	39.6	38.5	29.5	14.4
Sandy Clayey Loam	39.8	6.8	14.8	25.5	33	26.2	72
Loam	46.3	2.7	11.7	27	43.4	40.7	316.8

4.3.7 Determination of Hydraulic Conductivity

To determine the coefficient of hydraulic conductivity of the soil samples taken from the study area, falling head permeability tests have been performed in the Geo-Hydrology Laboratory of Hacettepe University Geological Engineering Department. With these laboratory tests, the hydrologic soil properties index table based on the soil texture proposed by Rawls et al. [119] has also been verified in terms of hydraulic conductivity. The soil samples in the permeameter cell were compacted (with an equipment including compactor and mold) until the in-situ strength value determined by the pocket penetrometer to reflect the in-situ compactness of the soil samples for the permeameter test. Determination of soil compactness and the testing apparatus is shown in Figure 4.6.



Figure 4.6: Testing apparatus and determination of compactness

The determination of hydraulic conductivity is performed based on the standard proposed by ASTM [127] using the equation below.

$$K = 2.3x \frac{r_t^2 \cdot L}{r_o^2 \cdot t} x \log \frac{h_1}{h_2} \quad (\text{Eq.4.1})$$

where;

K : Coefficient of hydraulic conductivity (m/s)

r_t^2 : Manometer radius (cm²)

r_o^2 : Radius of soil sample (cm²)

L : Length of soil sample (cm)

h_1 : Hydraulic head loss at t_1 (cm)

h_2 : Hydraulic head loss at t_2 (cm)

t : Time difference between the records of h_1 ve h_2 (s).

The comparison of the hydraulic conductivity values, determined by the laboratory tests and proposed by Rawls et al. [119] is shown in Figure 4.7.

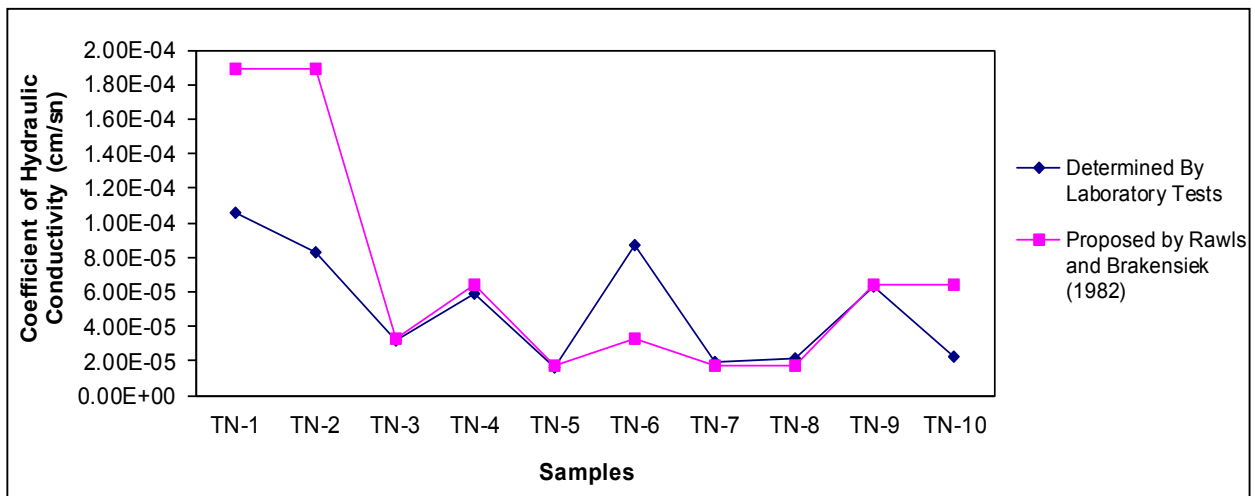


Figure 4.7: Comparison of the hydraulic conductivity values for the soils in the study area determined by laboratory tests and proposed by Rawls et al. [119]

Figure 4.7 shows that hydraulic conductivity test results of soil samples TN-3, TN-4, TN-5, TN-7, TN-8 and TN-9 are compatible with the hydraulic conductivity proposed by Rawls et al. [119]. However, in USDA soil texture ternary diagram, the soil samples TN-1 and TN-2 are located between the borderline of “loam” and “sandy loam” and the soil sample TN-10 is located near the “clay” borderline. The

hydraulic conductivity values determined by laboratory tests and proposed by Rawls et al. [119] for the soil samples TN-1, TN-2 and TN-10 are not compatible due to their location on the ternary diagram. However, the coefficient of correlation between the laboratory values and proposed values are determined as 0.76. Therefore, it is seen that the hydrologic properties of the soil samples mentioned in Table 4.8 proposed by Rawls et al. [119] based on the soil texture should be utilizable for the SMDR model. In this table only hydraulic conductivity values could be determined from the samples collected in the field. Other data were used as advised by Rawls et al. [119].

4.4 STRUCTURE of SMDR MODEL and ITS PARAMETRISATION

The SMDR model, executed for the reflection of the rainfall runoff process on landslide susceptibility concept in “Derebaşı landslide” is considered as a suitable model, since it represents a fully spatially distributed model based on the saturation excess runoff generation phenomenon.

4.4.1 Structure of the SMDR Model

SMDR model is a fully distributed hydrological model based on the variable source area concept, which simulates spatio-temporal soil moisture variations in a watershed. Variable source area is the concept that simulates the runoff generation locations in a watershed, varying spatially and temporally. Variable source areas are not stable, they appear in various locations and amounts depending on rainfall, temperature, topography, and vegetation within other factors. Owing to its modular structure, SMDR model can be utilized for several purposes and several watersheds.

According to Soil and Water Laboratory [26], SMDR model works on the following assumptions:

- 1- Gravity is the driving force of water movement.
- 2- For lateral flow, the hydraulic gradient can be approximated by the local slope.

- 3- The equilibrium moisture profile is uniform below the calculated water content and can be represented by Richards equation [128] (described in the following sections) above this water content.
- 4- The top soil overlies a shallow layer that can be qualified either as bedrock or restricting layer.
- 5- Water percolating through this shallow layer fills up a lumped linear subsurface reservoir. This last assumption is required due to the lack of actual knowledge about the geometry of fractures in and below the bounding layer. The linear reservoir approach assumes that a given constant percentage of the deep groundwater volume generates stream baseflow.
- 6- Surface runoff is primarily generated from areas in excess of water saturation.
- 7- Precipitation occurring on impervious areas does not infiltrate, but is added to an infiltration excess storage.
- 8- Surface runoff does not re-infiltrate and reaches the watershed outlet during “unit time”.

First three assumptions mentioned above, result in neglecting capillarity as a driving force [26].

SMDR model is a fully spatially distributed model where the soil hydrodynamic properties are defined at each point of the region for each defined time range [26]. Therefore, it does not require extensive calibration and is designed to use data that are readily available in electronic form [110]. In SMDR model the relevant watershed is divided into small cells which are representing the geological, topographical and soil hydrodynamic properties homogenously. For this reason, the smaller cell sizes increase the accuracy of the model. Nevertheless, it has been underlined that for the cell based models like SMDR, increasing the grid size resolution misrepresented the landscape curvature and increased simulated soil water contents [129].

4.4.1.1 Working Principle of SMDR Model

In SMDR model the vertical water movement is realized along the defined functional layers. It is assumed that three functional layers exist for each cell of the watershed. These functional layers are;

- 1) Evapotranspiration zone
- 2) Transmission zone
- 3) Underlying bounding layer

In SMDR model the evapotranspiration zone can be defined with the root zone of the dominant vegetative cover. If there is not efficient vegetative activity on site, the top 8 cm (3 inches) can be assumed as evapotranspiration zone and the size of the transmission zone depends on the root depth as well as on the depth to the bounding layer [26].

The cell based SMDR model is working based on the water mass balance calculations in the relevant watershed for each cell. For the daily water mass balance calculation of each cell inputs and outputs are listed below (see Figure 4.8):

Water inputs;

1. Daily precipitation
2. Lateral inflow from surrounding upslope cells

Water outputs;

1. Lateral outflow to surrounding downslope cells
2. Percolation
3. Evapotranspiration

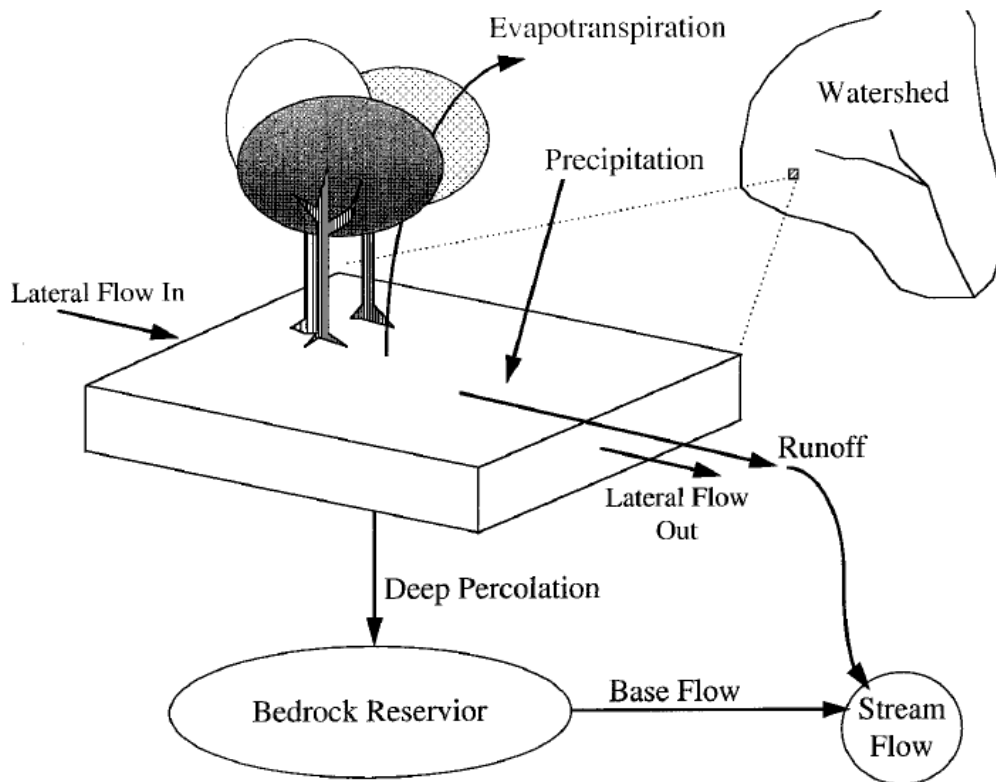


Figure 4.8: Conceptual model of water balance processes [130]

The saturation excess water is considered as runoff at the end of the selected time step (eg: day). In conclusion the water mass balance can be expressed as follows:

$$W^2 |\theta(t) - \theta(t - \Delta t)| = |RF(t) + SM(t)| + Qi(t) - Qo(t) - ET(t) - P(t) - SE(t) \quad (\text{eq.4.2})$$

Where;

W : Grid size (square) (m),

θ : Cell average water content ($\text{m}^3 \cdot \text{m}^{-3}$),

Δt : Time step (d),

RF : Rainfall volume (m^3)

SM : Snowmelt volume (m^3)

Qi : Volume of water received through lateral flow from surrounding upslope cells,

Qo : Volume of water lost through lateral flow to surrounding downslope cells,

ET : Volume of water lost by evapotranspiration,

P : Volume of water lost by percolation

SE: Saturation excess runoff.

For this equation the thickness of the soil is considered as 1m. Volumes are expressed in (m³)

4.4.1.2 Main Components of SMDR Model

SMDR model consists of 5 main components;

- Meteorological Components
 - Rainfall
 - Snowmelt
- Drainage Component
- Evapotranspiration Component
- Lateral Flow Component
- Percolation Component

4.4.1.2.1 Meteorological Components

The meteorological components utilized in water mass balance of SMDR model are rainfall and snowmelt. These components are calculated by daily average total precipitation and daily average temperature for each cell.

The effect of local topographic variations on daily average temperature is reflected in the model by the equation below (eq.4.3):

$$T_i = T_{ref} - 0.00637 (H_i - H_{ref}) \quad (\text{Eq. 4.3})$$

Where;

T_i : Local temperature of cell "i" (°C)

T_{ref} : Daily average temperature measured at reference point (°C)

H_i : Elevation of cell "i" (m)

H_{ref} : Reference elevation (m)

4.4.1.2.1.a Rainfall

In SMDR model the total precipitation is considered as rainfall and snowfall depending on local temperature. If the T_i temperature calculated by the equation 4.3, is above snowfall-rainfall limit which is defined by user (0°C is selected for this

study), precipitation is considered as rain. Otherwise, the precipitation is considered as snow. This consideration of the model can be expressed as follows (eq. 4.4, eq. 4.5 and eq.4.6);

$$\text{If, } T_i(t) > T_{s/r} \quad \longrightarrow \quad RF_i(t) = TP(t) \quad (\text{eq. 4.4})$$

$$\text{If, } T_i(t) \leq T_{s/r} \quad \longrightarrow \quad RF_i(t) = 0 \quad (\text{eq. 4.5})$$

and

$$SF_i(t) = TP(t) - RF_i(t) \quad (\text{eq. 4.6})$$

Where;

$T_i(t)$: Local temperature of cell "i" at time "t" (°C)

$T_{s/r}$: Snowfall – Rainfall limit (°C)

$RF_i(t)$: Rainfall of cell "i" at time "t" (mm)

$TP(t)$: Total precipitation at time "t" (mm)

$SF_i(t)$: Snowfall of cell "i" at time "t" (mm)

4.4.1.2.1.b Snowmelt

In SMDR model potential snowmelt is calculated as follows (eq. 4.7, eq. 4.8 and eq. 4.9);

$$\text{If, } T_i(t) > T_{SM} \quad \longrightarrow \quad SM_{pot;i}(t) = (m_i T_i + k_i) \Delta t \quad (\text{eq. 4.7})$$

$$\text{If, } T_i(t) \leq T_{SM} \quad \longrightarrow \quad SM_{pot;i}(t) = 0 \quad (\text{eq. 4.8})$$

Where;

$T_i(t)$: Local temperature of cell "i" at time "t" (°C)

T_{SM} : Temperature of snowmelt (°C)

$SM_{pot;i}(t)$: Potential snowmelt of cell "i" at time "t" (mm)

m_i : Snowmelt factor of cell "i" (mm. °C⁻¹ day⁻¹)

k_i : Snowmelt constant of cell "i" (mm.day⁻¹)

Δt : Time difference (day)

In equations 4.7 and 4.8 "m" and "k" depend on the vegetative cover: "m" is 2.3 mm. °C⁻¹ day⁻¹ in forested areas and 2.7 mm. °C⁻¹ day⁻¹ in non-forested areas and "k" is 0 mm.day⁻¹ in forested areas and 12.2 mm.day⁻¹ in non-forested areas [131].

In conclusion, snow amount existing on each cell (SC) is updated as follows (eq. 4.9);

$$SC = SF - SM_{pot} \quad (\text{eq. 4.9})$$

4.4.1.2.2 Drainage Component

Drainage component of SMDR model represents the vertical water flux for related cell. This vertical water movement in unsaturated zone of soil is calculated by the Richards [128] equation. Richards [128] equation is a differential equation which defines the water movement in unsaturated zone of soil integrating with the Darcy's [132] law and continuity equation [133]. In conclusion, the water movement in the unsaturated zone of soil is determined by the Richards [128] equation based on the water content conditions of soil profile.

Additionally, for the drainage through the macropores and cracks, macropore drainage limit (θ_{md}) is specified in SMDR model. Macropore drainage limit is defined as minimum water content below which the larger pores are not drained [26]. Below θ_{md} , drainage occurs only through the soil matrix and will be referred to as "matric" drainage. Because of the large difference of time scales of these phenomena, the 'matric' drainage can be neglected as long as the 'macropore' drainage takes place [26].

The continuity equation expressing the conservation of the water mass in a representative elementary volume of soil can be written as follows (eq. 4.10);

$$\frac{\partial \theta}{\partial t} = \frac{\partial q}{\partial z} \quad (\text{eq. 4.10})$$

Where;

θ : Volumetric water content of soil ($\text{m}^3 \cdot \text{m}^{-3}$)

t : Time (day)

q : Flow velocity ($\text{m} \cdot \text{day}^{-1}$)

z : Depth (m)

Flow velocity within the continuity equation is expressed as follows (eq. 4.11);

$$q = K(\theta) \frac{\partial H}{\partial z} \quad (\text{eq. 4.11})$$

Where;

$K(\theta)$: Hydraulic conductivity as a function of soil water content ($\text{m} \cdot \text{day}^{-1}$)

H : Hydraulic head (m)

On the other hand, Darcy's [132] law is valid under homogenous, isotropic and saturated porous media. Darcy's equation represents the flow rate under a specific hydraulic head, in a saturated porous medium which has a specific hydraulic conductivity. In contrast, the Richards [128] equation is an expression of the flow rate in a unsaturated porous medium. However, coefficient of hydraulic conductivity indicated in the Richards [128] equation vary as a function of volumetric soil water content [135].

Richards [128] equation derived by the combination of continuity equation of Darcy's law can be expressed as follows (eq. 4.12).

$$\frac{\partial \theta}{\partial t} = \frac{\partial}{\partial z} \left[K(\theta) \left(\frac{\partial h}{\partial z} - 1 \right) \right] \quad (\text{eq. 4.12})$$

The vertical water movement in a cell is only realized if the water content of soil reaches to the field capacity value. In conclusion, for the calculation of vertical water movement in SMDR model, the hydraulic conductivity as a function of water content is calculated using the equation (eq. 4.13) proposed by Bresler et al. [136].

$$K(\theta) = K_{\text{sat}} \cdot \exp \left(\alpha \frac{(\theta - \theta_{\text{sat}})}{(\theta_{\text{sat}} - \theta_r)} \right) \quad (\text{eq. 4.13})$$

Where;

K_{sat} : Saturated hydraulic conductivity (m.day⁻¹)

θ_{sat} : Volumetric water content at saturation (m³.m⁻³)

θ_r : Residual water content (m³.m⁻³)

α : Constant (proposed as 13 by the SMDR model) [26]

In this equation (eq. 4.13) proposed by Bresler et al. [136], volumetric water content at saturation (θ_{sat}) is considered as the effective soil porosity.

In conclusion, the hydraulic conductivity variations depending on the soil water content are determined by the "equation 4.13" proposed by Bresler et al. [136]. Then, the vertical flow velocity in unsaturated zone is determined by Richards [128] equation (eq. 4.13).

4.4.1.2.3 Evapotranspiration Component

Evapotranspiration is one of the water output parameter for water mass balance calculation of SMDR model. Transpiration and evaporation processes are integrated under this component and calculated for each cell.

The vertical distribution of soil water extraction rate is calculated by the empirical equation 4.14 proposed by Novak [137];

$$u(z) = \frac{E_{Ti}}{1 - \exp(-\omega)} \frac{\omega}{Z_A} \exp(-\omega / Z_A) \quad (\text{eq. 4.14})$$

Where;

$u(z)$: Root extraction rate at position z (m.day⁻¹)

E_{Ti} : Evapotranspiration rate (m.day⁻¹)

ω : Dimensionless coefficient

Z_A : Thickness of evapotranspiration zone (m)

In SMDR model the evapotranspiration is assumed to take place over a zone that corresponds to first 8 cm of each cell. Moreover, according to Novak [137] the dimensionless coefficient “ ω ” varies usually in a range 1-10 depending on the local vegetation density. The SMDR user manual documentation [26] indicates that in case of a lack of actual data the constant factor $\omega=5$ can be assumed for trees shrubs and crops. For this reason, the dimensionless coefficient in the equation 4.14 is assumed as $\omega=5$ due to the general vegetation type in Yenice Watershed based on the information acquired from Directorate of Yenice Regional Forestry (oral communication).

In SMDR model the variation of evapotranspiration rate based on the soil water content is expressed as follows (eq. 4.15, 4.16 and 4.17);

$$\text{If; } \theta < \theta_{wp} \quad E_{Ti} = 0 \quad (\text{eq. 4.15})$$

$$\text{If; } \theta_{wp} \leq \theta < \theta_{etl} \quad E_{Ti} = E_{TP-ref} \left(\frac{\theta - \theta_{wp}}{\theta_{etl} - \theta_{wp}} \right) \quad (\text{eq. 4.16})$$

$$\text{If; } \theta_{etl} \leq \theta \quad E_{Ti} = E_{TP-ref} \quad (\text{eq. 4.17})$$

Where;

E_{TP-ref} : Reference potential evapotranspiration rate (m.day⁻¹)

θ : Water content (m³.m⁻³)

θ_{wp} : Wilting point (m³.m⁻³)

θ_{etl} : Evapotranspiration limit (m³.m⁻³)

Within the context of evapotranspiration rate calculation, different methods are proposed by many researchers [138, 139, 140, 141 and 142]. These methods require knowledge of certain data such as relative humidity, wind speed, cloud cover, land cover albedo, emissivity coefficients, dew point temperature, and these data are not easily and readily available [26].

The reference potential evapotranspiration rate is determined by the Hargreaves [143] Method which considers the solar radiation (eq. 4.18).

$$E_{TP-ref} = 0.0023 \frac{R_a}{\lambda_H \rho_w} \sqrt{\delta_T} (T_{av} + 17.8) \quad (\text{eq. 4.18})$$

Where;

R_a : Solar Radiation (MJ.m⁻² day⁻¹)

δ_T : Difference between mean monthly maximum and mean monthly minimum temperatures (°C)

T_{av} : Daily average temperature (°C)

ρ_w : Density of water (kg.m⁻³)

λ_H : Latent heat of vaporization of water (MJ.kg⁻¹)

Hargreaves and Samani [143] proposed an equation for the calculation of latent heat of vaporization (eq. 4.19);

$$\lambda_H = 2.501 - 2.361 \cdot 10^{-3} \cdot T \quad (\text{eq. 4.19})$$

The calculation of the extra-terrestrial solar radiation received on a given day at a given latitude is expressed as follows (eq. 4.20);

$$R_a = \frac{1}{\pi} \gamma_{sc} d_r [\omega_s \sin(\phi) \sin(\delta) + \cos(\phi) \cos(\delta) \sin(\omega_s)] \quad (\text{eq. 4.20})$$

Where;

γ_{sc} : Solar constant (118.20 MJ.m⁻²gün⁻¹)

ω_s : Sunset hour angle (rad)

d_r : Relative distance between the earth and sun on a given day

ϕ : Latitude (rad)

δ : Angle between sunrays and the normal to the surface (rad)

d_r , δ and ω_s are calculated as follow (eq. 4.21, 4.22 and 4.23);

$$d_r = 1 + 0,033 \cos (2 \pi J/n_Y) \quad (\text{eq. 4.21})$$

Where;

J: Julian day number (e.g. January 2 = 2)

n_Y : Number of days of year Y

$$\delta = \frac{23.45\pi}{180} \sin\left(2\pi \frac{J - 80.75}{n_Y}\right) \quad (\text{eq. 4.22})$$

$$\omega_s = \arccos(-\tan(\phi)\tan(\delta)) \quad (\text{eq. 4.23})$$

4.4.1.2.4 Lateral Flow Component

In SMDR model the factor which controls the water transportation from upslope cells to downslope cells is the topographic situation of the interested watershed. To determine the flow direction, different approaches have been proposed by many researchers such as “D8” algorithm [144] “D ∞ ” algorithm [145], “Multi Flow Direction” algorithm [146].

D8 is a single direction algorithm which randomly assigns flow from the centre grid cell to one of its downslope neighbours with the probability proportional to slope [147]. In this flow direction algorithm, all of the water existing in the relevant cell is directed to one of its eight adjacent or diagonal neighbours with the steepest downward slope. Consideration of eight main direction for the D8 algorithm is an important limitation and disadvantage in terms of hydrological modelling, and therefore is not used by SMDR.

The water amount distributed from central cell to downslope cells with “multiple flow direction algorithm” [146] is realized by the expression as follows (eq. 4.25);

$$P_{ij} = \frac{(Z_i - Z_j)/L_j}{\sum_{j=1}^n [(Z_i - Z_j)/L_j]} \quad (\text{eq. 4.25})$$

P_{ij} : Water proportion transferred from cell “i” to cell “j”

Z_i and Z_j : Depths of the cells i and j

L_j : Distance from centre of the cell “i” to centre of the cell “j”

n : Number of neighbour cell situated downslope of cell “i”

The lateral outflow from each cell ($Q_{out\ i}$) is calculated by Darcy’s Law [132]. In this calculation the hydraulic gradient is considered as the local slope (eq. 4.26) [26].

$$Q_{out\ i} = w.K(\theta)_i.Di(dh/dL)_i \quad (\text{eq. 4.26})$$

Where;

w : Width of the cell (m)

$(dh/dL)_i$: The local slope of cell “i”

$K(\theta)_i$: Coefficient of hydraulic conductivity of cell “i”

In lateral flow component of SMDR model, the coefficient of hydraulic conductivity which varies as a function of volumetric water content is calculated as follows (eq. 4.27 and 4.28);

$$\text{If; } \theta_{sat} \geq \theta_i > \theta_{fc} \quad K(\theta)_i = (K_{sat} - K(\theta_{fc,i})) \left(\frac{\theta_i - \theta_{fc,i}}{\theta_{sat} - \theta_{fc,i}} \right) + K(\theta_{fc,i}) \quad (\text{eq. 4.27})$$

$$\text{If; } \theta_i < \theta_{fc} \quad K(\theta)_i = K_{sat} \exp \left(\alpha \frac{(\theta - \theta_{sat})}{(\theta_{sat} - \theta_r)} \right) \quad (\text{eq. 4.28})$$

4.4.1.2.5 Percolation Component

When a cell becomes saturated, the percolation component accounted for, and the vertical water movement to the reservoir realizes. For this component Darcy's Law [132] is valid because activation of percolation component take place under saturated soil condition. In this case, vertical hydraulic conductivity is utilized.

4.4.2 Input Data of SMDR Model and Data Production

The operation of SMDR model requires the input data within two basic formats, "raster maps" and "lookup tables".

These input data can be expressed in 4 main categories;

- 1) Topographic data
- 2) Geographic data
- 3) Agronomic data
- 4) Meteorological data

4.4.2.1 Raster Maps

5 types of raster maps are utilized by SMDR model, of which 3 are topographic, 1 is geographic and 1 is agronomic based maps. Topographic based maps are, "digital elevation model map", "watershed boundary map" and "aspect map". Geographic maps can be summarized as "vegetation map" and "soil type map".

Digital elevation model map is the cornerstone of the input raster maps by which the watershed boundary map and aspect maps are derived from. The watershed boundary map and aspect map are prepared by the geographic information system software ArcGIS 10.0 [148] (this software is utilized by Suyapı Engineering and Consulting Inc.). The vegetation characteristics map is acquired from Directorate of Yenice Regional Forestry. Soil type map is generated based on the integration of field observations and the USDA soil texture classification system.

4.4.2.1.1 Digital Elevation Model Map

Study area is located in 1/25000 scaled Zonguldak F28-c1 and F28-b4 topographic maps prepared by National Mapping Agency of Turkey [27]. Digital elevation model (DEM) of the study area with 10 m x 10 m cell size was generated on the basis of digitized elevation contours of 1/25 000 scaled topographic map with intervals of 10 m. From this digital elevation model thematic maps were derived by the software ArcGIS 10.0. Elevation range in the study area changes between 165 – 837m (Fig. 4.10). Additionally, the drainage network is determined based on DEM by Strahler [149] method (Fig. 4.10).

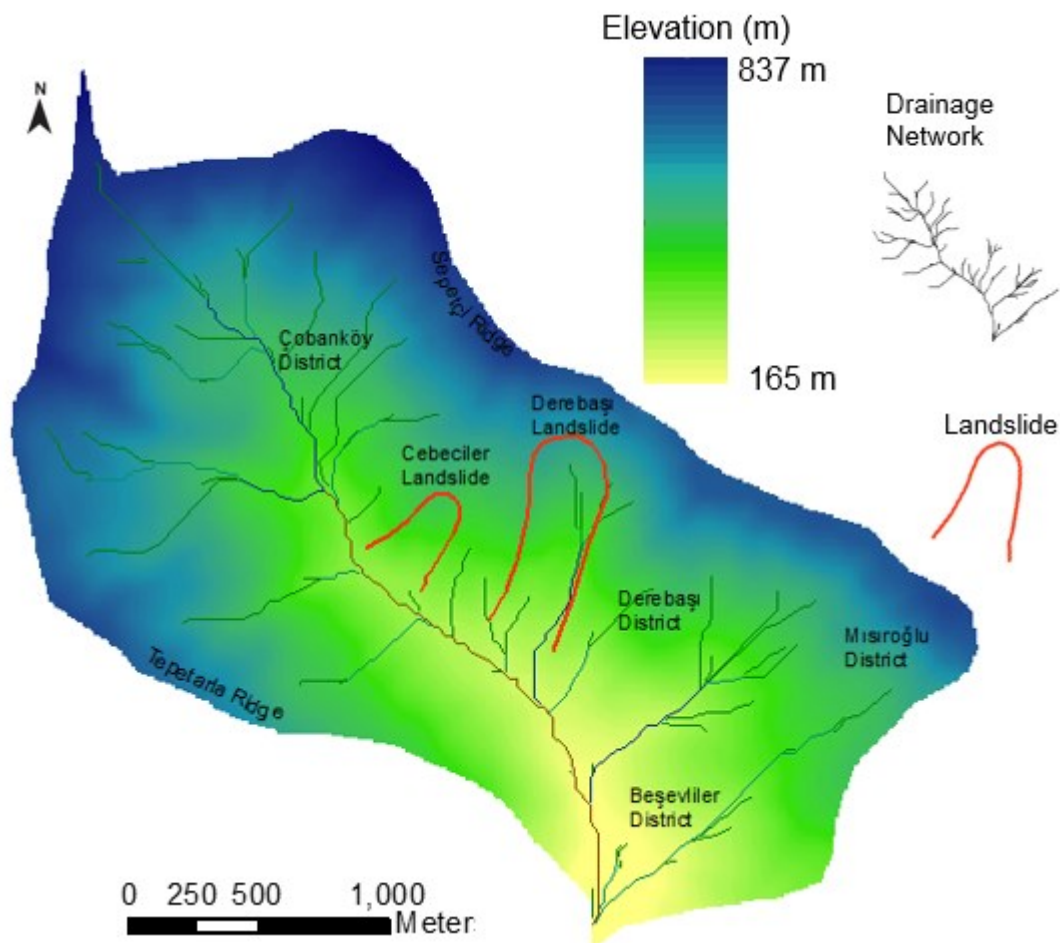


Figure 4.10: Digital elevation model of study area

4.4.2.1.2 Watershed Boundary Map

Watershed boundary map is derived from the digital elevation model and generated by ArcGIS software, version 10.1 [148]. Before generating watershed boundary map, sink errors were corrected to overcome the disorientation of water.

If a digital elevation model contains a sink all the water flux would be oriented from the upslope cells to the sink cell (Fig. 4.11.a and b). The small imperfections of digital elevation model were removed with performing the ArcGIS software fill function [148].

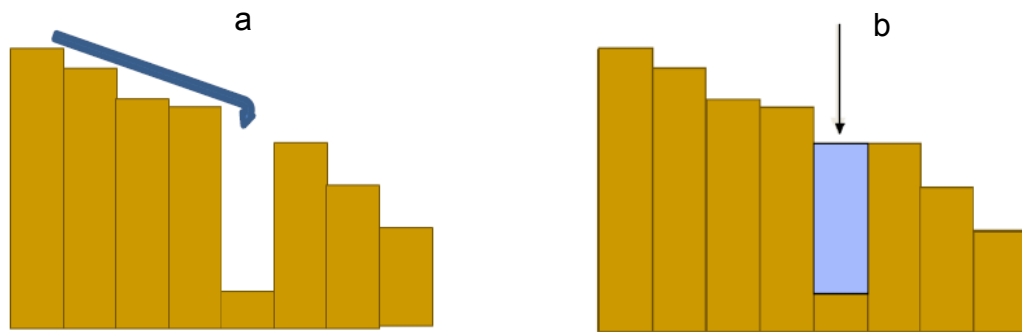


Figure 4.11 a) Sink error in digital elevation model, b) Filled sink in digital elevation model [148].

After removing the imperfection of digital elevation model, the cell based flow direction map is generated by D8 algorithm with ArcGIS 10.0 software [148]. Water flux is directed from the central cell to the cell which has the lowest elevation value. In Figure 4.12 each number represents an elevation value. In this case the water flux will be as shown in Figure 4.12.



Figure 4.12: Water flow direction [148]

Then flow accumulation map is generated by the software ArcGIS 10.0 [148]. This map shows the cell number in drainage area. In other words, with this map the drainage area and drainage network can be determined. Flow direction map and flow accumulation map is shown in Figure 4.13 a and b.

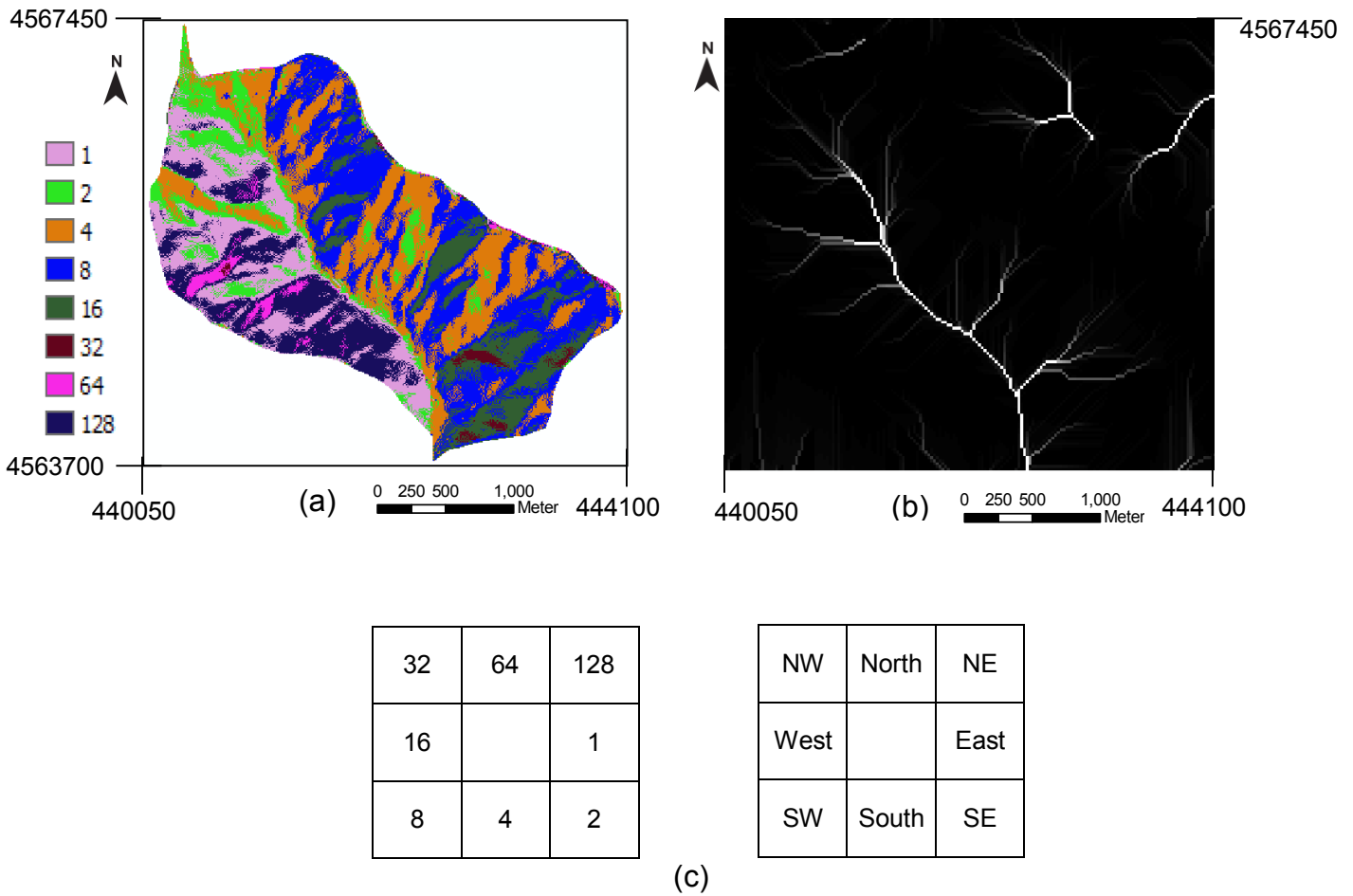


Figure 4.13 a) Flow direction map of study area b) Flow accumulation of study area c) Flow direction values for each direction

Flow direction values in Figure 4.13 a represents the directions presented in Figure 4.13 c

Watershed boundary map is determined by ArcGIS 10.0 [148] based on flow accumulation map with the indication of pour point (see Fig.4.14). The water mass balance of the SMDR model is calculated in the watershed boundary area. For this reason inside the watershed must have a value of “1” while external cells must have a value of “0” (see Figure 4.14).

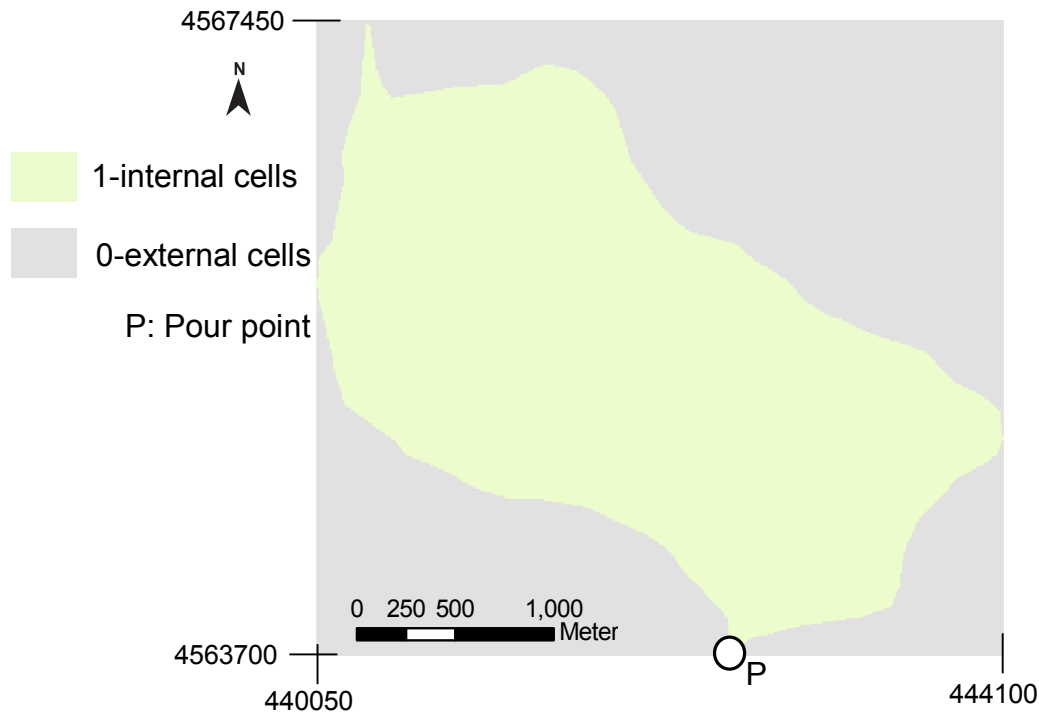


Figure 4.14: Watershed boundary map utilized in SMDR model as an input

4.4.2.1.3 Aspect Map

Aspect map is one of the thematic data generated from digital elevation model using with ArcGIS 10.0 software [148]. Aspect represents the dip direction of a surface [144]. Cell values of an aspect map vary between 0 and 359.9, these values correspond to the directions indicated below;

- | | |
|--------------------------|---------------------------|
| Between 0°-45° N-NE, | Between 180° -225° S-SW, |
| Between 45° -90° NE-E, | Between 225° -270° SW-W, |
| Between 90° -135° E-SE, | Between 270° -315° W-NW, |
| Between 135° -180° SE-S, | Between 315° -359.9° NW-N |
- And “-1” means horizontal

Aspect map is utilized for the lateral flow component of SMDR model. The aspect map of Yenice Watershed as an input parameter of SMDR model is shown on Figure 4.15.

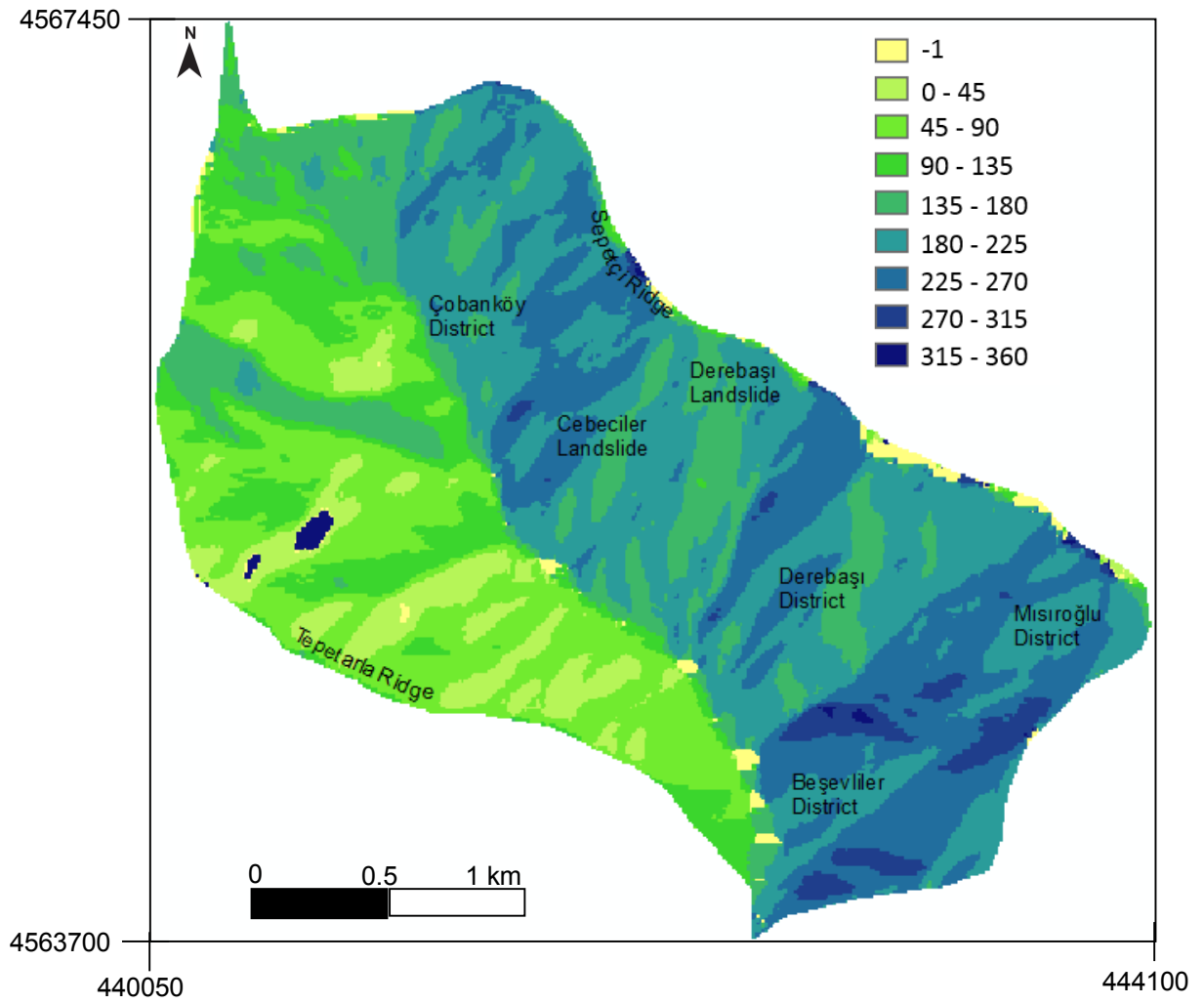


Figure 4.15: Aspect map utilized in SMDR model as an input

4.4.2.1.4 Vegetation Map

Vegetation map of the study area prepared at the occurrence date of the Derebaşı landslide (year 2000) is obtained from Directorate of Yenice Regional Forestry. This map (Fig. 4.16) is utilized with the vegetation characteristics table in evapotranspiration component of SMDR model.

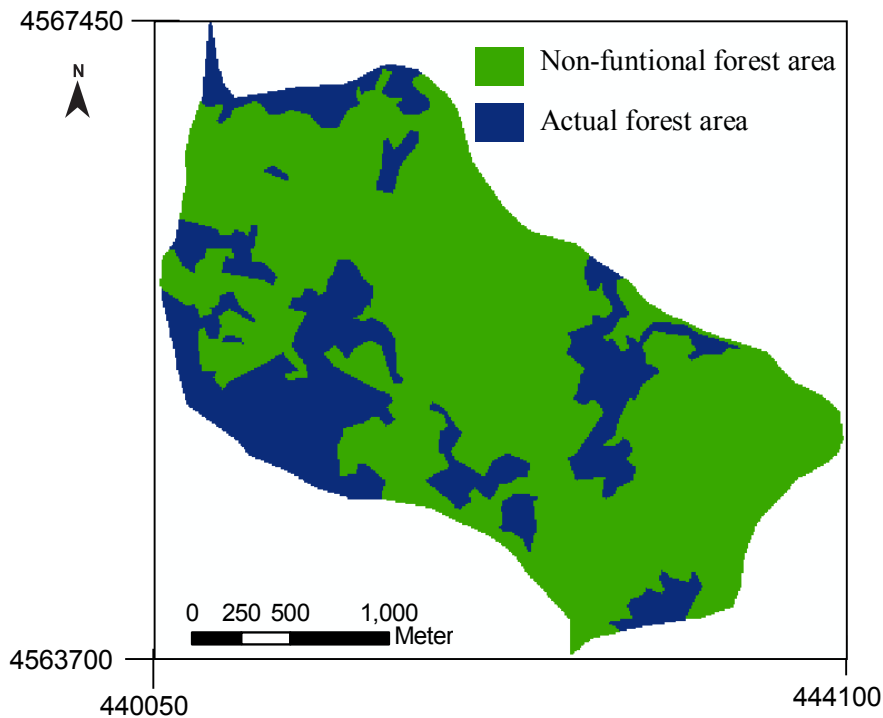


Figure 4.16: Vegetation map of Yenice Watershed for the year 2000[28]

4.4.2.1.5 Soil Type Map

Soil type map is drawn based on the field observations and laboratory tests (grain size distribution). The first step of determining soil type map borderlines is, mapping the soil type variations based on the field observations (Fig. 4.17.a) then collection of representative soil samples from watershed. Subsequently, laboratory tests were performed on the soil samples and the grain size distribution was determined for each analysed sample as explained in section 4.2 and 4.3. Both “Kriging” and “Inverse Distance Weighting” (IDW) methods were considered for the determination of the grain size percentage map, and IDW was found more representative, because it was found more compatible with the field observations. Therefore, IDW method was utilized to obtain the percentage map for clay, silt and sand (Fig. 4.17.b, c and d). Finally, the borderlines of the soil type map were revised by integration of observed and interpolated maps. Then, soil type map was redrawn based on the field observations and verified by Inverse distance weighting (Fig. 4.18). The required soil properties for soil characteristics table are compiled by the laboratory tests and estimated from soil texture through statistical relationships proposed by Rawls and Brakensiek [119, 120].

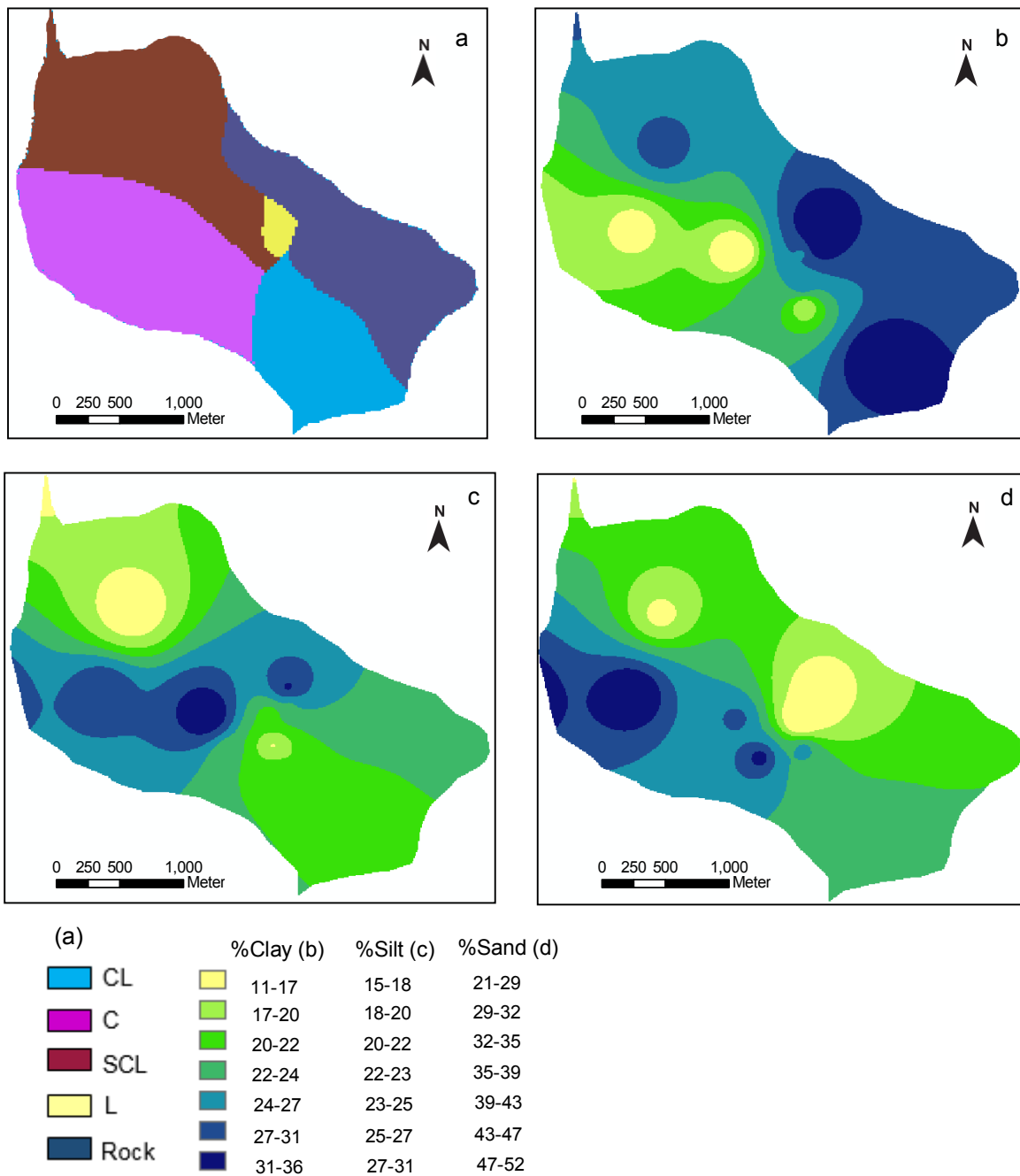


Figure 4.17: a) Map of soil type variations based on the field observations, b) Map of clay percentage based on IDW, c) Map of silt percentage based on IDW, d) Map of sand percentage based on IDW.

Figure 4.17 a, b, c and d shows that clay and sand percentage maps drawn based on the IDW method overlap with the soil type variations map based on the field observations. Consequently, the soil type variations map based on the field

observations is used as base for the soil type mapping. The unknown borderlines of soil type map were completed with personal engineering judgement from the clay and sand percentage maps drawn based on the IDW method and field observations. Then so obtained final soil type map is given in Figure 4.18.

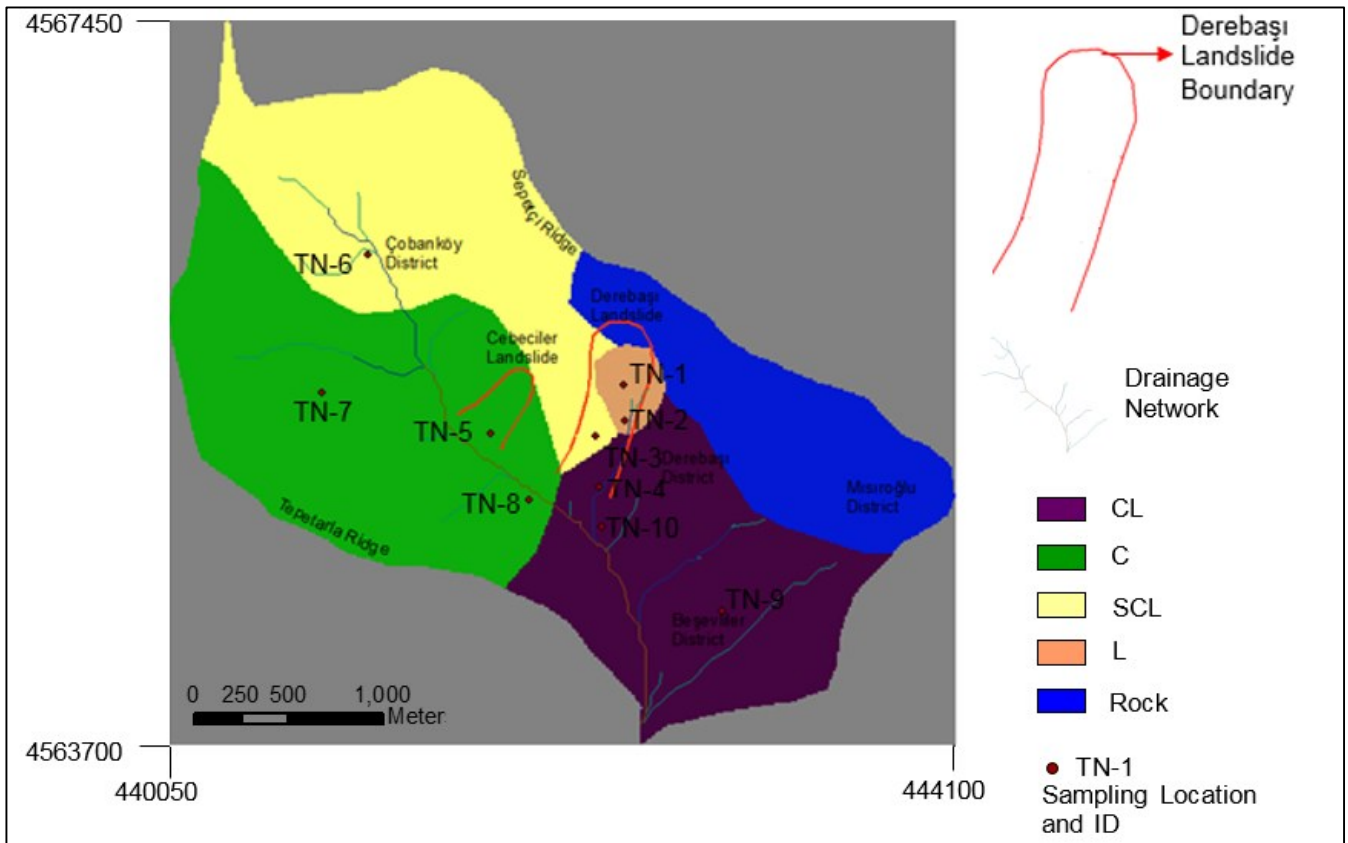


Figure 4.18: Soil type map of Yenice Watershed

The soil hydrodynamic properties of each soil type given in the soil type map is determined from laboratory tests and estimated from soil texture through statistical relationships proposed by Rawls and Brakensiek [119, 120], and given in detail in section 4.4.2.2.3.

4.4.2.2 Lookup Tables

The input tables of SMDR model make sense of the input maps and to product new raster maps. 3 main tables are required for running SMDR model;

- 1) Meteorological data table

- 2) Vegetation characteristics table
- 3) Soil characteristics table

4.4.2.2.1 Meteorological Data Table

Daily meteorological data for Yenice Station between the years 1989-2009 are obtained from “General Directorate of Meteorological Service of Turkey” [29]. These data consist of daily mean temperature, daily mean precipitation and daily mean potential evapotranspiration records. The monthly mean meteorological data table of the year 2000 (occurrence year of Derebaşı Landslide) prepared as an input data table of SMDR simulation is presented in Table 4.9.

Table 4.9: Monthly mean meteorological data of the year 2000 as an input data table of SMDR model.

Date	Mean Precipitation (mm)	Mean Temperature(C ^o)	Mean Potential Evapotranspiration (mm)
January 2000	11.5	4.8	0
February 2000	11.5	5.6	0
March 2000	14.1	8.7	0
April 2000	18.8	12.7	1.3
May 2000	21.8	16.6	3.2
June 2000	20.4	20.6	5.1
July 2000	12.1	23.5	5.3
August 2000	13.5	23.5	5.2
September 2000	19.3	19.1	4.3
October 2000	15.7	14.9	1.2
November 2000	18.6	8.8	0
December 2000	14.4	5.4	0

4.4.2.2.2 Vegetation Characteristics Table

Vegetation characteristics table (Table 4.10) converted to NLCD classification system, is obtained from Directorate of Yenice Regional Forestry [28]. In the study area two types of area exist according to the vegetation characteristics map, namely non-functional forest area and actual forest area. Actual forest area was interpreted as "43 land use class numbered mixed forest" and non-functional forest area was interpreted as "51 land use class numbered shrubland" by Directorate of Yenice Regional Forestry [28] in terms of NLCD classification format.

According to NLCD Land Cover Class Definitions [149] land use class 43 "mixed forest" and land use class 51 "shrubland" are defined as follow:

Mixed Forest Areas (43) are dominated by trees where neither deciduous nor evergreen species represent more than 75% of the cover present.

Shrubland Areas (51) dominated by shrubs; shrub canopy accounts for 25-100% of the cover. Shrub cover is generally greater than 25% when tree cover is less than 25%. Shrub cover may be less than 25% in cases when the cover of other life forms (eg. herbaceous or tree) is less than 25% and shrubs cover exceeds the cover of the other life forms.

Vegetation characteristics table used in SMDR model as an input data is presented in Table 4.10. This data is utilized for the vegetation development and nitrate - pesticide transport modelling module of SMDR model. For this reason the Table 4.10 is formed from the tables proposed by Soil and Water Laboratory [26] for each land use class number of NLCD.

Table 4.10: Vegetation characteristics table of Yenice Watershed entered to SMDR model

Column Number													
1	2	3	4	5	6	7	8	9	10	11	12	13	14
Land Use Class 43	Mixed Forest	1500	1500	1	2500	10	22.5	90	250	1000	0	Mar.20	Oct.15
Land Use Class 51	Shrubland	750	750	1	2500	7.5	12.5	95	200	1000	0	Mar.20	Oct.15

Where;

Column 1: Land Use Class number

Column 2: Land Use class description

Column 3: Minimum root depth - Z_{Rmin} (mm)

Column 4: Maximum root depth - Z_{Rmax} (mm)

Column 5: Base temperature - T_b (°C)

Column 6: Maximum Growing-Degree-Days - DD_{max}

Column 7: Development stages 1-2 limit - DD_{1-2} (% DD_{max})

Column 8: Development stages 2-3 limit - DD_{2-3} (% DD_{max})

Column 9: Development stages 3-4 limit - DD_{3-4} (% DD_{max})

Column 10: Minimum basal evapotranspiration coefficient - Kc_{min} (‰)

Column 11: Maximum basal evapotranspiration coefficient - Kc_{max} (‰)

Column 12: Planted Crop flag (0: Non-planted - 1: Planted)

Column 13: Planting Date (MM/DD)

Column 14: Harvest Date (MM/DD)

4.4.2.2.3 Soil Characteristics Table

Soil characteristics table represents the physical and hydrodynamic properties of each unit in soil type map. In the study area 4 types of soil class are determined according to USDA soil texture classification system. These soil classes are “clay”, “clayey loam”, “sandy clayey loam” and “loam”. The soil characteristics table used in SMDR model as an input data is presented in Table 4.11.

Table 4.11: Soil characteristics table of Yenice Watershed in SMDR format

1	2	3	4	5	6	7	8	9	10	11	12	13	14	15	16	17	18
1	CL	1	100	CL	15	0.6	46.4	7.5	19.7	12.1	31.8	39	31.5	28.6	31.8	48	480
2	C	1	100	C	9.3	0.54	47.5	9	27.2	12.4	39.6	38.5	29.5	35.6	39.6	14.4	144
3	SCL	1	100	SCL	29	0.55	39.8	6.8	14.8	10.7	25.5	33	26.2	23	25.5	72	720
4	L	1	100	L	14	0.47	46.3	2.7	11.7	15.3	27	43.4	40.7	24.3	27	316.8	3168

Each column of Table 4.11 is explained as follow;

Column 1 Soil number: It corresponds to the number specified in soil characteristics map.

Column 2 Soil ID: Name of soil

Column 3 Layer number: Only one layer is assumed for Yenice Watershed

Column 4 Depth (mm): Depth is assumed as 100 cm (depth of sampling).

Column 5 Main texture class: USDA soil texture classification system is utilized for texture class (see section 4.3.6).

Column 6 Rocks and gravel content (%): Rocks and gravel content is assumed as gravel content (see table 4.7)

Column 7 Organic matter content (%): This column is filled from Table 4.5

Column 8 Porosity (%): Porosity is determined by the proposition of Rawls et al. [119] as presented in Table 4.8.

Column 9 Residual water content (%): Residual water content is defined as the water content for which the gradient $d\theta/dh$ becomes zero and determined by the proposition of Rawls et al. [119] as presented in Table 4.8.

Column 10 Permanent wilting point (%): Permanent wilting point is defined as the minimum soil water content the plant requires not to wilt. It is physically assumed

as the wilting point is the water content at 1500 J/kg of negative hydraulic head. This parameter is determined by the proposition of Rawls et al. [119] as presented in Table 4.8.

Column 11 Available water capacity (%): This parameter is defined as the volume of water available to plants per unit soil of volume. Available water capacity is determined by the difference between field capacity and wilting point as defined in Soil and Water Laboratory [26].

Column 12 Water content at field capacity (%): This parameter is defined as the water content held in the soil after excess water has drained and the rate of downward movement has decreased. It is physically assumed as the field capacity is the bulk water content retained in soil at 33 J/kg of negative hydraulic head. This parameter is determined by the proposition of Rawls et al. [119] as presented in Table 4.8.

Column 13 Water content at saturation (%): This parameter is assumed to be equal to effective porosity (air entrapment is neglected). Effective porosity is determined by the proposition of Rawls et al. [119] as presented in Table 4.8.

Column 14 Maximum available water content (%): This parameter is determined by the definition of Soil and Water Laboratory [26] as the difference between water content at saturation and residual water content.

Column 15 Potential evapotranspiration limit (%): This parameter is defined as the minimum water content above which evapotranspiration takes place at the potential rate. Potential evapotranspiration limit is determined as proposed by Soil and Water Laboratory [26] with approximation that potential evapotranspiration limit is equal to 0.9 times field capacity ($\theta_{epl}=0.9 \times \theta_c$).

Column 16 Macroporal drainage limit (%): This parameter is defined as the minimum water content for which drainage occurs predominantly through macropores. Macroporal drainage limit is determined as proposed by Soil and Water Laboratory [26] with approximation that macroporal drainage limit is equal to field capacity.

Column 17 Vertical hydraulic conductivity (mm/day): This parameter is determined by the hydraulic conductivity test based on the standard proposed by ASTM [129] and verified by the proposition of Rawls et al. [119] as presented in figure 4.7. The mean soil hydraulic conductivity determined by laboratory tests for each soil textural class is presented in Table 4.12.

Table 4.12: Mean hydraulic conductivity determined by laboratory tests for each soil textural class

Soil Texture	mm/day
CL	41.5
C	16.5
SCL	51.1
L	81.4

Column 18 Horizontal hydraulic conductivity (mm/day): This parameter is determined as proposed by Soil and Water Laboratory [26] with approximation that horizontal hydraulic conductivity is equal to 10 times vertical hydraulic conductivity.

From this point on, the saturation degree will be considered as the main parameter controlling the landslide susceptibility in terms of water effect considering the triggering mechanism of Derebaşı Landslide (see section 3.1.2). To enlighten the triggering location of the Derebaşı landslide, landslide area is divided into 3 zones to observe the triggering location (Fig. 4.19) and saturation degree maps were analysed for 10 days before of landslide occurrence date. Saturation degree maps between the dates 25.05.2000 and 05.06.2000 obtained from the SMDR model is analysed for 3 different zones and the results are given in the Table 4.13.

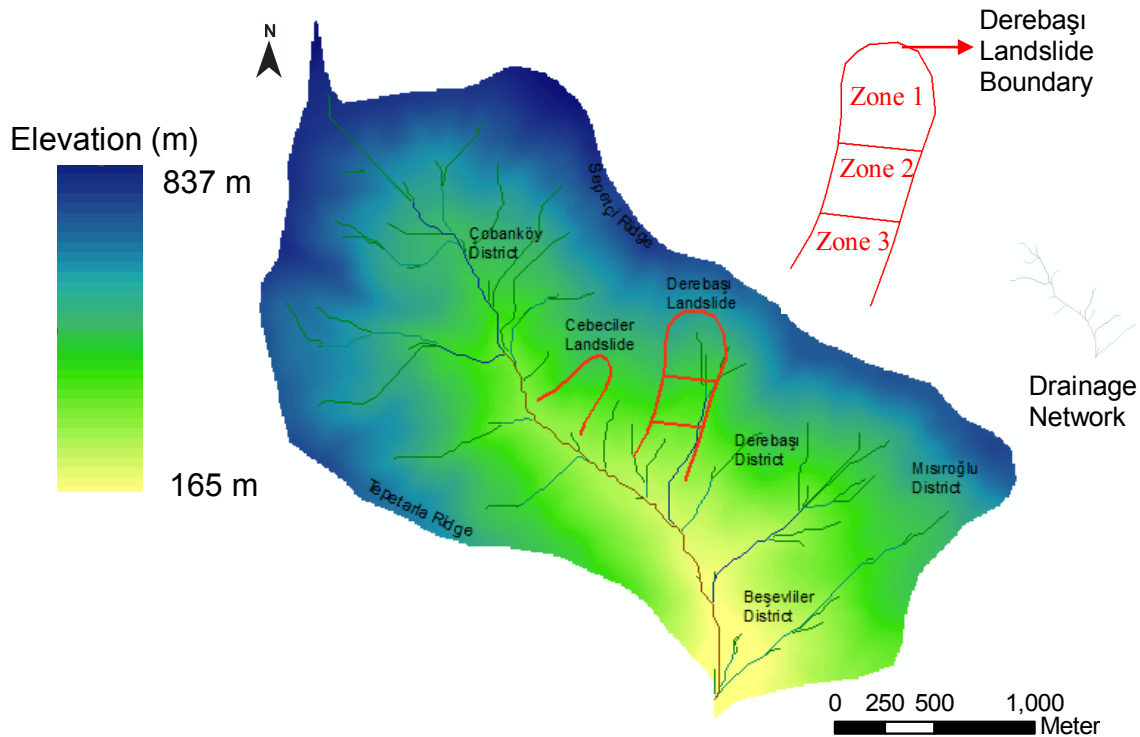


Figure 4.19: DEM of Study area and divided zones of Derebaşı Landslide area

Table 4.13: Number of pixels (frequency) for each saturation degree class of 3 different zones between the dates 25.05.2000 and 05.06.2000 obtained from the SMDR model and meteorological data

Date	Rainfall (mm)	Temp (C°)	ET (mm)	Saturation Degree			
				Class	Frequency Zone 1	Frequency Zone 2	Frequency Zone 3
25.05.2000	23.1	15.2	1	0.70 - 0.75	1	0	0
				0.75 - 0.80	2	0	0
				0.80 - 0.85	322	322	393
				0.85 - 0.90	721	379	446
				0.90 - 0.95	1	0	0
				0.95 - 1.00	0	0	0
26.05.2000	2.9	17.1	1	0.70 - 0.75	0	0	0
				0.75 - 0.80	4	0	0
				0.80 - 0.85	374	385	430
				0.85 - 0.90	668	316	409
				0.90 - 0.95	1	0	0
				0.95 - 1.00	0	0	0
27.05.2000	3.3	20.3	4.3	0.70 - 0.75	0	0	0
				0.75 - 0.80	4	0	0
				0.80 - 0.85	439	433	472
				0.85 - 0.90	600	268	367
				0.90 - 0.95	3	0	0
				0.95 - 1.00	1	0	0
28.05.2000	0.5	20	5.5	0.70 - 0.75	2	0	0
				0.75 - 0.80	5	0	0
				0.80 - 0.85	464	453	496
				0.85 - 0.90	567	248	343
				0.90 - 0.95	8	0	0
				0.95 - 1.00	1	0	0
29.05.2000	1.4	22.7	6.4	0.70 - 0.75	2	0	1
				0.75 - 0.80	11	0	6
				0.80 - 0.85	482	471	520
				0.85 - 0.90	540	230	312
				0.90 - 0.95	12	0	0
				0.95 - 1.00	0	0	0
30.05.2000	1.6	18.2	4.4	0.70 - 0.75	1	1	1
				0.75 - 0.80	12	4	8
				0.80 - 0.85	508	484	544
				0.85 - 0.90	512	212	286
				0.90 - 0.95	13	0	0
				0.95 - 1.00	1	0	0
31.05.2000	0.9	18.7	3.4	0.70 - 0.75	2	1	1
				0.75 - 0.80	13	8	13
				0.80 - 0.85	512	490	547
				0.85 - 0.90	501	200	278
				0.90 - 0.95	17	2	0
				0.95 - 1.00	2	0	0

01.06.2000	0	20.8	3.4	0.70 - 0.75	2	1	1
				0.75 - 0.80	24	16	22
				0.80 - 0.85	520	488	550
				0.85 - 0.90	478	192	265
				0.90 - 0.95	21	4	1
				0.95 - 1.00	2	0	0
02.06.2000	2.5	16.2	5.4	0.70 - 0.75	4	1	1
				0.75 - 0.80	33	28	40
				0.80 - 0.85	536	480	539
				0.85 - 0.90	447	184	257
				0.90 - 0.95	22	8	2
				0.95 - 1.00	5	0	0
03.06.2000	11.2	15.1	1.5	0.70 - 0.75	6	1	1
				0.75 - 0.80	43	38	64
				0.80 - 0.85	538	478	518
				0.85 - 0.90	429	172	251
				0.90 - 0.95	25	12	5
				0.95 - 1.00	6	0	0
04.06.2000	10.7	17.3	1.8	0.70 - 0.75	9	2	3
				0.75 - 0.80	52	57	90
				0.80 - 0.85	532	457	493
				0.85 - 0.90	415	172	247
				0.90 - 0.95	31	13	6
				0.95 - 1.00	8	0	0
05.06.2000	7.3	19.6	2.1	0.70 - 0.75	10	1	6
				0.75 - 0.80	68	79	119
				0.80 - 0.85	523	436	468
				0.85 - 0.90	399	164	237
				0.90 - 0.95	37	21	9
				0.95 - 1.00	10	0	0

In relation with the Table 4.13 the saturation degree map for June 5 2000 is presented in Figure 20.

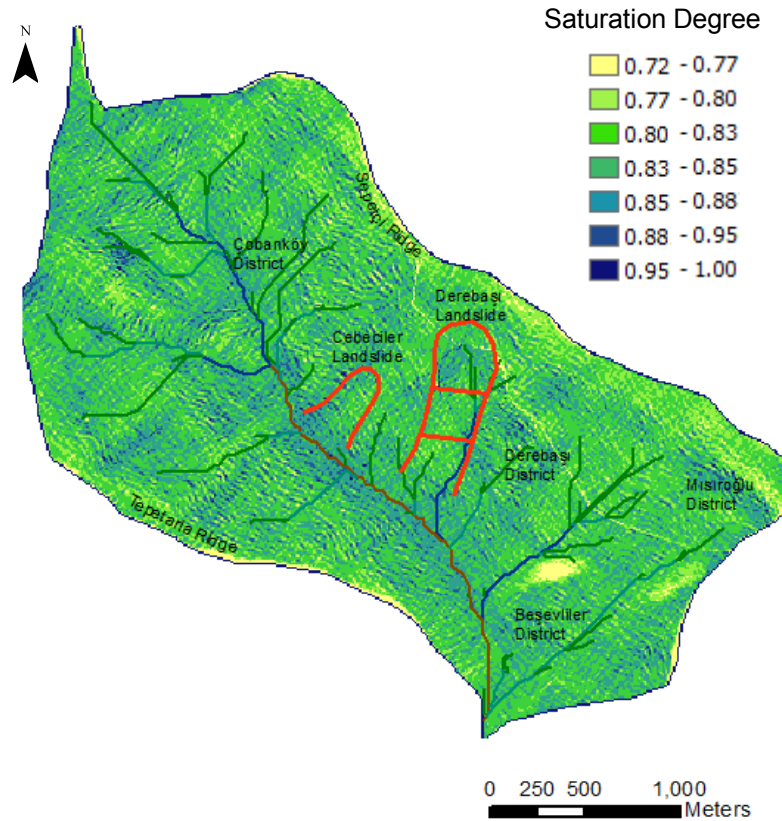


Figure 4.20: Saturation degree map of June 5 2000

Number of pixels (Frequency) of each saturation degree class is analysed from 10 days before the occurrence date of the Derebaşı landslide. The increase of pixels in zone 1 for the saturation degree classes 0.90-0.95 and 0.95-1.00 is remarkable. This prominent increase indicates that the Derebaşı landslide is triggered from zone 1 as reported by Disaster and Emergency Management Presidency. Another striking point of the Table 4.13 is that the precipitation amount for the occurrence date of Derebaşı Landslide is only 7.3 mm which is not the highest value.

On the other hand, as the landslides are the result of interdependent spatio-temporal processes, including static and dynamic factors, a mathematical expression must include both dynamic and static factors. However, static factors (eg: elevation, slope, aspect, topographic curvature, topographic wetness index, etc.) vary spatially and remain steady temporally and dynamic (triggering) factors (eg: earthquakes, water effect, human activities) vary temporally and remain steady spatially for a watershed scale. For this reason a mathematical relation between the landslide occurrence and dynamic data could not be composed.

To reflect the spatio-temporal effect of water on landslide susceptibility, saturation degree will be expressed as a newly introduced index, named from now on as the saturation degree index and utilized in frequency ratio analysis.

4.5 FREQUENCY RATIO ANALYSIS IN TERMS OF LANDSLIDE SUSCEPTIBILITY

To provide objectivity within the context of minimizing the uncertainties in weight assignment, statistical methods have been incorporated with the landslide susceptibility concept as a qualitative approach. Statistical analyses are popular because they provide a more quantitative analysis of slope instability, have the ability to examine various effects of each factor on an individual basis, and decide on the final input maps in an interactive manner [5]. Statistical methods in landslide susceptibility studies are commonly known as two types: “Multivariate statistical analysis” and “bivariate statistical analysis”. Frequency ratio analysis is categorized under bivariate statistical analysis.

In general, to predict the landsliding, the causal factors for landslides that occurred in the past are considered for the landslides in the future [150]. In this study, to reflect statistically the conceptual relation between the landslides which occurred in the past and their causal factors, the frequency ratio analysis is utilized in terms of landslide susceptibility. Frequency ratio is the ratio of occurrence probability to non-occurrence probability for specific attributes [151]. Frequency ratio can be expressed as the Venn diagram below (Fig. 4.21).

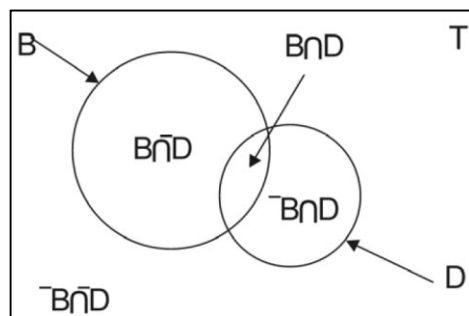


Figure 4.21: Venn diagram showing the frequency ratio concept [152] (T: Total area, B: Conditioning parameter present, D: Landslide occurrence present, \bar{B} : Conditioning parameter absent, \bar{D} : Landslide occurrence absent).

If the frequency ratio is greater than 1, greater is the relationship between a landslide and the specific factor's attribute, and if the ratio is less than 1, lesser will be the relationship between a landslide and the specific factor's attribute [153]. The frequency ratio (eq. 4.29) is shown in Table 4.14 for all parameters and each parameter class. As it is known from the reports of Disaster and Emergency Management Presidency, the Derebaşı landslide is triggered from zone 1, the zone 2 and 3 (Fig. 4.20) were considered as "out of landslide" in Table 4.13. The results of SMDR model in context of saturation degree verify also the triggering location of the Derebaşı landslide (see Appendix 2).

$$Fr_i = \frac{N_{pix(Si)} / N_{pix(Ni)}}{\sum N_{pix(Si)} / \sum N_{pix(Ni)}} \quad (\text{eq. 4.29}) \quad [152]$$

Where;

Fr_i : Frequency ratio of class "i",

$N_{pix(Si)}$: The number of pixels containing landslide in class "i",

$N_{pix(Ni)}$: Total number of pixels having class "i" in whole area of the watershed.

$\sum N_{pix(Si)}$: Total number of pixels containing landslide,

$\sum N_{pix(Ni)}$: Total number of pixels in the whole area of the watershed.

Table 4.14: Spatial relationships between each parameters and landslide – frequency ratio values

PARAMETERS	CLASS	NUMBER OF PIXELS WITHOUT LANDSLIDE	RATIO-a (%)	NUMBER OF PIXELS WITH LANDSLIDE	RATIO-b (%)	Frequency Ratio (b/a)
Slope (°)	0-10	7374	9.74	0	0.00	0.00
	10-20	32825	43.36	151	14.39	0.33
	20-30	31744	41.93	896	85.41	2.04
	>30	3756	4.96	2	0.19	0.04
Aspect (°)	0-45	5360	7.08	0	0.00	0.00
	45-90	12912	17.06	0	0.00	0.00
	90-135	8081	10.68	11	1.05	0.10
	135-180	10642	14.06	696	66.35	4.72
	180-225	21820	28.82	334	31.84	1.10
	225-270	14696	19.41	8	0.76	0.04
	270-315	1904	2.52	0	0.00	0.00
315-360	284	0.38	0	0.00	0.00	

Elevation (m)	150-300	9101	12.02	0	0.00	0.00
	300-450	19367	25.58	86	8.20	0.32
	450-600	22533	29.77	963	91.80	3.08
	600-750	22334	29.50	0	0.00	0.00
	750-900	2364	3.12	0	0.00	0.00
TWI	<16	7	0.01	0	0.00	0.00
	16-17	48204	63.68	1	0.10	0.00
	17-18	23745	31.37	985	93.90	2.99
	18-19	2765	3.65	63	6.01	1.64
	19-20	978	1.29	0	0.00	0.00
Soil Type	Clayey Loam	18130	23.95	0	0.00	0.00
	Clay	25342	33.48	0	0.00	0.00
	Sandy Clayey Loam	19944	26.35	169	16.11	0.61
	Loam	618	0.82	615	58.63	71.81
	Rock	11665	15.41	265	25.26	1.64
Saturation Degree (for 05.06.2000)	0.70-0.75	1281	1.69	12	1.14	0.68
	0.75-0.80	10014	13.23	68	6.48	0.49
	0.80-0.85	36291	47.94	523	49.86	1.04
	0.85-0.90	24575	32.46	399	38.04	1.17
	0.90-0.95	3168	4.18	37	3.53	0.84
	0.95-1.00	370	0.49	10	0.95	1.95
Permeability ($\times 10^{-5}$ m/s)	1.64-3.40	13954	18.43	0	0.00	0.00
	3.40-5.16	16628	21.97	0	0.00	0.00
	5.16-6.93	38724	51.16	0	0.00	0.00
	6.93-8.69	6300	8.32	633	60.34	7.25
	8.69-10.50	93	0.12	416	39.66	322.79

In Table 4.14 the slope and aspect maps are generated from digital elevation model by use of ArcGIS 10.0 [148], topographic wetness index map is composed by the equation 1.1. The saturation degree map for the occurrence date of the Derebaşı landslide is handled by the SMDR model. Finally, the permeability map is generated by the use of IDW method based on the laboratory test results.

In order to combine all weight values of different parameters an overall “Landslide Susceptibility” is computed by reclassifying the summation of each parameter’s frequency ratio values as in equation 4.30. So, the Unclassified Landslide Susceptibility (ULS),

$$\text{ULS} = \text{Fr} (\text{Slope Index}) + \text{Fr} (\text{Aspect Index}) + \text{Fr} (\text{Elevation Index}) + \text{Fr} (\text{Saturation Degree Index on June 5, 2000}) + \text{Fr} (\text{Soil Type Index}) + \text{Fr} (\text{Permeability Index}) \quad (\text{eq. 4.30})$$

Landslide susceptibility calculation processes for each stage is shown in Figure 4.22.

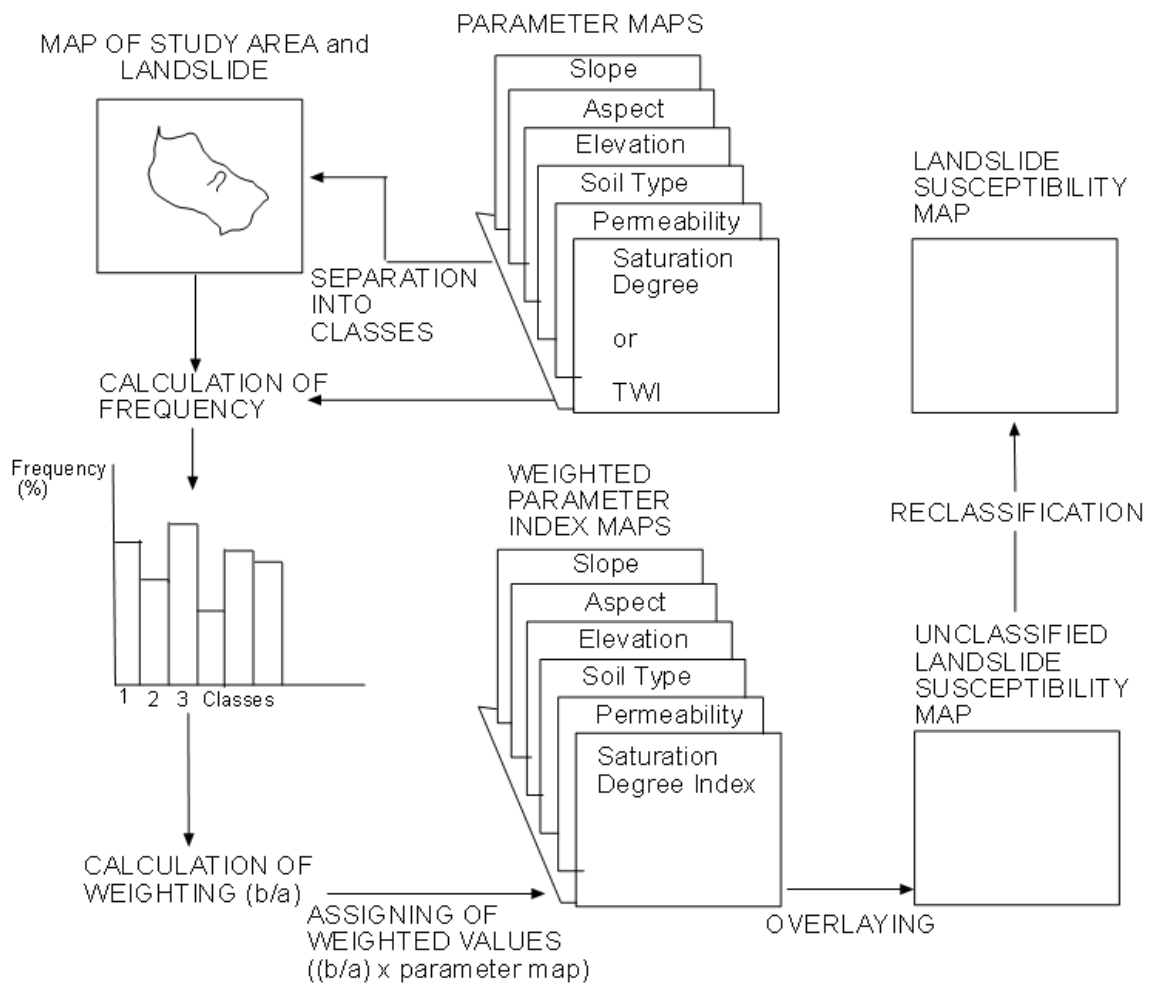


Figure 4.22: Work flow diagram of frequency ratio analysis concept for landslide susceptibility (modified from Akgün and Türk, [152]).

Parameter maps used in frequency ratio analyses and the resulting parameter index maps are given in Figures 4.23a, 4.23b, 4.24a, 4.24b, 4.25a, 4.25b, 4.26a, 4.26b, 4.27a, 4.27b, 4.28a, 4.28b, 4.29a, 4.29b.

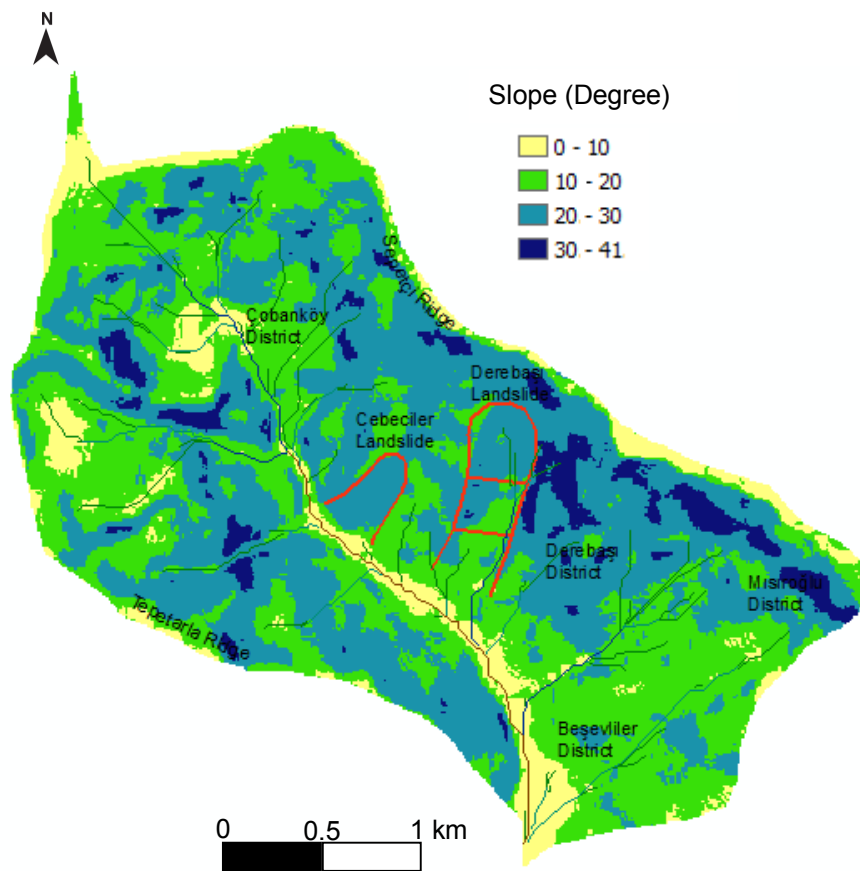


Figure 4.23.a) Slope Map of Yenice Watershed

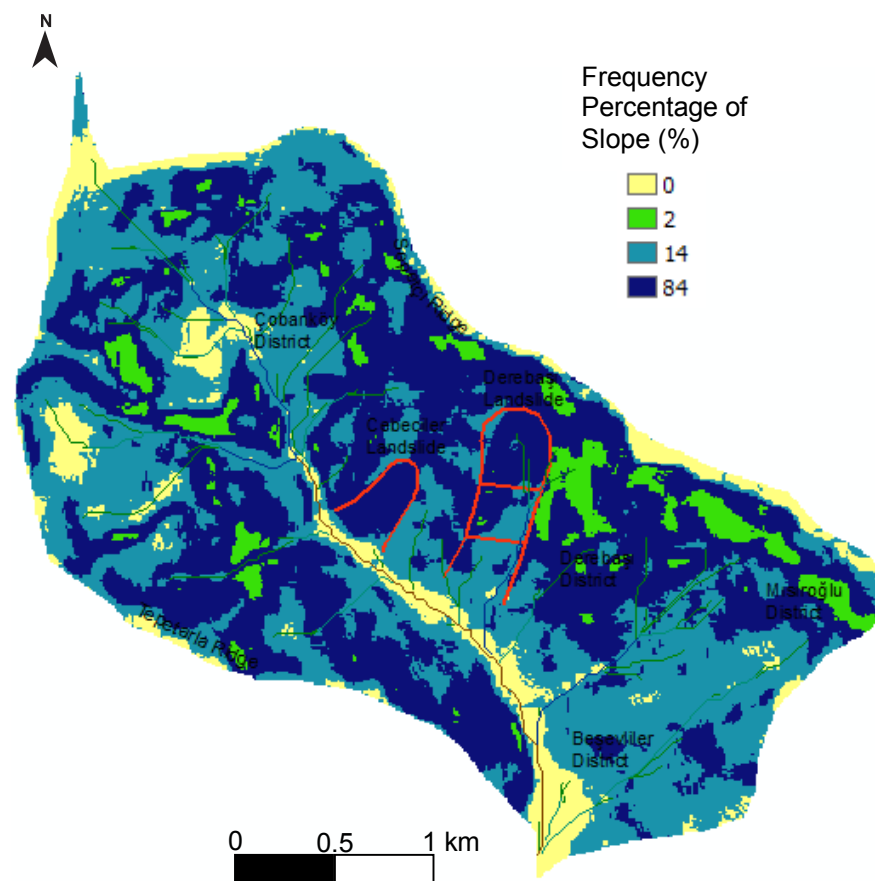


Figure 4.23.b) Slope Index Map of Yenice Watershed (Reclassified)

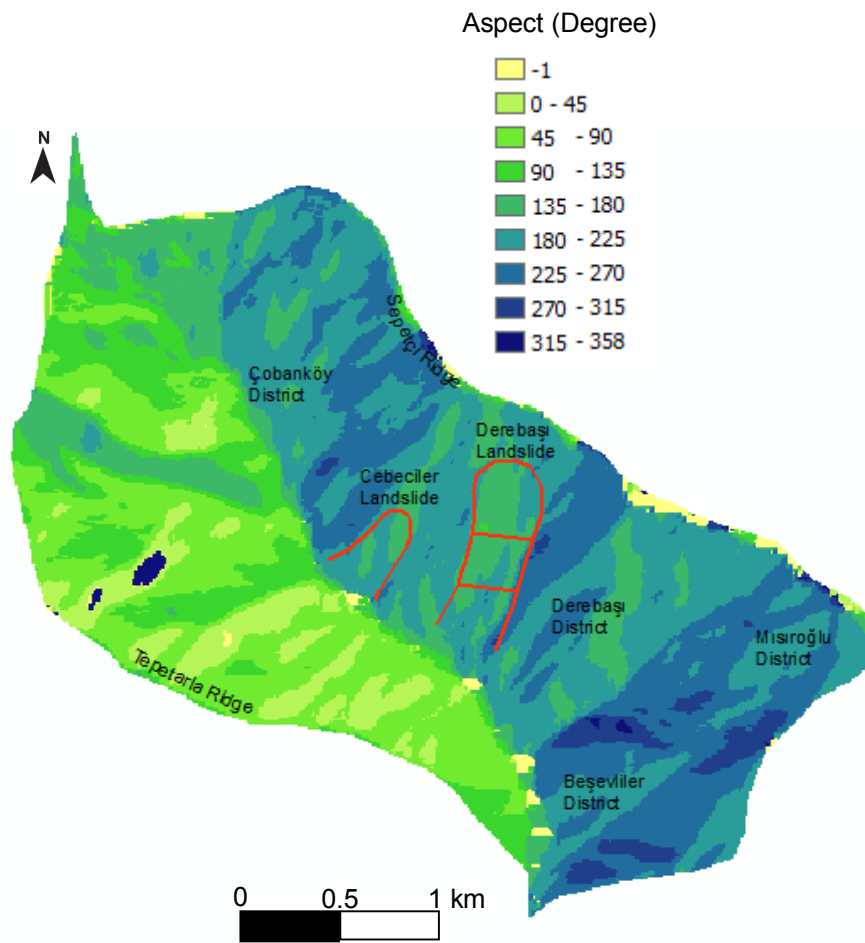


Figure 4.24.a) Aspect Map of Yenice Watershed

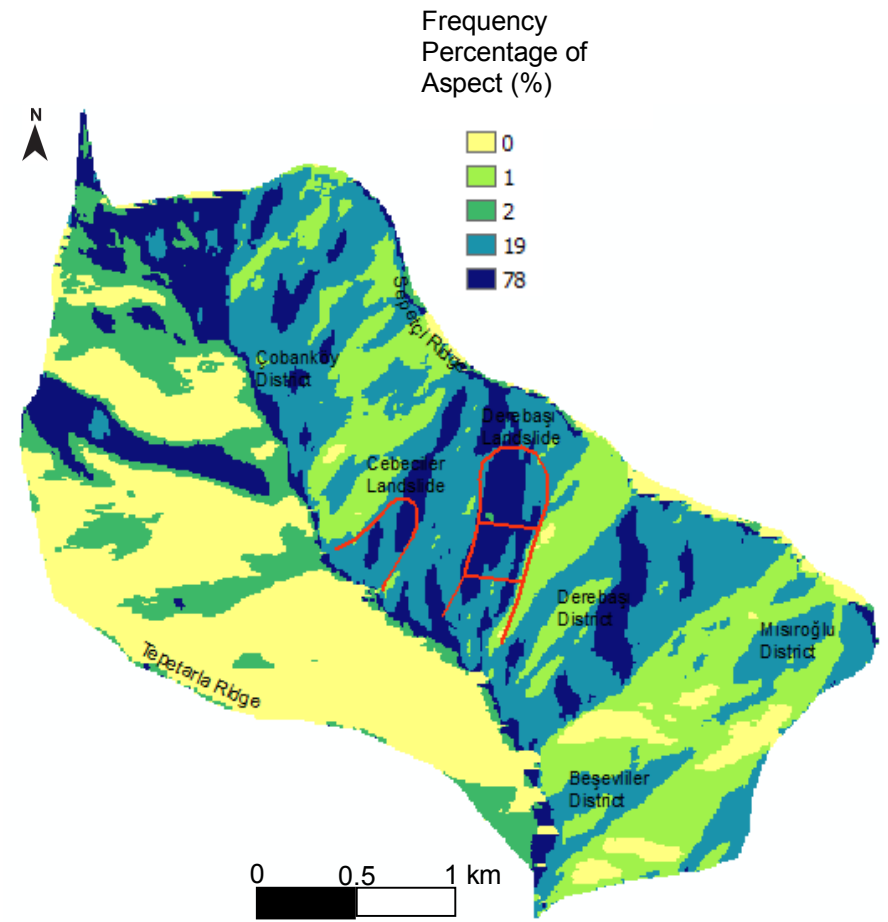


Figure 4.24.b) Aspect Index Map of Yenice Watershed (Reclassified)

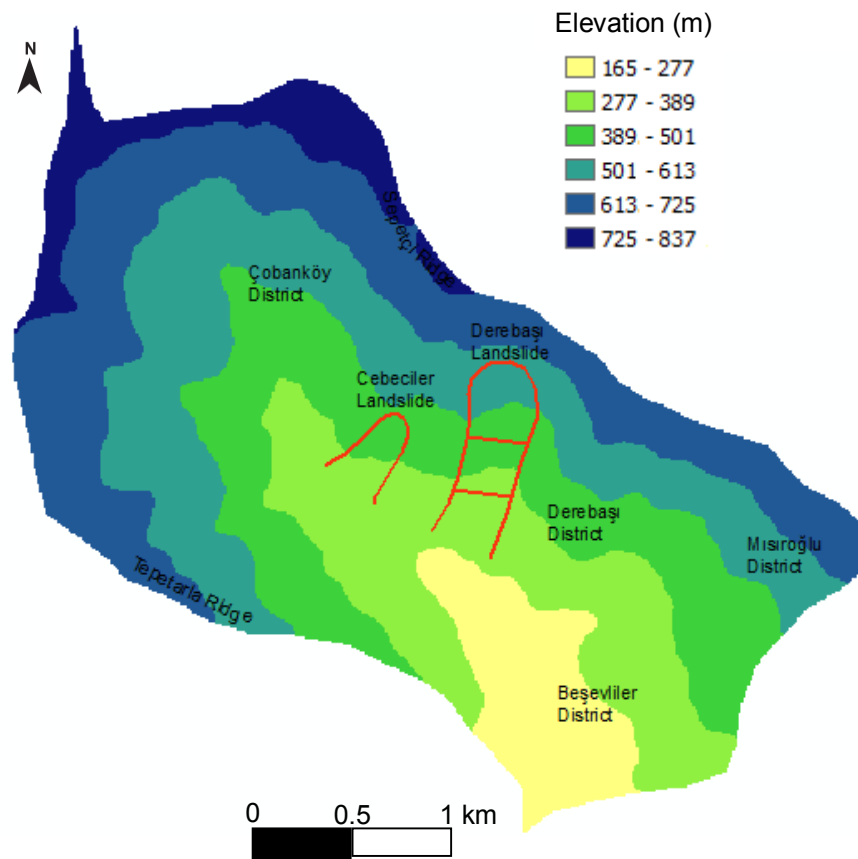


Figure 4.25.a) Elevation Map of Yenice Watershed

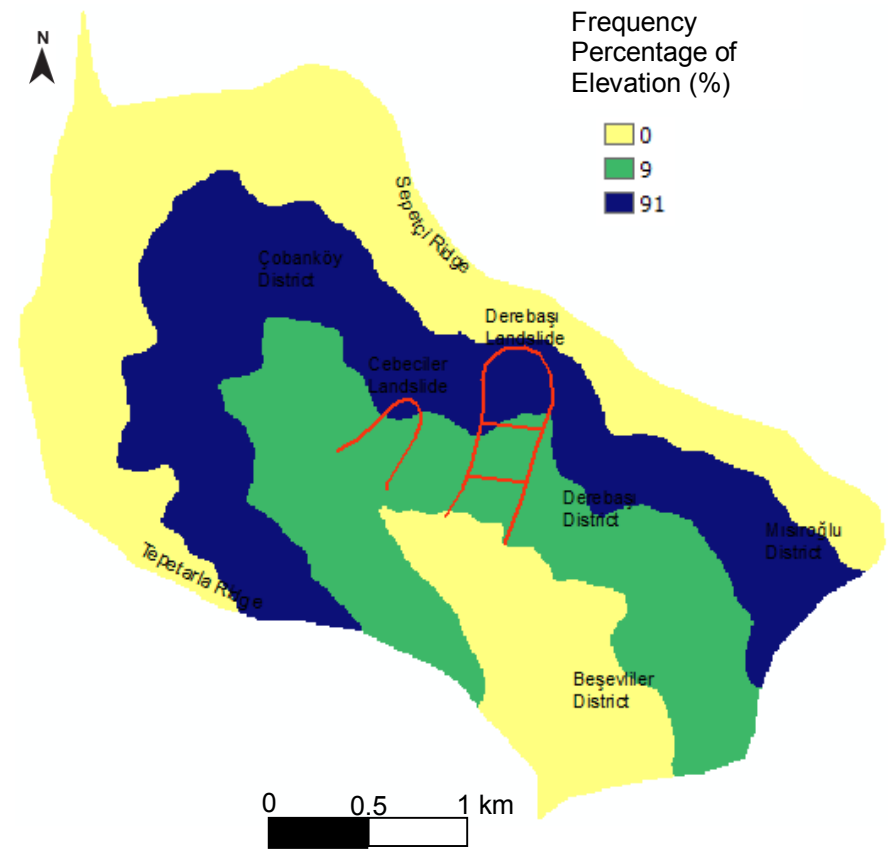


Figure 4.25.b) Elevation Index Map of Yenice Watershed (Reclassified)

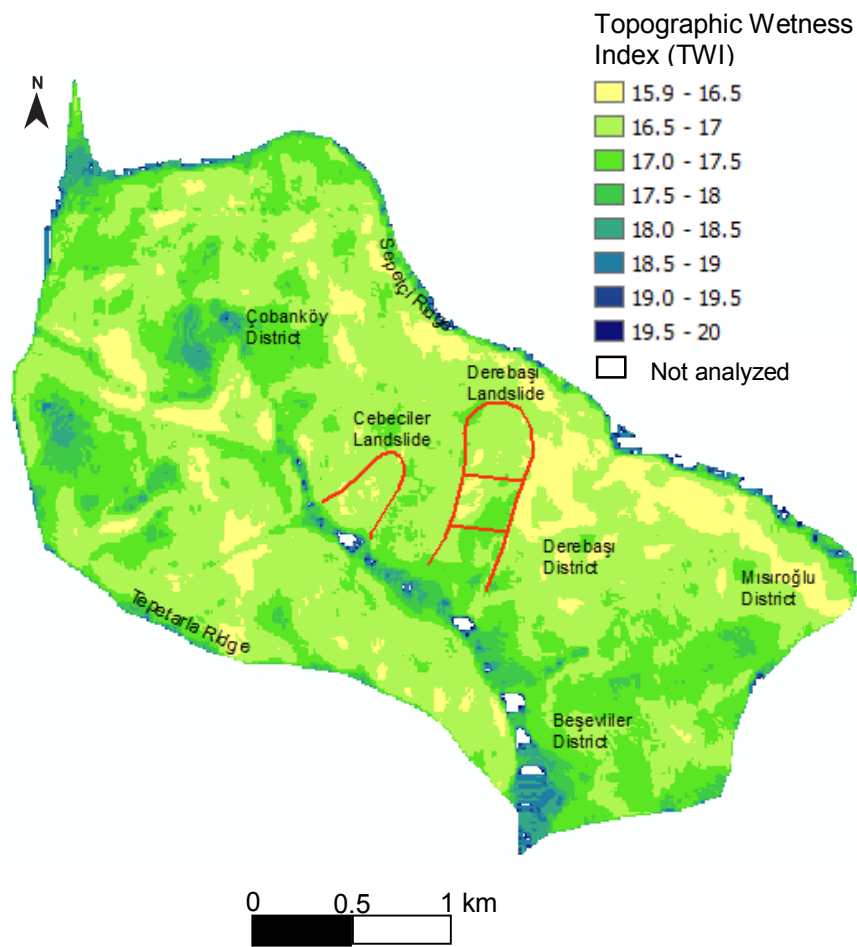


Figure 4.26.a) Topographic Wetness Index Map of Yenice Watershed

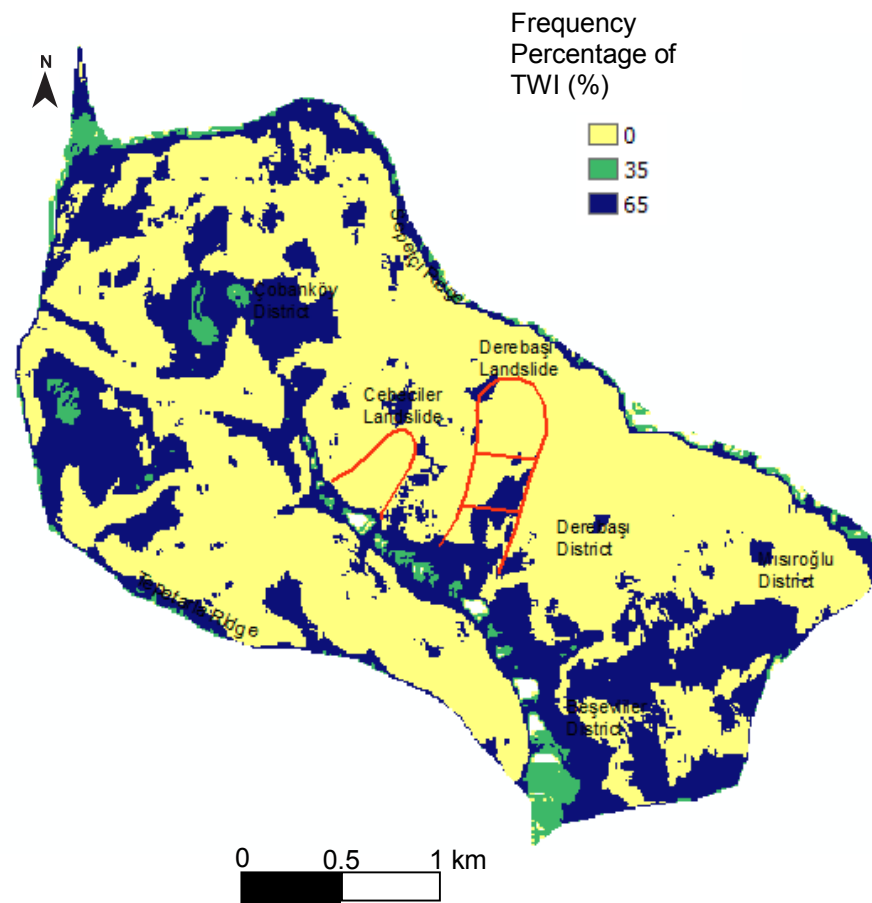


Figure 4.26.b) Topographic Wetness Index Frequency Map of Yenice Watershed (Reclassified)

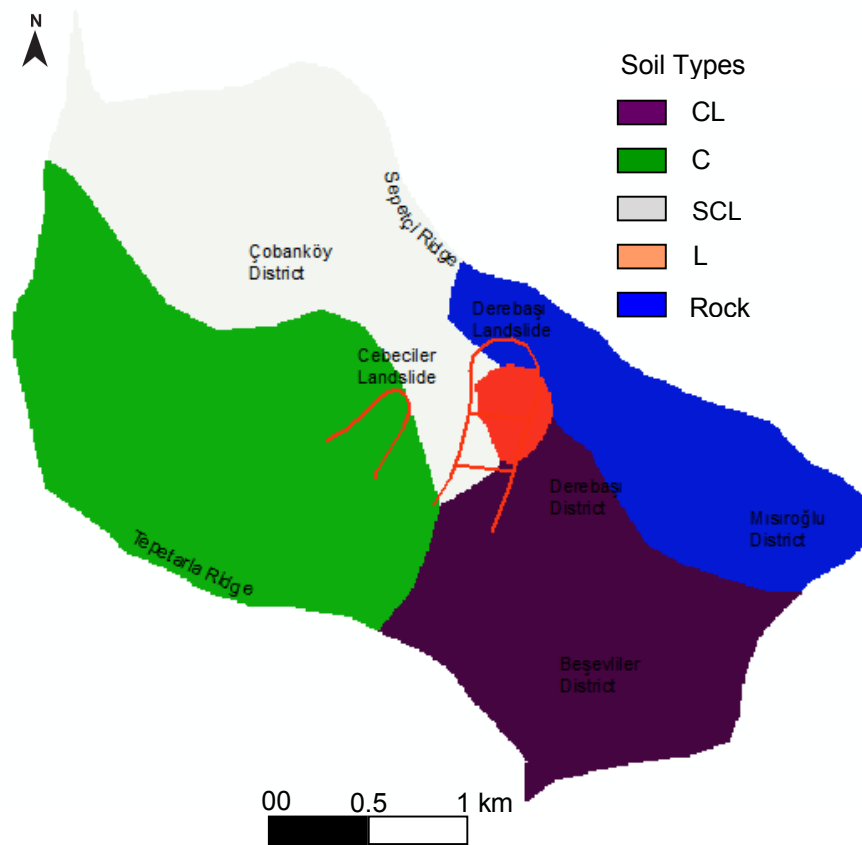


Figure 4.27.a) Soil Type Map of Yenice Watershed

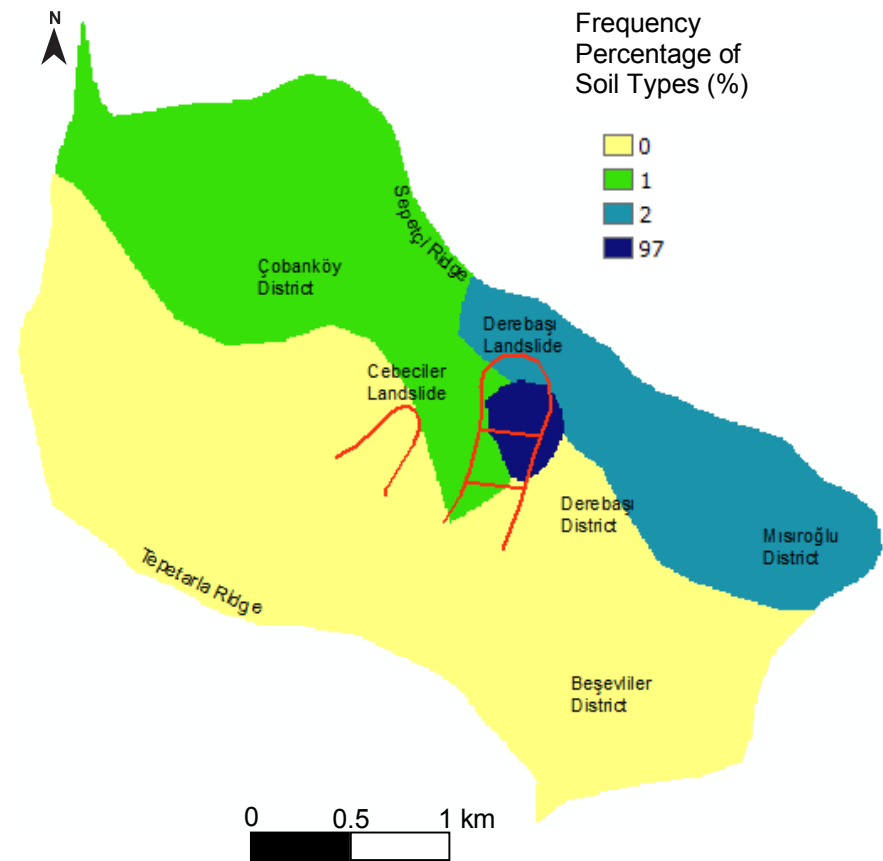


Figure 4.27.b) Soil Type Index Map of Yenice Watershed (Reclassified)

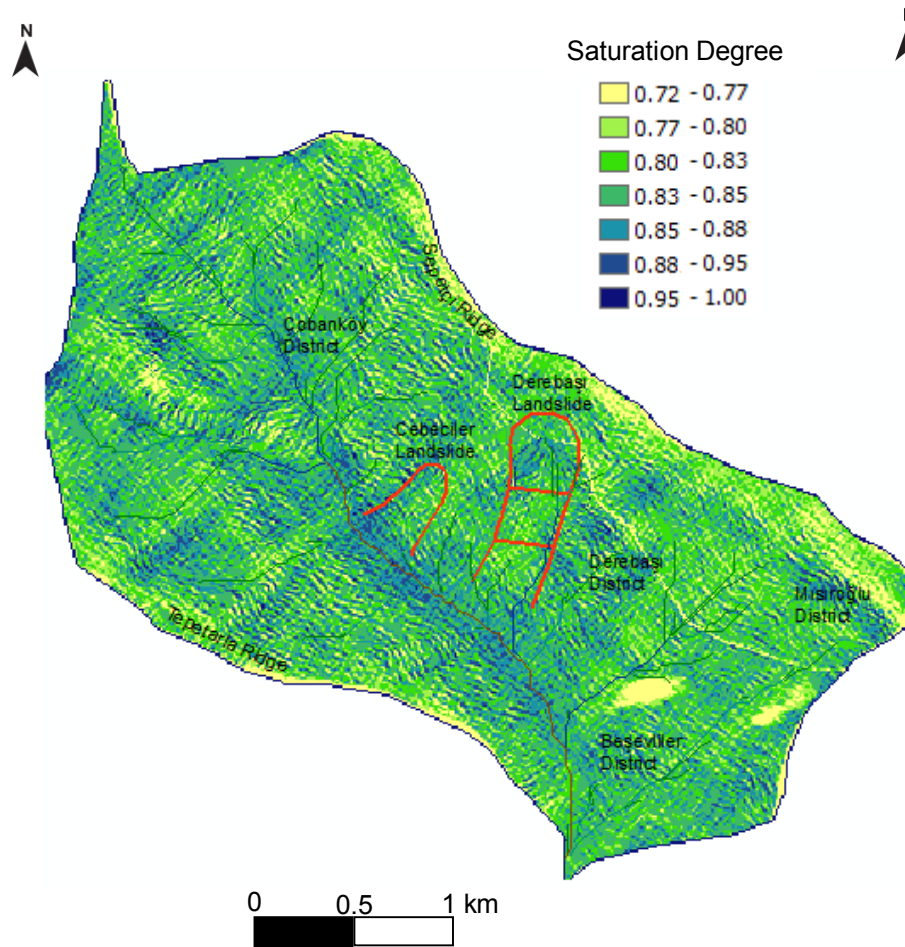


Figure 4.28.a) Saturation Degree Map of Yenice Watershed for the date 5 June 2000

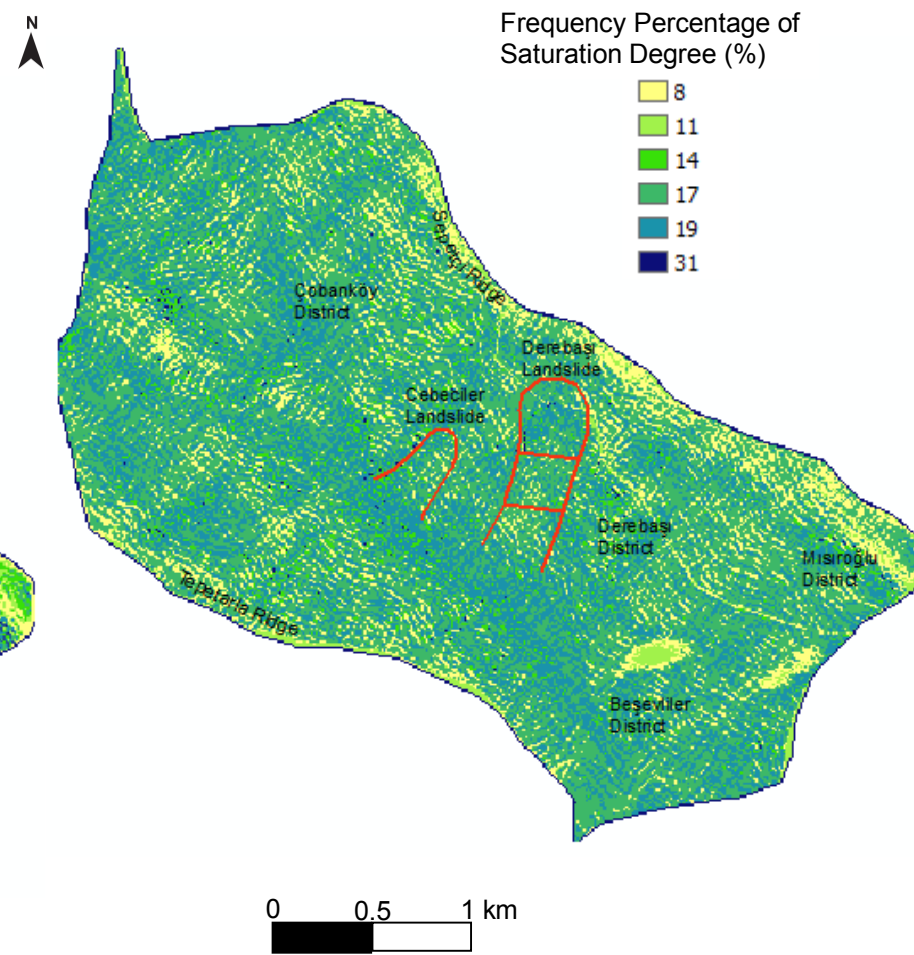


Figure 4.28.b) Saturation Degree Index Map of Yenice Watershed for the date 5 June 2000 (Reclassified)

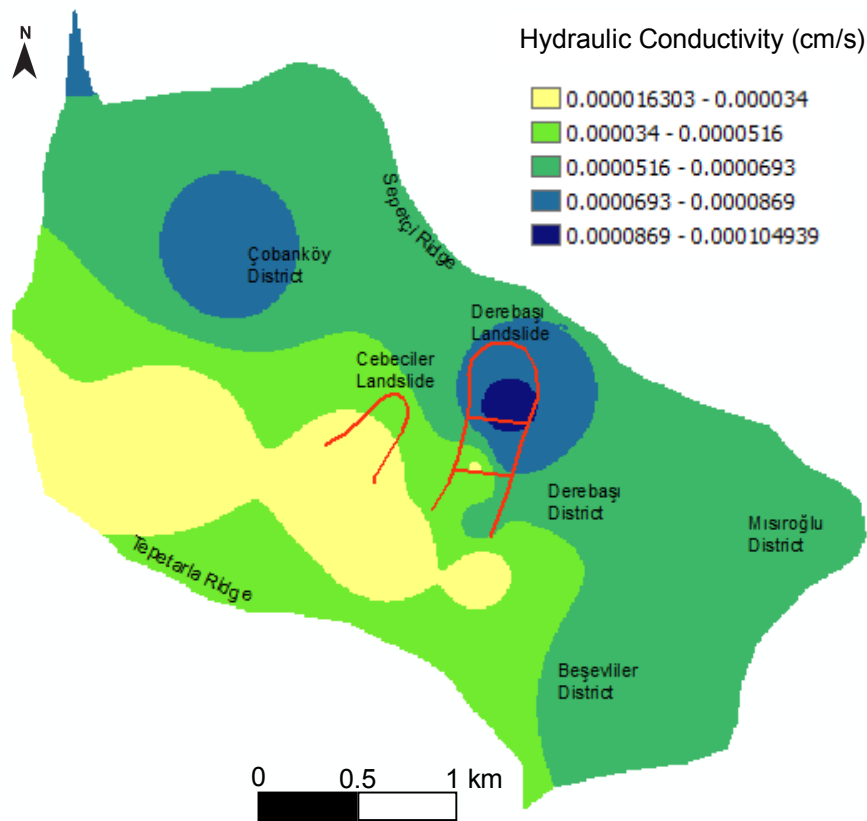


Figure 4.29.a) Hydraulic Conductivity Map of Yenice Watershed

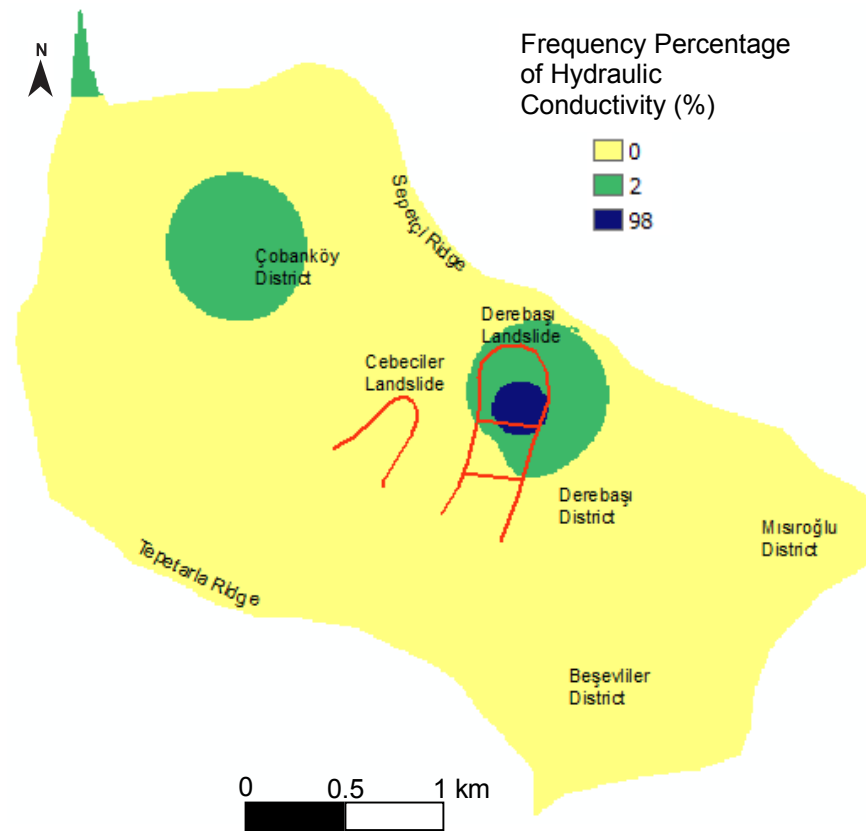


Figure 4.29.b) Soil Type Index Map of Yenice Watershed (Reclassified)

The reason for observation of circle-like geometries in Figure 4.29 is due to the limited number of samples tested. Unclassified landslide susceptibility map generated by weighted parameter values determined from Table 4.14 using the eq.4.30 is shown on Figure 4.30.

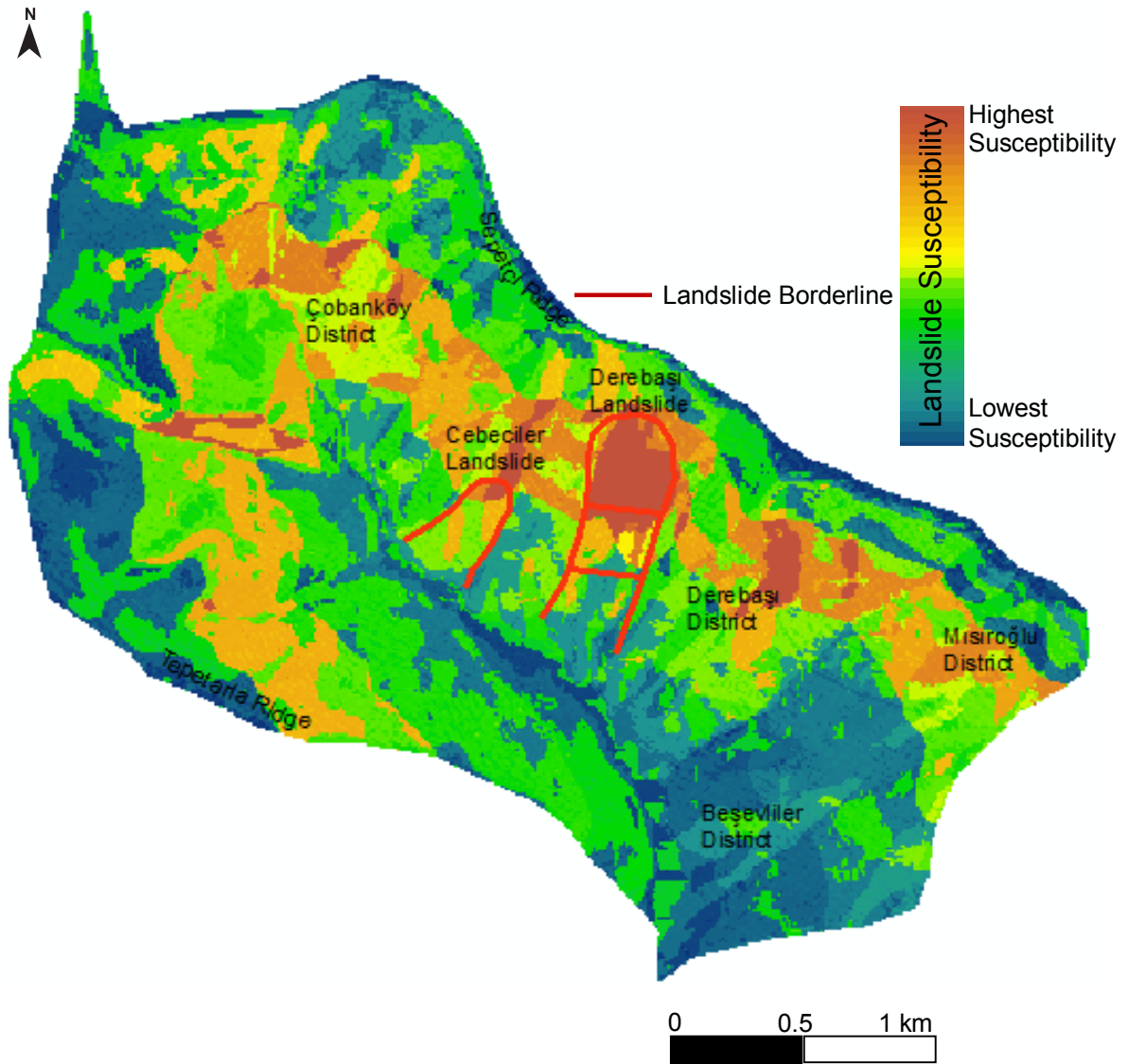


Figure 4.30: Unclassified landslide susceptibility map of Yenice Watershed computed by the eq. 4.30.

In this map (Figure 4.30), landslide susceptibility value represents the relative susceptibility to landslide occurrence, as higher values are associated with landslide susceptibility.

After reclassification process, the ultimate landslide susceptibility map is prepared in which the saturation degree index is utilized as a parameter (Fig. 4.31).

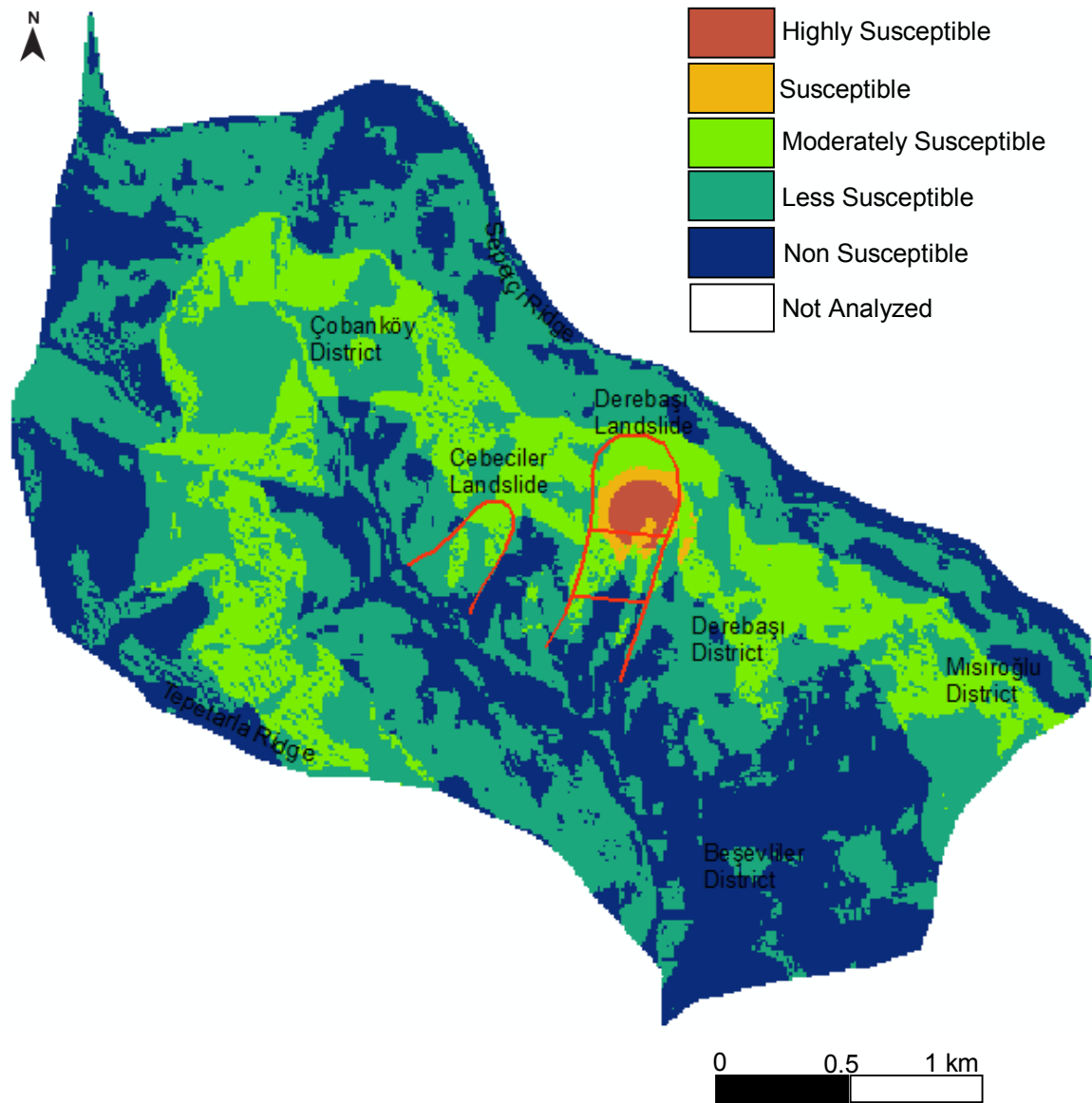


Figure 4.31: Ultimate landslide susceptibility map of Yenice Watershed generated with saturation degree index and determined after reclassification process

To emphasize the importance of the spatio-temporal water effect on landslide susceptibility phenomenon, the landslide susceptibility map is recalculated with equation 4.31 (Fig. 4.32). So, the ultimate Landslide Susceptibility (LS),

$$LS = Fr(\text{Slope Index}) + Fr(\text{Aspect Index}) + Fr(\text{Elevation Index}) + Fr(\text{TWI}) + Fr(\text{Soil Type Index}) + Fr(\text{Permeability Index}) \quad (\text{eq. 4.31})$$

Equation 4.31 involves only spatial parameters as well as the topographic wetness index (eq. 1.1) by contrast with Equation 4.30.

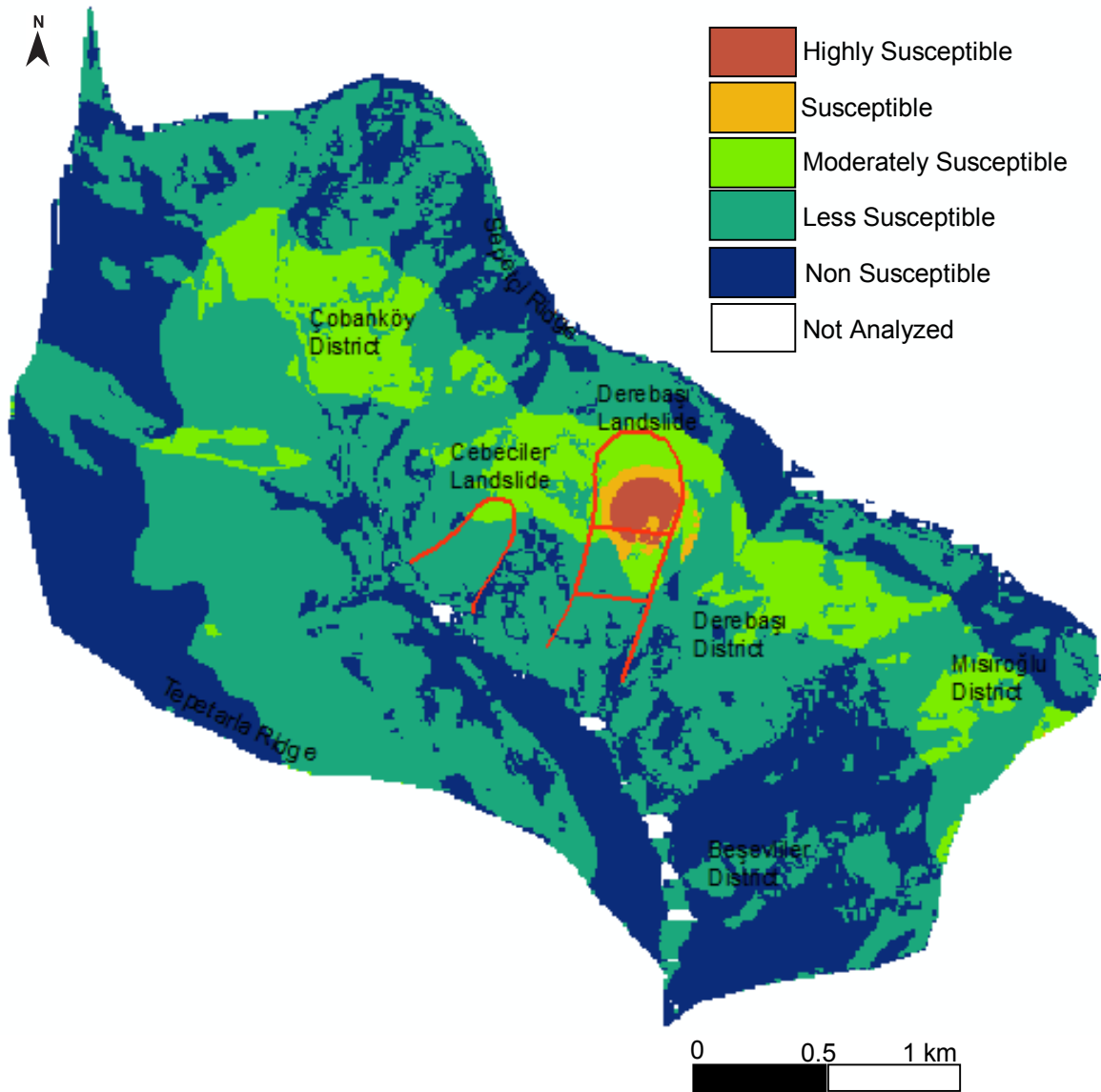


Figure 4.32: Landslide susceptibility map of Yenice Watershed generated with topographic wetness index

Comparing landslide susceptibility maps obtained using TWI (computed by eq. 4.30) and using SDI (computed by eq. 4.31) illustrates that the effect of saturation degree index is more accurate in Yenice Watershed especially for Derebaşı Landslide (see Figs. 4.31 and 4.32). This is because TWI is valid only for steady-state rainfall conditions as proposed by Moore et al. [21]. For this reason, expressing the landslide susceptibility spatially and temporally, reflects the triggering mechanisms and hydrodynamic processes. In addition, topographic wetness index cannot be calculated for the horizontal cells using the equation 1.1. Consequently,

in Figure 4.32 the landslide susceptibility values are undefined for the pixels where slope is zero.

To generate a mathematical expression including the saturation degree (SD) and saturation degree index (SDI) for utilization in landslide susceptibility concept, saturation degree index chart is composed (Fig. 4.33) from the Table 4.15.

Table 4.15: Spatial relationship between saturation degree and saturation degree index

Saturation Degree Class	Number of Pixels Without Landslide	Ratio-a (%)	Number of Pixels With Landslide	RATIO-b (%)	Frequency Ratio (b/a)	Saturation Degree Index
0.70-0.75	1281	1.69	12	1.14	0.68	0.11
0.75-0.80	10014	13.23	68	6.48	0.49	0.08
0.80-0.85	36291	47.94	523	49.86	1.04	0.17
0.85-0.90	24575	32.46	399	38.04	1.17	0.19
0.90-0.95	3168	4.18	37	3.53	0.84	0.14
0.95-1.00	370	0.49	10	0.95	1.95	0.31

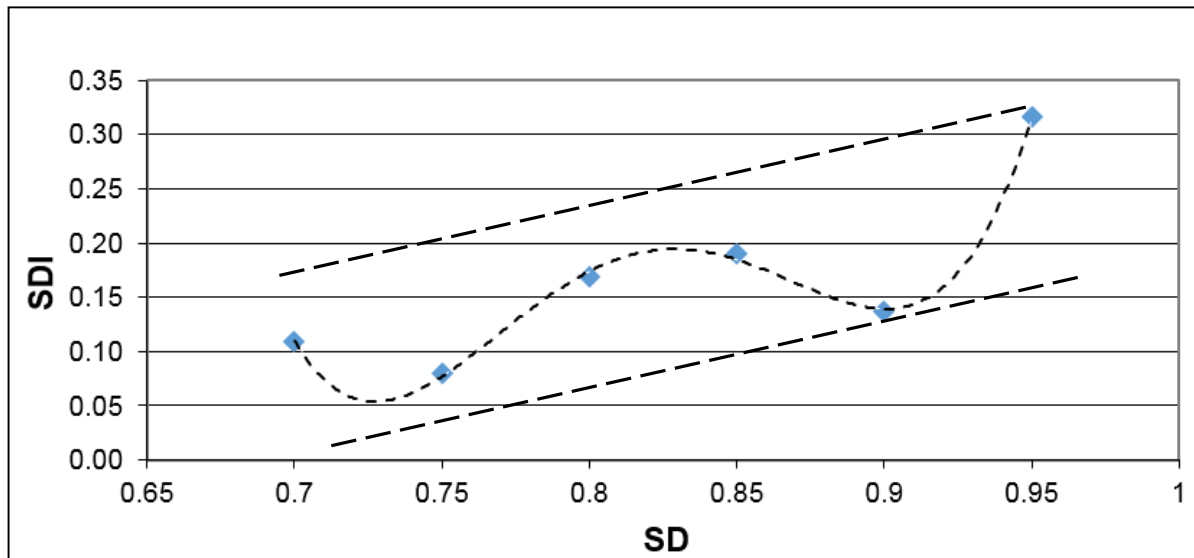


Figure 4.33: Relationship chart between the Saturation Degree Index (SDI) and Saturation Degree (SD)

The equation of the curve on the Figure 4.33 is;

$$SDI = 1648.1 \times SD^4 - 5398.3 \times SD^3 + 6605.7 \times SD^2 - 3578.3 \times SD + 724.07$$

(eq. 4.32)

Equation 4.32 can be expressed as a 3rd degree or 4th degree polynomial expression of the saturation degree index as a function of saturation degree between the upper and lower bound as shown in Figure 4.33. The coefficient of correlation for this equation is 0.99, best fitting the SD-SDI relationship. However, the equation 4.32 is valid only in Yenice Watershed especially for Derebaşı Landslide.

On the other hand, the utilization of Saturation Degree Index (SDI) employing with the frequency ratio analysis method is more realistic comparing with the utilization of topographic wetness index.

Furthermore, to verify the validity of using Saturation Degree Index (SDI), the same methodology was followed for Cebeciler Landslide too. The occurrence date of the Cebeciler landslide is unknown but year is recorded as 1998 by General Directorate of Natural Disaster [118] in the geological investigation report. Therefore, monthly mean meteorological data were compiled to identify landslide susceptibility maps for 12 months of the year 1998 (Fig. 4.34a, 4.34b, 4.35a, 4.35b, 4.36a, 4.36b, 4.37a, 4.37b, 4.38a, 4.38b, 4.39a, 4.39b, 4.40a, 4.40b, 4.41a, 4.41b, 4.42a, 4.42b, 4.43a, 4.43b, 4.44a, 4.44b, 4.45a, 4.45b). In this way, the estimation of occurring month of the Cebeciler landslide was targeted.

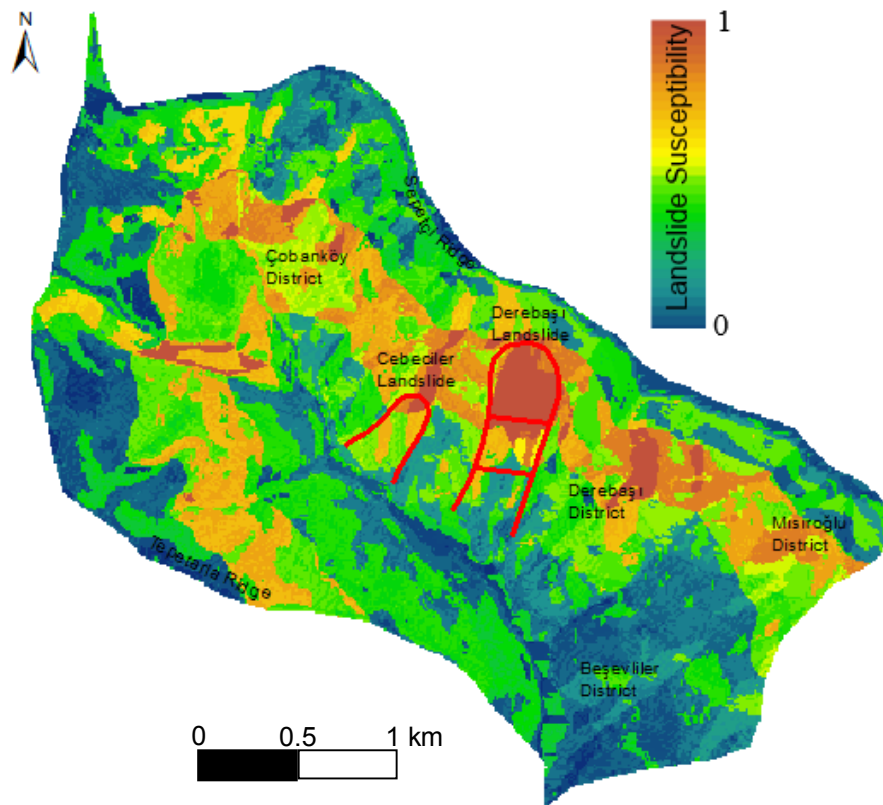


Figure 4.34a) Unclassified landslide susceptibility map of Yenice Watershed for January 1998

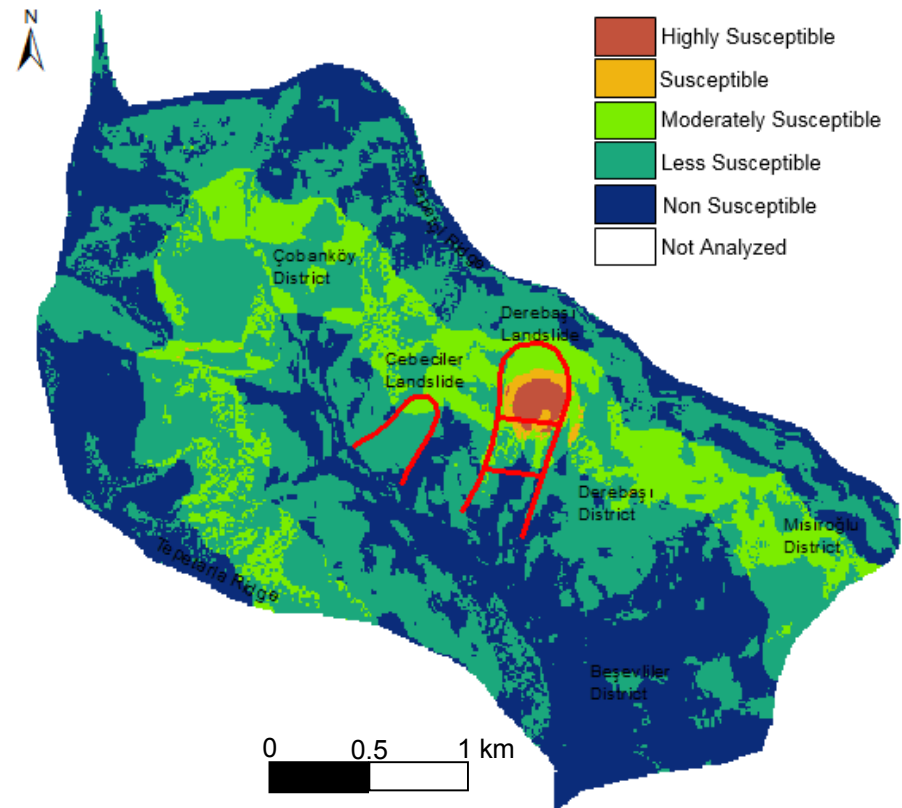


Figure 4.34b) Classified landslide susceptibility map of Yenice Watershed for January 1998

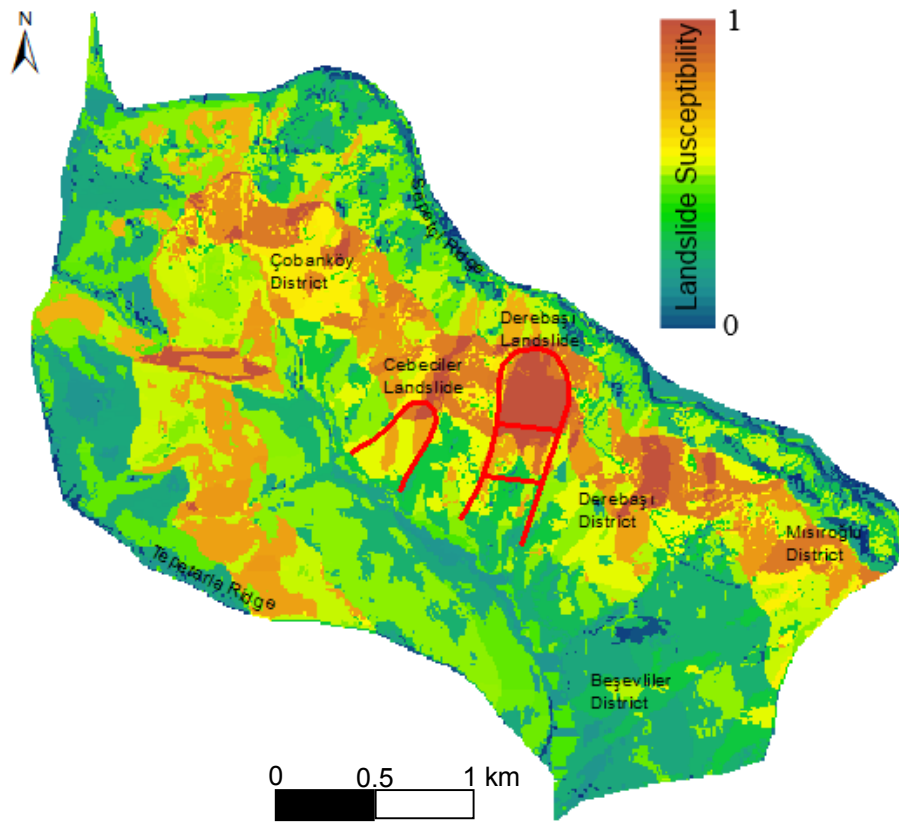


Figure 4.35a) Unclassified landslide susceptibility map of Yenice Watershed for February 1998

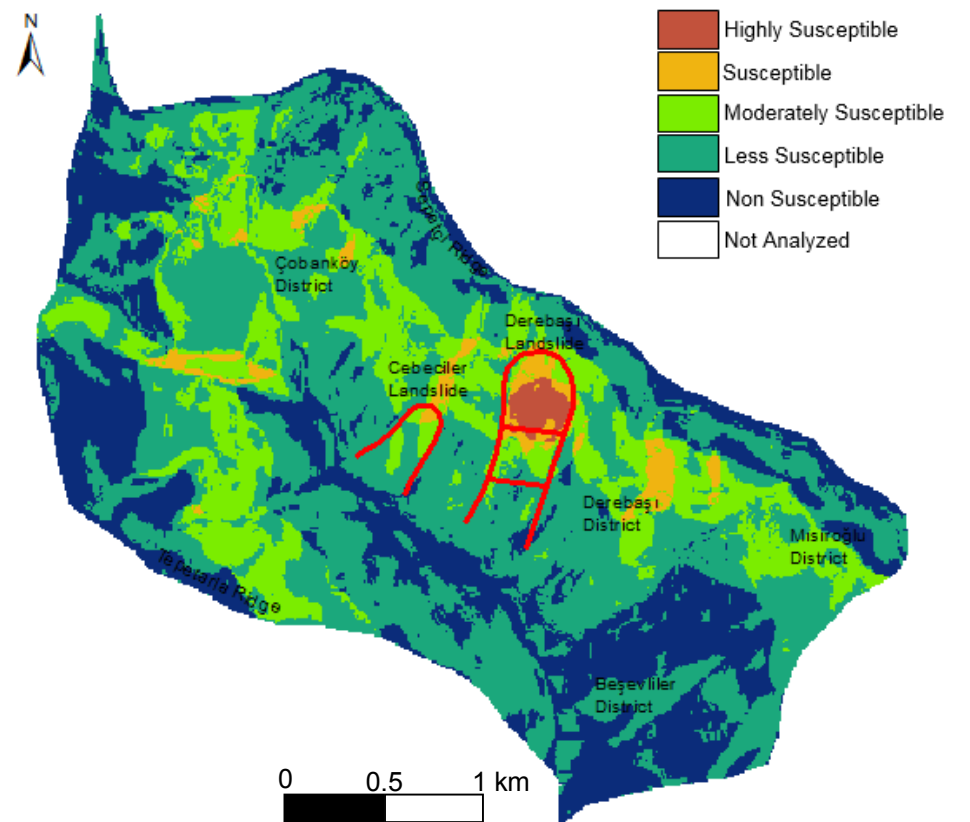


Figure 4.35b) Classified landslide susceptibility map of Yenice Watershed for February 1998

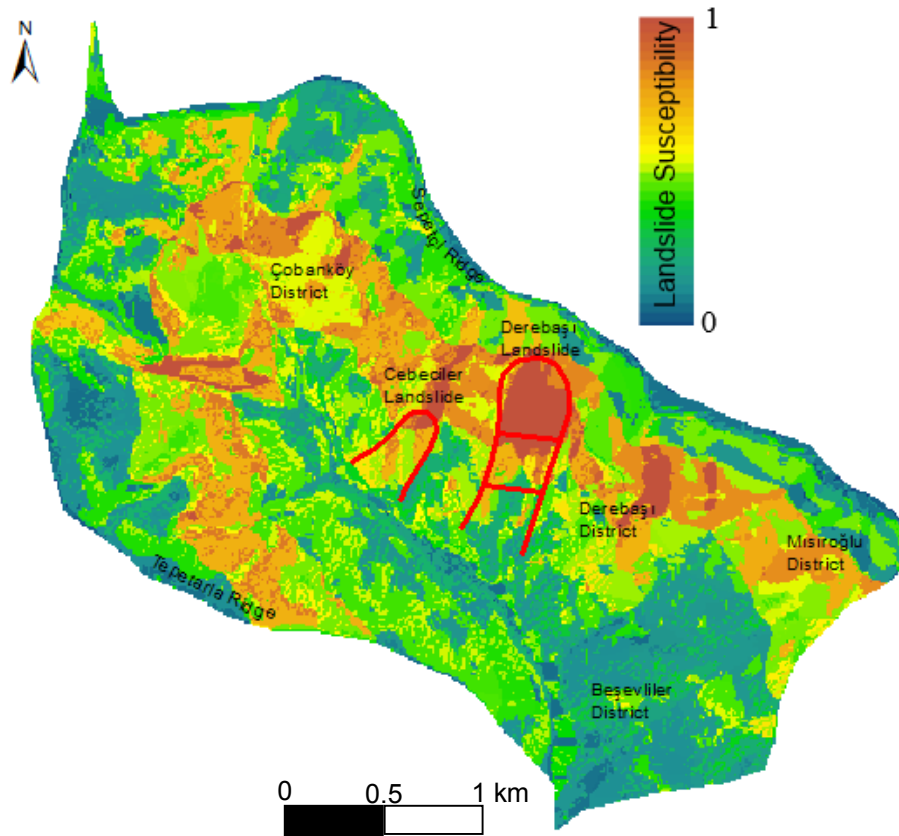


Figure 4.36a)Unclassified landslide susceptibility map of Yenice Watershed for March 1998

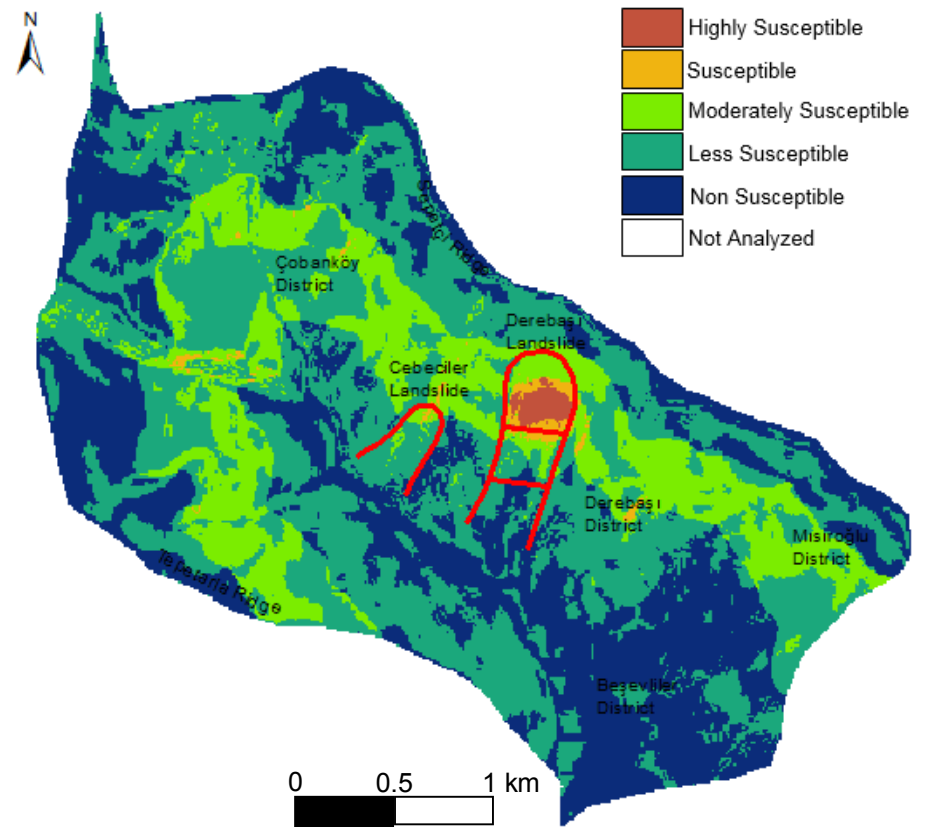


Figure 4.36b)Classified landslide susceptibility map of Yenice Watershed for March 1998

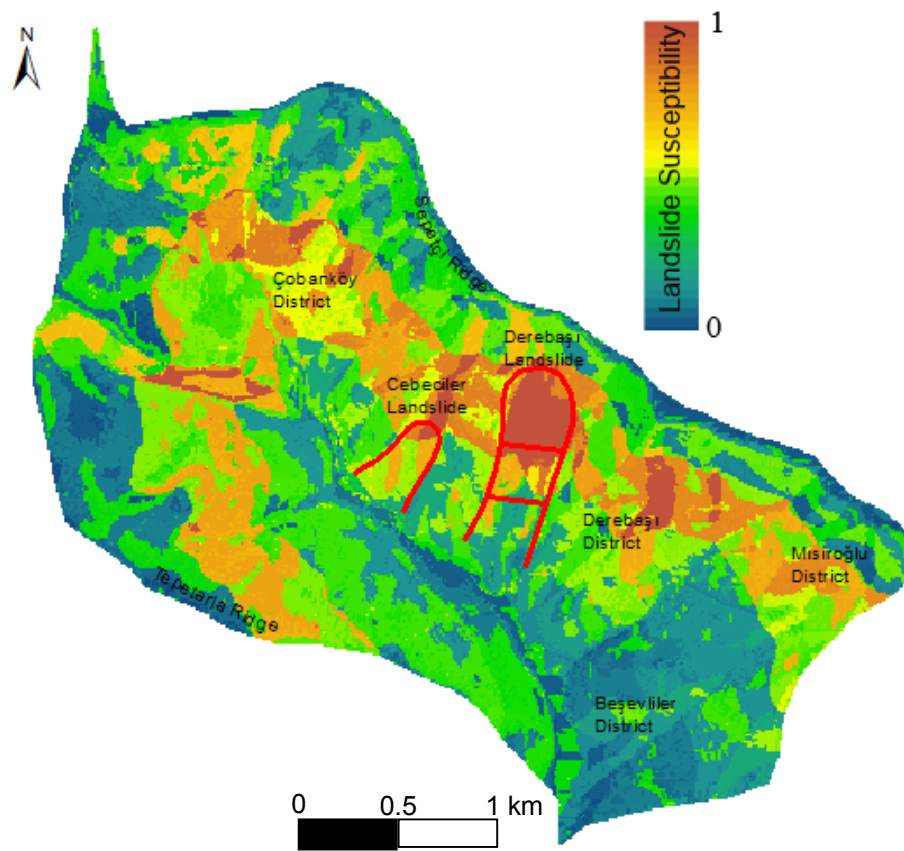


Figure 4.37a)Unclassified landslide susceptibility map of Yenice Watershed for April 1998

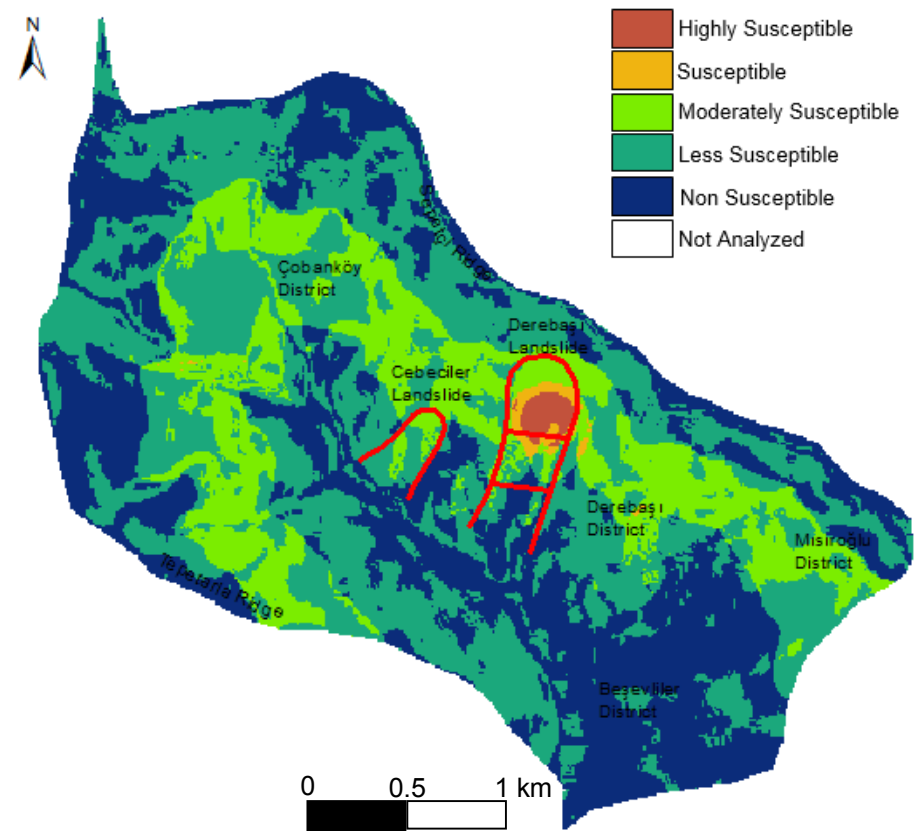


Figure 4.37b)Classified landslide susceptibility map of Yenice Watershed for April 1998

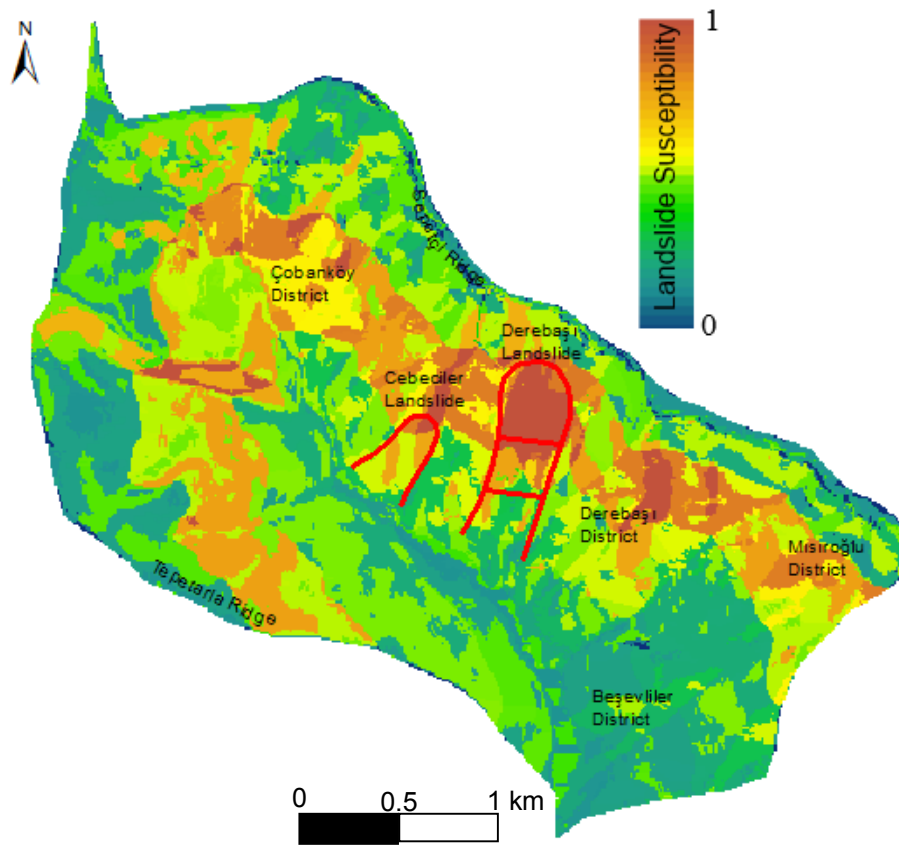


Figure 4.38a)Unclassified landslide susceptibility map of Yenice Watershed for May 1998

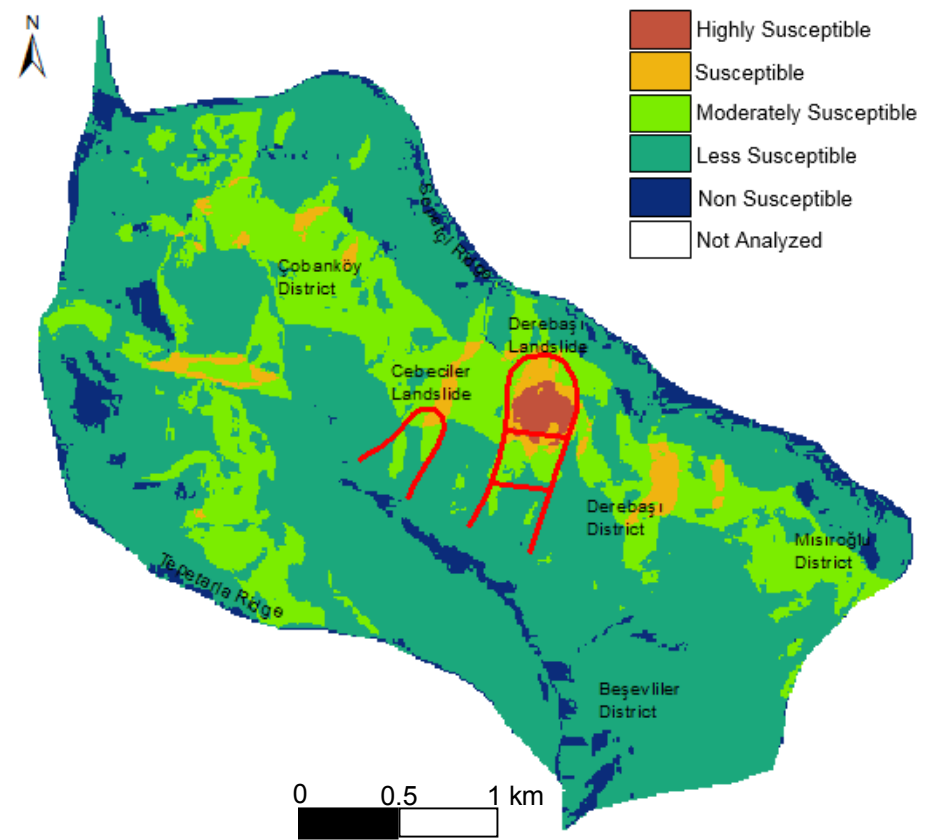


Figure 4.38b)Classified landslide susceptibility map of Yenice Watershed for May 1998

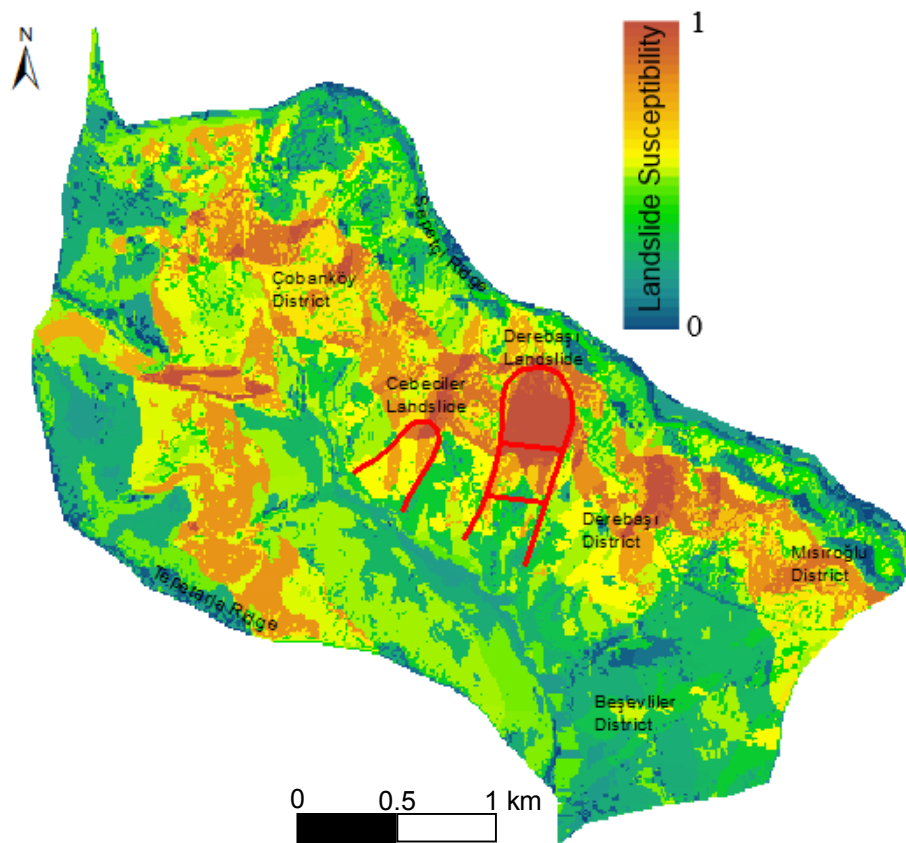


Figure 4.39a)Unclassified landslide susceptibility map of Yenice Watershed for June 1998

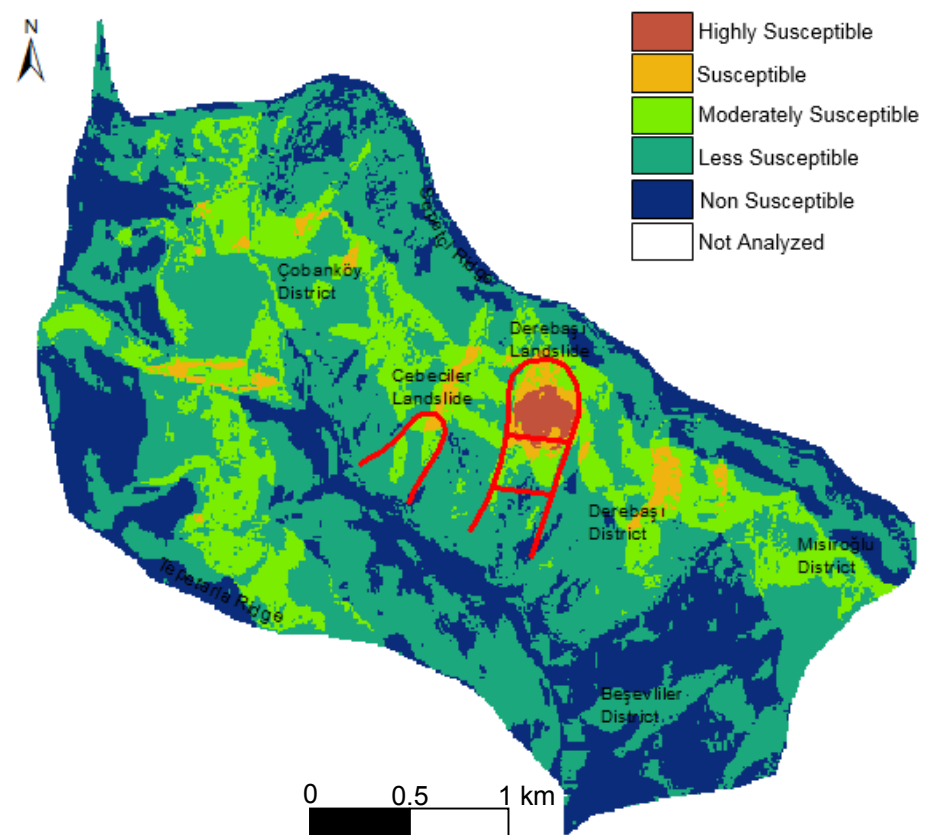


Figure 4.39b)Classified landslide susceptibility map of Yenice Watershed for June 1998

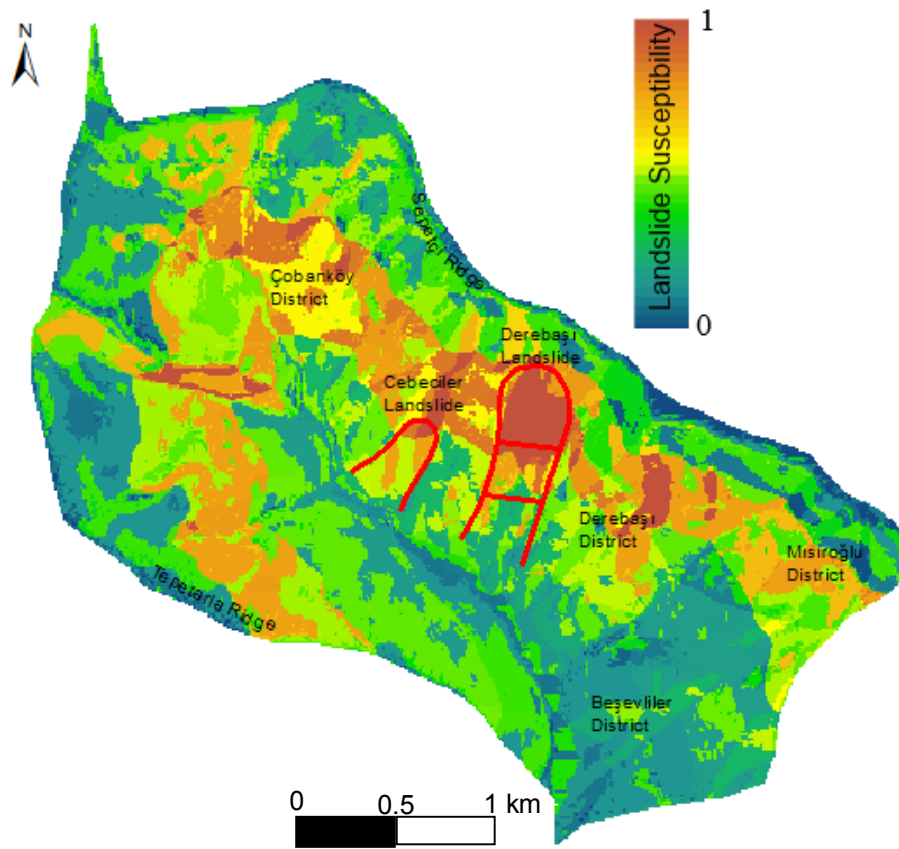


Figure 4.40a)Unclassified landslide susceptibility map of Yenice Watershed for July 1998

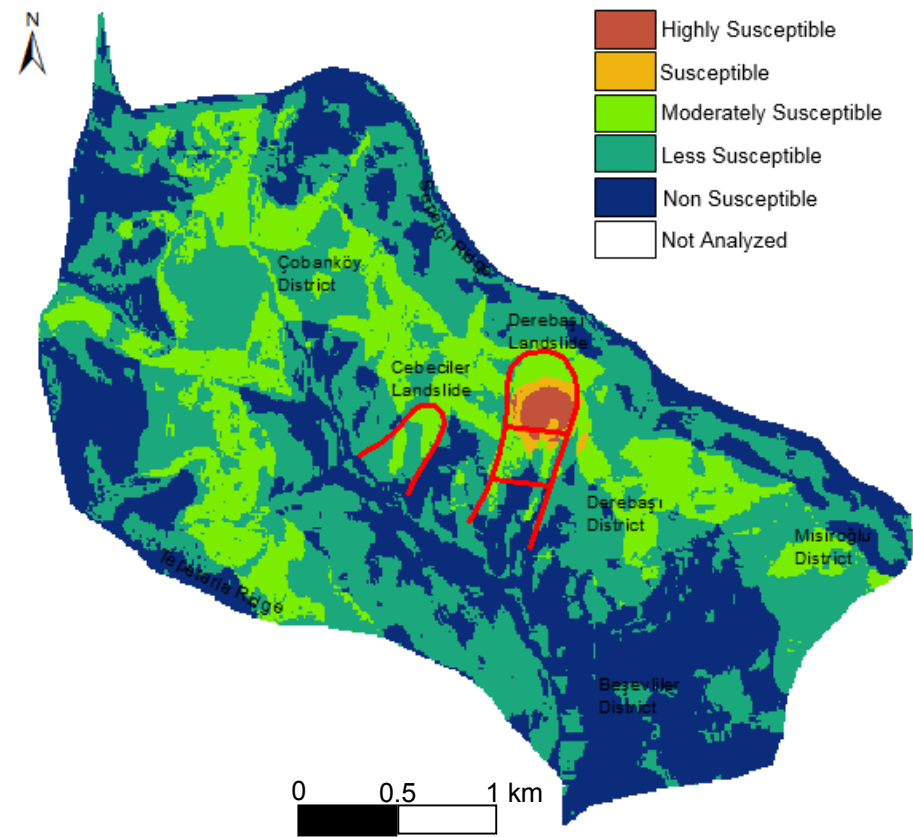


Figure 4.40b)Classified landslide susceptibility map of Yenice Watershed for July 1998

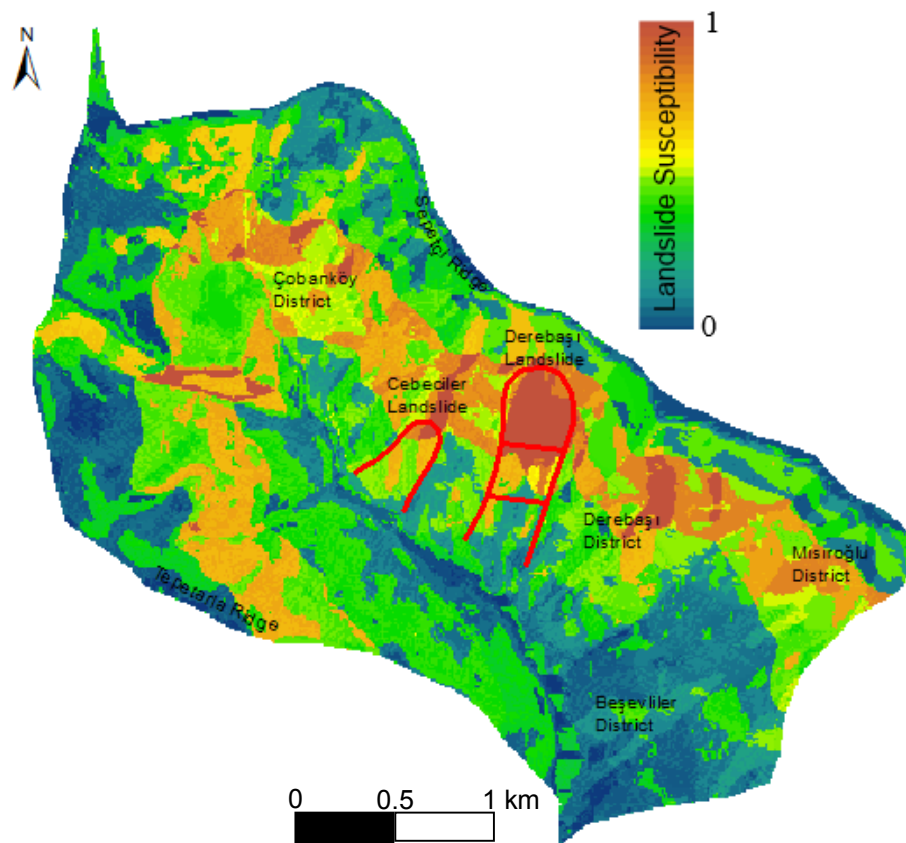


Figure 4.41a) Unclassified landslide susceptibility map of Yenice Watershed for August 1998

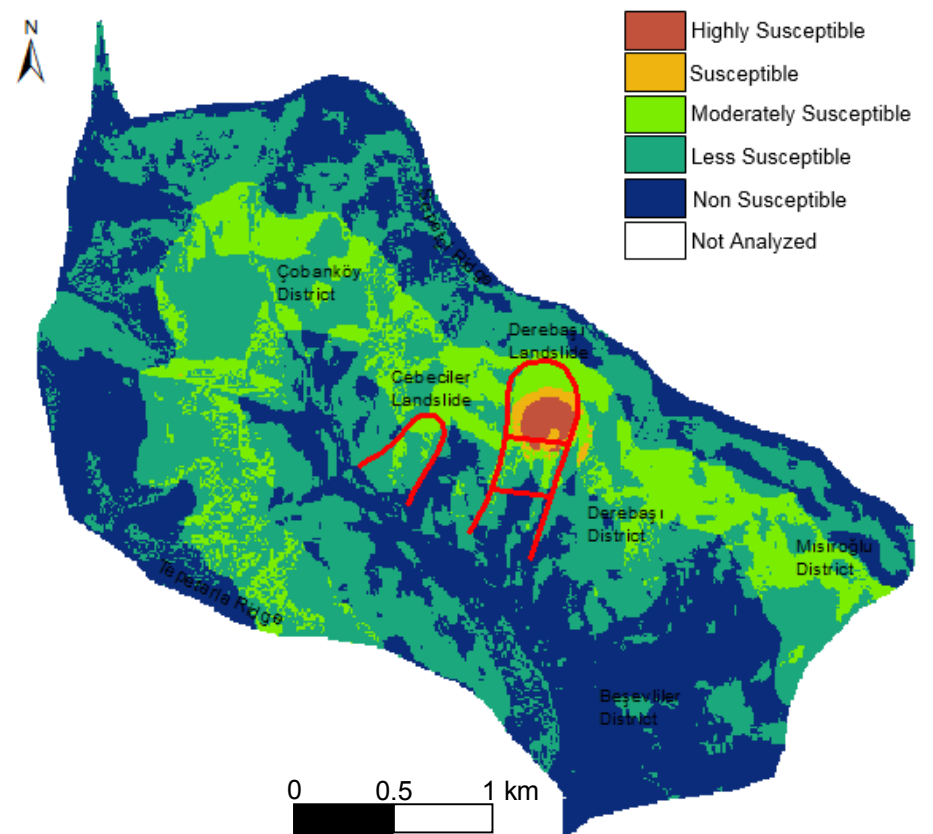


Figure 4.41b) Classified landslide susceptibility map of Yenice Watershed for August 1998

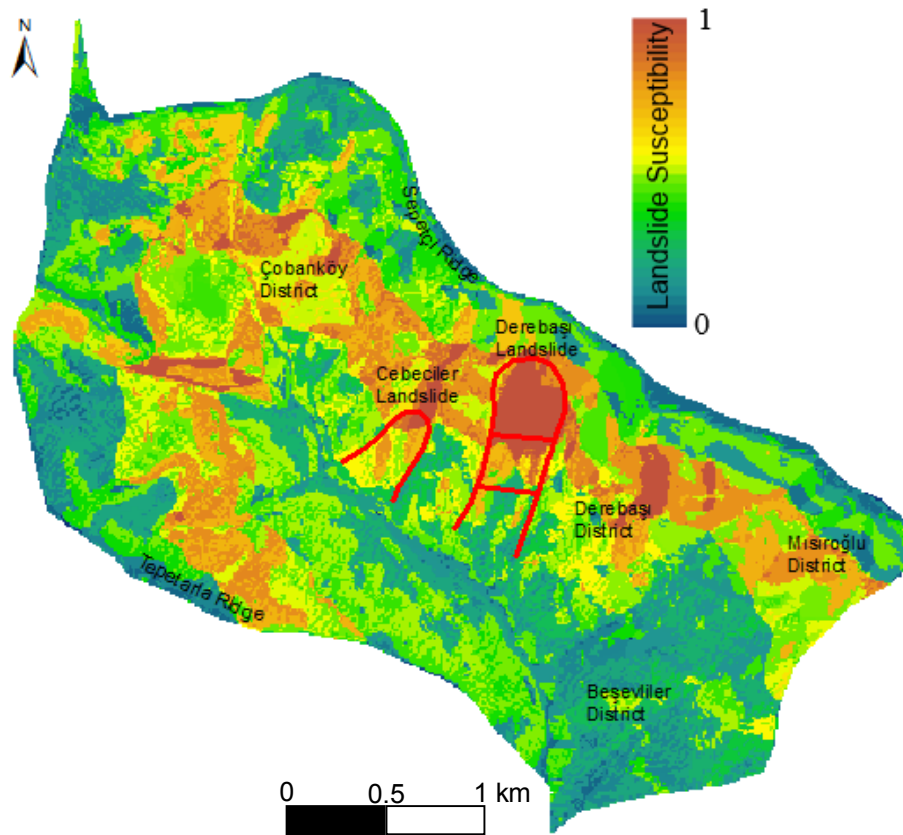


Figure 4.42a) Unclassified landslide susceptibility map of Yenice Watershed for September 1998

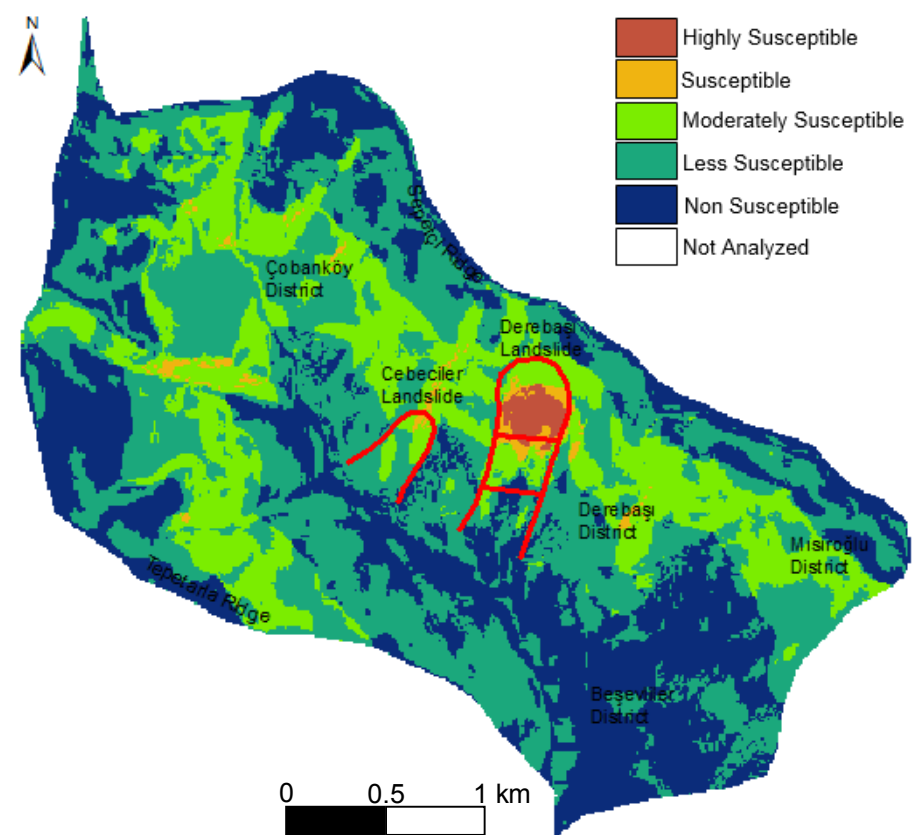


Figure 4.42b) Classified landslide susceptibility map of Yenice Watershed for September 1998

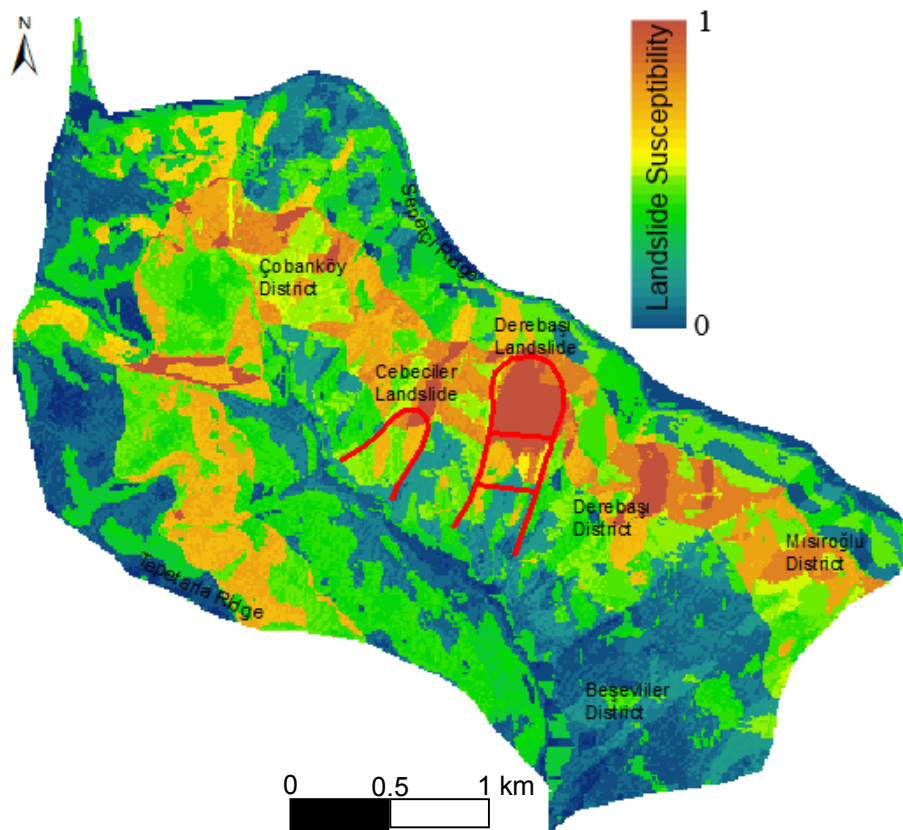


Figure 4.43a) Unclassified landslide susceptibility map of Yenice Watershed for October 1998

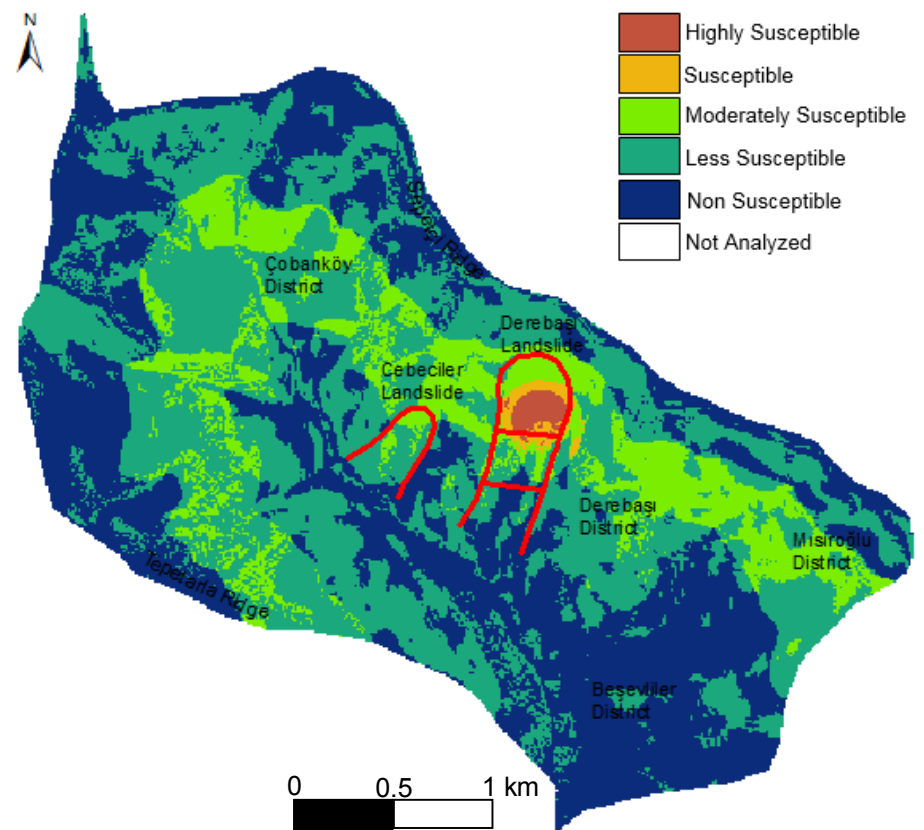


Figure 4.43b) Classified landslide susceptibility map of Yenice Watershed for October 1998

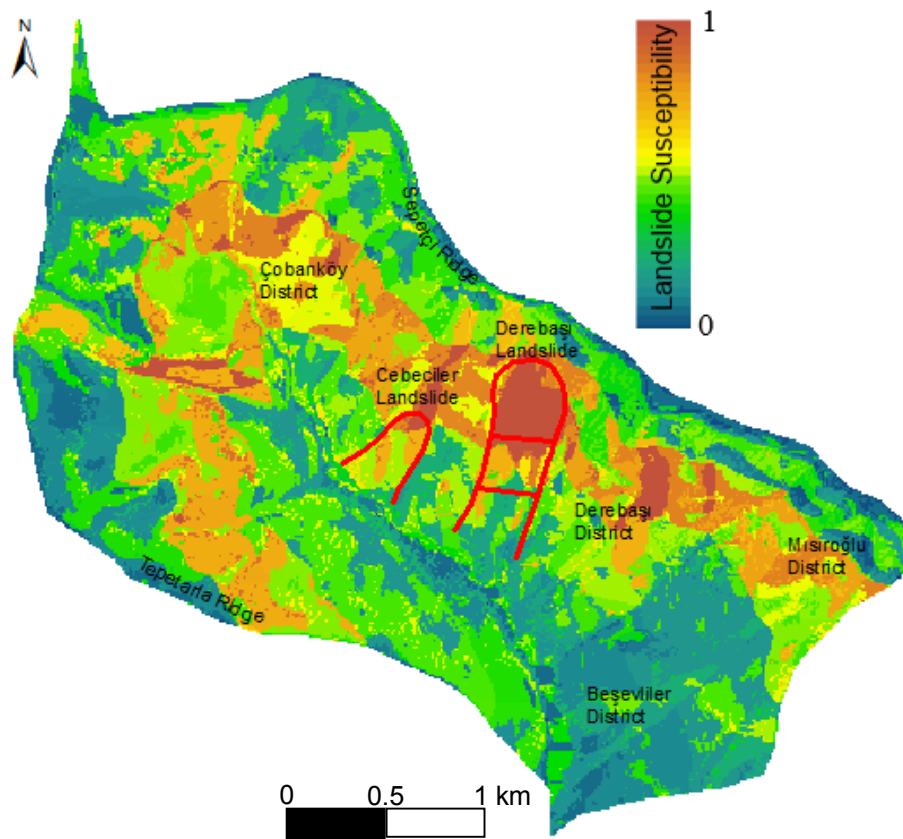


Figure 4.44a) Unclassified landslide susceptibility map of Yenice Watershed for November 1998

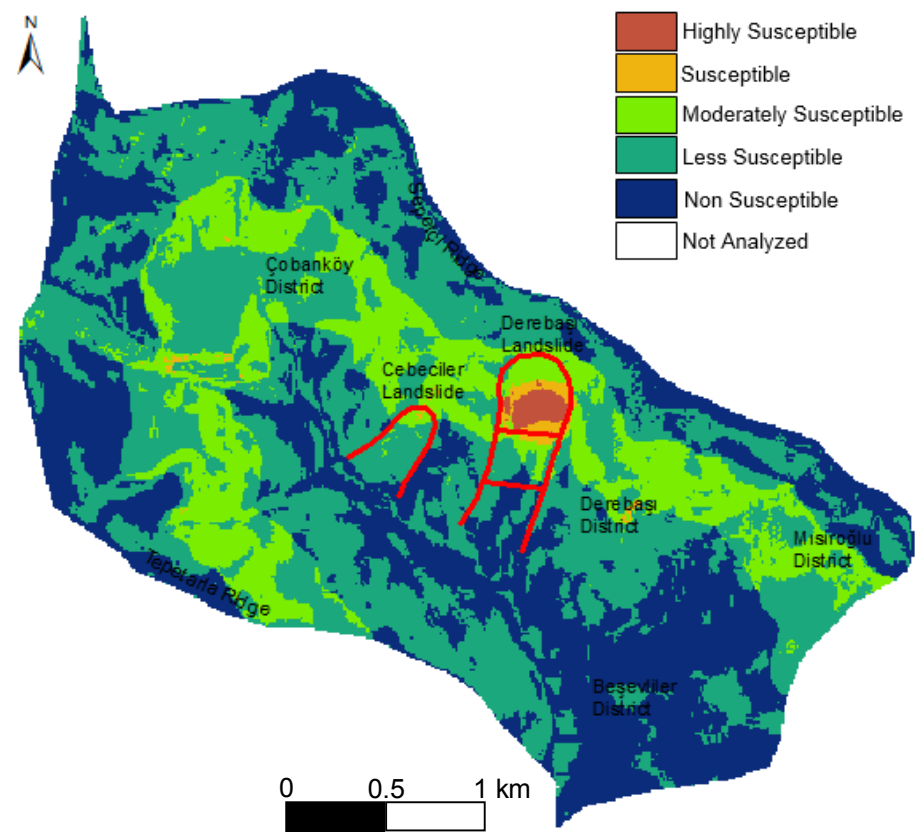


Figure 4.44b) Classified landslide susceptibility map of Yenice Watershed for November 1998

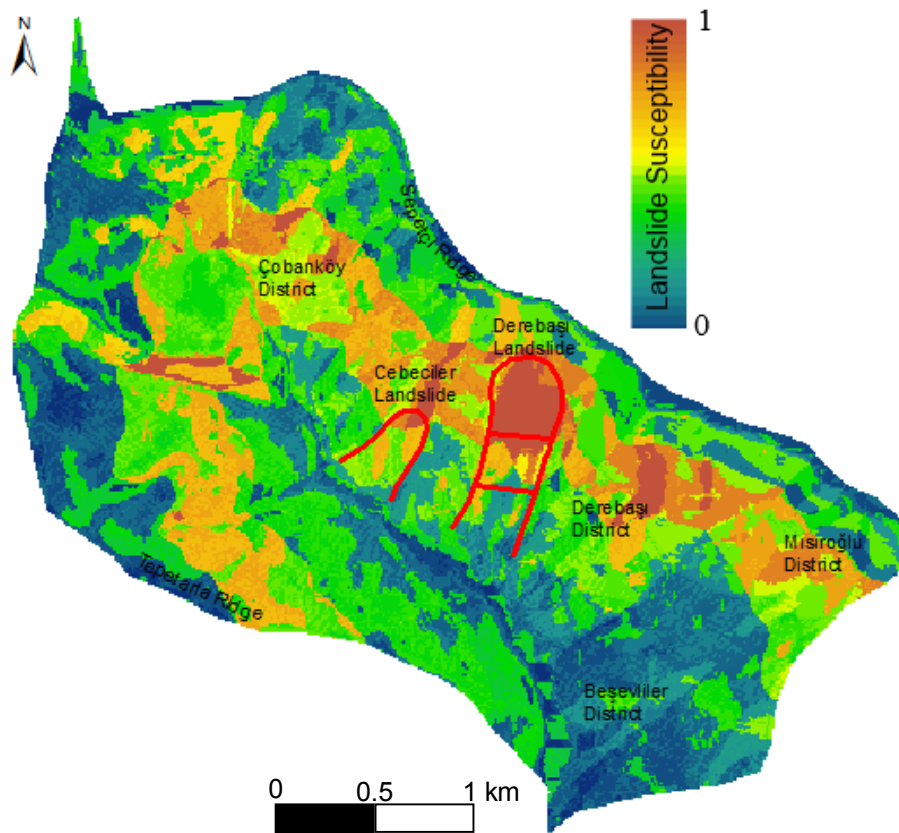


Figure 4.45a) Unclassified landslide susceptibility map of Yenice Watershed for December 1998

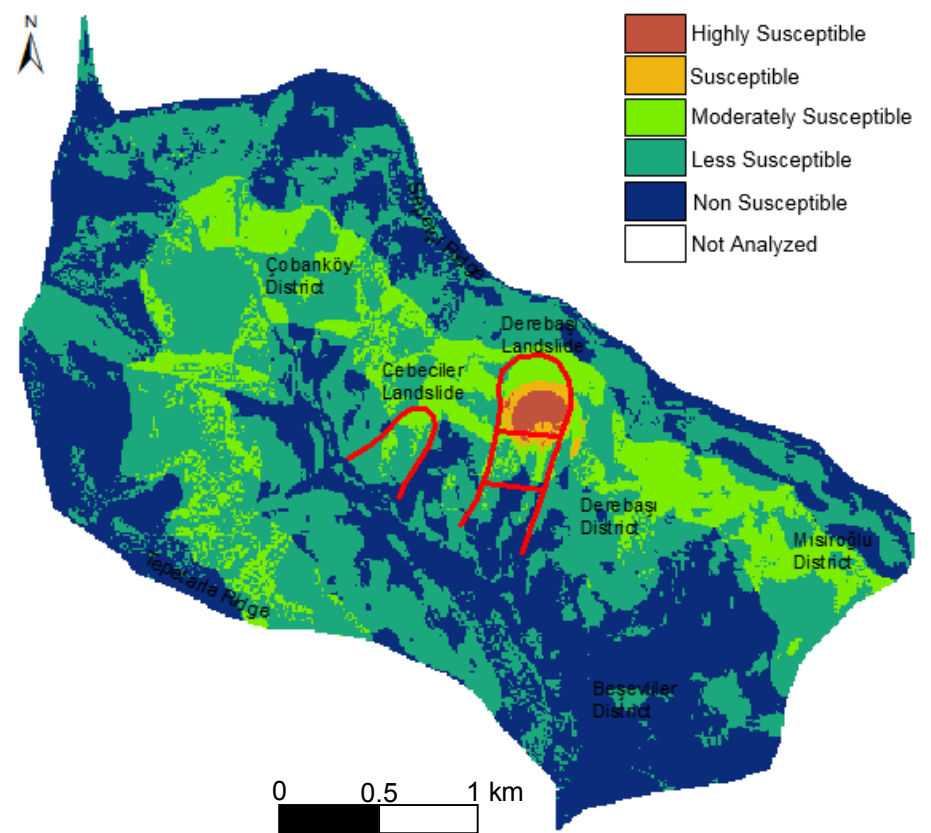


Figure 4.45b) Classified landslide susceptibility map of Yenice Watershed for December 1998

The spatial patterns of monthly landslide susceptibility in Yenice Watershed for the year 1998 are presented in the Figures 4.34a, 4.34b, 4.35a, 4.35b, 4.36a, 4.36b, 4.37a, 4.37b, 4.38a, 4.38b, 4.39a, 4.39b, 4.40a, 4.40b, 4.41a, 4.41b, 4.42a, 4.42b, 4.43a, 4.43b, 4.44a, 4.44b, 4.45a and 4.45b. It is observed that May is the most susceptible month of the year 1998 in Yenice Watershed for the Cebeciler landslide (see Figs. 4.38a and b). This result can be interpreted as the spatio-temporal frequency analysis approach using with saturation degree index for 12 months is valid also for the Cebeciler landslide (see Figs. 4.38a and b). By virtue of these results, a new approach for landslide susceptibility is proposed in order to reflect the temporal effects of water in terms of saturation degree for a watershed. For the application of this approach SMDR model executed with all the available monthly average meteorological data (1989 – 2009 for Yenice Watershed) and frequency ratio analysis is processed.

5. RESULTS and CONCLUSIONS

Throughout this study, a new perspective is proposed for existing landslide susceptibility concept in order to reflect the water effect in terms of saturation degree. In other words, a new index called as “saturation degree index” SDI is considered to integrate the surface water effect into the ordinary landslide susceptibility phenomenon. The following results and conclusions can be drawn from the present study;

- A new procedure is considered to produce spatio-temporal landslide susceptibility map. This procedure utilizes SMDR model and frequency ratio analysis in order to take into account the effect of water more deterministic point of view.
- Based on the seismic information obtained from “Kandilli Observatory and Earthquake Research Institute”, there was no significant earthquake record at or just before the occurrence date of Derebaşı landslide (Appendix 1), so the earthquake probability is discarded as triggering factor for Derebaşı Landslide. Additionally, no evidence or information was found about the human activity to trigger the Derebaşı landslide. On the other hand, there was not a heavy rainfall for a period of 10 days before the date of occurrence of the Derebaşı landslide (Table 4.13). Consequently, it is believed that the only triggering factor for the Derebaşı landslide could be the variance of the water flux in terms of saturation degree. To determine the saturation degree map in Yenice Watershed, SMDR model based on the saturation excess runoff phenomenon is performed. With this study it is expected to compensate the lack of spatial and temporal water effect on landslide susceptibility mapping.
- Topographic wetness index (TWI) is a conventional parameter which represents the spatial variations of water effect in a watershed. However, it is deduced that TWI cannot represent hydrodynamic processes due to its rendering intent. Additionally, this index is proposed for determining the wetness variations of large scaled watersheds under steady state rainfall conditions [21]. Furthermore, the TWI map of Yenice Watershed indicates that this index is not totally meaningful considering triggering mechanism of the Derebaşı and Cebeciler landslides (see Figs. 4.26a and b).

- The saturation degree map of Yenice Watershed for the occurrence date of the Derebaşı landslide was produced by SMDR model. The analysed saturation degree map shows that the Derebaşı landslide is triggered from zone-1 of landslide area (Table 4.13). Additionally, hydrological models based on the variable source area concept clarify more accurately the triggering processes of landsliding in context of landslide susceptibility phenomena.
- A mathematical relation is tried to be composed in order to standardise the water effect on landslide susceptibility as an index. Landslides are the result of interdependent spatio-temporal processes, including static and dynamic factors and so a mathematical expression must include both dynamic and static factors. However, static factors such as elevation, slope, aspect, topographic curvature, topographic wetness index, etc. vary spatially and remain steady temporally and dynamic (triggering) factors (e.g. earthquakes, water effect, human activities) vary temporally and remain steady spatially for a watershed scale. For this reason, it can be concluded that a mathematical expression relying on the landslide occurrence and dynamic parameters could not be composed.
- Slope angle, slope aspect, topographical elevation, soil type, permeability and saturation degree parameters were used as inputs for the frequency ratio analysis of landslide susceptibility mapping. Saturation degree index SDI and commonly used topographic wetness index TWI were utilized as input maps of frequency ratio analysis, and generated landslide susceptibility maps compared (see Figs. 4.31 and 4.32). Thus, it is considered that using SDI for landslide susceptibility is more effective, deterministic and accurate in terms of reflecting the temporal effect of water. In this way, it was possible to introduce a temporal dimension into the landslide susceptibility concept. In other words, up to present, landslide susceptibility phenomena answered the question “where”, but now, with this study landslide susceptibility phenomena may possibly enlighten the question “when”.
- SDI obtained from the methodology which combines the SMDR model with frequency ratio is tried to be expressed mathematically. And consequently, a mathematical relation is proposed (see eq. 4.32). However, this equation is

valid only in the Yenice Watershed especially for the Derebaşı landslide. Any analysis for any other watershed should be carried out with its own data.

- The methodology combining the SMDR model with frequency ratio is performed to handle the landslide susceptibility maps for each month of the year 1998. The obtained landslide susceptibility maps show noticeable difference in the Cebeciler landslide area and the most susceptible month for this area is May 1998 compared to other months (see Figs. 4.38 a and b). These monthly landslide susceptibility maps of the Yenice Watershed for the year 1998 indicate that the occurrence month of the Cebeciler landslide would most probably be May. The difference in the susceptibility in the Cebeciler landslide can be noticed at the crown (see Figs. 4.38 a and b). Thereby, the methodology suggested for the Derebaşı landslide in the Yenice Watershed has been verified for another area, the Cebeciler landslide.
- Finally, a new methodology is proposed using attainable meteorological data. The landslide susceptibility maps for 12 months were generated from the monthly mean meteorological data between the years 1989 – 2009 for Yenice Watershed (Figs 5.1a, 5.1b, 5.2a, 5.2b, 5.3a, 5.3b, 5.4a, 5.4b, 5.5a, 5.5b, 5.6a, 5.6b, 5.7a, 5.7b, 5.8a, 5.8b, 5.9a, 5.9b, 5.10a, 5.10b, 5.11a, 5.11b, 5.12a and 5.12b). These maps the most susceptible months are June and May, while September and November can be noticed as susceptible. This integrated approach is promising an incorporated methodology for better quantification of parameters and accurate representation of spatial and temporal landslide susceptibility. The aim of the study was to show the quantitative unbiased approach in the context of surface water effect uncertainties as a triggering factor for landslide susceptibility. Besides, Figures 4.34a, 4.34b, 4.35a, 4.35b, 4.36a, 4.36b, 4.37a, 4.37b, 4.38a, 4.38b, 4.39a, 4.39b, 4.40a, 4.40b, 4.41a, 4.41b, 4.42a, 4.42b, 4.43a, 4.43b, 4.44a, 4.44b, 4.45a and 4.45b validate the applicability of proposed methods, approaches and landslide susceptibility classification index.

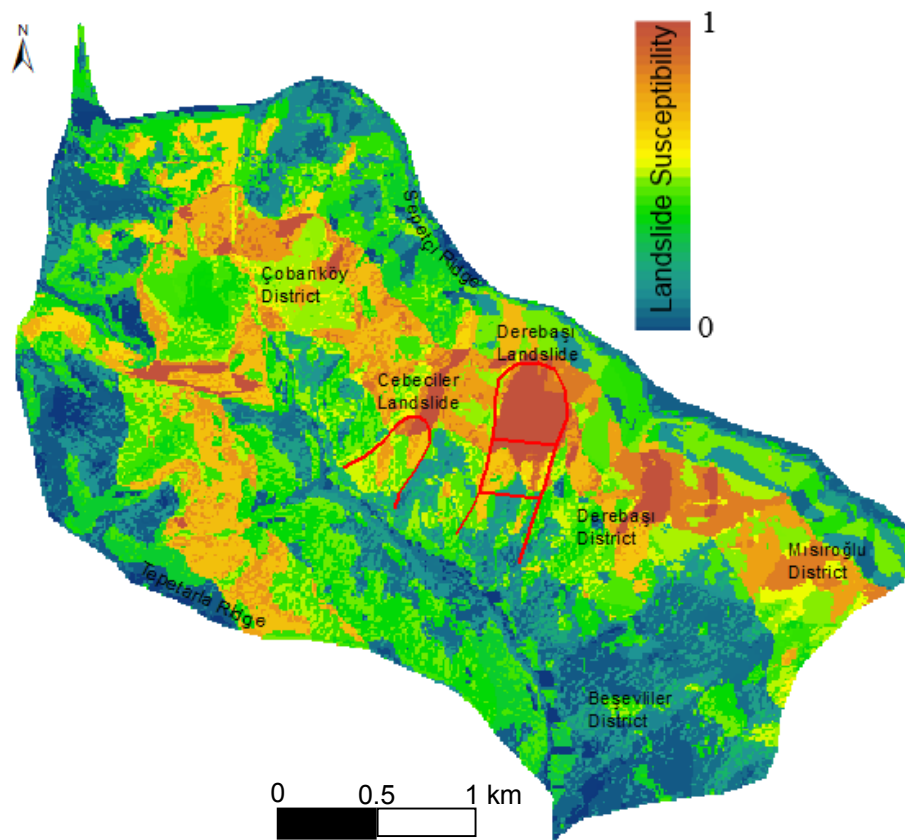


Figure 5.1a) Unclassified landslide susceptibility map of Yenice Watershed for January

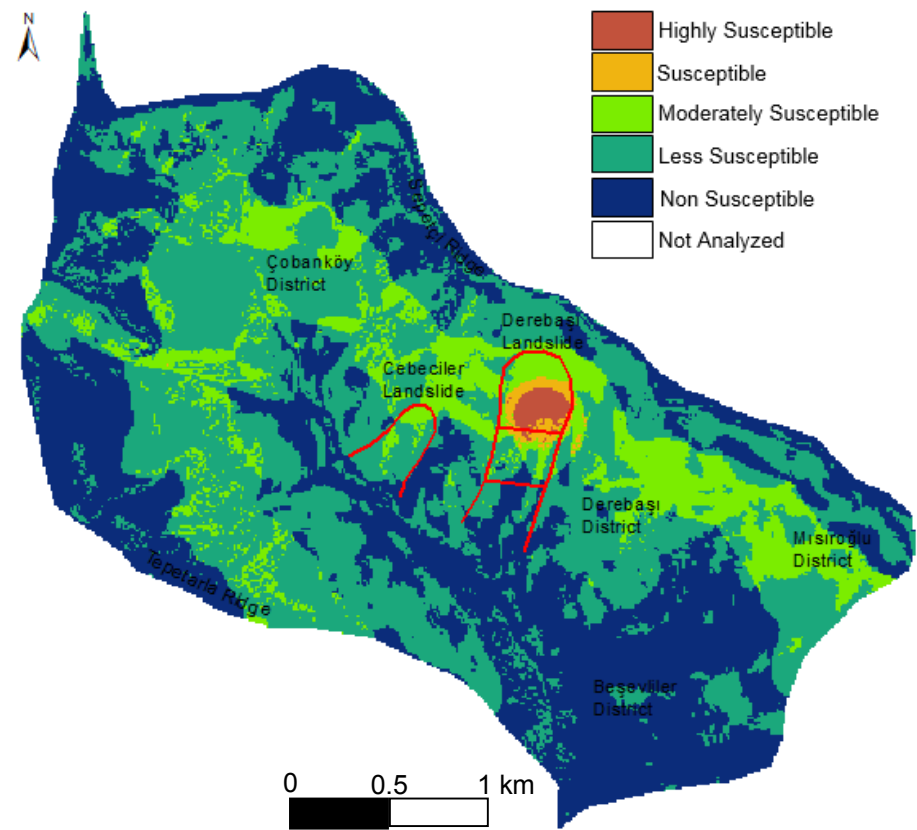


Figure 5.1b) Classified landslide susceptibility map of Yenice Watershed for January

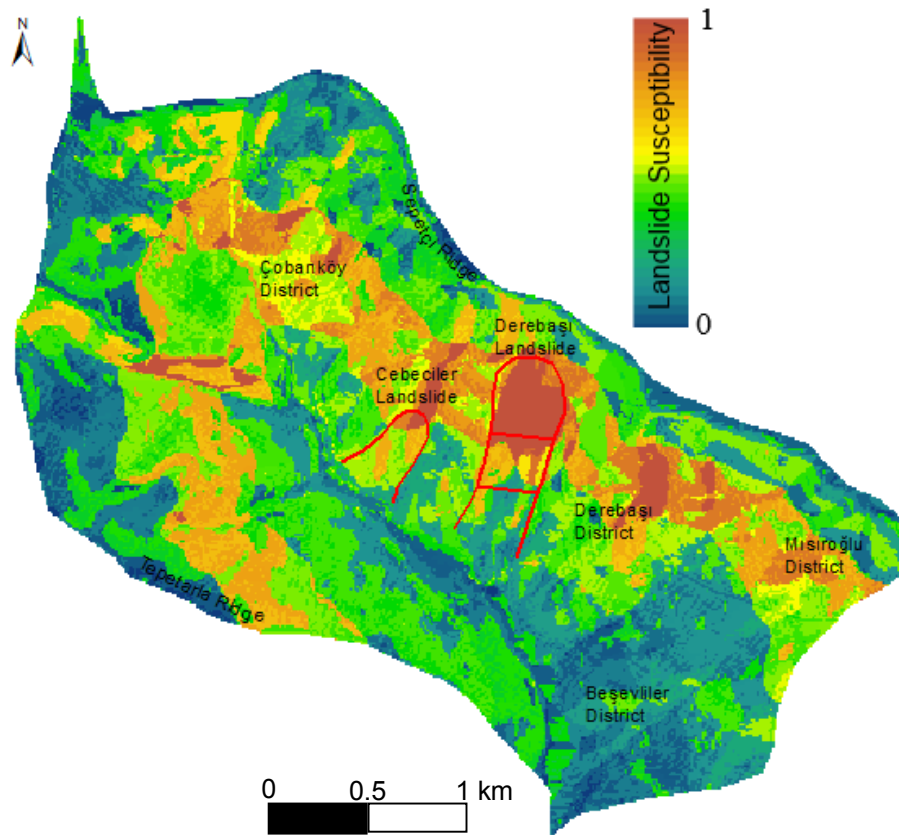


Figure 5.2a) Unclassified landslide susceptibility map of Yenice Watershed for February

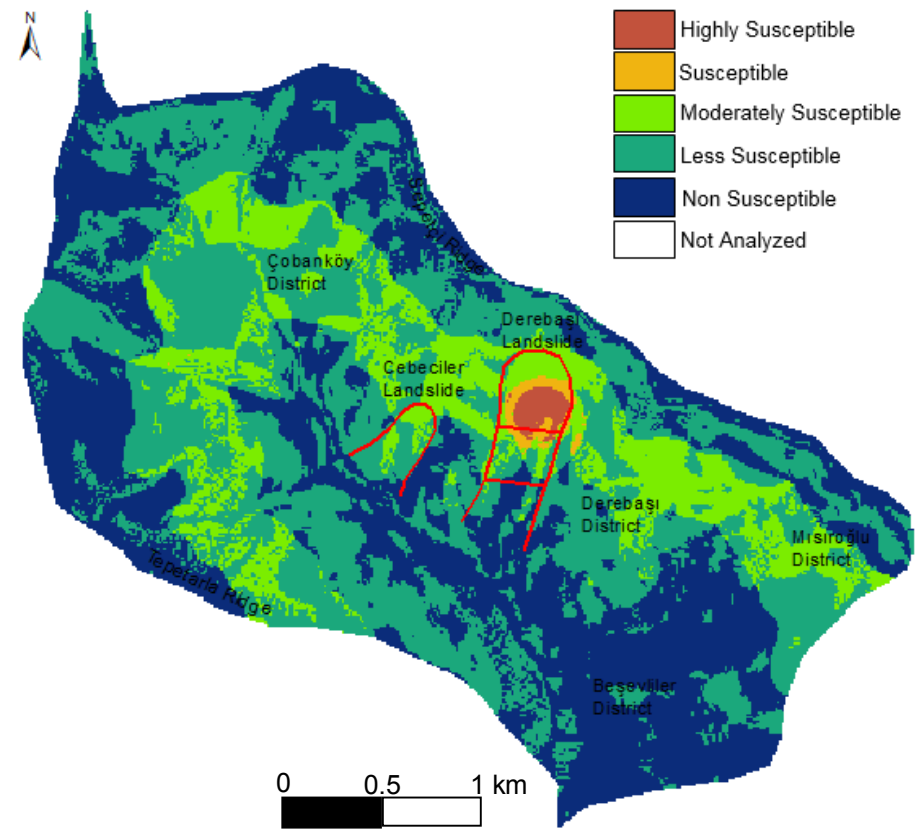


Figure 5.2b) Classified landslide susceptibility map of Yenice Watershed for February

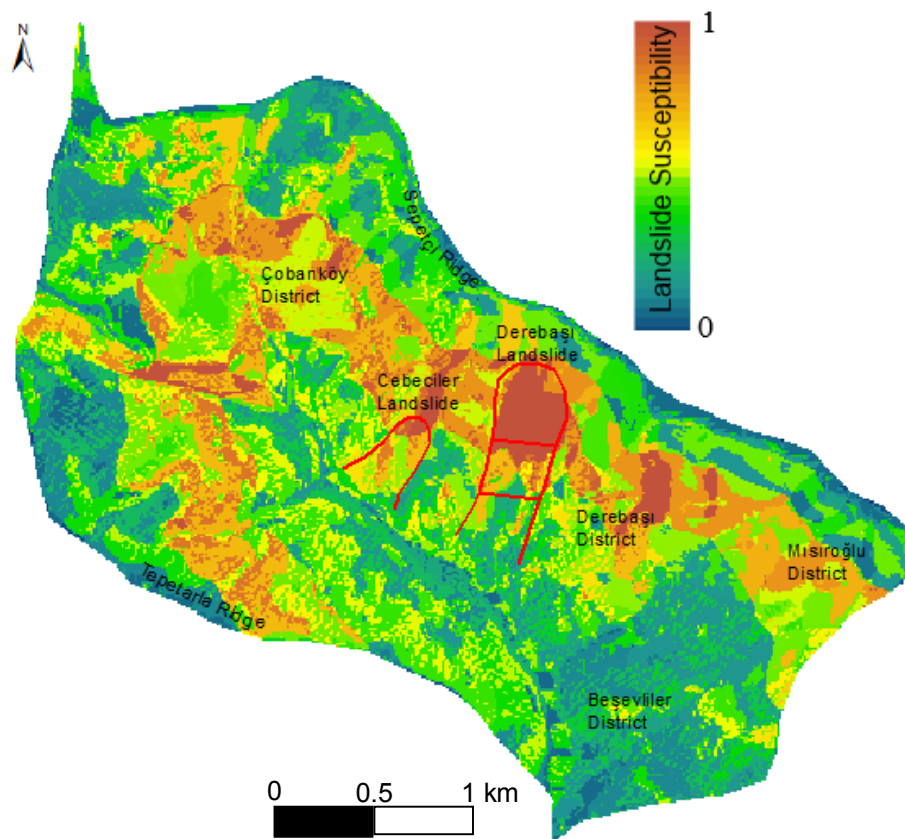


Figure 5.3a) Unclassified landslide susceptibility map of Yenice Watershed for March

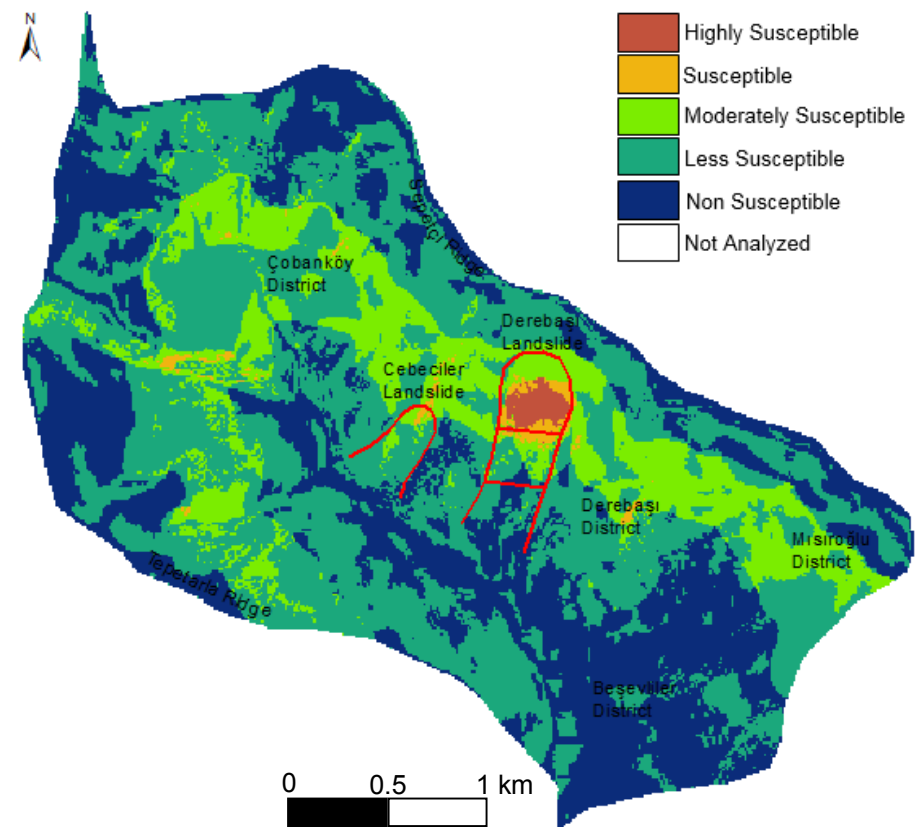


Figure 5.3b) Classified landslide susceptibility map of Yenice Watershed for March

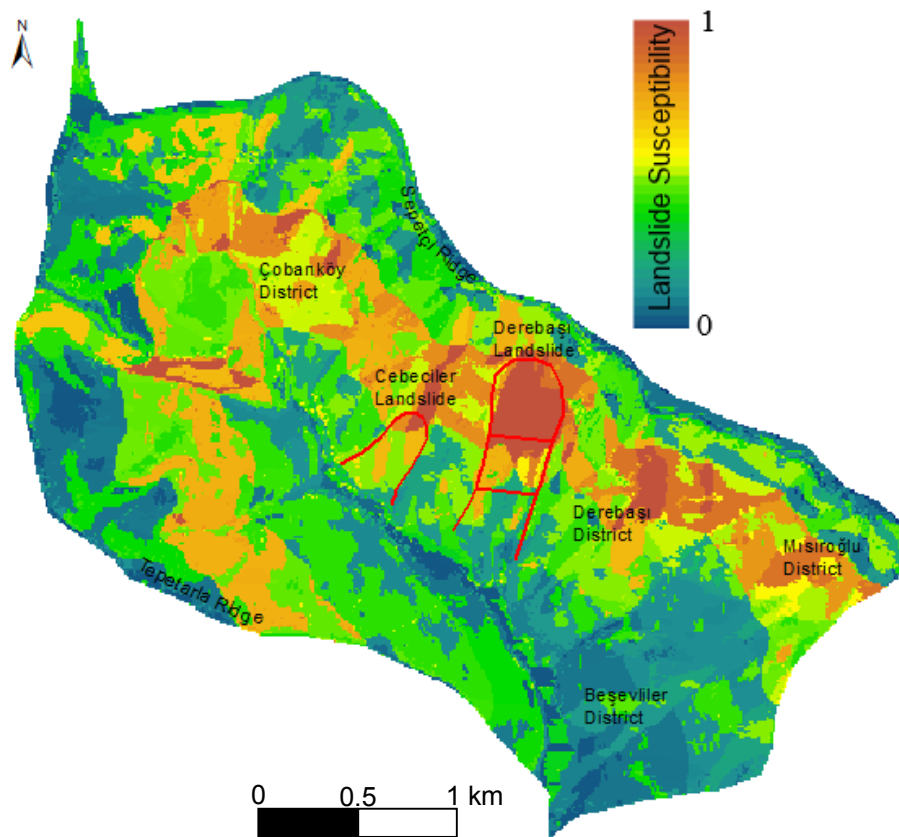


Figure 5.4a) Unclassified landslide susceptibility map of Yenice Watershed for April

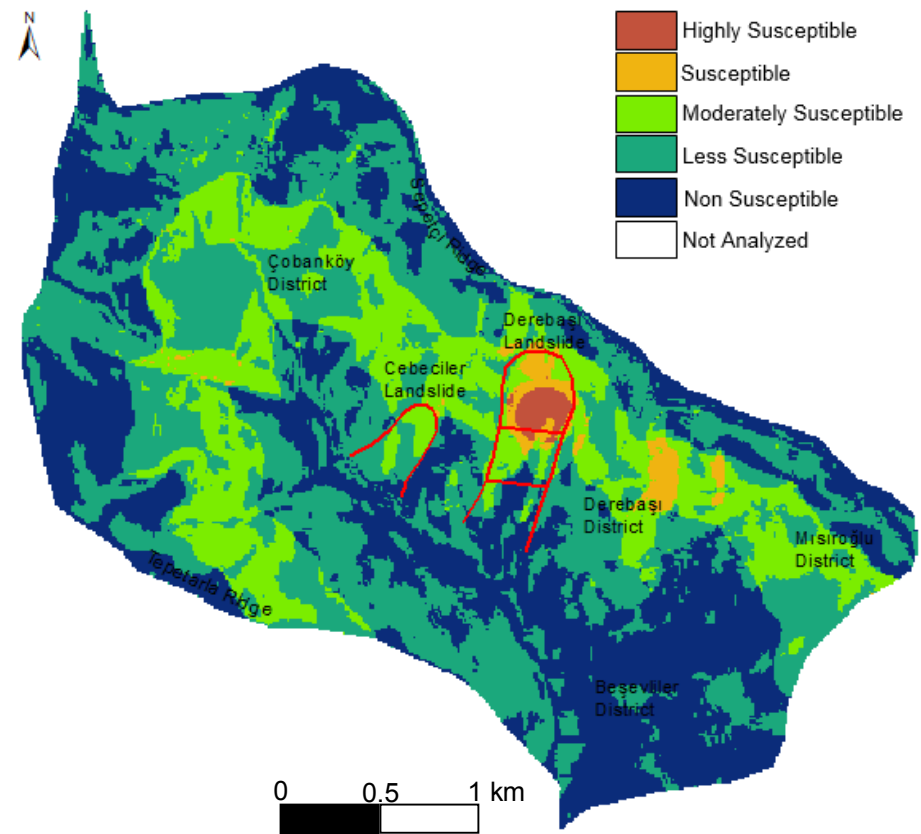


Figure 5.4b) Classified landslide susceptibility map of Yenice Watershed for April

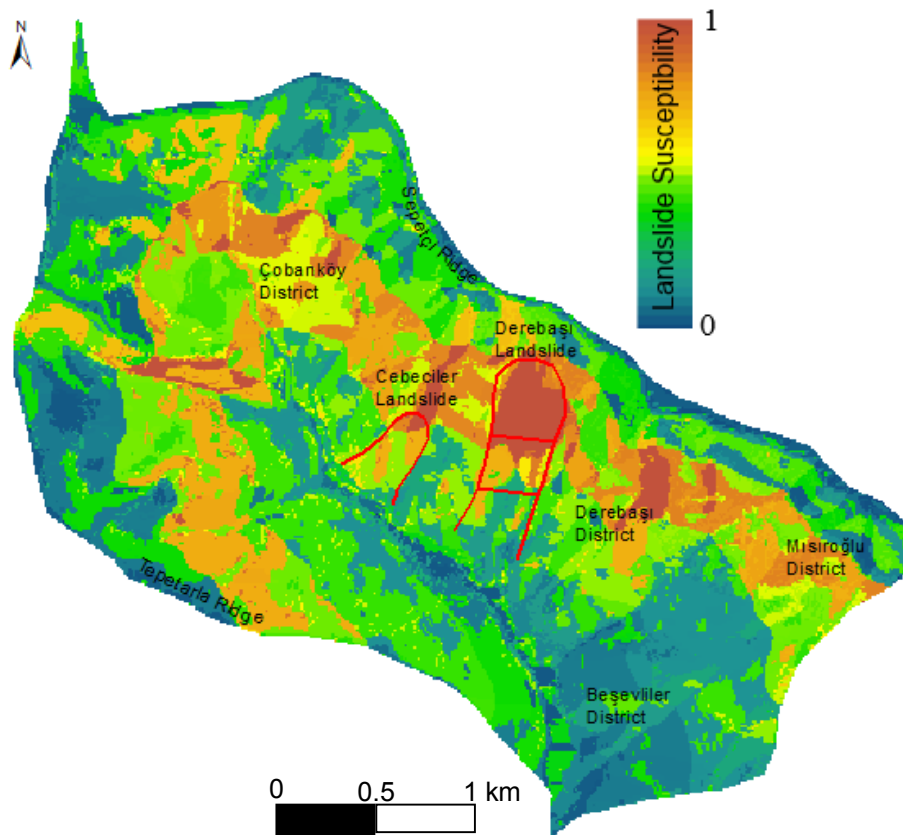


Figure 5.5a) Unclassified landslide susceptibility map of Yenice Watershed for May

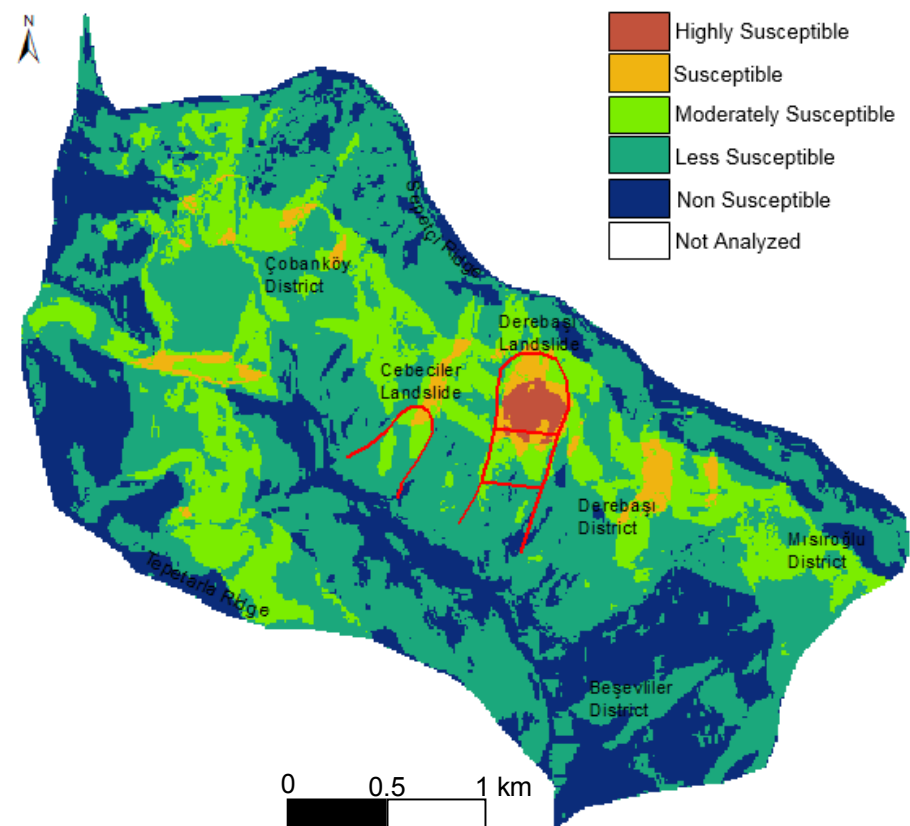


Figure 5.5b) Classified landslide susceptibility map of Yenice Watershed for May

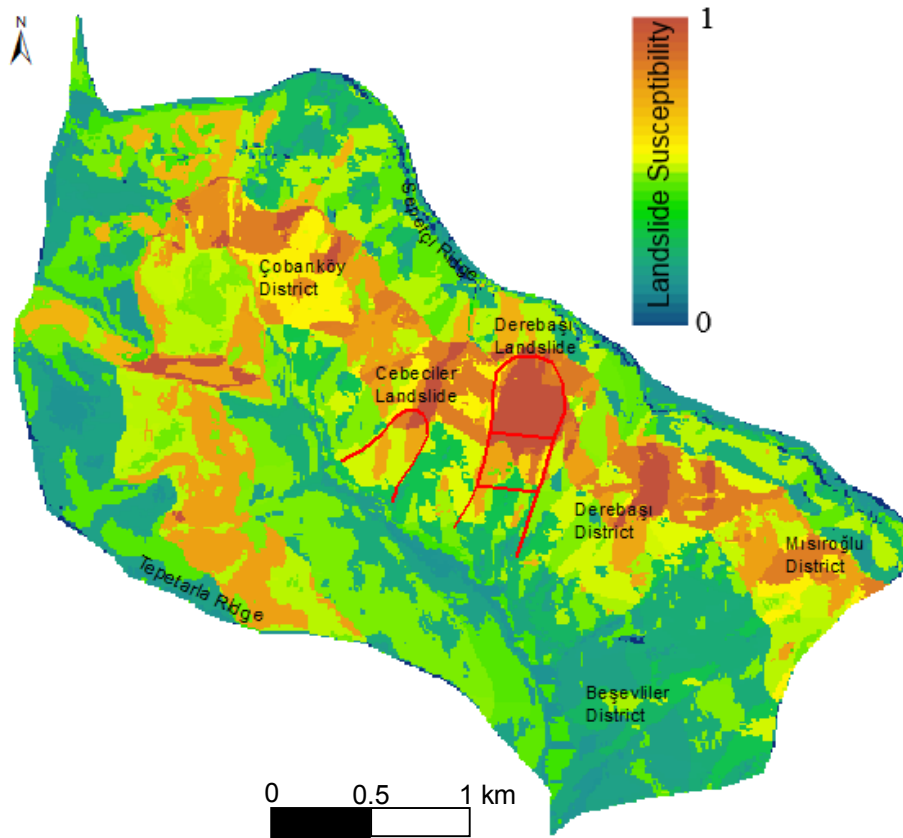


Figure 5.6a) Unclassified landslide susceptibility map of Yenice Watershed for June

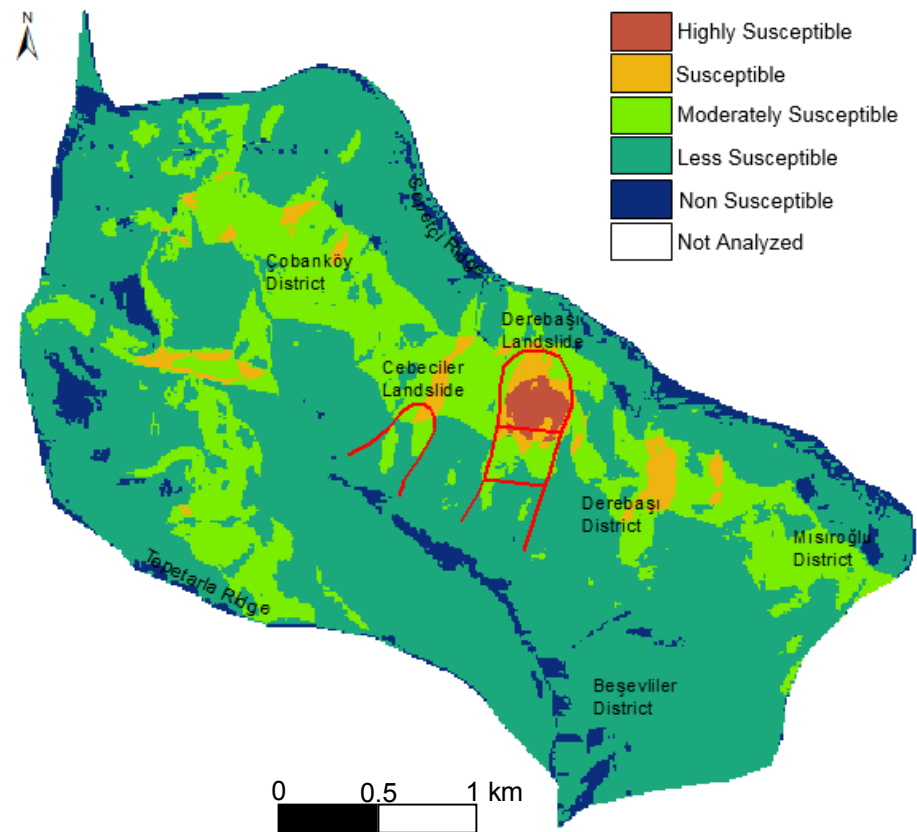


Figure 5.6b) Classified landslide susceptibility map of Yenice Watershed for June

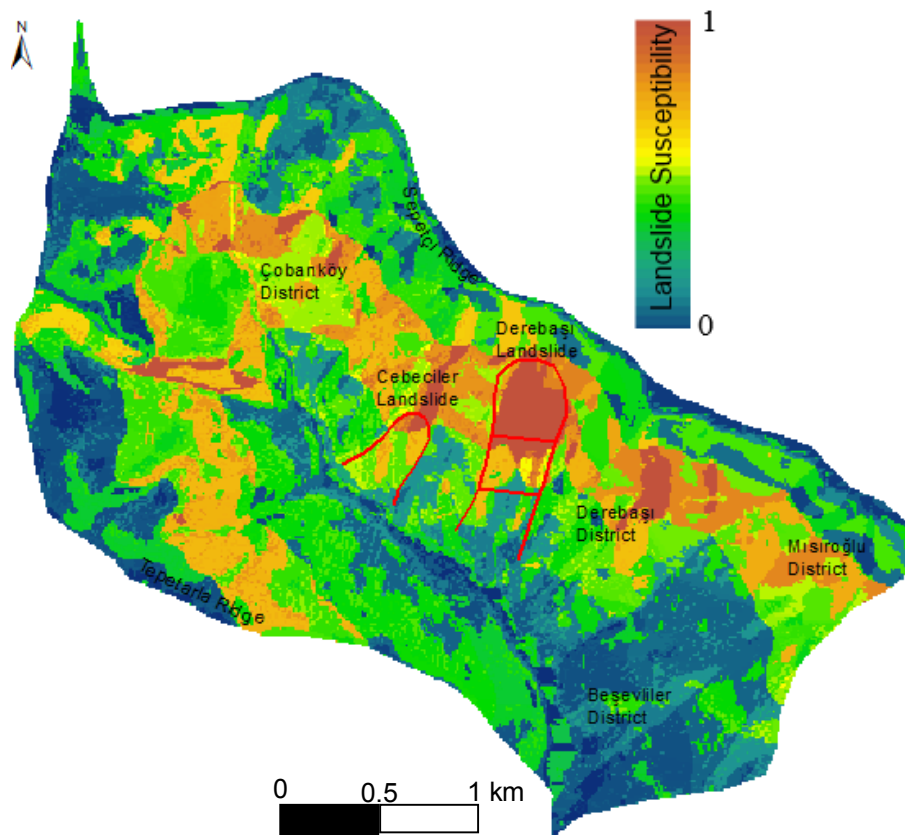


Figure 5.7a) Unclassified landslide susceptibility map of Yenice Watershed for July

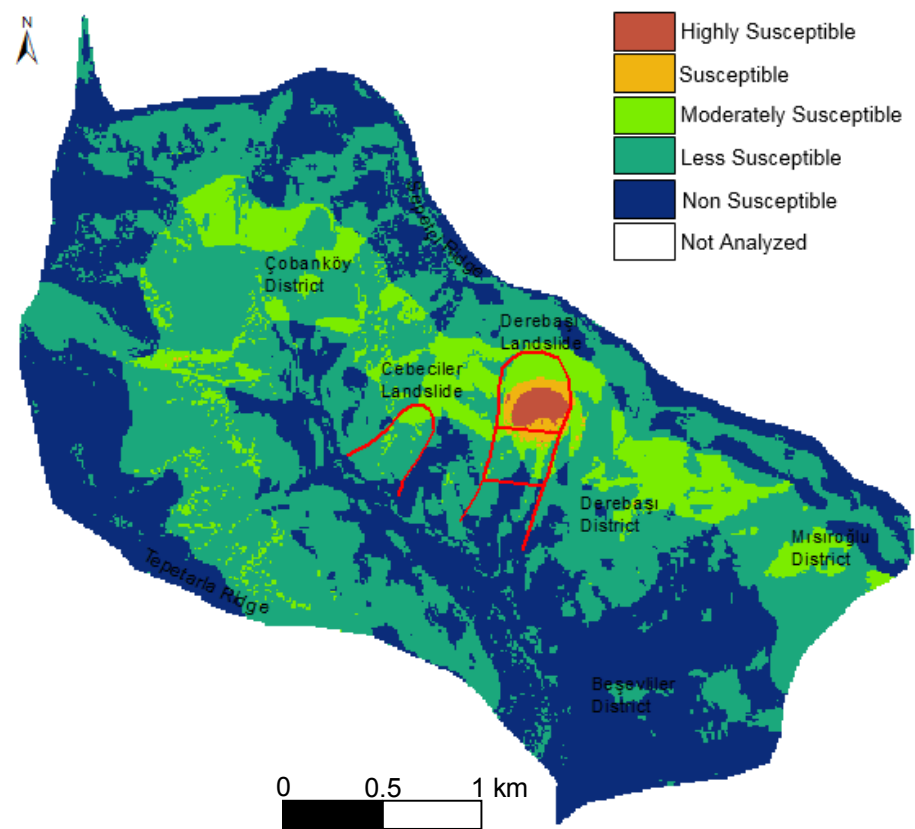


Figure 5.7b) Classified landslide susceptibility map of Yenice Watershed for July

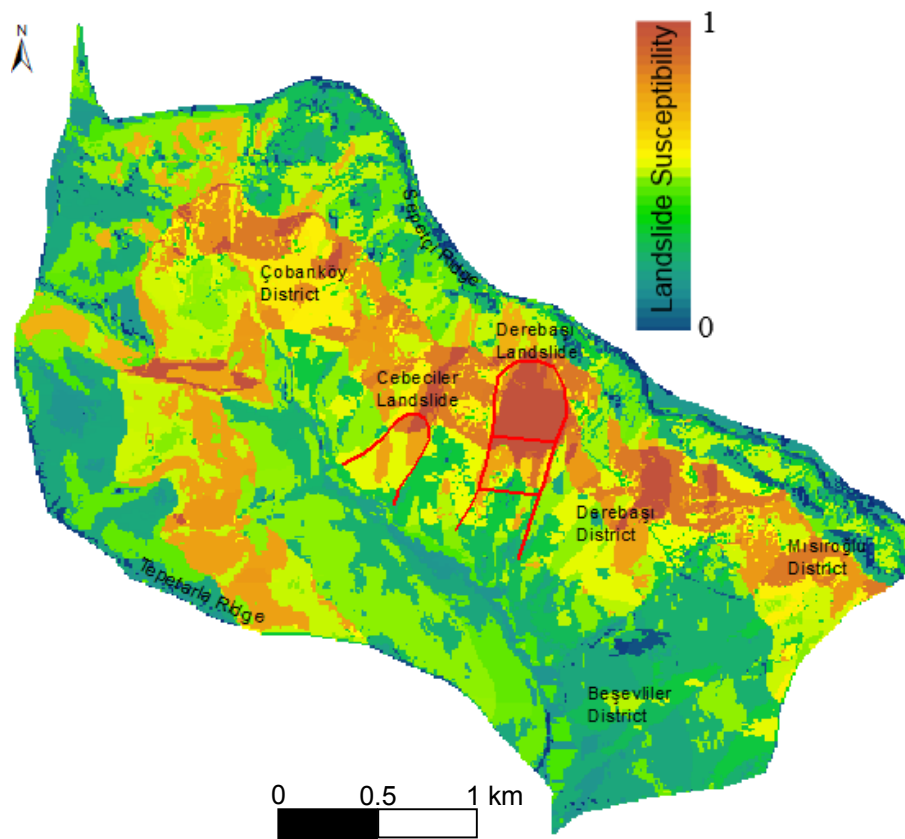


Figure 5.8a) Unclassified landslide susceptibility map of Yenice Watershed for August

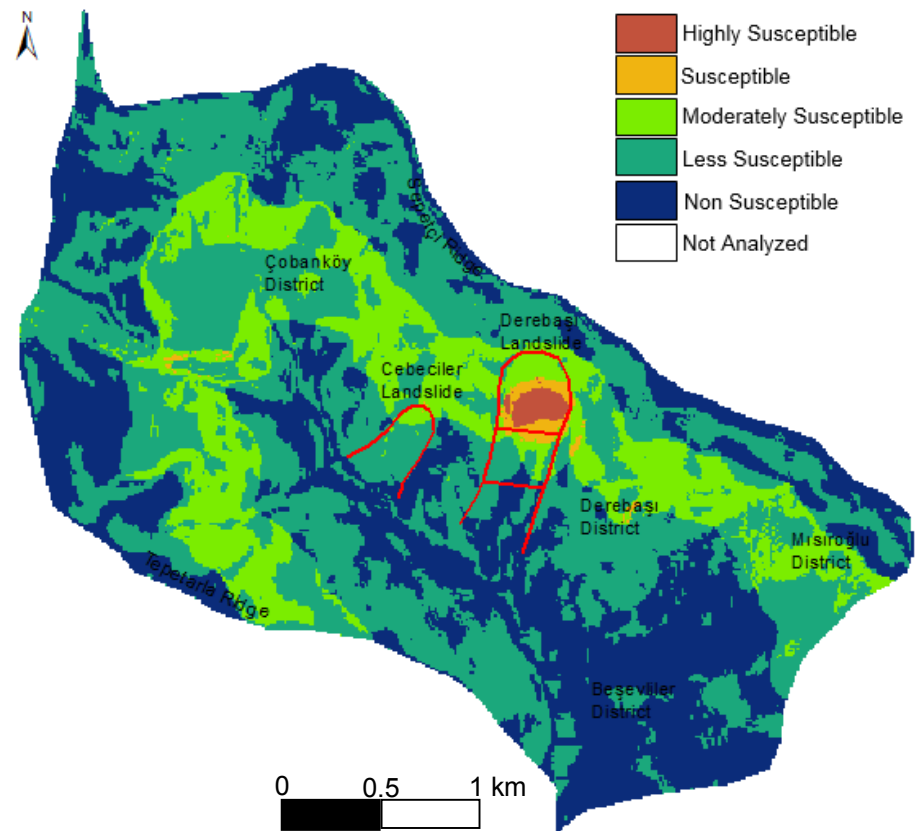


Figure 5.8b) Classified landslide susceptibility map of Yenice Watershed for August

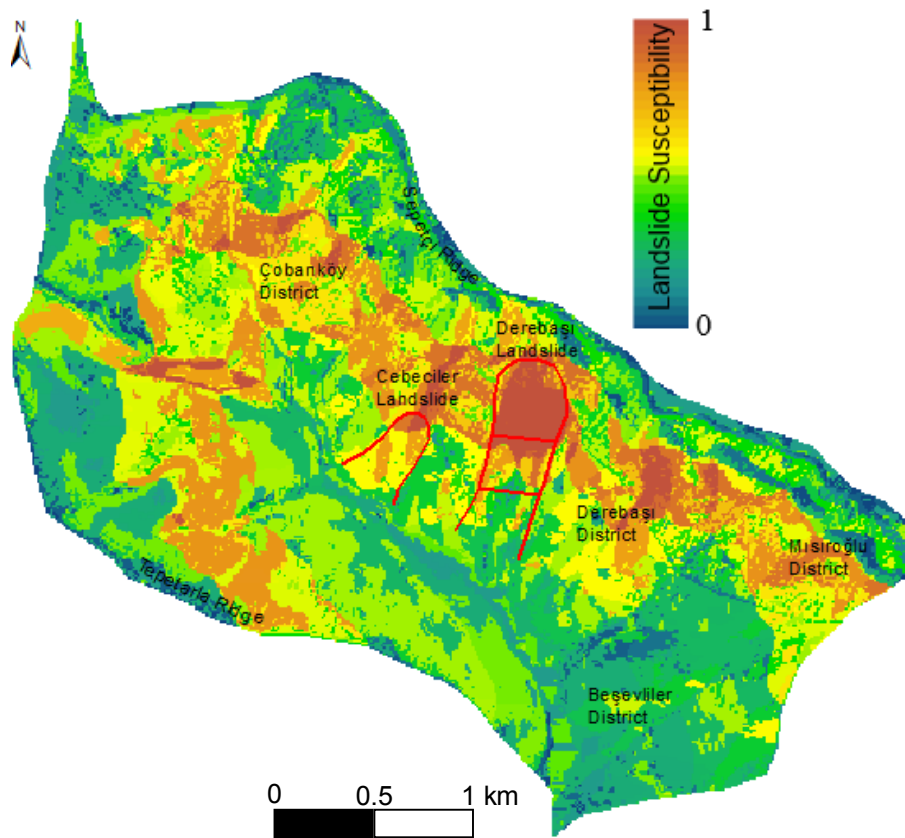


Figure 5.9a) Unclassified landslide susceptibility map of Yenice Watershed for September

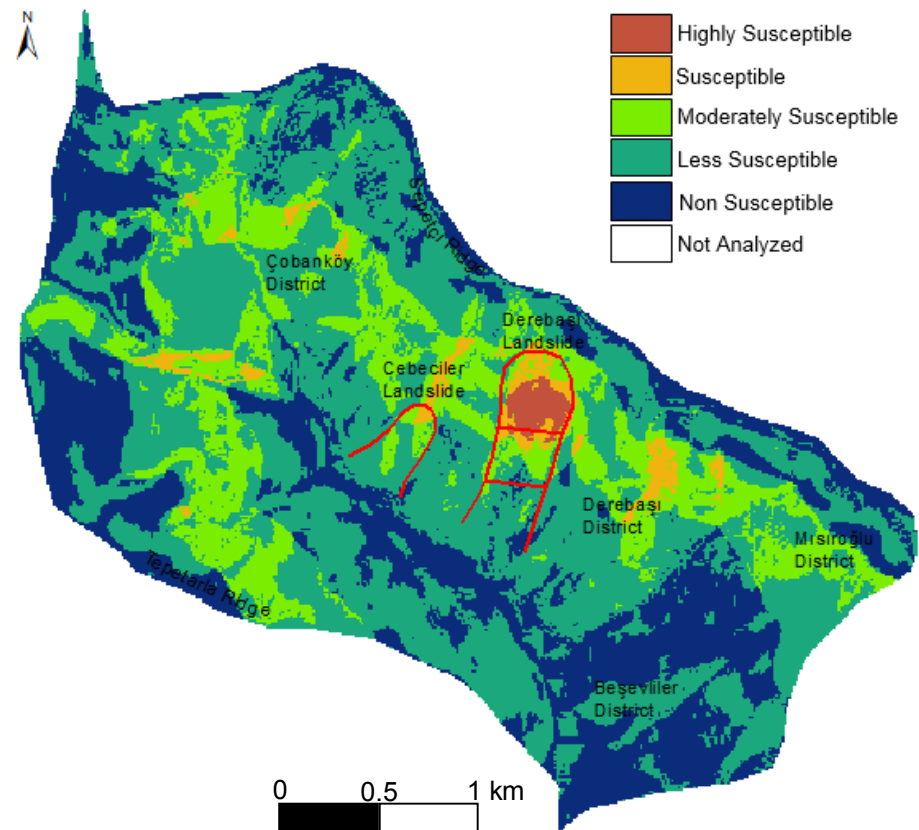


Figure 5.9b) Classified landslide susceptibility map of Yenice Watershed for September

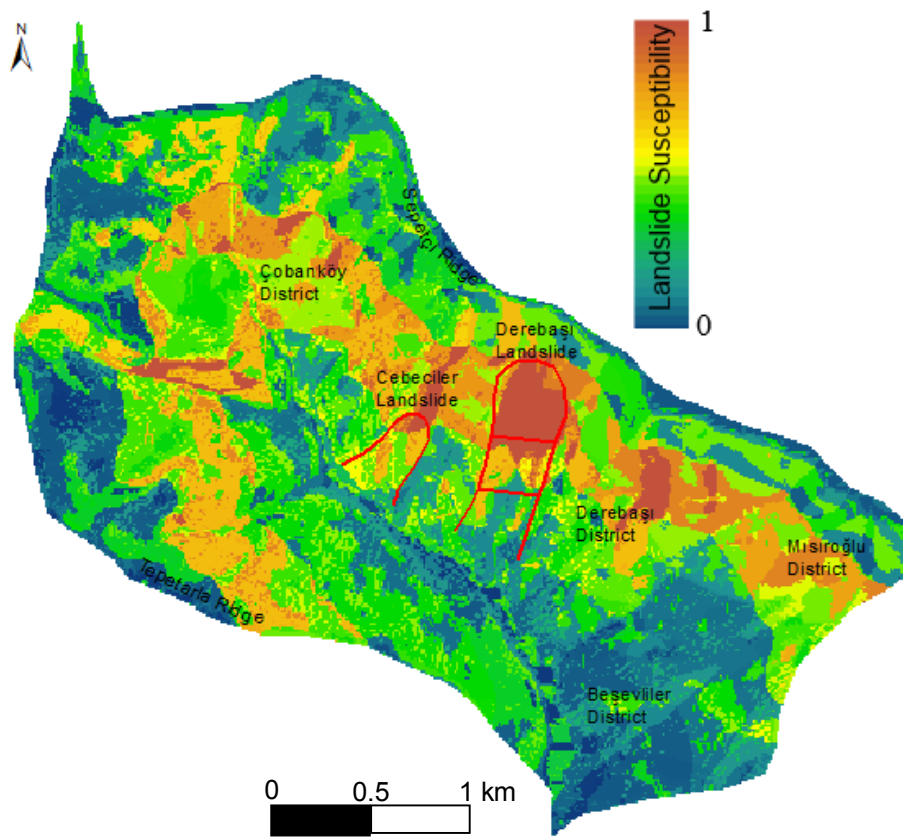


Figure 5.10a) Unclassified landslide susceptibility map of Yenice Watershed for October

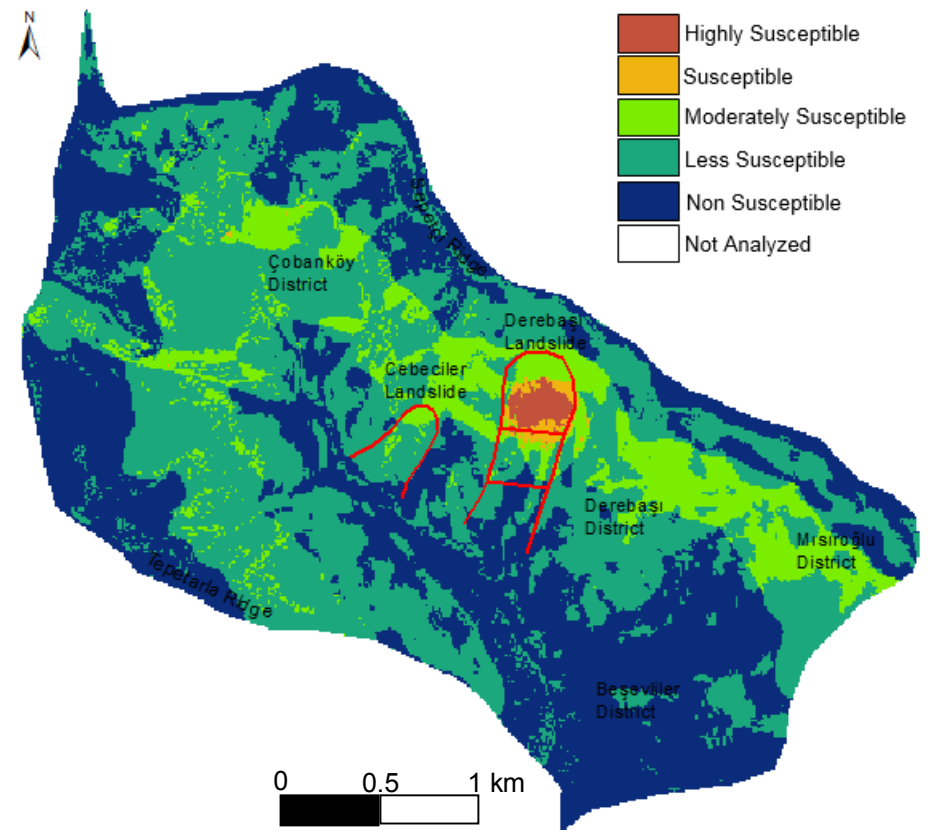


Figure 5.10b) Classified landslide susceptibility map of Yenice Watershed for October

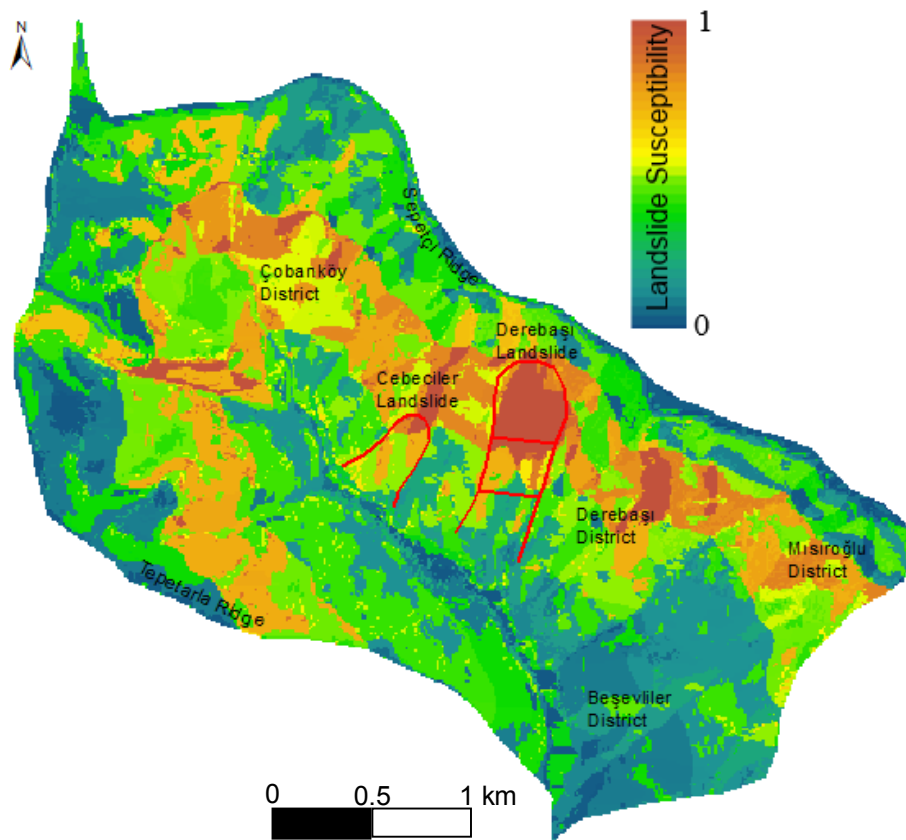


Figure 5.11a) Unclassified landslide susceptibility map of Yenice Watershed for November

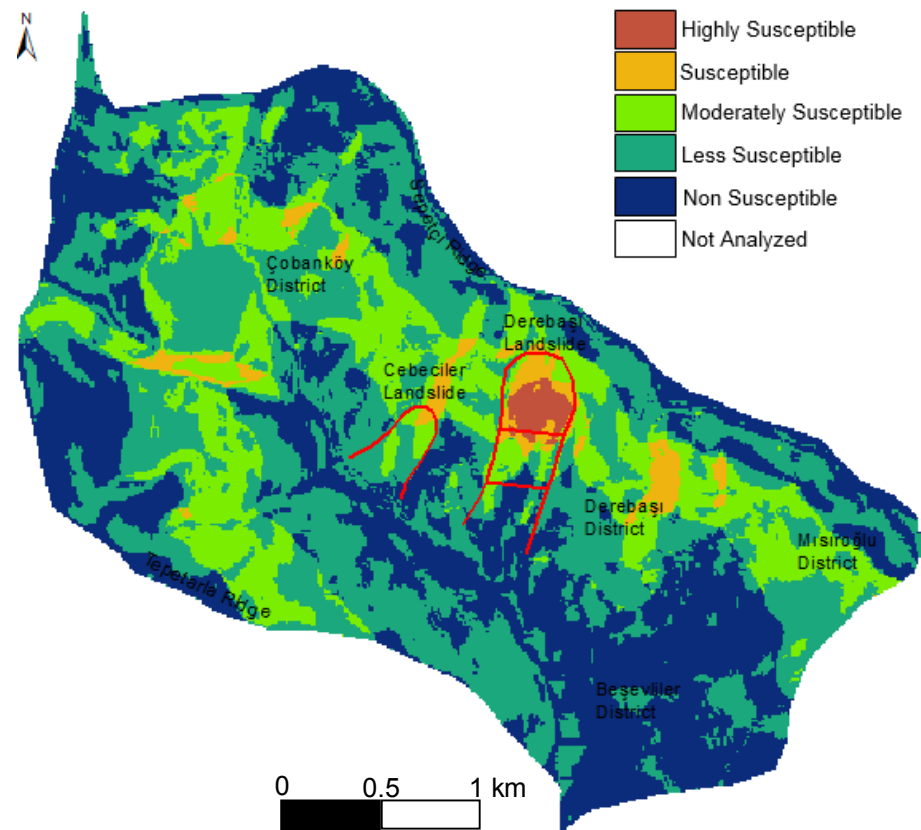


Figure 5.11b) Classified landslide susceptibility map of Yenice Watershed for November

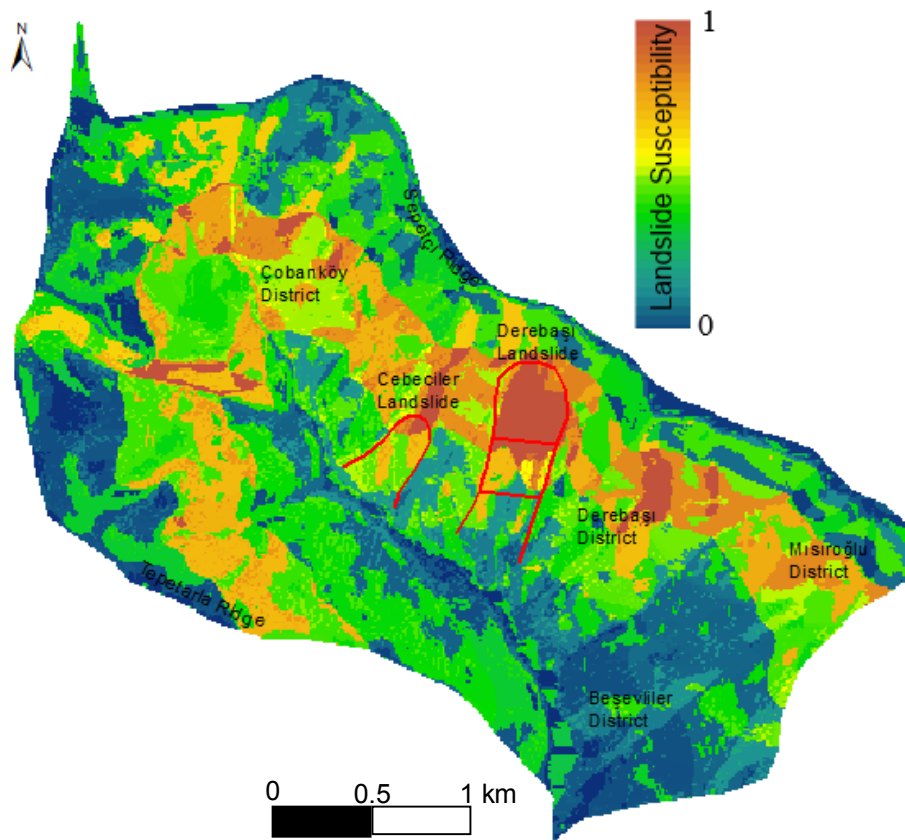


Figure 5.12a) Unclassified landslide susceptibility map of Yenice Watershed for December

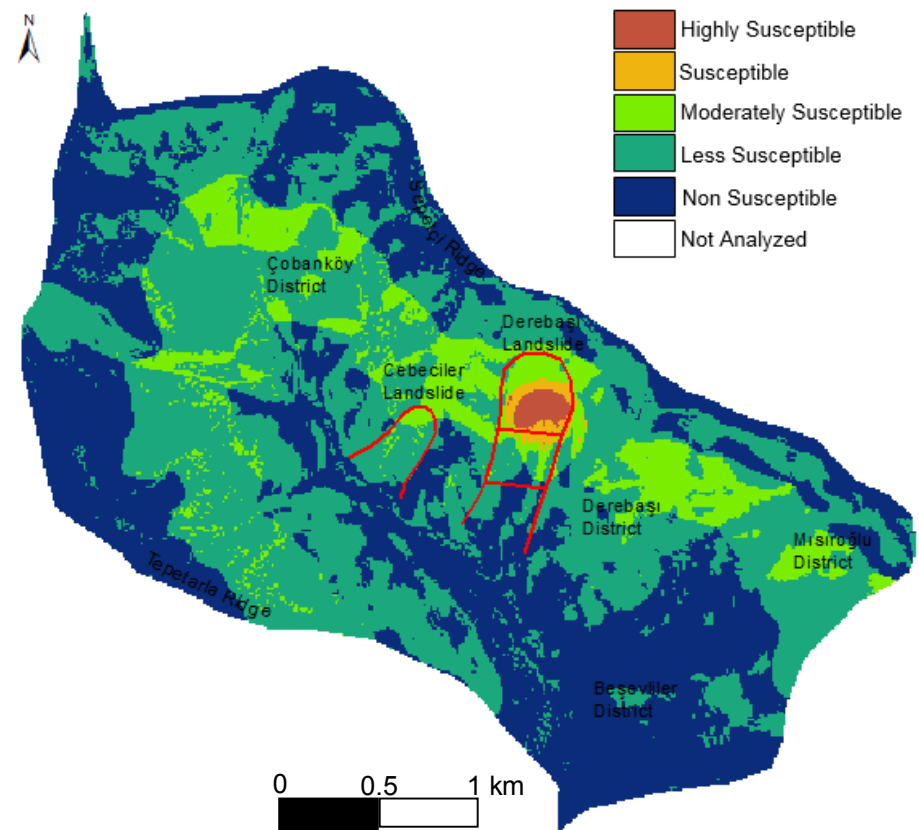


Figure 5.12b) Classified landslide susceptibility map of Yenice Watershed for December

- This method is developed to reflect the spatio-temporal effect of water on landslide susceptibility as a landslide triggering factor for a watershed which embodies a landslide. For the watersheds which have no landslide generation, or in case of existence of significant seismic records, the improvement stages of this method should be treated as the subject of the future research studies.
- Finally, in context of data accessibility, for the countries which have a soil characteristics database as SSURGO [154] in USA, this method is simple and expeditious. However, for the countries which do not have a soil database, execution of this method requires sites works including the soil mapping and sampling, and laboratory works. This issue necessitates time and financial possibilities for the particular studies.

REFERENCES

- [1] Schuster, R. L., Fleming, R. W., Economic losses and fatalities due to landslides, *Bulletin of the Association of Engineering Geologists* 11–28, **1986**.
- [2] Ercanoğlu, M., Landslide Susceptibility Assessment of SE Bartın (West Black Sea region, Turkey) by artificial neural networks, *Natural Hazards and Earth System Science*, 5, 979-992, **2005**.
- [3] Baltacı, H., Şen, L.Ö., Karaca, M., Doğu Karadeniz bölgesi heyelan-yağış ilişkisinin incelenmesi ve minimum eşik değerlerinin belirlenmesi, *Uluslararası Katılımlı I. Meteoroloji Sempozyumu*, 27-28 Mayıs, Devlet Meteoroloji İşleri Genel Müdürlüğü, 356-363, Ankara, **2010**.
- [4] Van Westen, C. J., Lulie Getahun, F., Analyzing the evolution of the Tessina landslide using aerial photographs and digital elevation models, *Geomorphology*, 54, 77-89, **2003**.
- [5] Aleotti, P., Chowdury, R., Landslide hazard assessment: summary review and new perspectives, *Bulletin of Engineering Geology and the Environment*, 21- 44, **1999**.
- [6] Guzzetti, F., Carrara, A., Cardinali, M., Reichenbach, P., Landslide hazard evaluation: a review of current techniques and their application in a multi-scale study, Central Italy. *Geomorphology*, 31, 181–216, **1999**.
- [7] Gokceoğlu, C., Aksoy, H., Landslide susceptibility mapping of the slopes in the residual soils of the Mangen region (Turkey) by deterministic stability analyses and image processing techniques. *Engineering Geology*, 44, 147–161, **1996**.
- [8] Dai, F. C., Lee, F. C., Landslide characteristics and slope instability modelling using GIS, Lantau Island, Hong Kong. *Geomorphology*, 42, 213-228, **2002**.
- [9] Ercanoğlu, M., Aksoy, H., Ankara Kalesi ve civarındaki kaya şevleri için potansiyel duraysızlık haritası. *Yerbilimleri*, 23, 189-206, **2004**.
- [10] Aksoy, H., Ercanoğlu, M., Kaya şevleri için kinematik analiz yöntemine yeni bir yaklaşım. *Erdoğan Yüzer Mühendislik Jeolojisi Sempozyumu*, 6-7 Eylül, İstanbul, 188-196, **2007**.
- [11] Carrara, A., Pike, R., GIS technology and models for assessing landslide hazard and risk *Geomorphology*, 94, 257-260, **2008**.
- [12] Alexander, D. E., A brief survey of GIS in mass-movement studies, with reflections on theory and methods. *Geomorphology*, 94, 261-267, **2008**.
- [13] Temiz, N., *Batı Karadeniz bölgesi (Bartın, Karabük, Zonguldak yörelerinde) kütle hareketlerinin ve bunları denetleyen jeolojik ve morfolojik özelliklerinin CBS ve Uzaktan Algılama yöntemi ile araştırılması*, Yüksek Lisans Tezi, Hacettepe Üniversitesi Fen Bilimleri Enstitüsü, Ankara, **2000**.

- [14] Ercanoğlu, M., Gökçeoğlu, C., Assessment of landslide susceptibility for a landslide-prone area (North of Yenice, NW Turkey) by fuzzy approach, *Environmental Geology*, 41, 720–730, **2002**.
- [15] Ercanoglu, M., *Bulanık mantık ve istatistiksel yöntemlerle heyelan duyarlılık haritalarının üretilmesi: Batı Karadeniz Bölgesi (Kumluca Güneyi-Yenice Kuzeyi)*, Doktora Tezi, Hacettepe Üniversitesi Fen Bilimleri Enstitüsü, Ankara, **2003**.
- [16] Gökçeoğlu, C., Aksoy, H., Ercanoğlu, M., Yenice (Karabük) Kuzeyi Heyelanlarının İncelenmesi ve Heyelan Duyarlılık Haritalarının Oluşturulması, *Hacettepe Üniversitesi Bilimsel Araştırmalar Birimi Araştırma Projesi*, 207s Ankara, **2003**.
- [17] Ercanoğlu, M., Gökçeoğlu, C., Use of fuzzy relations to produce landslide susceptibility map of a landslide prone area (West Black Sea Region, Turkey), *Engineering Geology*, 75, 229–250, **2004**.
- [18] Ercanoglu, M., Gokceoglu, C., Van Asch Th. W. J., Landslide susceptibility zoning North of Yenice (NW Turkey) by multivariate statistical techniques, *Natural Hazards*, 32, 1–23, **2004**.
- [19] Temiz, N., Aksoy, H., Ercanoğlu, M., Batı Karadeniz Bölgesi'nde potansiyel taşkın alanlarının belirlenmesine yönelik bir çalışma. *Türkiye Jeoloji Bülteni*, 47, 41-48, **2004**.
- [20] Yılmaz, Ç., Topal, T., Süzen, M. L., GIS-based landslide susceptibility mapping using bivariate statistical analysis in Devrek (Zonguldak-Turkey), *Environmental Earth Science*, 65 (7), 2161-2178, **2012**.
- [21] Moore, I. D., Grayson, W. D., Ladson, A. R., Digital terrain modelling: A review of hydrological, geomorphological and biological applications, *Hydrological Processes*, 5, 3-30, **1991**.
- [22] Giannecchini, R., Galanti, Y., D'Amato Avazi, G., Critical rainfall thresholds for triggering shallow landslides in the Serchio River Valley (Tuscany, Italy), *Natural Hazards and Earth, System Science*, 12, 829-842, **2012**.
- [23] Kuthari, S., *Establishing precipitation tresholds for landslide initiation along with slope characterisation using GIS based modelling*, MSc. Thesis, Indian Institute of Remote Sensing, **2007**.
- [24] Ayalew L., The effect of seasonal rainfall on landslides in the highlands of Ethiopia, *Bulletin of Engineering Geology and the Environment*, 58, 9–19, **1999**.
- [25] Calcaterra, D., Parise, M., Palma, B., Pelella, L., The influence of meteoric events in triggering shallow landslides in pyroclastic deposits of Campania, Italy, *In: Proceedings 8th International Symposium on Landslides*, (eds: Bromhead E, Dixon N, Ibsen ML), 1, 209-214, Cardiff, UK, **2000**.

[26] Soil and Water Laboratory, *SMDR – The Soil Moisture Distribution and Routing model, version 2.0 – documentation*, Department of Biological and Environmental Engineering, Cornell University, Ithaca, New York, **2003**.

[27] National Mapping Agency of Turkey, *1/25000 scaled Zonguldak F28-c1 and F28-b4 topographic maps*, **1999**.

[28] Directorate of Yenice Regional Forestry, *Vegetation characteristics map of Yenice Watershed*, **2013**.

[29] General Directorate of Meteorological Service of Turkey, *Meteorological data of Yenice Station*, **2013**.

[30] Türkiye İstatistik Kurumu, *Adrese Dayalı Nüfus Kayıt Sistemi (ADNKS) Sonuçları*, **2009**.

[31] Google Maps, Türkiye İstatistik Kurumu, <https://www.google.com/maps/@41.234651,32.2085587,10z>, (2014).

[32] Tüysüz, O., Aksay, A., Yiğitbaş, E., *Batıkaradeniz Bölgesi litostratigrafi birimleri. Stratigrafi Komitesi litostratigrafi birimleri serisi-1*, MTA Genel Müdürlüğü Eğitim Serisi, Ankara, **2004**.

[33] Hyppolyte, J.C., Müller, C., Kaymakçı, N., Sangu, E., *Dating of the Black Sea Basin: new nannoplankton ages from its inverted margin in the Central Pontides (Turkey)*, *Geological Society, London, Special Publications*, 340, 113-136, **2010**.

[34] Tüysüz, O., *Geology of the Cretaceous sedimentary basins of the Western Pontides*. *Geological Journal*, 34, 75–93, **1999**.

[35] Derman, S., Sayılı, A., İnaltı Formation: a key unit for regional geology. (Eds: Erler, A., Ercan, T., Bingöl, E., Örcen, S.) *Proceedings of the International Symposium on the Geology of the Black Sea Region*. Mineral Research and Exploration Institute of Turkey (MTA), 104–108, Ankara **1995**.

[36] Okay, A. I., Tüysüz, O., Satır, M., Özkan, S., Altın, D., Sherlock, S., Eren, R. H., *Cretaceous and Triassic subduction-accretion, high pressure – low temperature metamorphism, and continental growth in the Central Pontides, Turkey*. *Geological Society of America Bulletin*, 118, 1247–1269, **2006**.

[37] Deveciler, E., *Alaplı-Bartın-Cide (B.Karadeniz) jeoloji raporu*, MTA yayınları, Derleme No: 7938, Ankara, **1986**.

[38] Demir, B., Ercan, S., *Yenice ilçesindeki heyelanlar üzerine bazı gözlemler, Türkiye 3. Ulusal Heyelan Sempozyumu Özleri Kitabı*, Çukurova Üniversitesi, Adana, **1999**.

[39] Yergök, A.F., Akman, I.L., İplikçi, E., Karabalık, N., Keskin, I., Mengi, H., Umut, M., Armağan, F., Erdoğan, K., Kaymakçı, M., Çetinkaya, A., *Batı Karadeniz Bölgesinin Jeolojisi 1*, MTA, Derleme No: 8273, Ankara, **1987**.

- [40] Ministry of Public Works and Settlement, *Earthquake zonation map of Turkey*, **1996**.
- [41] Republic of Turkey Prime Ministry, Disaster and Emergency Management Presidency, *The active fault and earthquake location map of Turkey*, **2013**.
- [42] Lee, E.M., Jones, D. K. C., *Landslide Risk Assessment*, Thomas Telford, London, **2004**.
- [43] Varnes, D. J., *Landslide types and processes*. In: *Landslide and Engineering Practice*. (ed: Eckel, E. B.), Highway Research Board Special Report, 29, 20-47, **1978**.
- [44] Cruden, D. M., Varnes, D. J., *Landslide types and processes*, In: *Landslides Investigation and Mitigation*, Transportation Research Board (eds: Turner, A. K., Schuster, R. L.), Special Report 247, Washington D.C., US, **1996**
- [45] Ladd, G. C., Landslides, subsidences and rockfall. *American Railway Engineering Association Bulletin*, 37, 72 p., **1935**.
- [46] Sharpe, C. F. S., Landslides and related phenomena. *Columbia University Press*, New York, USA, 137, **1938**.
- [47] Campbell, D. A., Types of soil erosion prevalent in New Zealand. *International Association of Scientific Hydrology*, Brussels, 2, 82–95, **1951**.
- [48] Varnes, D. J., Landslide types and processes. In: *Landslide and Engineering Practice* (ed: Eckel, E. B.), Special Report 29. Highway Research Board, National Research Council, Washington DC, pp 20–47, **1958**
- [49] Crozier, M. J., Techniques for the morphometric analysis of landslips. *Geomorphologie*, 17, 78–101, **1973**.
- [50] Wieczorek, G. F., Preparing a detailed landslide-inventory map for hazard evaluation and reduction, *Bulletin of Associated Engineering Geologist*, 21, 337–342, **1984**.
- [51] Hungr, O., Evans, S. G., Bovis. M. J., Hutchnison. N. J., A review of the classification of landslides of the flow type, *Environment and Engineering Geoscience*, 7, 221–238, **2001**.
- [52] British Geological Survey, Types of Landslides, http://www.bgs.ac.uk/landslides/how_does_BGS_classify_landslides.html (2014).
- [53] USGS, Landslides types and processes, <http://pubs.usgs.gov/fs/2004/3072/fs-2004-3072.html> (2014)

- [54] Varnes, D. J., International association of engineering geology commission on landslides and other mass movements on slopes: *landslide hazard zonation: a review of principles and practice*. UNESCO, 63, Paris, **1984**.
- [55] Hoek, E., Bray, J. W., *Rock slope engineering*. Taylor and Francis, UK, 358, **1981**.
- [56] Sidle, R. C., Ochiai, H., *Landslides: processes, prediction, and landuse*. American Geophysical Union, Washington DC, 18, 312, **2006**.
- [57] Deveciler, E., *Alaplı-Bartın-Cide (B.Karadeniz) jeoloji raporu*, MTA yayınları, Derleme No: 7938, 58 s, **1986**.
- [58] Fell, R., Corominas. J., Bonnard, C., Cascini, L., Leroi, E., Savage, W. Z., Guidelines for landslide susceptibility, hazard and risk zoning for land use planning, *Engineering Geology*, 102, 85–98, **2008**.
- [59] Gulla, G., Antronico, L., Laquinta, P., Terranova, O., Susceptibility and triggering scenarios at a regional scale for shallow landslides, *Geomorphology*, 99, 39–58, **2008**.
- [60] Gorsevski, P. V., Gessler, P. E., Boll, J., Elliot, W. J., Foltz, R. B., Spatially and temporally distributed modeling of landslide susceptibility. *Geomorphology*, 80, 178–198, **2006**.
- [61] Ray, R. L., Jacobs, J. M., Cosh M. H., Landslide susceptibility mapping using downscaled AMSR-E soil moisture: A case study from Cleveland Corral, California, *US Remote Sensing of Environment*, 114, 2624–2636, **2010**.
- [62] Ray, R. L., Jacobs, J. M., Pedro de Alba, Impacts of unsaturated zone soil moisture and groundwater table on slope instability, *Journal of Geotechnical and Geoenvironmental Engineering*, 136, 1448 – 1458, **2010**.
- [63] Carrara, A., Cardinali, M., Detti, R., Guzzetti, F., Pasqui, V., Reichenbach, P., GIS techniques and statistical models in evaluating landslide hazard. *Earth Surface Processes and Landforms*, 16, 427–445, **1991**.
- [64] Hutchinson, J. N., Keynote paper: landslide hazard assessment. In: *Landslides, Proceedings 6th International Symposium on Landslides* (ed: Bell, D. H.), Christchurch, New Zealand, pp 1805–1841, **1995**.
- [65] Turner, A. K., Schuster, R. L., Landslides: Investigation and Mitigation. National Research Council, Transportation Research Board Special Report No 247, 673, Washington DC, USA, **1996**.
- [66] Guzzetti F (2004) Landslide mapping, hazard assessment and risk evaluation: Limits and potential. In: *Proceeding International Symposium on Landslide and Debris Flow Hazard Assessment, National Center for Research on Earthquake Engineering*, 7-8 October, Taipei, 1-17, **2004**.

- [67] Alkeveli, T., *Aster Uydu Verilerinin Heyelan Envanter Haritalamalarına Yönelik Kullanımının Araştırılması: Yenice-Gökçebey (Batı Karadeniz Bölgesi)*. Yüksek Lisans Tezi, Hacettepe Üniversitesi Fen Bilimleri Enstitüsü, 84, **2009**.
- [68] Verstappen, H. T., *Applied geomorphology: geomorphological surveys for environmental development*. Elsevier, Amsterdam, 437, **1983**.
- [69] Leroi, E., Landslide hazard-risk maps at different scales: Objectives, tools and developments. Rotterdam, Netherlands, 35–51, **1996**.
- [70] Van Westen, C. J., Van Asch, T. W. J., Soeters, R., Landslide hazard and risk zonation - why is it still so difficult? *Bulletin of Engineering Geology and the Environment*, 65, 167–184, **2006**.
- [71] Anbalagan, R., Landslide hazard evaluation and zonation mapping in mountainous terrain, *Engineering Geology*, 32, 269–277, **1992**.
- [72] Saaty, T. L., *The analytic hierarchy process*. McGraw-Hill Book Co, New York, **1980**.
- [73] Ayalew, L., Yamagishi, H., Ugawa, N., Landslide susceptibility mapping using GIS-based weighted linear combination, the case in Tsugawa area of Agano River, Niigata prefecture, Japan, *Landslides*, 1, 73–81, **2004**.
- [74] Hasekiogulları, G., *Heyelan duyarlılık haritalarının üretilmesinde parametre etkilerinin değerlendirilmesi*, Hacettepe Üniversitesi Fen Bilimleri Enstitüsü, yüksek lisans tezi, 116, **2010**.
- [75] Süzen, M. L., Doyuran, V., A Comparison of the GIS based landslide susceptibility assessment method: multivariate versus bivariate, *Environmental Geology*, 45, 665-679, **2004**.
- [76] Carrara, A., Catalano, E., Sorriso-Valvo, M., Reali, C., Orso, I., Digital terrain analysis for land evaluation, *Geologia Applicata ed Idrogeologia*, 13, 69 – 117, **1978**.
- [77] Parise, M., Jibson, R. W., A seismic landslide susceptibility rating of geologic units based on analysis of characteristics of landslides triggered by the 17 January, 1994 Northridge, California Earthquake, *Engineering Geology*, 58, 251–270, **2000**.
- [78] Uromeihy, A., Mahdaviyar, M. R., Landslide hazard zonation of the Khorshrostan area, Iran, *Bulletin of Engineering Geology and the Environment*, 58, 207–213, **2000**.
- [79] Yin, K. L., Yan, T. Z., Statistical prediction model for 592 slope instability of metamorphosed rocks, *Proceeding 5th International Symposium on Landslides*, Lausanne, Switzerland, 1269–1272, **1988**.
- [80] Van Westen, C. J., Rengers, N., Terlien. M. T. J., Soeters, R., Prediction of the occurrence of slope instability phenomena through GIS-based hazard zonation, *Geology Rundschau*, 86, 404–414, **1997**.

- [81] Çevik, E., Topal, T., GIS-based landslide susceptibility mapping for a problematic segment of the natural gas pipeline, Hendek (Turkey), *Environmental Geology*, 44, 949–962, **2003**.
- [82] Lee, S., Min, K., Statistical analysis of landslide susceptibility at Yongin, Korea, *Environmental Geology*, 40, 1095–1113, **2001**.
- [83] Süzen, M. L., Doyuran, V., Data driven bivariate landslide susceptibility assessment using geographical information systems: a method and application to Asarsuyu Catchment, Turkey, *Engineering Geology*, 71, 303–321, **2004**.
- [84] Carrara, A., Multivariate models for landslide hazard evaluation. *Mathematical Geology* 15, 403–426, **1983**.
- [85] Eshghabadi, S. M., Solaimani, K., Omdivar, E., Landslide susceptibility mapping using multiple regression and GIS tools in Tajan Basin, North of Iran, *Environment and Natural Resources Research*, 2, 43-51, **2012**.
- [86] Ohlmacher, G. C., Davis, J. C., Using multiple logistic regression and GIS technology to predict landslide hazard in northeast Kansas, USA, *Engineering Geology*, 69, 331-343, **2003**.
- [87] Reger, J. P., Discriminant analysis as a possible tool in landslide investigations. *Earth Surface Processes and Landforms*, 4, 267–273, **1979**.
- [88] Dong, J. J., Tung, Y. H., Chen, C. C., Liao, J. J., Pan, Y. W., Discriminant analysis of the geomorphic characteristics and stability of landslide dams, *Geomorphology*, 110, 162-171, **2009**.
- [89] Gorsevski, P. V., Gessler, P., Foltz, R. B., Spatial prediction of landslide hazard using discriminant analysis and GIS, *GIS in the Rockies 2000 Conference and Workshop Applications for the 21st Century, Denver, Colorado*, 25-27, **2000**.
- [90] Carrara, A., Cardinali, M., Guzzetti, F., Uncertainty in assessing landslide hazard and risk. *International Test Commission Journal*, 2, 172–183, **1992**.
- [91] Yeşilnacar, E., Topal, T., Landslide susceptibility mapping: A comparison of logistic regression and neural networks methods in a medium scale study, Hendek region (Turkey), *Engineering Geology*, 79, 251-266, **2005**.
- [92] Yılmaz, I., Landslide susceptibility mapping using frequency ratio, logistic regression, artificial neural networks and their comparison: A case study from Kat landslides (Tokat – Turkey), *Computer and Geosciences*, 35, 1125-1138, **2009**.
- [93] Baeza, C., Corominas, J., Assessment of shallow landslide susceptibility by means of multivariate statistical techniques. *Earth Surface Process and Landform*, 26, 12, 1251–1263, **2001**.

- [94] Wang, H., Liu, G., Xu, W., Wang, G., GIS-based landslide hazard assessment: an overview, *Progress in Physical Geography*, 29, 548–567, **2005**.
- [95] Zadeh, L. A., Fuzzy sets, *Information and Control*, 8, 338–353, **1965**.
- [96] Garrett, J., Where and why artificial neural networks are applicable in civil engineering? *Journal of Computing in Civil Engineering*, 8, 129–130, **1994**.
- [97] Kanungo, D. P., Arora., M. K., Sarkar, S., Gupta, R. P., A comparative study of conventional, ANN black box, fuzzy and combined neural and fuzzy weighting procedures for landslide susceptibility zonation in Darjeeling Himalayas, *Engineering Geology*, 85, 347–366, **2006**.
- [98] Wu, W., Sidle, R. C., A distributed slope stability model for steep forested basins, *Water Resources Research*, 31, 2097–2110, **1995**.
- [99] Wu, W., Sidle, R. C., Application of a distributed shallow landslide analysis model (dSLAM) to manage forested catchments in coastal Oregon, *International Association of Hydrological Sciences*, 245, 213–221, **1997**.
- [100] Hammond, C., Prellwitz, R., Miller, S., Landslide hazard assessment using Monte Carlo simulation, *Proceeding Sixth International Symposium on Landslides*, Christchurch, New Zealand, 2, 959–964, **1992**.
- [101] Montgomery, D. R., Dietrich, W. E., A physically based model for the topographic control of shallow landsliding, *Water Resources Research*, 30, 1153–1171, **1994**.
- [102] Güner, Y., *Filyos Vadisinin ve Dolayının Jeomorfolojisi*, MTA, 87-90, Ankara, **1975**.
- [103] Koçyiğit, A., Karabük – Safranbolu Tersiyer havzası kuzey kenarının stratigrafisi ve niteliği, *Türkiye Jeoloji Kurumu Bülteni*, 30, 61-69, **1987**.
- [104] Okay, A. I., Tectonic units and sutures in the Pontides, Northern Turkey, *Kluwer Academic Publications*, 109-116, **1989**.
- [105] Biryol, B.C., *Neotectonics and evolution of the Eskipazar Basin, Karabük Turkey*, MSc Thesis, Middle East Technical University Graduate School and Applied Sciences, 124, **2004**.
- [106] Kuterdem, K., *Eskipazar (Karabük Güneyi) ve Kuzey Anadolu Fay Zonu (KAFZ) arasındaki bölgenin morfolotektonik özelliklerinin coğrafi bilgi sistemleri ile belirlenmesi*, Yüksek Lisans Tezi, Hacettepe Üniversitesi Fen Bilimleri Enstitüsü, 94, **2005**.
- [107] Akın, M., *Eskipazar (Karabük) Travertenlerinin Bozunmasının araştırılması*, Doktora Tezi, Ankara Üniversitesi Fen Bilimleri Enstitüsü, 263, **2008**.

- [108] SUYAPI, Tefen Regülatörü ve Hes Kesin Projesi Mühendislik Jeolojisi Raporu, *Orman ve Su İşleri Bakanlığı DSİ Genel Müdürlüğü 23. Bölge Müdürlüğü*, 52 s. **2012**.
- [109] Veith, T. L., Srinivasan, M. S., Gburek, W. S., Process Representation in Watershed-scale Hydrologic Models: an Evaluation in an Experimental Watershed. (eds: Renard, K. G., McElroy, S. A., Gburek, W. J., Canfield, H. E., Scott, R., L.), *First Interagency Conference on Research in The Watersheds* October 27-30 US Department of Agriculture Research Service Washington DC, **2003**.
- [110] Gerard-Marchant, P., Hively, W. D., Steenhuis, T. S., Distributed hydrological modeling of total dissolved phosphorus transport in an agricultural landscape, part I: distributed runoff generation, *Hydrology and Earth System Science*, 10, 245–261, **2006**.
- [111] Easton, Z. M., Gérard-Marchant, P., Walter, M. T., Petrovic, A. M., Steenhuis, T. S., Hydrologic assessment of an urban variable source watershed in the northeast United States, *Water Resources Research*, 43, **2007**.
- [112] De Alwis, D. A., Easton, Z. M., Dahlke, H. E., Philpot, W. D., Steenhuis, T. S., Hydrology and Earth System Sciences Unsupervised classification of saturated areas using a time series of remotely sensed images, *Hydrology and Earth System Science*, 11,1609–1620, **2007**.
- [113] Campos, I., Coterillo, I., Marco, J., Modelling of a watershed: A distributed parallel application in a Grid Framework, *Computing and Informatics*, 27, 285–296, **2008**.
- [114] Rao, N.S., Easton, Z.M., Schneiderman, E. M., Zion, M.S., Lee, D. R., Steenhuis, T. S., Modeling watershed-scale effectiveness of agricultural best management practices to reduce phosphorus loading, *Journal of Environmental Management*, 90, 1385–1395, **2009**.
- [115] Frey, M. P., Schneider, M. K., Dietzel, A., Reichert, P., Stamm, C., Predicting critical source areas for diffuse herbicide losses to surface waters: Role of connectivity and boundary conditions, *Journal of Hydrology*, 365, 23–26, **2009**.
- [116] Frey, M. P., Stamm, C., Schneider, M. K., Reichert, P., Using discharge data to reduce structural deficits in a hydrological model with a Bayesian inference approach and the implications for the prediction of critical source areas. *Water Resources Research*, 47,18, **2011**.
- [117] ASTM WK27337 New Test Method for Pocket Penetrometer Test, *ASTM Publication*, **2010**.
- [118] Republic of Turkey Prime Ministry, Disaster and Emergency Management Presidency, *Landslide Investigation Reports of Yenice County, Karabük, Turkey*, **2000**.

- [119] Rawls, W. J., Brakensiek, D. L., et Saxton, K.E., Estimation of soil water properties. Transactions of the *American Society of Agricultural Engineers*, 25: 1316-1328, **1982**.
- [120] Rawls, W., and D. Brakensiek, Prediction of soil water properties for hydrologic modeling, *Watershed Management in the Eighties*, 293–299, **1985**.
- [121] ASTM D-854, Standard Test Methods for Specific Gravity of Soil Solids by Water Pycnometer, *ASTM Publication*, 972, **2000**.
- [122] ASTM D-2216, Standard Test Methods for Laboratory Determination of Water (Moisture) Content of Soil and Rock by Mass, *ASTM Publication*, 972, **2000**.
- [123] ASTM D-2974, Standard Test Methods for Moisture, Ash and Organic Matter of Peat and Other Organic Soils, *ASTM Publication*, 972, **2000**.
- [124] ASTM D-422-63, Standard Test Method for Particle Size Analysis of Soils, *ASTM Publication*, 972, **2000**.
- [125] ASTM D-4318, Standard Test Method for Liquid Limit, Plastic Limit and Plasticity Index of Soils, *ASTM Publication*, 972, **2000**.
- [126] USDA Soil Survey Staff, Natural Resources Conservation Services, A Basic System of Soil Classification for Making and Interpreting Soil Surveys, *United States Department of Agriculture*, second edition, **1999**.
- [127] ASTM D-5084, Standard Test Methods for Measurement of Hydraulic Conductivity of Saturated Porous Materials Using a Flexible Wall Permeameter, *ASTM Publication*, 972, **2000**.
- [128] Richards, L., Capillary conduction of liquids through porous mediums, *Physics*, 1, 318–333, **1931**.
- [129] Kuo, W. L., Steenhuis, T., McCulloch, C., Mohler, C., Weinstein, D., DeGloria, S., Swaney, D., Effect of grid size on runoff and soil moisture for a variable-source-area hydrology model, *Water Resources Research*, 35, 3419–3428, **1999**.
- [130] Frankenberger, J., Brooks, E., Walter, M., Steenhuis, T., A GIS-based variable source area hydrology model, *Hydrological Processes*, 13, 805–822, **1999**.
- [131] U.S. Army Corps of Engineers, Engineering and design: Runoff from snowmelt, *Tech. Rep. EM 1110-2-1406*, U.S. Army Corps of Engineers, Government Printing Office, Washington, D.C., **1960**.
- [132] Darcy, H., *Les fontaines publiques de la Ville de Dijon*, vol. Annexe D, Dalmont, Paris, **1856**.
- [133] Ngnepieba, P., Dimet, F. X., Boukong, A., Nguetseng, G., Identifications des paramètres: une application à l'équation de Richards. *ARIMA*, 1, 127-157, **2002**.

- [135] Canoğlu, M. C., Approche quantitative des flux d'eau dans le système sol-nappe du Marais Poitevin, Thèse de Master, HYDRASA, Poitiers, **2007**.
- [136] Bresler, E., Russo, D., Miller, R., Rapid estimate of unsaturated hydraulic conductivity function, *Soil Science Society of America Journal*, 42, 170–172, **1978**.
- [137] Novak, V., Estimation soil-water extraction patterns by roots, *Agricultural Water Management*, 12, 271–278, **1987**.
- [138] American Society of Civil Engineers, *Evapotranspiration and Irrigation Water Requirements*, Manuals and Reports on Engineering Practice, New York, **1990**.
- [139] Shuttleworth, W., *Evaporation*, chapter 4, in *Maidment*, 1–53, **1993**.
- [140] Alexandris, S., Kerkides, P., Liakatas, A., Daily reference evapotranspiration estimates by the “Copais” approach, *Agricultural Water Management*, 82, 371–386, **2006**.
- [141] Allen, R. G., Assessing integrity of weather data for use in reference evapotranspiration estimation, *Journal of Irrigation and Drainage Engineering*, 122(2), 97–106, **1996**.
- [142] Pauwels, V. R. N., Samson, R., Comparison of different methods to measure and model actual evapotranspiration rates for a wet sloping grasslands, *Agricultural Water Management*, 82, 1–24, **2006**.
- [143] Hargreaves, G., Samani, Z., Reference crop evapotranspiration from temperature, *Applied Engineering in Agriculture*, 1, 96–99, **1985**.
- [144] O’Callaghan, J., Mark, D., The extraction of drainage networks from digital elevation data, *Computing Vision Graphics Image Processing*, 28, 323–344, **1984**.
- [145] Tarboton, D., A new method for the determination of flow directions and upslope areas in grid digital elevation models, *Water Resources Research*, 33, 309–319, **1997**.
- [146] Quinn, P., Beven, K., Chevallier, P., Planchon, O., The prediction of hillslope flow paths for distributed hydrological modeling using digital terrain models, *Hydrological Process*, 5, 59–80, **1991**.
- [147] Choi, Y., Yi, H., Park, H. D., A new algorithm for grid-based hydrologic analysis by incorporating stormwater infrastructure, *Computers and Geosciences*, 37, 1035–1044, **2011**.
- [148] ESRI, Environmental Systems Research Institute, **2010**.
- [149] United States Environmental Protection Agency, NLCD 1992 Classification System, <http://www.epa.gov/mrlc/definitions.html#1992>, (**2014**).

[150] Chung, C. F., Fabbri, A. G., Probabilistic prediction models for landslide hazard mapping, *Photogrammetric Engineering and Remote Sensing*, 65, 1389–1399, **1999**.

[151] Bonham-Carter, G. F., Geographical information systems for geoscientists modeling with GIS, *Computer Methods in Geosciences*, Pergamon, Netherlands, 13, 398, **1996**.

[152] Akgün, A., Türk, N., İki ve çok değişkenli istatistik ve sezgisel tabanlı heyelan duyarlılık modellerinin karşılaştırılması: Ayvalık (Balıkesir, Kuzeybatı Türkiye) Örneği, *Jeoloji Mühendisliği Dergisi*, 34, 85-112, **2010**.

[153] Avinash, K. G., Ashamanjari, K. G., A GIS and frequency ratio based landslide susceptibility mapping: Aghnashini river catchment, Uttara Kannada, India, *International Journal of Geometrics and Geosciences*, 1, 343-354, **2010**.

[154] USDA, Natural Resources Conservation Services, Description of SSURGO (soil survey geographic database), United States Department of Agriculture, http://www.nrcs.usda.gov/wps/portal/nrcs/detail/soils/survey/?cid=nrcs142p2_053627

APPENDICES

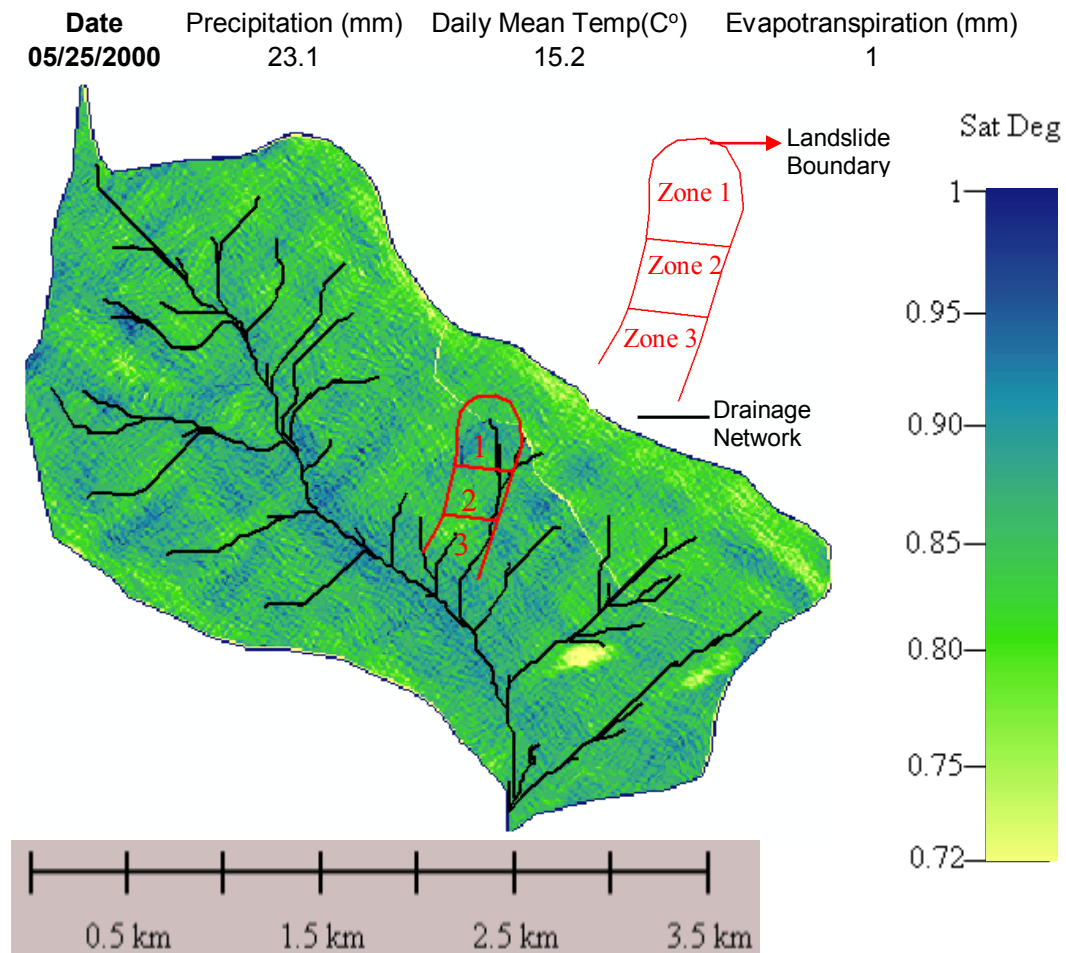
APPENDIX 1. Seismic parameters of the earthquakes that occurred in the period of 01.06.2000-10.06.2000 for a radius of 300km from Yenice Watershed.

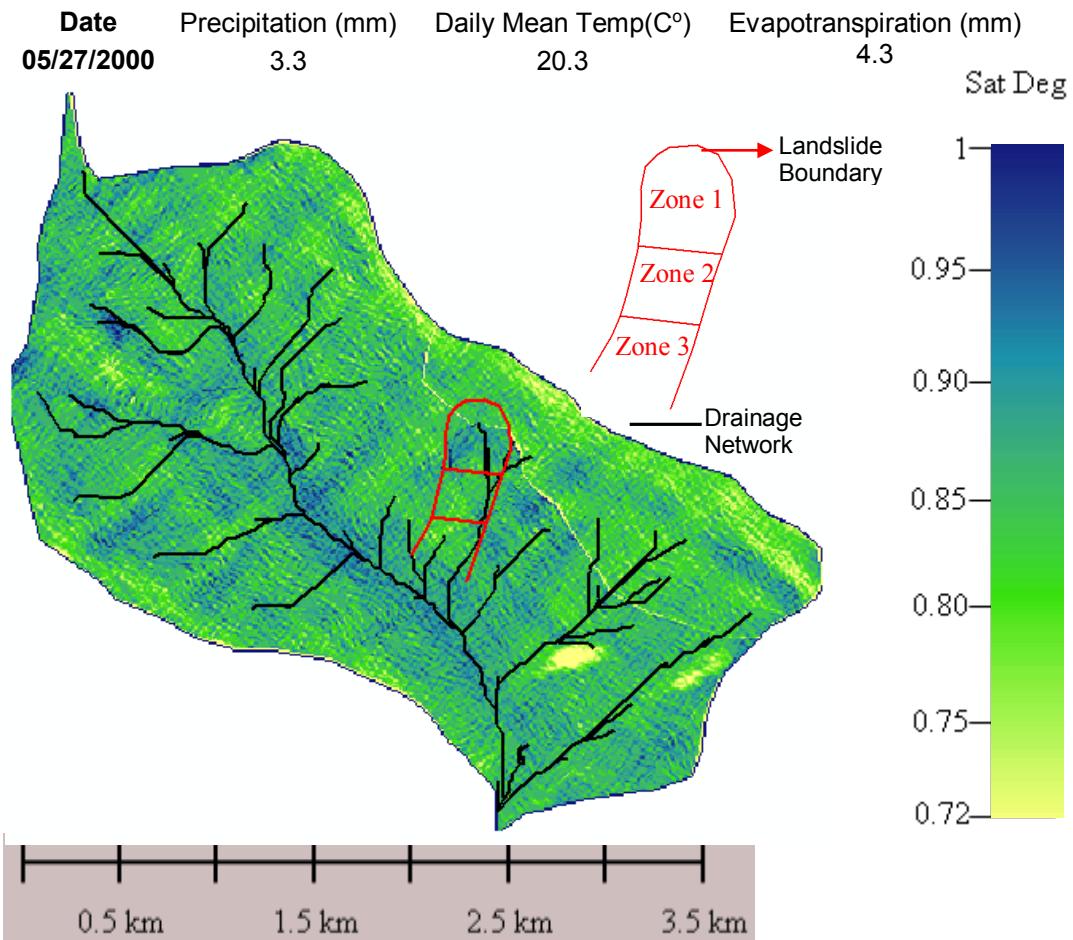
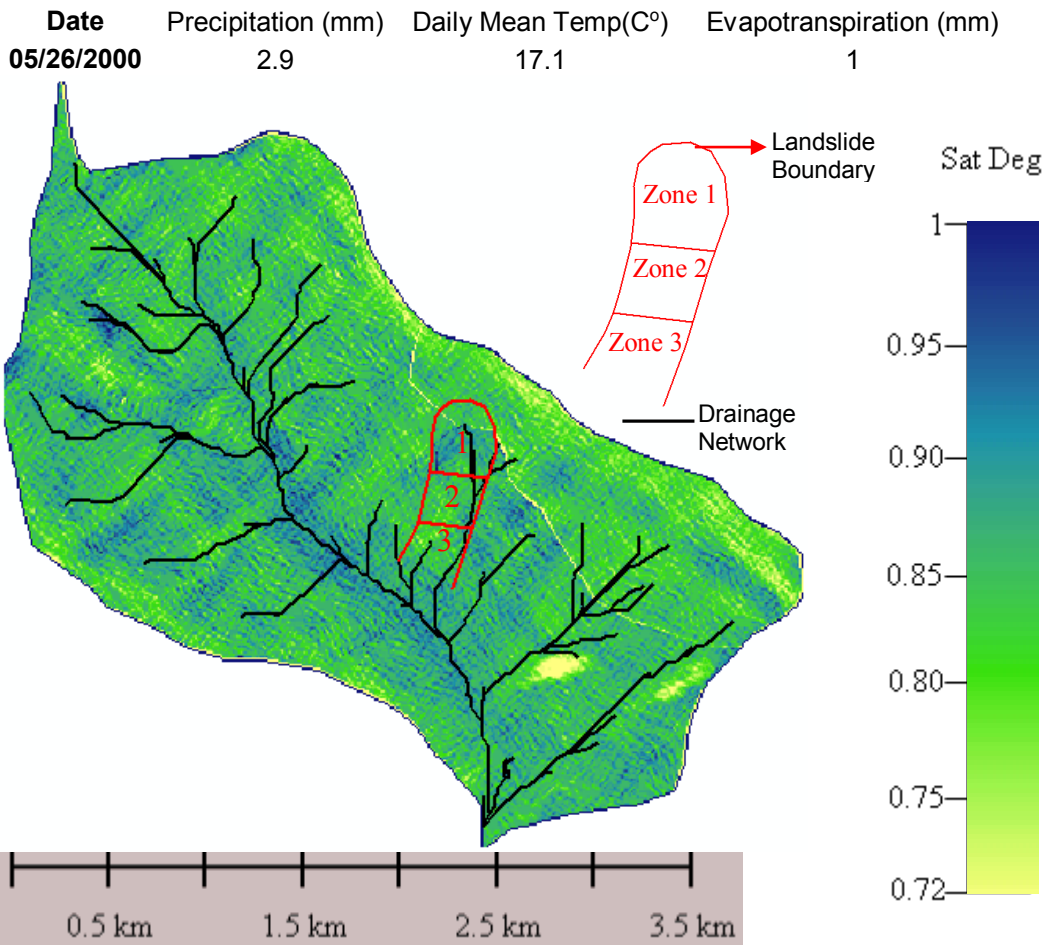
Occurrence Date	Latitude	Longitude	Depth (km)	Maximum Magnitude	Location
10.06.2000	40.77	31	2	2.7	ACMA-GOLYAKA (DUZCE) [North West 0.7 km]
10.06.2000	40.51	29.51	12	2.6	KERAMET-ORHANGAZI (BURSA) [East 3.1 km]
10.06.2000	40.64	33	7	3.8	BUGUOREN-ORTA (ÇANKIRI) [South East 0.7 km]
10.06.2000	40.88	32.98	0	3.1	CALCIOREN-CERKES (ÇANKIRI) [North East 2.5 km]
10.06.2000	40.66	33.13	10	3.1	KIRSAKAL-ORTA (ÇANKIRI) [West 1.7 km]
10.06.2000	40.44	29.24	13	2.8	GEDELEK-ORHANGAZI (BURSA) [South West 2.5 km]
10.06.2000	40.79	32.97	31	3.2	KARAMUSTAFA-CERKES (ÇANKIRI) [West 1.4 km]
10.06.2000	39.55	29.5	12	2.8	TAVSANLI (KÜTAHYA) [North East 0.8 km]
10.06.2000	40.72	33	13	3.2	GUZELYURT-CERKES (ÇANKIRI) [South West 2.0 km]
10.06.2000	40.56	33.03	0	3.1	GOKCEOREN-ORTA (ÇANKIRI) [North West 2.3 km]
10.06.2000	40.63	33.05	0	3.7	YUVA-ORTA (ÇANKIRI) [North East 1.4 km]
10.06.2000	40.68	33	3	3.4	HACILAR-CERKES (ÇANKIRI) [South East 3.5 km]
09.06.2000	40.8	32.95	0	3	KADIOZU-CERKES (ÇANKIRI) [South West 2.7 km]
09.06.2000	40.93	32.97	0	3.5	ULUKOY-CERKES (ÇANKIRI) [South East 1.8 km]
09.06.2000	40.6	29.21	9	2.7	YENIMAHALLE-TERMAL (YALOVA) [South East 1.1 km]
09.06.2000	40.61	29.26	6	2.9	SAFRAN- (YALOVA) [East 1.3 km]
09.06.2000	40.5	32.97	0	3.9	ULUAGAC-CUBUK (ANKARA) [North East 4.3 km]
09.06.2000	40.73	33.01	1	3.5	GUZELYURT-CERKES (ÇANKIRI) [West 0.7 km]
09.06.2000	39.71	29.41	0	2.6	YORGUC-TAVSANLI (KÜTAHYA) [West 1.4 km]
09.06.2000	41.1	29.37	5	2.6	KOCULLU-CEKMEKOY (ISTANBUL) [North East 3.0 km]
09.06.2000	41.2	32.77	0	3.5	KUZYAKAOTE-SAFRANBOLU (KARABÜK) [North 1.1 km]
09.06.2000	40.86	33.17	0	3.1	YESILOZ-KURSUNLU (ÇANKIRI) [South West 2.2 km]
09.06.2000	40.84	32.98	1	3.7	ALIOZU-CERKES (ÇANKIRI) [North East 2.5 km]
09.06.2000	41.7	32.5	9	3.1	CANAKCILAR-AMASRA (BARTIN) [South 0.9 km]
09.06.2000	40.82	32.99	3	3	KADIOZU-CERKES (ÇANKIRI) [North East 1.4 km]
09.06.2000	40.75	32.95	0	4.5	YESILOZ-CERKES (ÇANKIRI) [South East 2.5 km]
09.06.2000	40.74	30.98	5	2.9	BAKACAK-GOLYAKA (DUZCE) [North West 0.4 km]
09.06.2000	40.82	33.01	31	3.2	SUSUZ-ATKARACALAR (ÇANKIRI) [South West 1.6 km]
09.06.2000	41	32.83	6	2.8	KARASAR- (KARABÜK) [South East 2.8 km]
09.06.2000	40.67	33.02	32	3.3	KISAC-ORTA (ÇANKIRI) [North West 2.7 km]
08.06.2000	41.03	32.85	0	3.2	SULUK-OVACIK (KARABÜK) [South West 0.7 km]
08.06.2000	40.63	33.03	3	3.1	YUVA-ORTA (ÇANKIRI) [North West 1.4 km]
08.06.2000	40.51	32.88	31	3	YILDIRIMELOREN-CUBUK (ANKARA) [North 4.8 km]
08.06.2000	40.69	32.98	0	4.3	HACILAR-CERKES (ÇANKIRI) [South East 1.7 km]
08.06.2000	40.34	33.06	0	3.4	SELE-CUBUK (ANKARA) [North East 1.7 km]
08.06.2000	40.8	33.13	0	3.2	CARDAKLI-ATKARACALAR (ÇANKIRI) [South East 0.8 km]
08.06.2000	40.69	33.02	0	3.2	HACILAR-CERKES (ÇANKIRI) [South East 4.2 km]
08.06.2000	39.59	29.42	1	2.7	KAYAARASI-TAVSANLI (KÜTAHYA) [South West 3.1 km]
08.06.2000	41.52	32.72	2	3.1	KARAKISLA-ULUS (BARTIN) [East 3.7 km]
08.06.2000	40.78	31.66	0	2.6	HAMZABEY- (BOLU) [South East 0.5 km]
08.06.2000	40.92	32.83	16	3	MEYDANKOY-CERKES (ÇANKIRI) [North West 0.0 km]
08.06.2000	40.83	31.49	0	3.4	KIZILAGIL- (BOLU) [North West 6.3 km]
08.06.2000	40.8	32.93	0	3.5	BOZOGLU-CERKES (ÇANKIRI) [North East 1.9 km]
07.06.2000	41.66	32.51	16	2.9	GENCALI- (BARTIN) [South East 1.9 km]
07.06.2000	40.89	31.69	10	3.4	MESCICELE- (BOLU) [North West 5.8 km]
07.06.2000	41.34	32.82	0	3	YOLBASI-SAFRANBOLU (KARABÜK) [North 1.0 km]

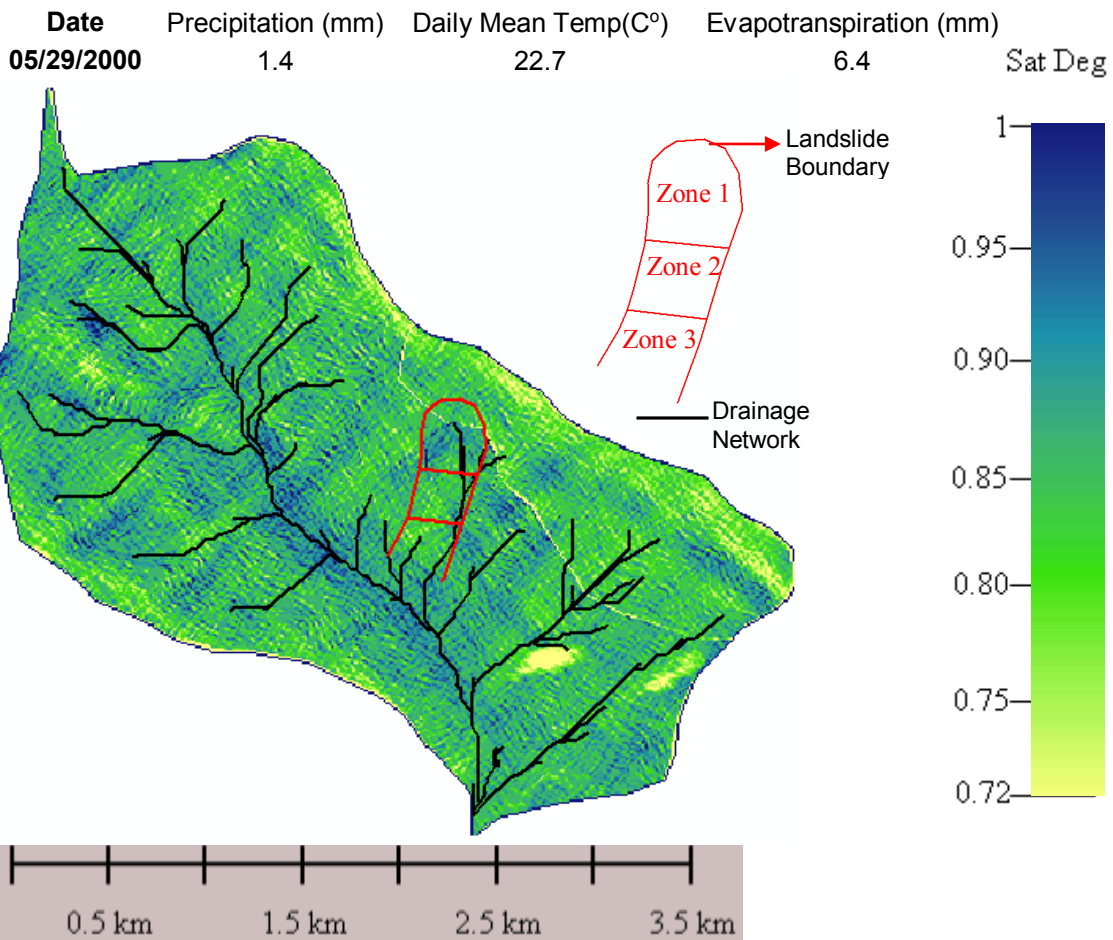
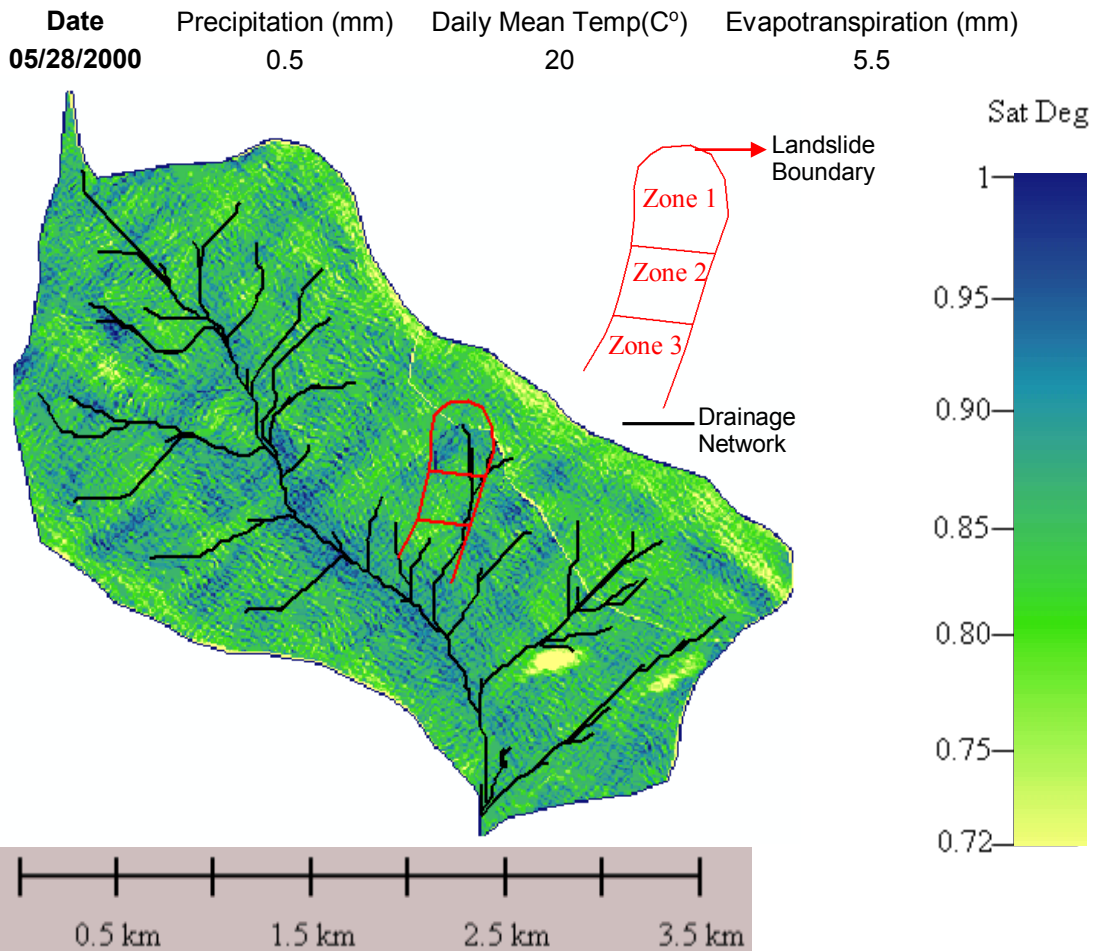
07.06.2000	40.58	33.11	9	3.1	YAYLAKENT-ORTA (ÇANKIRI) [South East 1.6 km]
07.06.2000	39.55	29.65	16	2.7	COBANKOY-TAVSANLI (KÜTAHYA) [North West 2.0 km]
07.06.2000	41.11	29.54	5	2.8	ERENLER-SILE (İSTANBUL) [West 1.6 km]
07.06.2000	40.39	33.11	6	3.2	DAGKALFAT-CUBUK (ANKARA) [North West 1.5 km]
07.06.2000	40.92	32.9	0	3	CAYLI-CERKES (ÇANKIRI) [North West 0.5 km]
07.06.2000	40.71	32.99	0	3.1	HACILAR-CERKES (ÇANKIRI) [North East 1.5 km]
07.06.2000	40.76	33.08	9	3.3	ILIPINAR-ATKARACALAR (ÇANKIRI) [South West 5.1 km]
07.06.2000	40.83	33.36	32	3	SUMUCAK-KURSUNLU (ÇANKIRI) [North East 1.2 km]
07.06.2000	40.64	33.06	7	3.4	SALUR-ORTA (ÇANKIRI) [South West 0.6 km]
07.06.2000	40.92	33.68	21	3.7	HACIHASAN-ILGAZ (ÇANKIRI) [North East 0.5 km]
06.06.2000	40.59	32.97	3	3	DEREBAYINDIR-ORTA (ÇANKIRI) [North West 1.8 km]
06.06.2000	40.44	33.02	4	2.9	AVCIOVA-CUBUK (ANKARA) [West 0.2 km]
06.06.2000	40.53	33.05	1	3.1	OZLU-ORTA (ÇANKIRI) [North West 1.5 km]
06.06.2000	40.49	33.04	6	3.4	OZLU-ORTA (ÇANKIRI) [South West 3.7 km]
06.06.2000	40.34	33.14	12	3	KUYUMCUKOY-CUBUK (ANKARA) [North West 1.9 km]
06.06.2000	40.65	33.07	11	3.4	SALUR-ORTA (ÇANKIRI) [North East 0.9 km]
06.06.2000	40.61	33.1	6	3.1	ORTA (ÇANKIRI) [South West 1.9 km]
06.06.2000	40.44	33.13	11	3.4	KOSRELIK-CUBUK (ANKARA) [West 2.3 km]
06.06.2000	40.44	33.09	0	3.6	KOSRELIK-CUBUK (ANKARA) [West 5.7 km]
06.06.2000	40.57	33.12	1	3.5	ELMALIK-ORTA (ÇANKIRI) [North West 2.8 km]
06.06.2000	40.69	33.17	0	3.5	SAKAELI-ORTA (ÇANKIRI) [North 1.1 km]
06.06.2000	40.44	33.17	1	2.9	KOSRELIK-CUBUK (ANKARA) [South East 1.1 km]
06.06.2000	40.62	33.06	8	3.5	YUVA-ORTA (ÇANKIRI) [East 1.7 km]
06.06.2000	41.09	32.79	0	2.9	KAMISKOY- (KARABÜK) [North West 1.3 km]
06.06.2000	40.51	33.02	0	3.8	OZLU-ORTA (ÇANKIRI) [South West 3.6 km]
06.06.2000	40.57	33.2	20	3.3	YENICE-ORTA (ÇANKIRI) [North West 2.5 km]
06.06.2000	40.41	33.21	4	2.9	KUTLUSAR-SABANOZU (ÇANKIRI) [North West 1.9 km]
06.06.2000	40.55	33.1	4	3.2	KAYILAR-ORTA (ÇANKIRI) [North East 1.5 km]
06.06.2000	40.48	33.12	1	3	KOSRELIK-CUBUK (ANKARA) [North West 5.2 km]
06.06.2000	40.66	33.06	0	3.1	SALUR-ORTA (ÇANKIRI) [North 1.7 km]
06.06.2000	40.57	33.03	4	2.9	HASANHACI-ORTA (ÇANKIRI) [South West 2.8 km]
06.06.2000	40.5	33.08	2	2.9	OZLU-ORTA (ÇANKIRI) [South East 2.7 km]
06.06.2000	39.97	33.23	31	3	ELMADAG (ANKARA) [North 5.3 km]
06.06.2000	40.57	33.02	0	2.9	ORTABAYINDIR-ORTA (ÇANKIRI) [East 2.9 km]
06.06.2000	39.62	29.51	18	2.6	TUNCBILEK-TAVSANLI (KÜTAHYA) [East 4.0 km]
06.06.2000	40.87	32.93	1	3	CALCIOREN-CERKES (ÇANKIRI) [North West 2.4 km]
06.06.2000	40.58	33	0	3.1	DEREBAYINDIR-ORTA (ÇANKIRI) [East 1.3 km]
06.06.2000	40.37	33.34	0	3.4	KINIK-KALECIK (ANKARA) [South 2.6 km]
06.06.2000	40.71	33.07	4	3	GUZELYURT-CERKES (ÇANKIRI) [South East 4.9 km]
06.06.2000	40.61	32.91	9	4.3	ORTAKOY-KIZILCAHAMAM (ANKARA) [North East 2.1 km]
06.06.2000	40.57	32.98	0	3.2	ORTABAYINDIR-ORTA (ÇANKIRI) [North West 0.7 km]
06.06.2000	40.56	33.02	1	3.5	ORTABAYINDIR-ORTA (ÇANKIRI) [South East 3.0 km]
06.06.2000	40.57	32.99	0	3.5	ORTABAYINDIR-ORTA (ÇANKIRI) [North East 0.6 km]
06.06.2000	40.83	32.94	8	3.2	ALIOZU-CERKES (ÇANKIRI) [West 1.0 km]
06.06.2000	40.59	33.01	1	3.2	DODURGA-ORTA (ÇANKIRI) [South East 2.1 km]
06.06.2000	40.9	32.94	6	3	KABAKKOY-CERKES (ÇANKIRI) [South West 1.8 km]
06.06.2000	40.76	32.97	7	3.4	YALIOZU-CERKES (ÇANKIRI) [South West 1.6 km]
06.06.2000	40.47	33.09	8	3.2	OZLU-ORTA (ÇANKIRI) [South East 6.0 km]
06.06.2000	40.5	33.07	0	3.2	OZLU-ORTA (ÇANKIRI) [South East 2.3 km]
06.06.2000	41.41	32.63	3	3	ONCULER-ULUS (BARTIN) [South East 3.9 km]
06.06.2000	40.49	33.18	0	3.4	BUYUKYAKALI-SABANOZU (ÇANKIRI) [North West 2.5 km]
06.06.2000	40.61	33.07	2	3.1	BUGDUZ-ORTA (ÇANKIRI) [North East 1.5 km]
06.06.2000	42.02	32.28	31	3.3	AMASRA AÇIKLARI-BARTIN (KARADENİZ)
06.06.2000	40.66	33.02	0	3	KISAC-ORTA (ÇANKIRI) [North West 1.6 km]

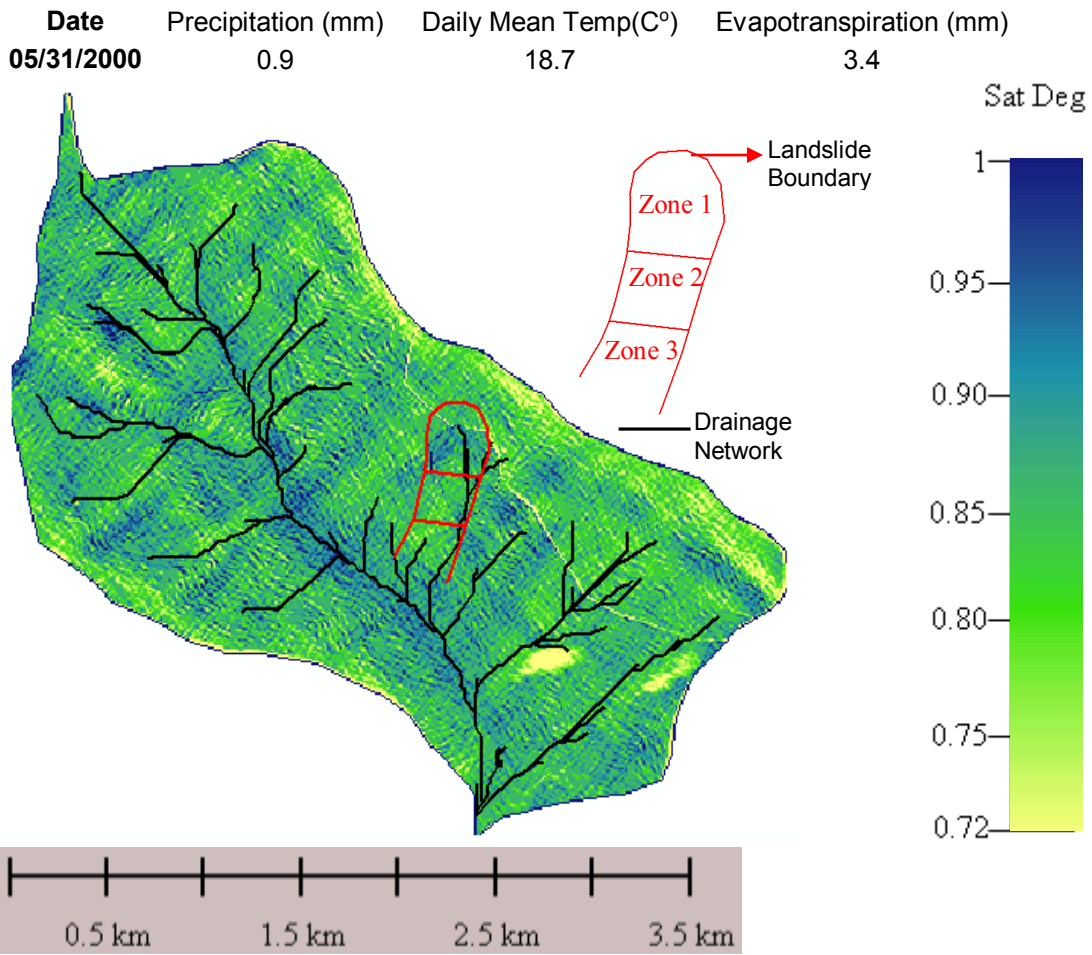
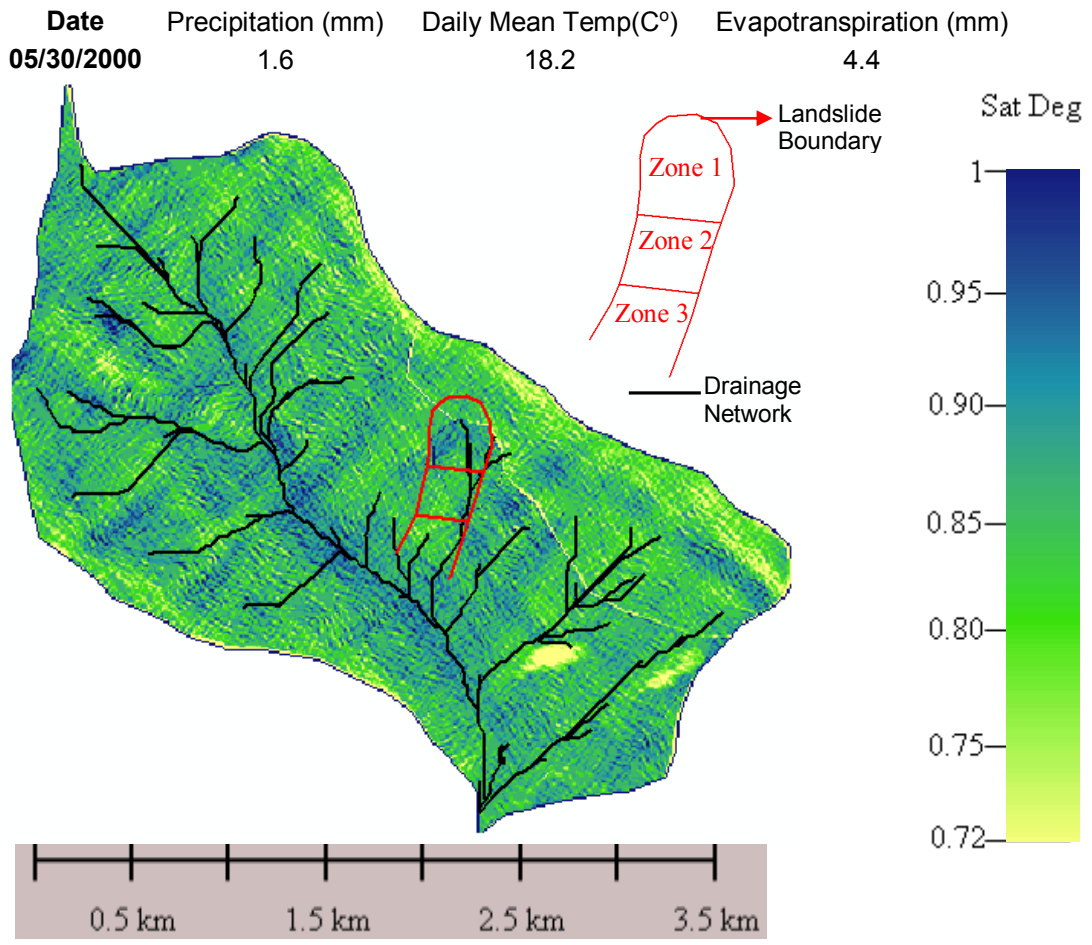
06.06.2000	40.8	32.98	0	2.9	KARAMUSTAFA-CERKES (ÇANKIRI) [North West 1.2 km]
06.06.2000	40.6	32.98	2	3	DODURGA-ORTA (ÇANKIRI) [South West 1.0 km]
06.06.2000	40.57	32.89	13	3.3	INCECIK-ORTA (ÇANKIRI) [South West 2.1 km]
06.06.2000	40.85	32.9	0	3.3	SIHDOGAN-CERKES (ÇANKIRI) [West 0.2 km]
06.06.2000	40.57	33.04	0	3.8	GOKCEOREN-ORTA (ÇANKIRI) [North West 2.3 km]
06.06.2000	40.77	32.95	10	3.2	YESILOZ-CERKES (ÇANKIRI) [South East 0.7 km]
06.06.2000	40.65	33.07	0	3.1	SALUR-ORTA (ÇANKIRI) [North East 0.9 km]
06.06.2000	40.7	32.99	5	5.6	HACILAR-CERKES (ÇANKIRI) [South East 1.5 km]
03.06.2000	40.67	31.79	18	3.1	KOLKOY- (BOLU) [South 5.6 km]
02.06.2000	39.48	29.93	7	2.7	ANDIZ- (KÜTAHYA) [South East 3.8 km]
02.06.2000	40.82	30.88	10	3	CUKURHAN-HENDEK (SAKARYA) [South 1.2 km]
02.06.2000	40.72	28.99	27	2.7	ÇINARCIK AÇIKLARI-YALOVA (MARMARA DENİZİ)
01.06.2000	40.74	30.9	8	2.7	DEGIRMENTEPE-GOLYAKA (DUZCE) [South East 1.8 km]
01.06.2000	39.7	29.54	4	2.5	KOZCAGIZ-DOMANIC (KÜTAHYA) [East 2.0 km]

APPENDIX 2. Saturation degree maps of last ten days before the occurrence date of Derebaşı Landslide

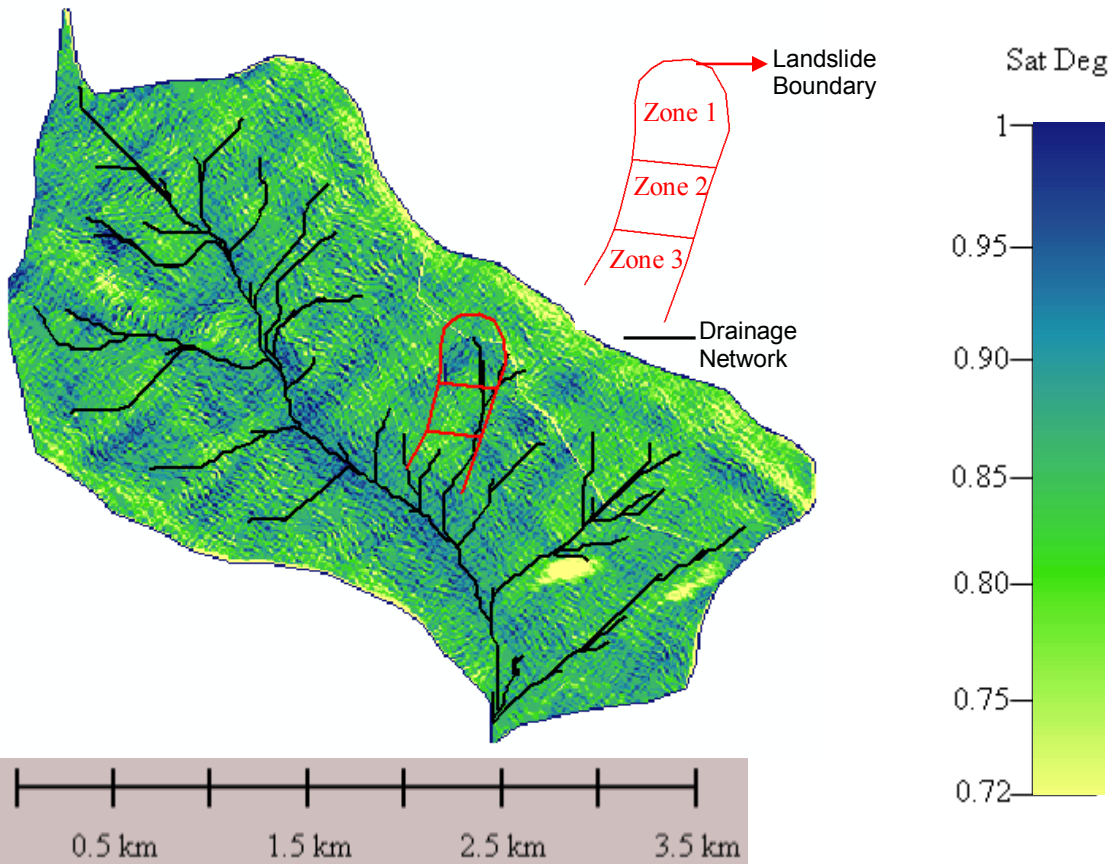




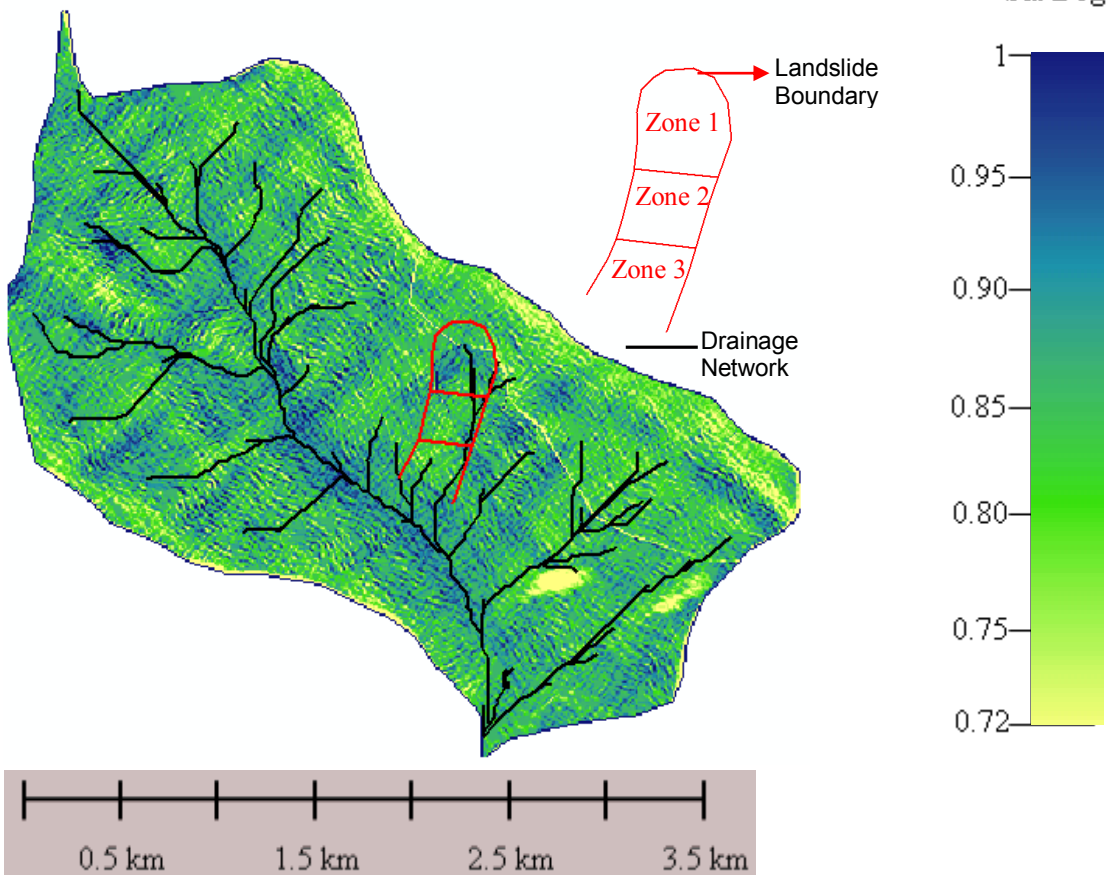




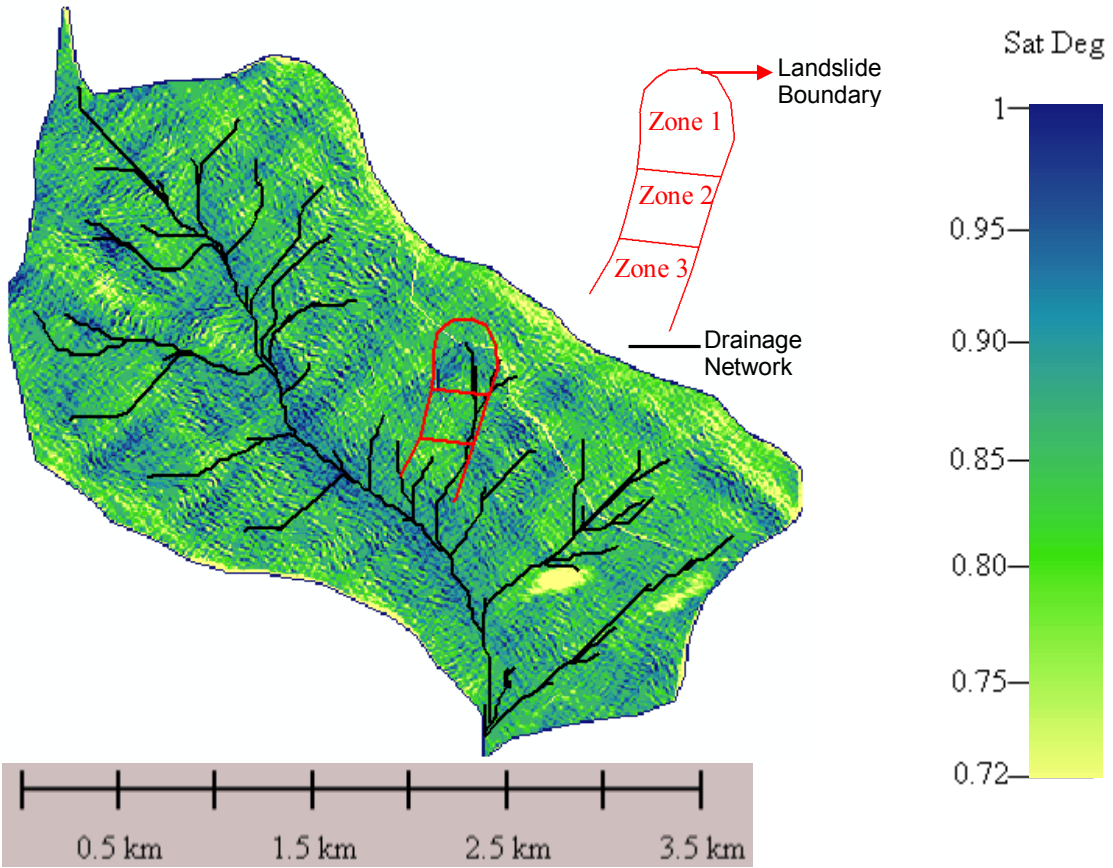
Date	Precipitation (mm)	Daily Mean Temp(C°)	Evapotranspiration (mm)
06/01/2000	0	20.8	3.4



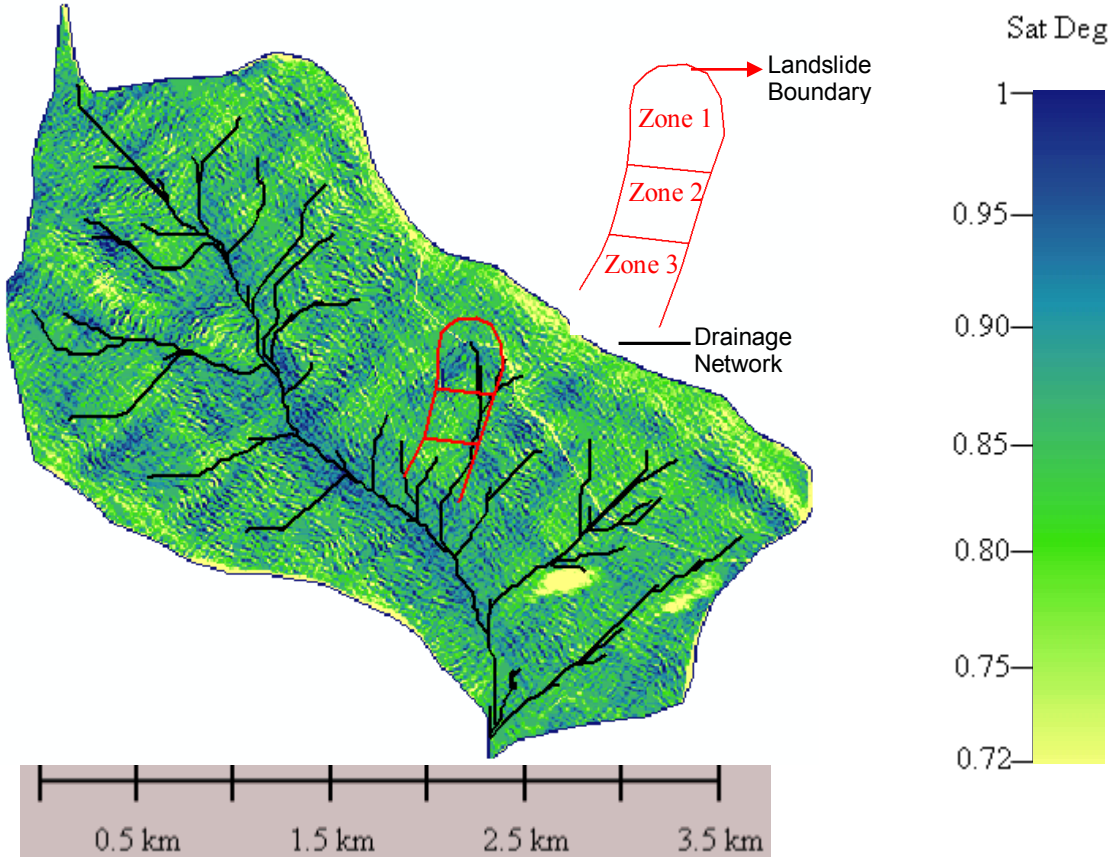
Date	Precipitation (mm)	Daily Mean Temp(C°)	Evapotranspiration (mm)
06/02/2000	2.5	16.2	5.4



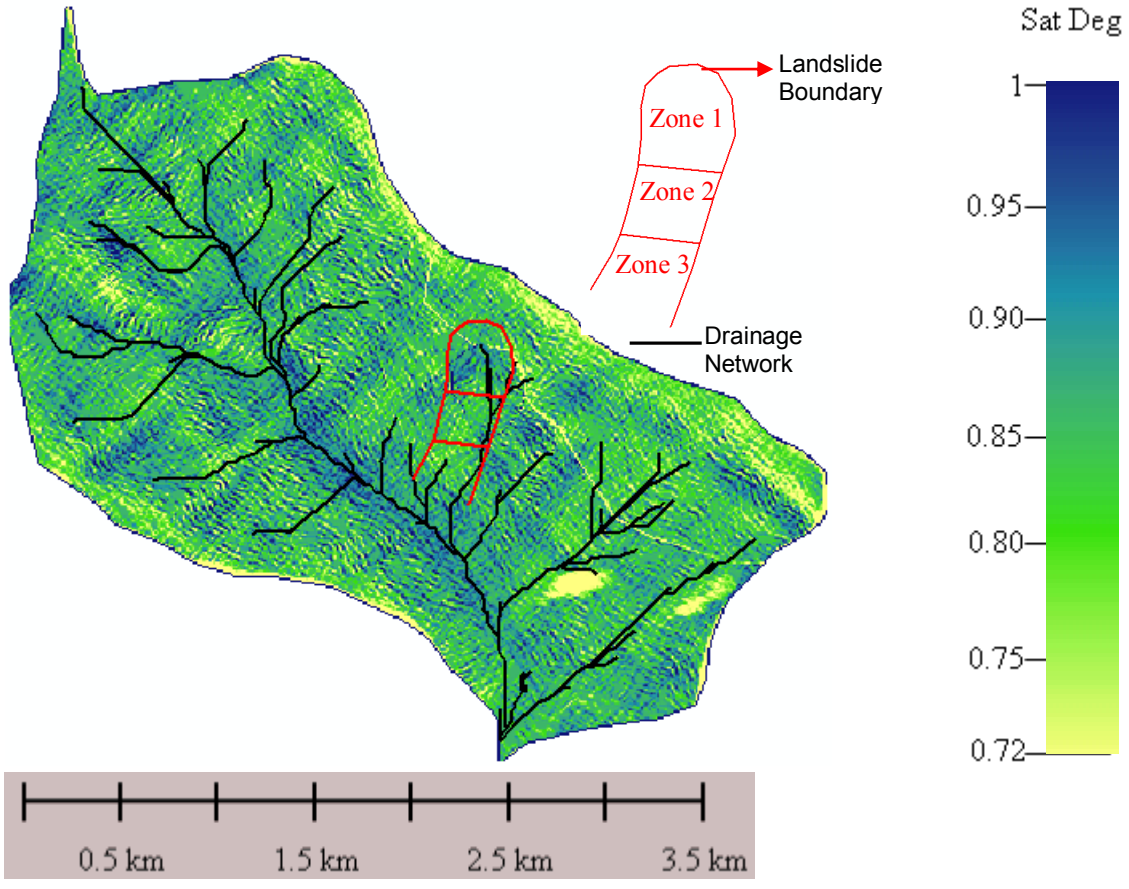
Date	Precipitation (mm)	Daily Mean Temp(C°)	Evapotranspiration (mm)
06/03/2000	11.2	15.1	1.5



Date	Precipitation (mm)	Daily Mean Temp(C°)	Evapotranspiration (mm)
06/04/2000	10.7	17.3	1.8



Date Precipitation (mm) Daily Mean Temp(C°) Evapotranspiration (mm)
06/05/2000 7.3 19.6 2.1



CURRICULUM VITAE

Credentials

Name, Surname : Mustafa Can Canođlu

Place of Birth : Ankara

Marital Status : Married

E-mail : can.canoglu@suyapi.com.tr, cancanoglu2005@yahoo.com

Address : Mustafa Kemal Mahallesi, 2128. Sokak, No:6, ZIP:06510, Çankaya, Ankara / TURKEY

Education

High School (1994 - 2001): Lycée Tevfik Fikret d'Ankara.

BSc. (2001-2006): Hacettepe University Geological Engineering Department

MSc. (2006-2007): Université de Poitiers, Faculté des Science Fondamentale et Appliquée, HydrASA.

PhD. (2008-2015): Hacettepe University Geological Engineering Department

Foreign Languages

French (Proficient – DALF C1)

English (Advanced)

Work Experience

2007-2008: Sial Geoscience Eng. Cons. Inc.

2008-2010: Spektra Jeotek Industry and Trade Co.

2010-...: Suyapı Engineering Consulting Inc.

Areas of Experiences

Hydrogeology, Engineering Geology, Applied Geotechnics, Drilling and Grouting.

Projects and Budgets

Publications

Integrated Approach Determining Spatio-Temporal Variations of the Saturation Degree Index as a Parameter in Landslide Susceptibility (***Unsubmitted Proof***).

Oral and Poster Presentations